# ANALYSIS OF A FOUR STATE SWITCHABLE HYDRO-PNEUMATIC SPRING AND DAMPER SYSTEM

**CHRISTIAAN LAMBERT GILIOMEE**

Submitted in partial fulfilment of the requirements for the degree

**M Eng (Mechanical Engineering)**

in the

Department of Mechanical and Aeronautical Engineering
Faculty of Engineering, Built Environment and Information Technology
University of Pretoria

2003

# ANALYSIS OF A FOUR STATE SWITCHABLE HYDRO-PNEUMATIC SPRING AND DAMPER SYSTEM

By

Christiaan Lambert Giliomee

Study leaders: Prof. JL van Niekerk, Mr. PS Els

Department of Mechanical and Aeronautical Engineering

University of Pretoria

## Summary

Spring and damper characteristics determine to a large extent the ride quality and handling of a vehicle. Since the requirements for good ride and good handling are conflicting, adjustable suspension elements are developed. In this study a two-state semi-active hydro-pneumatic spring, in conjunction with a two-state semi-active hydraulic damper is investigated. A mathematical model of the spring/damper system is developed and verified with measured data.

Two types of tests were performed on a prototype spring/damper unit, namely characterisation tests and single degree of freedom tests. The characterisation tests included characterising the hydro-pneumatic spring, the hydraulic damper, as well as the hydraulic valves in terms of valve response times. For the single degree of freedom tests, the step response, random input response and sine sweep response were determined.

Simulation models of the characterisation setup, as well as the single degree of freedom setup were constructed in Matlab Simulink. A real gas, thermal time constant model was used for modelling the hydro-pneumatic spring, while a look-up table was used for the damper characteristics. A hydraulic flow model was developed from first principles and first order valve dynamics were also included in the models.

Good correlation was obtained between measured and simulated data for the characteristation tests, as well as the single degree of freedom tests. The spring/damper model can be incorporated into a full 3D vehicle model in order to predict the ride and handling of a vehicle fitted with such a system.

# ANALISE VAN ‘N VIER-TOESTAND SKAKELBARE HIDROPNEUMATIESE VEER- EN DEMPERSTELSEL

Deur
Christiaan Lambert Giliomee

Studie leiers: Prof. JL van Niekerk, Mnr. PS Els

Departement Meganiese en Lugvaartkundige Ingenieurswese

Universiteit van Pretoria

## Opsomming

Veer- en demperkarakteristieke bepaal tot ‘n groot mate die ritgemak en hantering van ‘n voertuig. Aangesien die vereistes vir goeie ritgemak en goeie hantering teenstrydig is, word verstelbare suspensie elemente ontwikkel en gebruik. In hierdie studie word ‘n twee-toestand semi-aktiewe hidropneumatiese veer, gekoppel met ’n twee-toestand semi-aktiewe hidrouliese demper ondersoek. ’n Wiskundige model van die veer- en demperstelsel is ontwikkel en geverifieer met gemete data.

Twee tipes toetse is uitgevoer op die veer- en demperstelsel, naamlik karakteriseringstoetse en enkelvryheidsgraad toetse. Die karakteriseringstoetse het behels die karakterisering van die hidropneumatiese veer, die hidrouliese demper, asook die bepaling van die kleprespons tye. Enkelvryheidsgraad toetse het ingesluit trap respons, willekeurige en sinusvormige opwekking toetse.

Simulasiemodelle van die karakteriseringsopstelling, asook die enkelvryheidsgraad opstelling is geprogrammeer in Matlab Simulink. ‘n Werklike gas, termiese tydskonstante model is gebruik vir die hidropneumatiese veer model, terwyl oplees tabelle gebruik is vir die demper model. Die hidrouliese vloei model is afgelei uit eerste beginsels en eerste orde klep dinamika is ook ingesluit in die modelle.

Goeie korrelasie tussen gemete en gesimuleerde data is verkry vir die karakteriseringstoetse, asook die enkelvryheidsgraad toetse. Die veer- demperstelsel kan nou in ‘n volledige drie-dimensionele voertuig model ingebou word om die ritgemak en hantering van ’n voertuig met so ’n suspensie te voorspel.

*All models are wrong. Some are useful.*

J. Box

# ACKNOWLEDGEMENTS

Prof. Wikus van Niekerk

Mr. Schalk Els

Dr. Stefan Nell

Yolandé Giliomee

# INDEX

# ABBREVIATIONS

| | | |
|---|---|---|
| 2D | - | Two dimensional |
| 3D | - | Three dimensional |
| A/D | - | Analogue to Digital |
| ADAMS | - | Automatic Design and Analysis of Mechanical Systems |
| APC | - | Armoured Personnel Carrier |
| APG | - | Aberdeen Proving Grounds |
| ASC | - | Adaptive Suspension Control |
| AFV | - | Armoured Fighting Vehcile |
| ATV | - | All Terrain Vehicle |
| BWR | - | Benedict-Webb-Rubin |
| D/A | - | Digital to Analogue |
| DADS | - | Dynamic Analysis and Design System |
| EAS | - | Electronically Controlled Air Suspension |
| FRF | - | Frequency Response Function |
| GVM | - | Gross Vehicle Mass |
| HIL | - | Hardware in the Loop |
| HSS | - | Hydro-pneumatic Suspension System |
| MBT | - | Main Battle Tank |
| PRC | - | Programmed Ride Control |
| RAM | - | Random Access Memory |
| RMS | - | Root Mean Square |
| SDOF | - | Single Degree of Freedom |
| TEMS | - | Toyota Electronically Modulated Suspension |
| TACOM | - | Tank Automotive Command |
| USMC | - | United States Marine Core |
| VTF | - | Vehicle Test Facility |

# LIST OF FIGURES

# 1 INTRODUCTION

## 1.1 Preamble

The basic concept of land vehicle transportation has not changed much in the last few decades, although much progress was made in improving and optimising vehicle design and technology. The quest to always go faster, further and more comfortably, has lead in recent years to the development of advanced suspension systems. An improved suspension system allows a vehicle to achieve higher speeds over rougher terrain, and results in better handling, as well as improved ride comfort.

Passive suspension systems (suspensions without controllable elements), always represent a compromise between ride comfort and handling, since a stiff suspension is required for good handling, while a more compliant suspension is needed for good ride comfort. Implementing a controllable suspension (adaptive, slow-active, semi-active, fully-active see Chapter 2 for definitions) is therefore an attempt to narrow the gap between the opposing requirements for optimal ride comfort and handling.

This study focuses on a semi-active suspension system, consisting of a two-state switchable hydraulic damper, as well as a two-state switchable hydro-pneumatic spring. The different elements of the spring/damper system are characterised and a mathematical model is developed to predict the system performance.

In Chapter 1, an introduction and background is given. The background leading up to the development of the semi-active hydro-pneumatic spring/damper system, investigated in this study, is supplied and the working principle of the spring/damper system is explained. The purpose and scope, defining the extent of the research, is also discussed.

In Chapter 2, a brief discussion of the applicable literature is presented. The literature survey includes hydro-pneumatic springs and semi-active dampers, with specific reference to the application of this technology in heavy off-road vehicles.

Chapter 3 describes the development of the mathematical model of the semi-active spring/damper system. The mathematical model, as well as all the sub-models, is discussed in detail, with reference to the applicable literature.

In Chapter 4, the characteristics of the two-state hydro-pneumatic spring, the two-state hydraulic damper and the solenoid valve are presented. The experimental setup used to characterise the

semi-active hydro-pneumatic spring/damper system, as well as the single degree of freedom setup is described. Single degree of freedom test results are also presented in Chapter 4.

In Chapter 5, the mathematical model is verified using experimental data obtained from the characterisations and the single degree of freedom tests. The deficiencies of the current mathematical model are highlighted and areas for further refinement are defined.

In Chapter 6, conclusions are reached and recommendations made for future research into modelling this type of suspension system.

## 1.2 Background

In this section the background leading up to the development of the semi-active spring/damper system is presented.

The current research activity began in 1990, with a literature survey into advanced suspension systems (Nell 1990). This survey was part of an investigation conducted for the South African armaments procurement agency (Armscor). The literature survey concluded that future military vehicles would be highly mobile in order to enhance the survivability of the vehicle. This can be achieved by, amongst others, increasing the power to weight ratio or by optimising the suspension (Hohl 1986). An optimised passive suspension will however only be optimal for a certain combination of obstacle and vehicle speed (Nell 1991).

One way of enhancing the vibration isolation or ride comfort limited mobility of a vehicle is to introduce semi-active dampers (detail about the working of a semi-active damper can be found in Chapter 2). The development of semi-active dampers for wheeled vehicles started with simulations of a vehicle fitted with semi-active dampers, using DADS (Dynamic Analysis and Design System) software. The simulation results confirmed results obtained by other researchers in this field (Salemka & Beck 1975; Miller & Nobles 1988; Hrovat & Margolis 1981, Nell & Steyn 1994).

The first semi-active damper prototype is shown in Figure 1-1. In this figure, the external control valve and connecting pipes can clearly be seen.

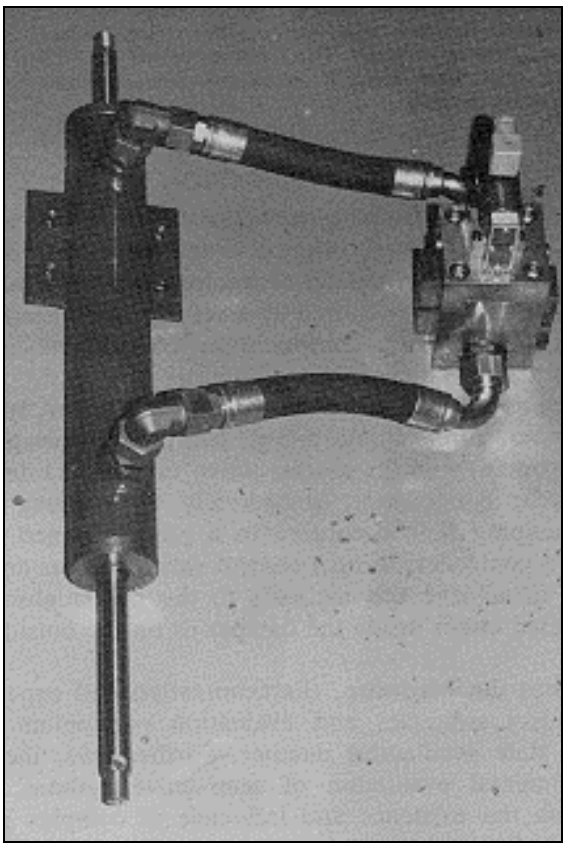

**Figure 1-1: First experimental semi-active damper**

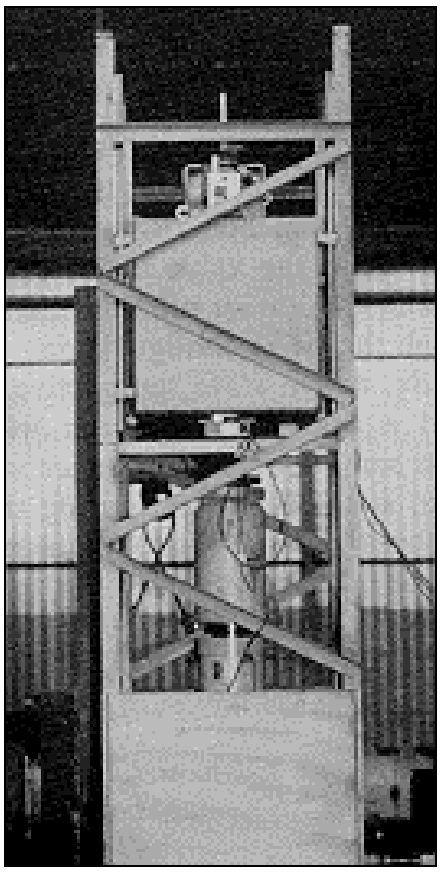

**Figure 1-2: First single degree of freedom test rig**

This damper was designed for a vehicle with a wheel load of approximately 2,5 metric tons. The semi-active damper was tested on a SDOF (single degree of freedom) test rig consisting of a 2,5 ton sprung mass (supported in linear bearings) and a linear coil spring. A 250*kN* Schenck hydraulic actuator was used to provide the required road inputs. The semi-active damper control signal was supplied by a personal computer. Figure 1-2 shows a photograph of the single degree of freedom test rig.

Three well-known semi-active damper control strategies were evaluated on the single degree of freedom test rig. They were the strategies of Karrnopp, Hölscher and Huang, and Rakheja and Sankar (Nell & Steyn 1994). It was found that the acceleration feedback strategy of Hölscher and Huang (Nell & Steyn 1994) proved to be the most successful at reducing the RMS acceleration on the sprung mass.

Nell (1993) developed an alternative control strategy, taking into account roll, pitch, lateral and vertical vehicle motion. This control strategy was evaluated on a 4x4 mine protected vehicle with a GVM of 12 tons, shown in Figure 1-3.

**Figure 1-3: 4x4 mine protected test vehicle fitted with semi-active dampers**

The semi-active dampers used on the 4x4 test vehicle can be seen in Figure 1-4. In this figure the external damper valve block, as well as the piping, is still clearly visible.

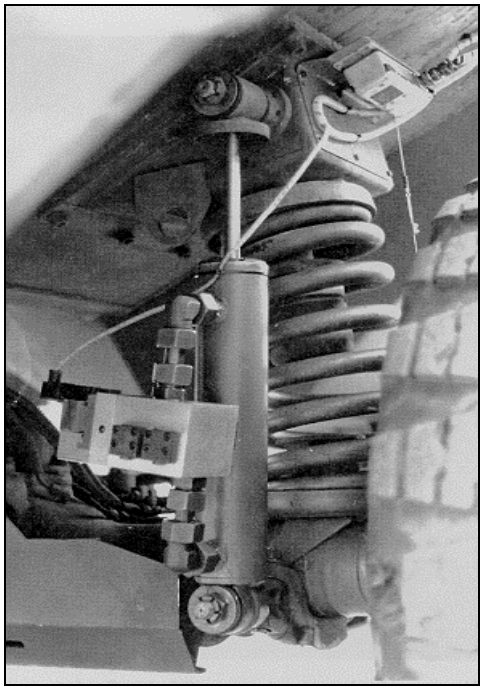

**Figure 1-4: Semi-active damper fitted to 4x4 test vehicle**

Tests were performed at speeds of between 15*km/h* and 55*km/h* over the Belgian paving track at the Gerotek Vehicle Test Facility and other typical off-road terrains. Improvements in ride comfort of up to 48% were recorded, with an average improvement of around 25%.

The next generation of semi-active dampers were fitted to a 6x6 armoured personnel carrier with a GVM of 17,4 tons. Semi-active dampers were fitted to all six wheel stations of the vehicle and were controlled by a dedicated computer, making use of solid state gyroscopes and accelerometers as input parameters. Figure 1-5 shows the vehicle during a high speed double lane change manoeuvre.

**Figure 1-5: 6x6 armoured personnel carrier fitted with semi-active dampers**

The ride comfort of the vehicle was improved by between 4% and 31% over different off-road terrains and at different vehicle speeds, while the maximum double lane change speed was improved by 9,4%. Roll velocity was also reduced and almost neutral steering was achieved.

Figure 1-6 shows the semi-active damper fitted to the 6x6 test vehicle. This damper was improved by including the valve block and ducts into a single assembly, bolted to the side of the damper i.e. the packaging was improved.

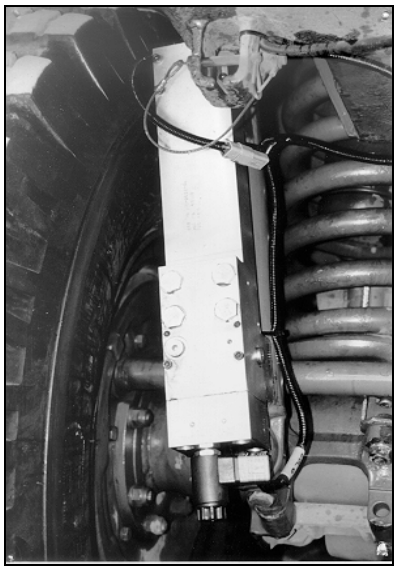

**Figure 1-6: Semi-active damper fitted to 6x6 APC**

The next step in semi-active damper research was the development of a semi-active rotary damper. The rotary damper was as a joint venture between Reumech Ermetek from South Africa and Horstman Defence Systems from the United Kingdom. Horstman Defence Systems was responsible for the damper design and manufacturing, while Ermetek developed the controller, integrated the damper onto the vehicle and installed the control valves and sensors. The test vehicle used to evaluate the performance of these dampers was the GV6 self-propelled howitzer shown in Figure 1-7.

**Figure 1-7: GV6 self-propelled howitzer fitted with semi-active rotary dampers**

The GV6 is a 6x6 vehicle of 47 tons GVM and is normally fitted with conventional translational dampers. Figure 1-8 shows a photograph of the semi-active rotary damper fitted to the experimental vehicle.

**Figure 1-8: Semi-active rotary damper fitted to the experimental vehicle**

The rotary damper supplies a maximum damping torque of 28*kNm* in the "on" state. Ride comfort tests were performed over the APG (Aberdeen Proving Grounds) track, Belgian paving track and the Fatigue track at the Gerotek VTF (Vehicle Test Facility). An improvement of between 25% and 58% in pitch velocity was achieved over the APG track, while improvements of between 7% and 15% were attained over the Belgian paving and Fatigue tracks. Figure 1-9 indicates the typical improvement in pitch velocity over the APG track at a vehicle speed of 24*km/h*.

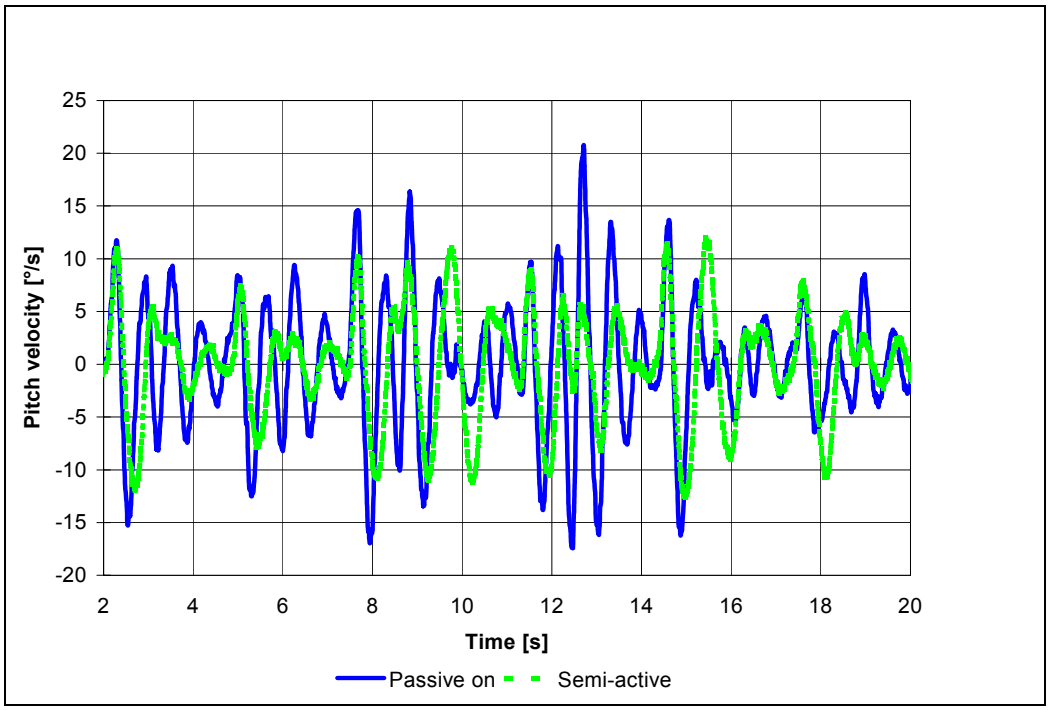


**Figure 1-9: Pitch velocity of the GV6 vehicle over the APG track**

Laboratory tests revealed that the valve response times are between 60 and 250 milliseconds, which is considered slow for semi-active control (Els & Giliomee 1998). Since the valve response times are dependent on the damper velocity, better performance increase was achieved over rougher terrains, such as the APG track.

The next evolution in semi-active suspensions, which is also the subject of this study, was developed during 1996/97. This system consists of a two-state semi-active hydraulic damper and a two-state semi-active hydro-pneumatic spring. The semi-active spring/damper system was developed for a vehicle with a static wheel load of 3000*kg*. The system was developed as result of two previous studies conducted by Nell and Steyn (1994) and Els (1993), into semi-active dampers and hydro-pneumatic springs. A brief explanation of the working principle of this suspension unit is supplied in the next paragraph.

The switching between high and low characteristics for both spring and damper are made possible by channelling hydraulic fluid with solenoid valves (refer to Figure 1-10). The spring/damper unit consists of a hydraulic strut (1), two Nitrogen filled accumulators (2&3), a hydraulic damper (4) and two solenoid valves (5&6).

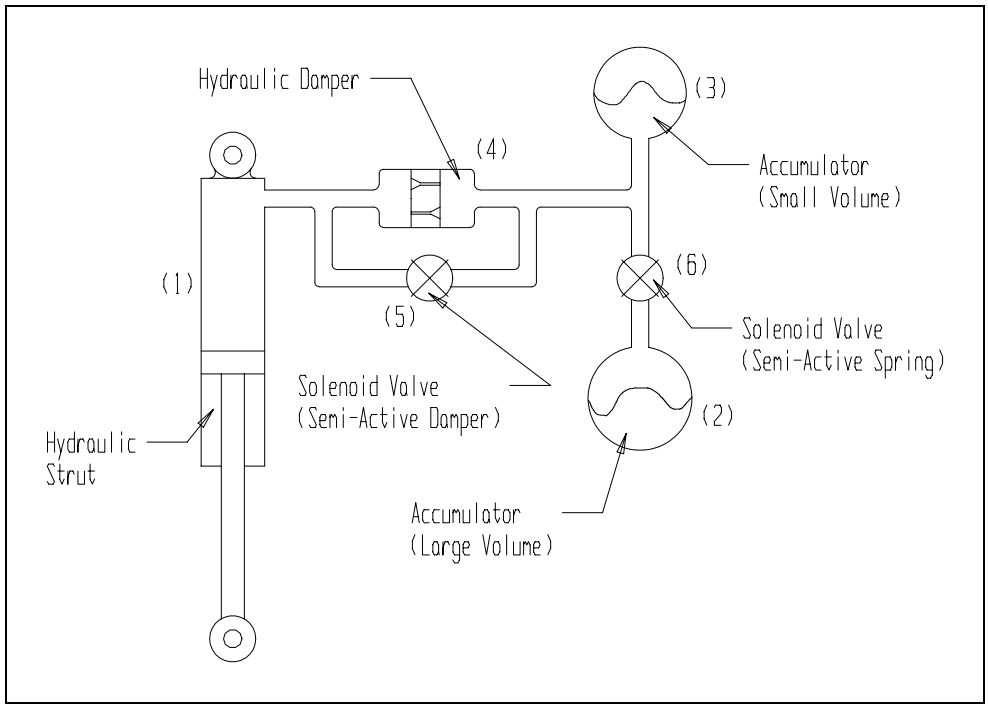


**Figure 1-10: Schematic layout of the semi-active spring/damper unit**

The low spring rate is achieved by compressing a large volume of gas consisting of two separate chambers (2&3). By sealing off one of the chambers (2), a smaller gas volume (3) is compressed and a higher spring rate is achieved. Spring rates can be individually tailored by changing the two gas volumes. For low damping the hydraulic damper (4) is short-circuited by opening a by-pass valve (5). For high damping this valve is closed and the hydraulic fluid is forced through the damper resulting in a higher damping force.

The characteristics of this suspension unit, as well as the tests and test results are discussed in detail in Chapter 4. The mathematical model of the suspension system is explained in Chapter 3.

## 1.3 Purpose and scope of this study

This study investigates the properties and mathematical modelling of an existing semi-active hydro-pneumatic spring/damper system. The reason for conducting this study is that semi-active suspension systems are currently the only means of further improving the ride comfort and handling of heavy off-road vehicles, cost effectively. Semi-active suspensions are cheaper than active suspensions because no external hydraulic power source is needed and inexpensive solenoid valves can be used to control the unit. Semi-active suspension systems are therefore commercially viable and worthwhile investigating.

A mathematical model of the semi-active spring/damper unit is developed to be used in a 3D multi-body vehicle simulation model. It is important to be able to simulate a full vehicle including the hydraulics, since the results will be used to size components such as pipe diameters, accumulator volumes, strut stroke and other components (designed for strength and durability). The mathematical model was developed in Simulink, which makes it modular, flexible and easy to integrate into a full vehicle simulation model in third party software such as DADS (Dynamic Analysis and Design System) or ADAMS (Advanced Dynamic Simulation of Mechanical Systems). An alternative and less complex model for first order 3D simulations is also proposed.

The following aspects are addressed in this study:

- Literature study about hydro-pneumatic springs and the modelling thereof
- Literature study of semi-active dampers
- Mathematical modelling of the semi-active spring/damper unit
- Measured spring, damper and valve characteristics
- Single degree of freedom (quarter car) rig tests
- Validation of the mathematical model
- Conclusions and recommendations

*****

# 2 HISTORICAL AND LITERATURE OVERVIEW

## 2.1 Preamble

In this chapter, an overview is given of semi-active dampers, hydro-pneumatic springs and hydraulic oil flow. Since a large amount of research has been done on adjustable dampers, this overview only covers discretely variable dampers, with a fast valve response (fast enough to control body resonance modes up to $2Hz$). This chapter focuses on literature concerned with large off-road vehicles, but in cases where the applicable technology has not yet be demonstrated on heavy vehicles, reference is made to commercial and passenger vehicles. Systems similar to the one investigated in this study are also discussed.

## 2.2 Suspension classification

Before semi-active dampers are discussed, it is necessary to define the term: semi-active. There exist many different opinions on the definition of semi-active suspensions. Some authors generalise the word “active” to any suspension system employing an external power supply and signal processing. This definition would however make it difficult to distinguish between a suspension powered by an external hydraulic pump and a suspension using only a small electric current to switch a valve. The difference between passive, adaptive, semi-active and fully active suspension systems are explained in the following paragraphs.

### a.) Passive suspension

If a graph of suspension displacement or velocity is plotted against suspension (spring or damper) force, the workspace of a passive suspension is in the first and third quadrants, since both spring and damper forces oppose the direction of displacement and velocity. The force elements in a passive suspension are not adjustable and cannot be controlled. Figure 2-1 is a graphical representation of a passive suspension workspace. The shaded area indicates the workspace, while the line indicates typical force element characteristics.

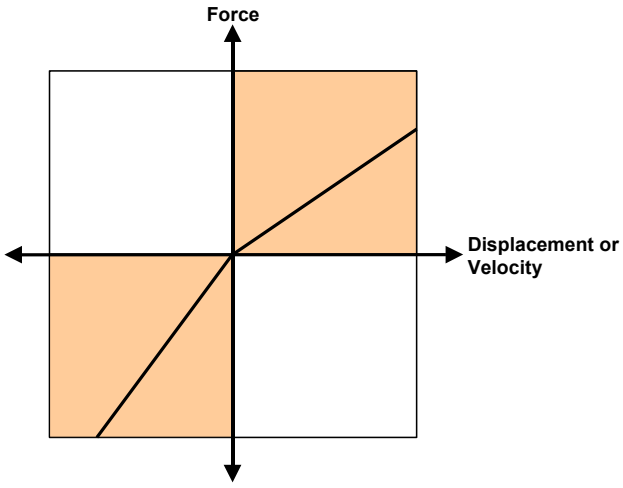


**Figure 2-1: Passive suspension workspace**

## b.) Adaptive or slow active suspension

The workspace of an adaptive or slow active suspension is the same as for a passive suspension, but the force element characteristics can be altered. The main difference between adaptive and semi-active suspensions is the rate at which the characteristics can be changed. For an adaptive suspension, the switching time is slower than the sprung mass natural frequency and requires minimal energy input to switch (see Figure 2-2).

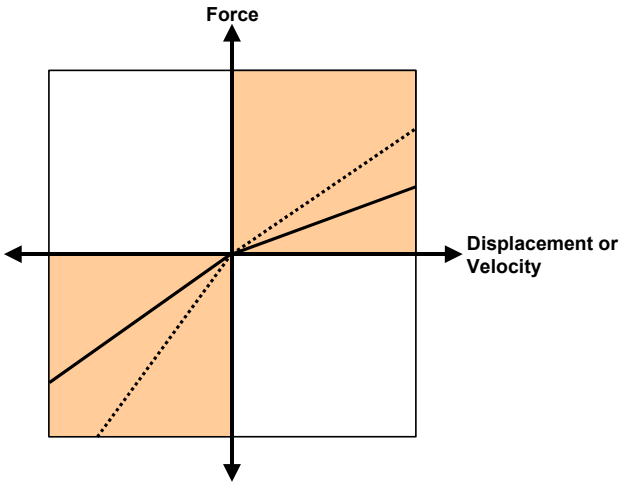


**Figure 2-2: Adaptive suspension workspace**

## c.) Semi-active suspension

The semi-active suspension workspace is the same as the passive and adaptive suspensions and like the adaptive suspension, the force element characteristics can be altered. Spring and/or damper characteristics of a semi-active suspension can be altered rapidly (faster than the sprung

mass natural frequency). The energy required to switch between characteristics is still low, but generally higher than an adaptive suspension (see Figure 2-3). Other than the switching signal, no energy is added to the system from an external source.

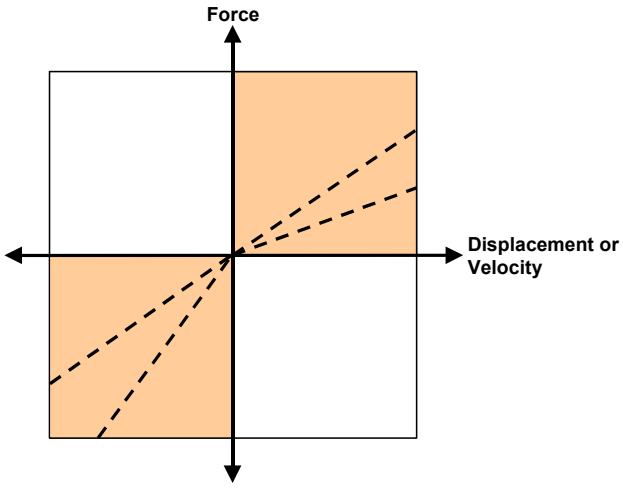


**Figure 2-3: Semi-active suspension workspace**

## d.) Active suspension

The workspace of an active suspension is in all four quadrants, because a positive force can be exerted for negative velocities or displacements and vice versa. The bandwidth of an active suspension is similar to that of a semi-active suspension, but the energy consumption is considerably higher. An external power source is required for this type of suspension.

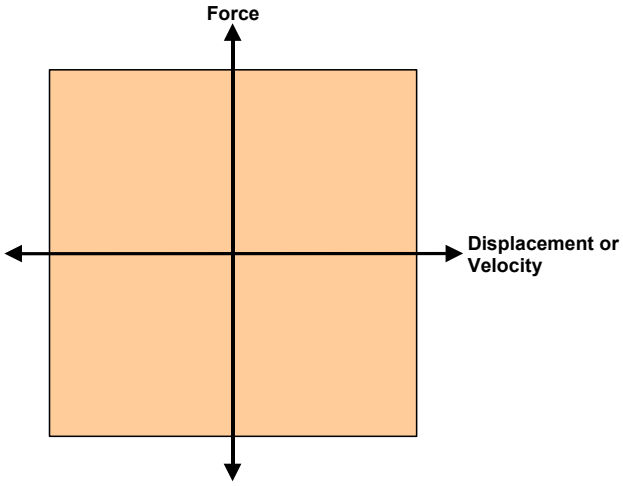


**Figure 2-4: Active suspension workspace**

## 2.3 Semi-active dampers

### 2.3.1 Background

Semi-active dampers were conceptualised in the 1970's and numerous configurations and control strategies were simulated and tested since then. Semi-active dampers greatly influence the vehicle dynamics (ride comfort and handling). This is also the main reason for developing semi-active dampers, namely to improve ride comfort without compromising handling and stability, by switching between hard and soft damper characteristics.

Most semi-active damper studies are conducted on passenger car sized vehicles. Experimental test rigs mostly consist of quarter car models with a sprung mass of ±250*kg* and an unsprung mass of ±50*kg*. Not many papers describe the development, or modelling, of semi-active dampers for heavy off-road vehicles (sprung mass of 2500*kg* to 3000*kg*).

Numerous so-called semi-active suspension systems were fitted to production vehicles, but most of these suspensions can be classified as adaptive. The reason for the confusion is that most of these suspensions are fast acting (as is semi-active suspensions), but they are employed in an adaptive manner. Examples of such suspension systems are:

- TEMS Toyota Electronic Modulated Suspension Toyota Soarer 1983 (Yokoya et al 1984).
- ASC Adaptive Suspension Control by Armstrong 1989 (CAR July 1989).
- 1987 Thunderbird Turbo Coupe Programmed Ride Control (PRC) Suspension (Soltis 1987).
- 1984 Continental Mark VII/Lincoln Continental Electronically-Controlled Air Suspension (EAS) System (Chance 1984).

Semi-active suspension development in the past mainly focussed on semi-active dampers, although some semi-active roll control devices and semi-active springs were also developed in more recent years.

### 2.3.2 Semi-active damper control

Modern and classical control theory accounts for very little of the control strategies successfully implemented on heavy off-road vehicles. Other control strategies similar to these were developed for implementation on vehicle platforms where not all the control parameters can be measured.

Many studies have been done to compare theory and experiments. In most of these studies, it was found that simulations are optimistic and often do not include all the physical phenomena and limitations.

Although the aim of this study is not to develop or test new control laws for semi-active suspension elements, some of the well-known strategies were used in the development and testing of the spring/damper unit in this study. The control strategies of Karnopp (Barak 1989), Hölscher and Huang (Nell 1993; Nell & Steyn 1994), and Rakheja and Sankar (1985:398-403) were used to determine the performance potential of the semi-active spring/damper system. The detail of these control strategies is described by Nell (1993).

## 2.4 Hydro-pneumatic springs

A hydro-pneumatic spring consists of two fluids acting upon each other, usually gas over oil. A compressible gas, such as Nitrogen is used as the springing medium, while a hydraulic fluid is used to convert pressure to force. In a pneumatic or air spring the external force directly compresses the gas and in a hydro-pneumatic suspension hydraulic fluid is used.

### 2.4.1 Historical overview

Hydro-pneumatic suspensions have been introduced on battle tanks in the 1950's. The first hydro-pneumatic struts were fitted to a prototype tracked vehicle, as a result of research done by two German companies, Frieseke and Höpfner from Erlangen and Borgwald from Bremen into the use of compressible fluids in suspension systems (Hilmes 1982). Since then, several other military vehicles were fitted with hydro-pneumatic suspensions, but most of them did not go into production due to reliability problems and short life span of the mechanical components. Initially, confidence in this type of suspension was low, due to sealing and design problems. These problems were later solved, but ride height change due to heat transfer to the compressed gas, still proved to be cumbersome, especially on tracked vehicles, where track tension is important.

The first production tracked vehicle fitted with a hydro-pneumatic suspension was the Swiss Strv-103 Main Battle Tank (MBT). This vehicle was fitted with a rigidly mounted main weapon and the height adjustable hydro-pneumatic suspension was used to tilt the vehicle upward or downward (Hilmes 1982). Several other military vehicles have since been fitted with hydro-

pneumatic suspensions. These include vehicles such as the Swiss Mowag Piranha (Figure 2-5), the British Challenger MBT and the French Giat Vextra (Figure 2-6).

**Figure 2-5: Mowag Piranha**

**Figure 2-6: Giat Vextra**

Since the introduction of more reliable sealing techniques, hydro-pneumatic springs have become more popular and are occasionally used in passenger cars, as well as in some large off-road vehicles. This type of suspension system is popular due to its non-linear characteristic and versatility. The non-linear characteristic causes the spring rate to increase as the load is increased. It also reduces body roll and pitching, results in more constant wheel loads and usually eliminates the necessity for a sophisticated bumpstop. Many controllable suspension systems make use of hydro-pneumatic springs because the hydraulic fluid can easily be channelled through ducts, orifices and valves. By adding, or removing, hydraulic fluid, the vehicle dynamics and ride height can be altered.

Hydro-pneumatic suspensions are not commonly used on commercial vehicles due to the high capital cost involved. Instead, pneumatic suspensions consisting of air bellows are mostly used on freight carrying vehicles. Hydro-pneumatic suspensions are found on passenger vehicles, where the design is simplified to minimise manufacturing costs.

Numerous hydro-pneumatic suspensions or suspension components are available on the world market. The internal working of these units all differ, but the basic principal, i.e. compressing a gas, is the same. Technical details of some of these units are supplied in Appendix A.

### 2.4.2 Modelling of hydro-pneumatic springs

Depending on the degree of complexity and accuracy required from the mathematical model, various mathematical models of hydro-pneumatic and pneumatic springs are available. Some of these models are discussed in more detail in the following paragraphs:

#### a.) Polytropic process

Hydro-pneumatic springs are often approximated as a politropic process, which is easy to model. In a politropic process the following pressure-volume relationship governs:

$$PV^n = \text{constant} \tag{2-1}$$

with

$P$ – Gas pressure
$V$ – Gas volume
$n$ – Polytropic constant

The following processes can be modelled as a polytropic process:

$n = 0$ Isobaric (Pressure stays constant)
$n = 1$ Isothermal (Temperature stays constant)
$n = k$ Isentropic (Entropy stays constant)
$n = \infty$ Isochroic

A reversible adiabatic process is isentropic, therefore a hydro-pneumatic spring can be modelled by using a polytropic constant between isothermal (1) and adiabatic ($k$), which is dependent upon the specific heat capacity of the gas. The value of $k$ for Nitrogen (ideal gas) is 1,4 at 300$K$.

Since hydro-pneumatic accumulators usually have thick walls to handle the high pressures, it invariably results in a high thermal capacity. This means that the gas compression and expansion process in a practical hydopneumatic spring, at realistic excitation frequencies, is close to adiabatic. A politropic constant of 1,35 is often used in mathematical models of hydro-pneumatic springs (Meller 1987). The following equation, proposed by Meller (1987), can be used to determine the hydro-pneumatic spring rate in the static position.

$$c = \frac{npA^2}{V}$$

with
$c$ – Gas spring rate
$n$ – polytropic exponent (1.35) (2-2)
$p$ – effective pressure
$A$ – pressure loaded area
$V$ – gas volume

Figure 2-7 shows the ideal gas, hydro-pneumatic spring characteristics for an isothermal an adiabatic process.

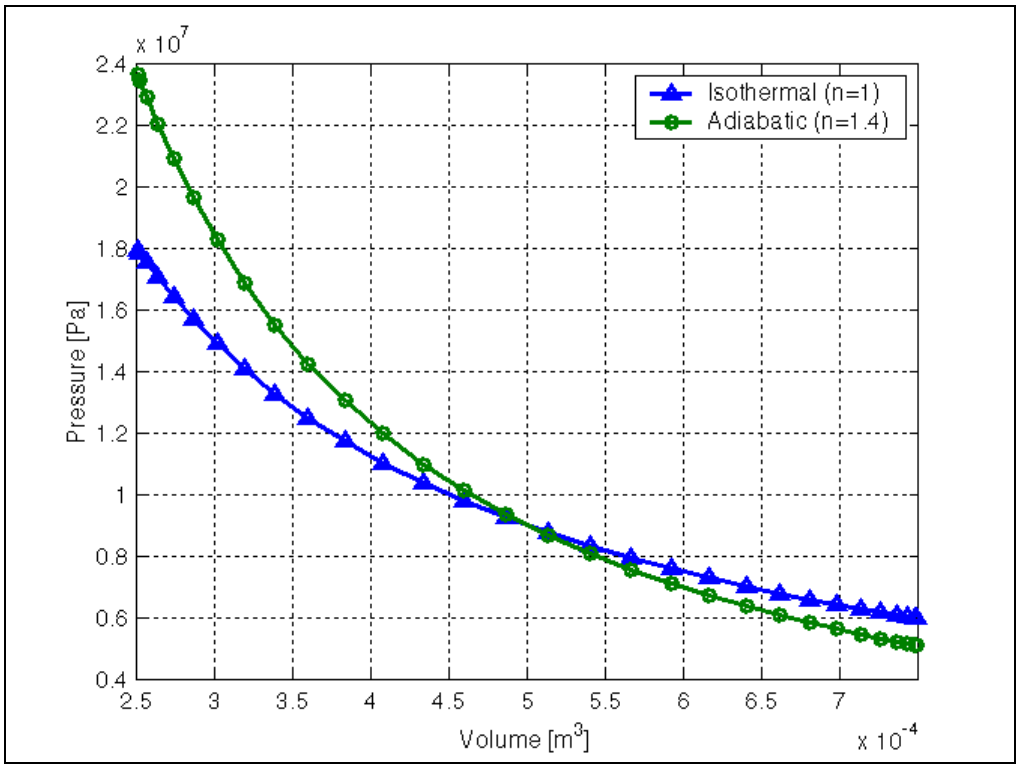


**Figure 2-7: Isothermal and adiabatic spring rates (ideal gas)**

In this approach, no provision is made for heat transfer to the surroundings. This approach was used by Horton and Crolla (1986), TACOM (1975), Félez and Vera (1987) and Meller (1987), amongst others.

## b.) Ideal gas approach

The ideal gas equation of state can also be used to determine the pressure volume relationship of a compressible medium like Nitrogen. Ideal gas assumptions are however only useful at low densities. The ideal gas equation of state can be written as follows:

$$PV = mRT \quad (2\text{-}3)$$

with

$P$ – Gas pressure

$V$ – Gas volume

$m$ – Gas mass

$R$ – Specific gas constant (296.8 J/kgK for Nitrogen @ 300K)

$T$ – Gas temperature [K]

Applying the conservation of mass theorem in a closed system and assuming that $R$ stays constant (ideal gas assumption), the ideal gas equation can also be written as:

$$\frac{P_1V_1}{T_1} = \frac{P_2V_2}{T_2}$$

where (2-4)

$P_1, V_1, T_1$ – Properties at first state

$P_2, V_2, T_2$ – Properties at second state

Because of its simplicity, this equation is very convenient to use for thermodynamic calculations.

### c.) Real gas approach

For pressures and temperatures above the critical point the ideal gas approach may result in significant errors, therefore a real gas approach has to be used. The critical temperature ($T_c$) of Nitrogen is 126,2$K$ and critical pressure ($P_c$) 3,39$MPa$ (Van Wylen and Sonntag 1985). Figure 2-8 indicates the compressibility factor ($Z$) of Nitrogen, as a function of both temperature and pressure. From this figure it is clear that the compressibility factor is very sensitive to the pressure and that the ideal gas approach will only hold for pressures lower than those normally found in hydro-pneumatic suspension systems (Els 1993) (see Appendix A).

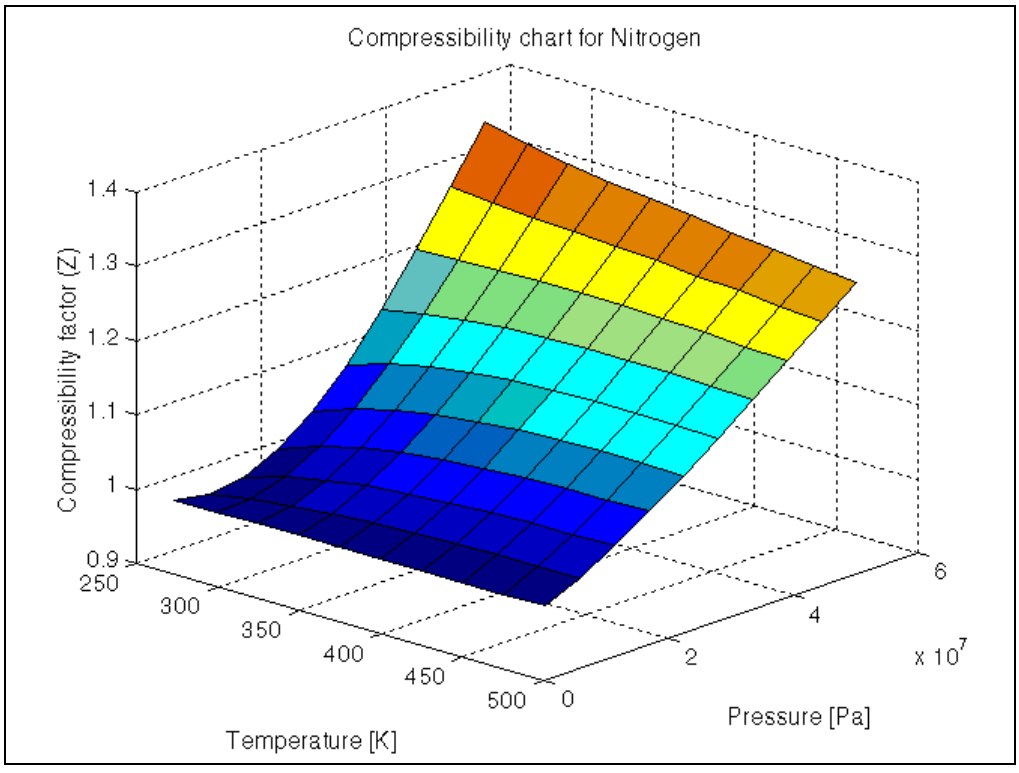


**Figure 2-8: Nitrogen compressibility**

An accurate equation of state, which is an analytical representation of P-v-T behaviour, is often required for computational models. Several different equations of state have been used. Most of

these are accurate only up to some density less than the critical density, though few are reasonably accurate to approximately 2,5 times the critical density. All equations of state fail badly when the density exceeds the maximum density for which the equation was developed.

The best-known and oldest equation of state is the Van der Waals equations first proposed in 1873. A simple equation of state namely the Redlich-Kwong equation was developed in 1949 and is considerably more accurate than the Van der Waals equation (Van Wylen & Sonntag 1985).

The Beattie-Bridgeman equation of state is an empirical equation first proposed in 1928 (Van Wylen & Sonntag 1985). This equation is reasonably accurate for densities lower than 0.8 times the critical density. A more complex equation of state, that is suitable for higher densities, is the Benedict-Webb-Rubin (BWR) equation of state developed in 1940. This equation has eight empirical constants and is essentially an extension of the Beattie-Bridgeman equation through the addition of the high density terms. The BWR equation can be written as follows:

$$P = \frac{RT_g}{v} + \left( \frac{B_0 RT_g - A_0 - {C_0}/{T_g^2}}{v^2} \right) + \left( \frac{bRT_g - a}{v^3} \right) + \frac{a\alpha}{v^6} + \left( \frac{c\left(1 + {\gamma}/{v^2}\right)e^{-\gamma/v^2}}{v^3 T_g^2} \right) \qquad (2\text{-}5)$$

with

$T_a$ - Ambient temperature

$T_g$ - Gas temperature

$C_v$ - Specific heat capacity of the gas

$P$ - Gas pressure

$V$ - Gas volume

$v$ - Gas specific volume

$a, A_0, b, B_0, c, C_0, \alpha, \gamma$ - constants for nitrogen gas

The first term of this equation can be recognised as the ideal gas term, while the rest of the terms are correction terms, compensating for the non-ideal behavior. The BWR equation was used with great success by Pourmovahed and Otis (1990), as well as by Els (1993). The gas pressures for the study conducted by Pourmovahed and Otis (1990) varied between 1 and 19.5*MPa*, while static pressures of between 6 and 10*MPa* and maximum pressure of 40*Mpa* were used in the study of Els (1993).

### d.) Thermal time constant, real gas approach

In 1993 the real gas, time constant model, described by Pourmovahed and Otis (1990) and Otis and Pourmovahed (1985), was adapted and applied to hydro-pneumatic springs by Els (1993). This model takes into consideration the heat transfer effects between the gas and the surroundings. The following equations describe the heat transfer between the gas and the surroundings (Els & Grobbelaar 1999):

$$\dot{T} = \frac{(T_a - T_g)}{\tau} - \frac{T_g}{C_v}\left(\frac{\partial P}{\partial T_g}\right)_v \dot{v} \tag{2-6}$$

with
$T_a$ - Ambient temperature
$T_g$ - Gas temperature
$\tau$ - Thermal time constant
$C_v$ - Specific heat capacity of the gas
$P$ - Gas pressure
$v$ - Gas specific volume

According to Pourmovahed and Otis (1990), the thermal time constant can either be determined through calculations or through experimental testing. The thermal time constant can be determined experimentally by observing the gas pressure for a step change in the gas volume. During the step change in gas volume, the gas is compressed and the temperature rises. As the gas cools down the pressure reduces. The thermal time constant, $\tau$, is the time it takes the gas pressure or temperature to drop by 63,2% to the final equilibrium pressure or temperature (see Figure 2-9).

Although the thermal time constant is not constant (varies with the heat transfer coefficient), it was found that a constant value could be assumed, if extreme accuracy is not required (Pourmovahed & Otis 1990). The thermal time constant for the accumulators used in this study, as determined by Els (1993), is approximately 6$s$.

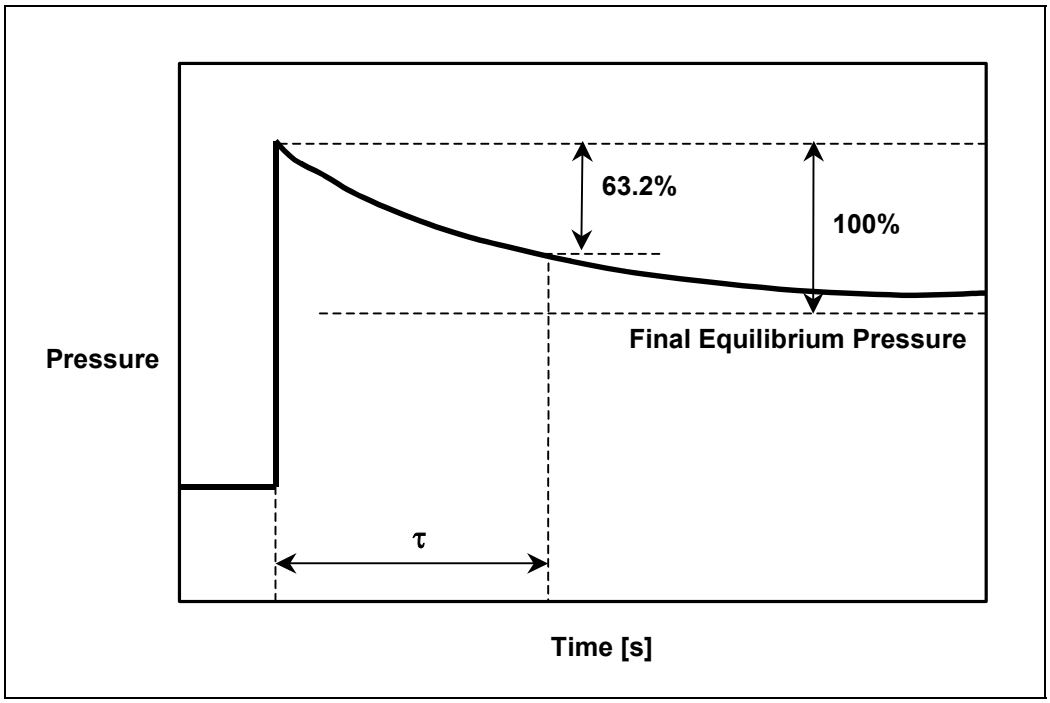


**Figure 2-9: Experimental determination of the thermal time constant**

Heat transfer may account for up to 30% of the thermal losses (at specific excitation frequencies), which results in the characteristic hysteresis loop of a hydro-pneumatic spring. Figure 2-10 shows the hydro-pneumatic spring characteristic when heat transfer effects are taken into consideration.

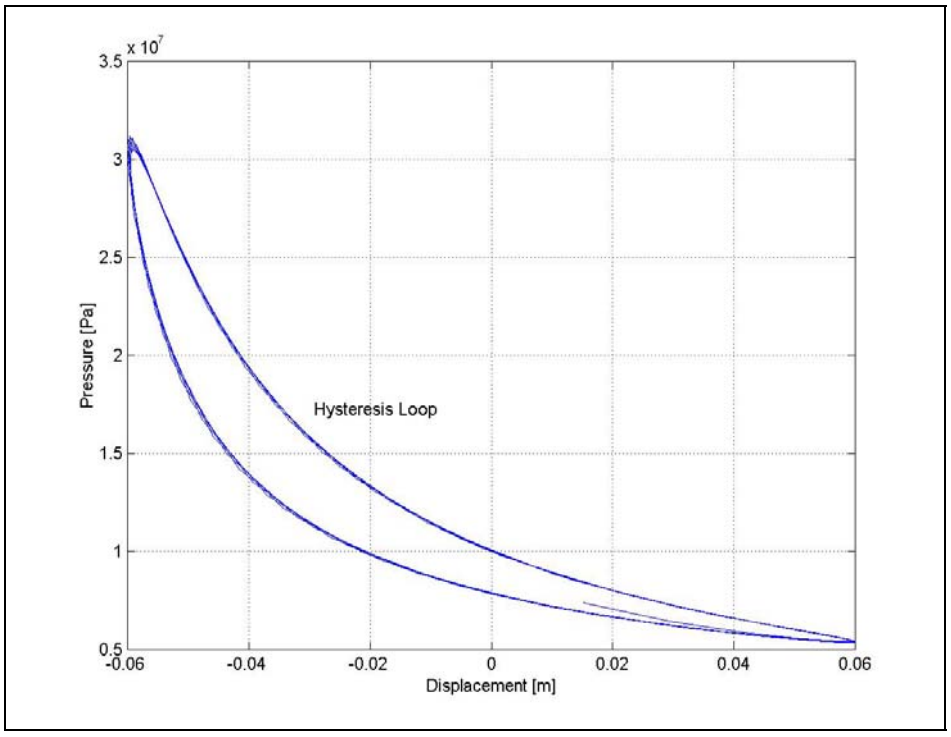


**Figure 2-10: Characteristic hysteresis loop of a hydro-pneumatic spring (sinusoidal excitation)**

The thermal losses are dependent on the excitation frequency, as well as the excitation amplitude. At low excitation frequencies, sufficient time is available for heat transfer to the surroundings, resulting in the isothermal characteristic. At higher excitation frequencies, the heat transfer process is too slow and the adiabatic characteristic is achieved. For excitation frequencies between isothermal and adiabatic, energy is transferred to the surroundings during the compression stage and not completely recovered during the expansion stage. This phenomenon results in the hysteresis loop, clearly visible in Figure 2-10. The area enclosed by the hysteresis loop indicates the amount of thermal damping at that specific excitation frequency.

Figure 2-11 indicates the amount of thermal damping for different excitation frequencies and amplitudes. From this figure, it can be seen that the thermal damping is frequency dependent and that for this specific case, the peak loss is below any frequency that is of interest in vehicle suspensions.

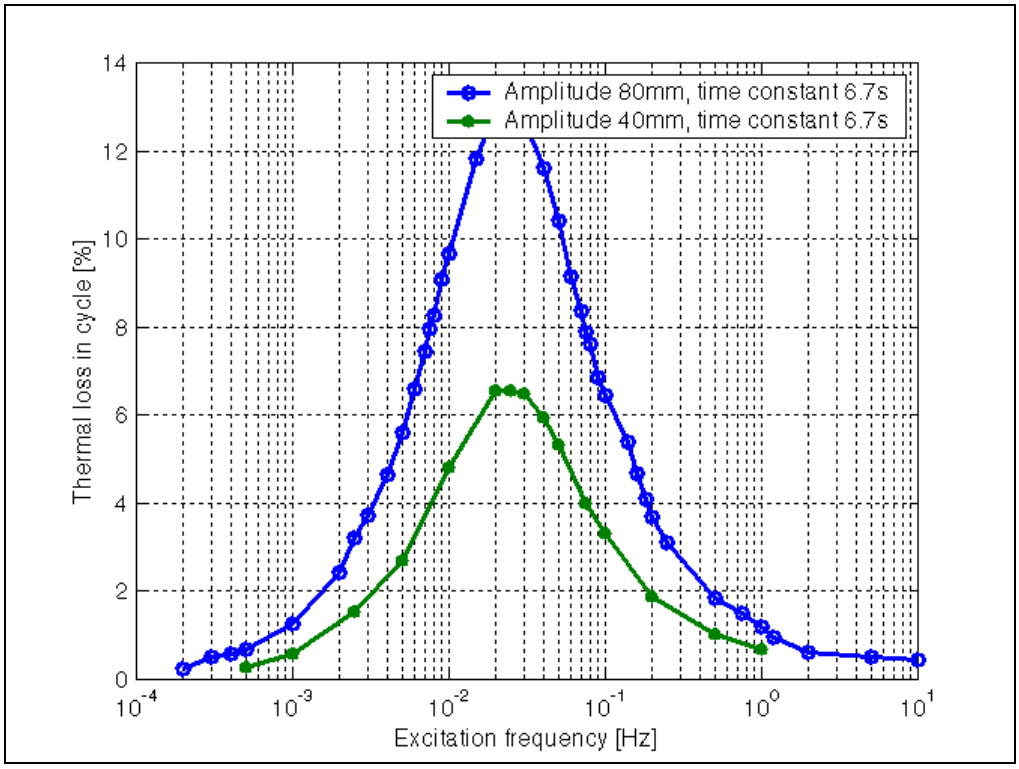


**Figure 2-11: Thermal damping**

In previous work of Pourmovahed and Otis (1984), a linear anelastic model was compared with the thermal time constant method. Figure 2-12 shows schematically the anelastic model, in which the spring ($k1$) and the damper ($c$) model the hysteresis loop in the spring characteristic.

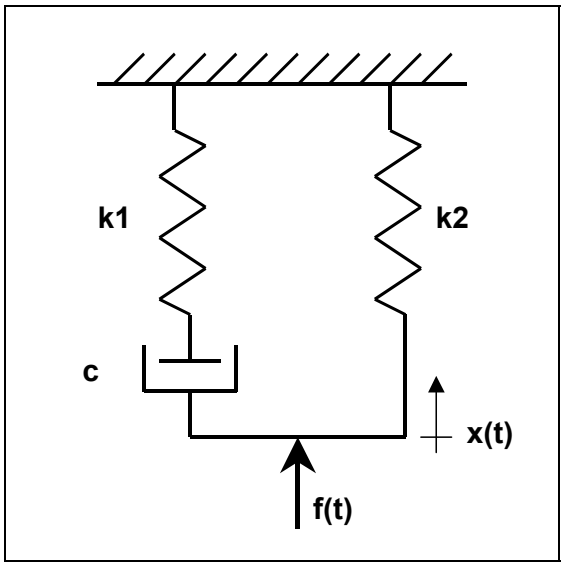


**Figure 2-12: Anelastic model for modelling heat transfer in accumulators**

The anelastic model was shown to be mathematically the same as the time constant model. The thermal time constant and real gas approach is used in the modelling of the semi-active spring/damper system investigated in this study (see Chapter 3 for more detail).

### e.) Bond graphs

The bond graph method was developed for simplifying the process of deriving the equations for mathematical models. This method was used by Félez and Vera (1987) to model a hydro-pneumatic spring system. In their model the damper is treated as a resistive element, while the hydro-pneumatic spring is a capacitive element. A polytropic process was used to model the capacitance of the hydro-pneumatic spring.

The bond graph method can also be used to model the parallel accumulator system of this study, but the causality laws at the split results in derivative, as well as integral equations, which can be troublesome to solve.

## 2.4.3 Controllable hydro-pneumatic / pneumatic suspensions

Several examples of controllable hydro-pneumatic or pneumatic springs can be found in the literature. The idea of obtaining more than one spring rate by changing the gas volume is not new. Karnopp en Heess (1991) suggested connecting two accumulators in parallel, in order to obtain different spring rates. They remark that it is possible to vary the spring rate, but it is not possible to directly control the force, as can be done with dampers.

The Electronic Modulated Air Suspension System for the 1986 Soarer of Toyota is fitted with an adjustable pneumatic spring and damper (Hirose et al 1988). Valve response times of 70*ms* were attained through an electromagnetic drive system. Modulating a rotary valve between a main and smaller air chamber alter the spring rate. The same principle is used for adjusting the damper characteristics. The spring and damper characteristics are not adjusted individually and a combination of input driven (steering, clutch, throttle or brake input) and reaction driven (measured acceleration, velocity and displacement) control strategies are used. Although fast response times are achieved the control of this suspension can be classified as adaptive rather than semi-active, since the reaction driven strategies react to vehicle speed and ride height, not body motion.

A controllable parallel accumulator suspension system was proposed by TACOM (1975). Figure 2-13 shows the variable spring rate concept. This system was proposed as an operator controlled system.

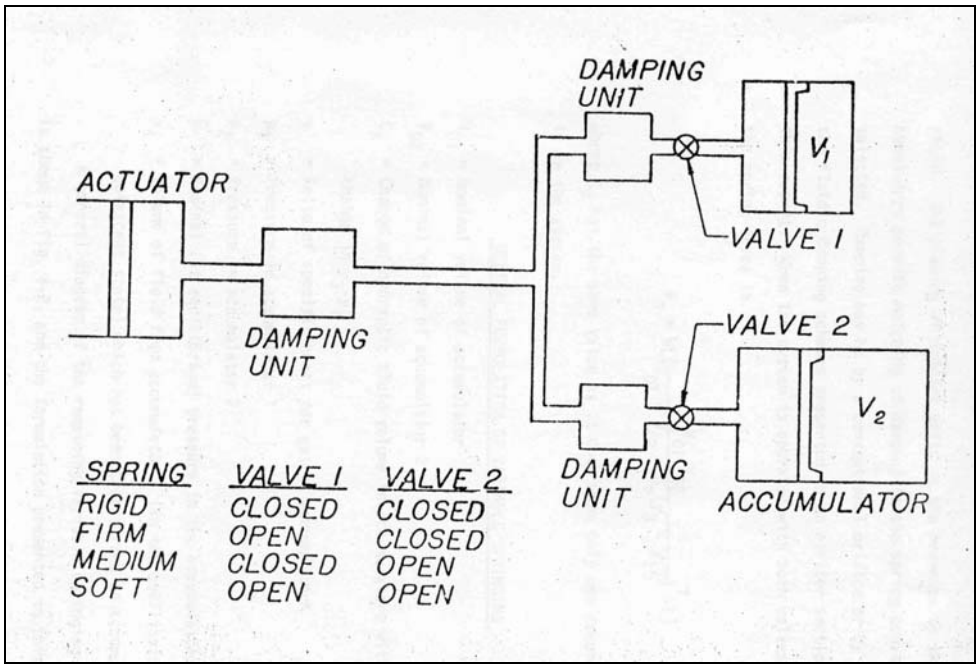


**Figure 2-13: Variable spring rate suspension (parallel accumulators)**

Another controllable spring system proposed by TACOM (1975) is an accumulator system connected in series. In principle, this concept works the same as accumulators connected in parallel. It is unknown if prototypes of these suspension concepts were ever built.

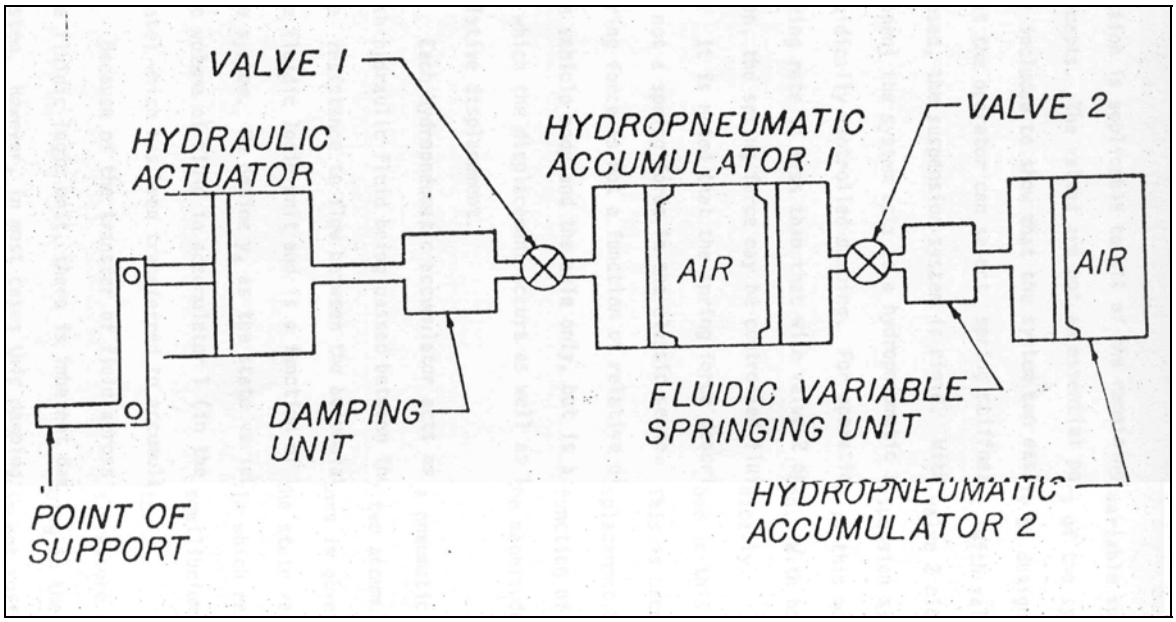


**Figure 2-14: Variable spring rate suspension (series accumulators)**

The twin-accumulator suspension described by Abd El-Tawwab (1997) was investigated. The twin accumulator suspension consists of two hydro-pneumatic springs in parallel and a control valve in series with each of the accumulators (see Figure 2-15).

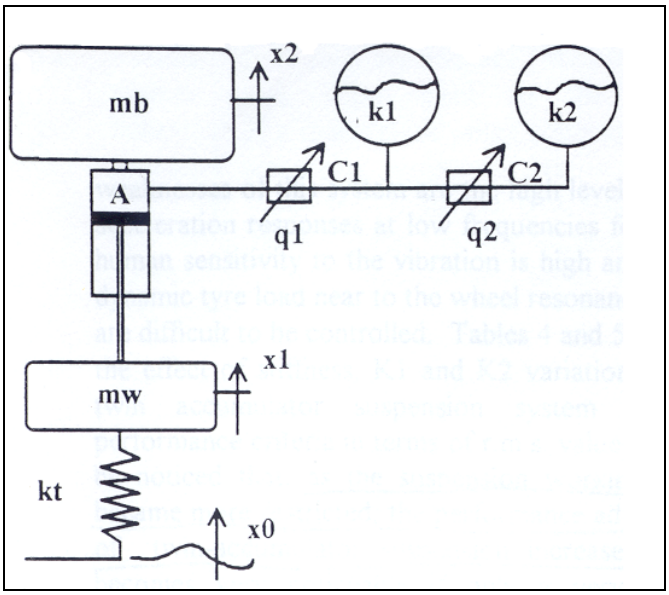


**Figure 2-15: Twin accumulator suspension**

The valves in this case are not switchable and have constant throttle properties. The accumulator parameters and throttle valve values can be chosen to result in an optimised, passive twin-accumulator suspension.

## 2.5 Closing

In closing the following conclusions can be made:

- Hydropneumatic springs are popular due the their non-linear characteristics.
- The semi-active hydro-pneumatic spring of this study was conceptually proposed by Karnopp & Heess (1991).
- No examples of semi-active hydro-pneumatic springs (exactly like to the one discussed in this study) could be found in the literature.
- An ideal gas approach is used by most researchers to model hydro-pneumatic springs.
- For pressures found in practical hydro-pneumatic springs, the ideal gas approach results in significant errors.
- The time constant approach for modelling heat transfer effects in hydro-pneumatic springs is in good agreement with experimental results.
- Parallel and serial accumulator suspension systems have been proposed, but not on the same scale (wheel loads) as in this study.
- Several systems employing controllable dampers have been developed and is currently used in production vehicles.
- The majority of controllable dampers employ fast acting valves, with adaptive control strategies.

**********

# 3 MATHEMATICAL MODELLING

## 3.1 Preamble

In this chapter, the mathematical modelling of the semi-active hydro-pneumatic spring/damper system is discussed. This includes a description of the different mathematical sub-models, as well as the integration of the sub-models. A complete discussion on the correlation between the measured and simulated results is provided in Chapter 5.

A real gas thermal time constant approach is used to model the hydro-pneumatic springs, while incompressible, inviscid flow is used to model the hydraulic pipe flow. A look-up table, with first order delay, is implemented to approximate the semi-active damper. Two variations of the basic mathematical model were constructed. The first model is used for modelling the characterisation process (Refer to Chapter 4 for characterisation detail). For these simulations the strut is subjected to different displacement inputs and valve switching signals. The damper is not included for these simulations, since no damper was present during the characterisation tests.

The second model simulates a single degree of freedom setup. This model includes the strut, as well as the single degree of freedom mass dynamics. Control signals recorded during the tests are used to switch both the spring and damper valves.

An alternative model to the real gas thermal time constant model (which is quite a sophisticated model) is also briefly discussed in this chapter. This model is based on the anelastic model, discussed in Chapter 2 and is less complicated than the real gas model.

The mathematical sub-models will be discussed separately in the following paragraphs.

## 3.2 Mathematical sub-models

### 3.2.1 Hydro-pneumatic spring model

As mentioned previously, a real gas thermal time constant approach is used for modelling the hydro-pneumatic springs. The reason for using a real gas approach is that the pressures and temperatures of the Nitrogen inside the spring are much higher than the critical values (refer to Chapter 2 for a more complete discussion). An ideal gas approach would therefore not be suitable for modelling the spring/damper unit of this study.

The hydro-pneumatic spring model, adapted by Els (1993), from the thermal time constant approach suggested by Pourmovahed and Otis (1990) is applied for the hydro-pneumatic springs. The BWR equation of state (Cooper & Goldfrank 1967) was used to determine the gas pressure.

The way the model approximates the hydro-pneumatic spring characteristics is by solving the gas temperature differential equation, which is a function of gas temperature, ambient temperature, specific volume and time. The model of Els (1993) was re-coded in Matlab/Simulink format and is solved using a fourth order Runge Kutta integration routine (ODE45) in Matlab. Equation 3-1 indicates the temperature differential equation taken from Els (1993).

$$\dot{T}_g = \frac{(T_a - T_g)}{\tau} - \frac{\dot{v}}{C_v}\left[\frac{RT_g}{v}\left(1+\frac{b}{v^2}\right)+\frac{1}{v^2}\left(B_0RT_g+\frac{2C_0}{T_g^2}\right)-\frac{2c}{v^3T_g^2}\left(1+\frac{\gamma}{v^2}\right)e^{-\frac{\gamma}{v^2}}\right] \qquad (3\text{-}1)$$

with

$\dot{T}$ - Change in gas temperature $[K/s]$
$T_a$ - Ambient temperature $[K]$
$T_g$ - Gas temperature $[K]$
$\tau$ - Thermal time constant $[s]$
$C_v$ - Specific heat capacity of the gas $[J/kgK]$
$\dot{v}$ - Change in gas specific volume $[m^3s/kg]$
$R$ - Specific gas constant $[J/kgK]$
$b, B_0, C_0, c, \gamma$ - BWR constants

From the gas temperature the gas pressure is determined, by making use of the Benedict-Webb-Rubin (BWR) equation of state (Cooper & Goldfrank 1967). The BWR equation has previously been shown to give adequate results for hydro-pneumatic spring units of similar volume, pressure and geometry. Equation 3-2 shows the BWR equation of state used to determine the gas pressure.

$$P = \frac{RT_g}{v} + \left(\frac{B_0RT_g - A_0 - C_0/T_g^2}{v^2}\right) + \left(\frac{bRT_g - a}{v^3}\right) + \frac{a\alpha}{v^6} + \left(\frac{c\left(1+\gamma/v^2\right)e^{-\gamma/v^2}}{v^3T_g^2}\right) \qquad (3\text{-}2)$$

with

$T_a$ - Ambient temperature $[K]$
$T_g$ - Gas temperature $[K]$
$\tau$ - Thermal time constant $[s]$
$C_v$ - Specific heat capacity of the gas $[J/kgK]$
$P$ - Gas pressure $[Pa]$
$R$ - Universal gas constant $[J/kgK]$
$V$ - Gas volume $[m^3]$
$v$ - Gas specific volume $[m^3/kg]$
$a, A_0, b, B_0, c, C_0, \alpha, \gamma$ - BWR constants for nitrogen gas

Values for the BWR constants of Nitrogen can be found in Cooper and Goldfrank (1967) and are repeated here in metric units: $a$ = 0.15703387, $A_0$ = 136.0474619, $b$ = 2.96625e-6, $B_0$ = 0.001454417, $c$ = 7.3806143e-5, $C_0$ = 1.0405873e-6, $\alpha$ = 5.7863972e-9, $\gamma$ = 6.7539311e-6

Figure 3-1 displays a schematic representation of the Simulink model of the hydro-pneumatic spring. From this figure it can be seen that the hydro-pneumatic spring model requires one input variable, namely floating piston displacement, while the gas temperature and pressure are the two main outputs of this block.

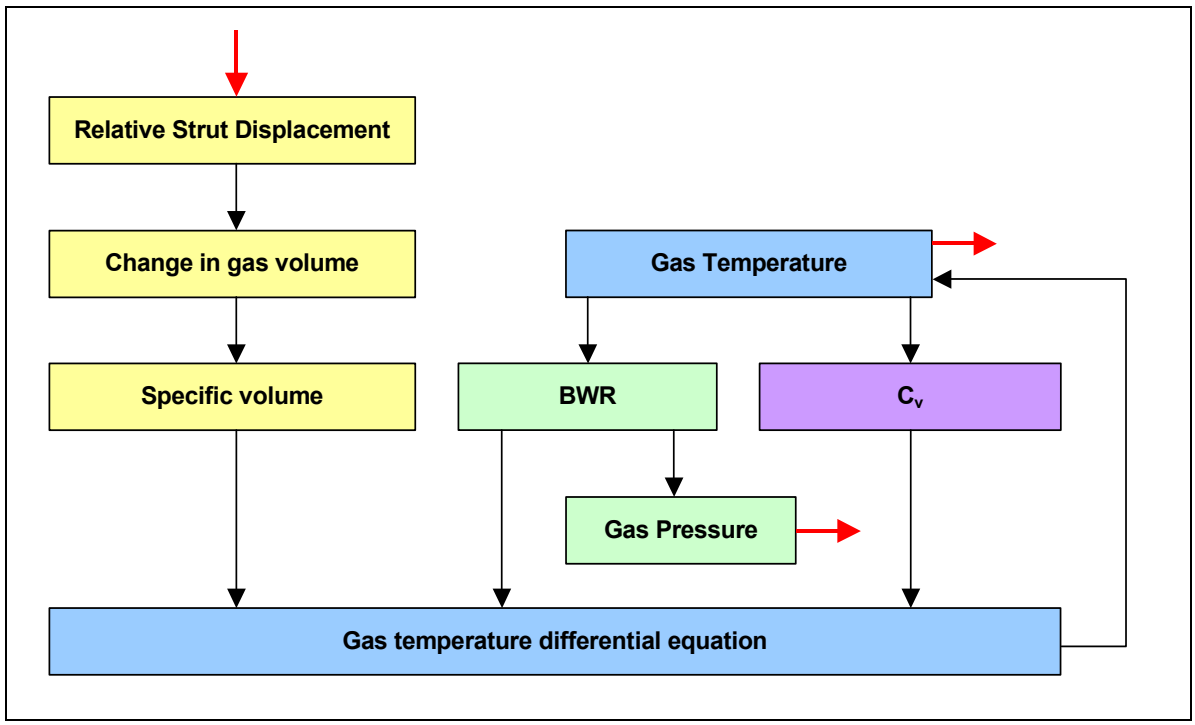


**Figure 3-1: Simulink model of the hydro-pneumatic spring**

From Figure 3-1, it can be seen that the specific heat capacity is calculated at each time step, as a function of gas temperature. The following equation is used to determine the ideal gas specific heat capacity (Els 1993):

$$C_v^0 = R\left(\frac{N_1}{T_g^3} + \frac{N_2}{T_g^2} + \frac{N_3}{T_g} + (N_4 - 1) + N_5 T_g + N_6 T_g^2 + N_7 T_g^3 + \frac{N_8 y^2 e^y}{(e^y - 1)^2}\right) \quad (3\text{-}3)$$

with

$C_v^0$ - Ideal gas specific heat capacity $[J/kgK]$
$R$ - Universal gas constant $[J/kgK]$
$T_g$ - Gas temperature $[K]$
$y = \frac{N_9}{T_g}$
$N_1 - N_9$ - Constants (Els 1993)

In the model of Els (1993) the ideal gas specific heat capacity is corrected (for pressure) to obtain the real gas specific heat capacity. It was however found that the ideal gas and real gas specific heat capacities differ by less than 0.0001% for the typical pressures and temperatures encountered in this study. The correction of the ideal gas specific heat capacity was therefore neglected.

A complete breakdown of the hydro-pneumatic spring model is provided in Appendix B.

### 3.2.2 Hydraulic damper model

The hydraulic damper was only present for the SDOF simulations and not for the characterisation simulations. Since the damper consists of a discrete two-state damper, it was decided to make use of a look-up table, where the damper characteristic can be found by interpolating on one of two graphs. The valve response of the damper valve, as well as the spring valve was modelled as a first order delay, based on measured valve response times. The valve models are discussed in paragraphs 3.2.4 and 3.2.5.

The damper characteristics used for the simulations were determined experimentally, as described in Chapter 4. Figure 3-2 shows the "on" and "off" damper characteristics.

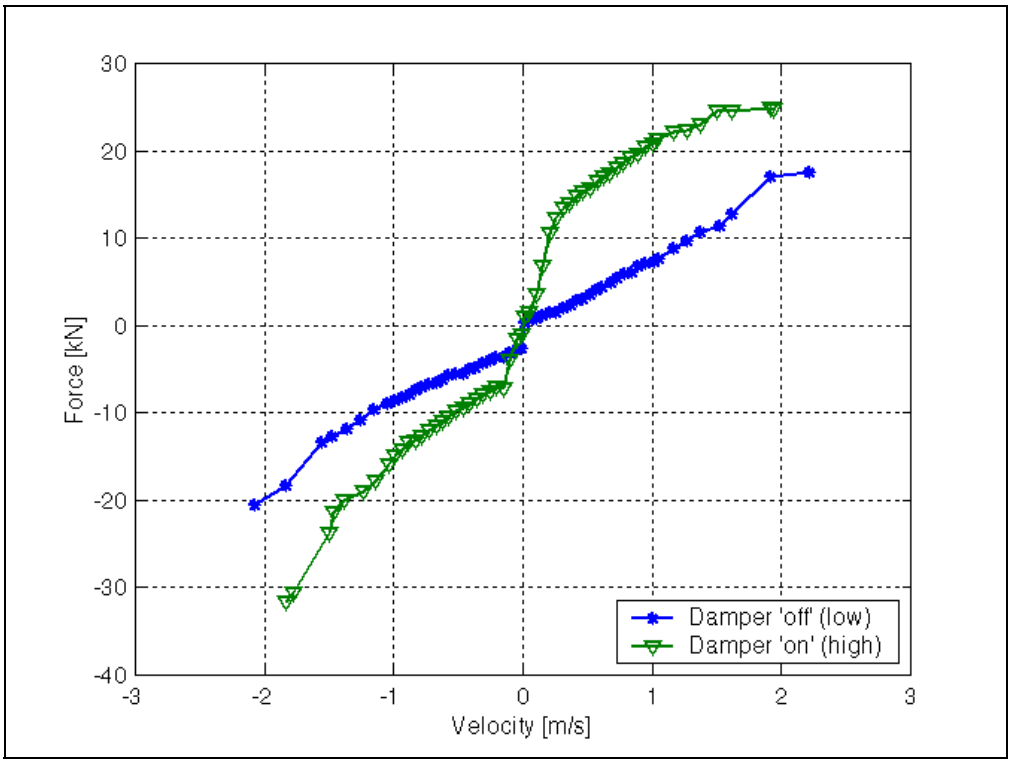


**Figure 3-2: Semi-active damper characteristic**

A 2D linear interpolation scheme was used to determine the damper force, dependant on the state of the semi-active damper valve, i.e. "on" or "off". Figure 3-3 indicates the Simulink model incorporating the damper look-up for the "on" and "off" states, as well as the damper switching signal input.

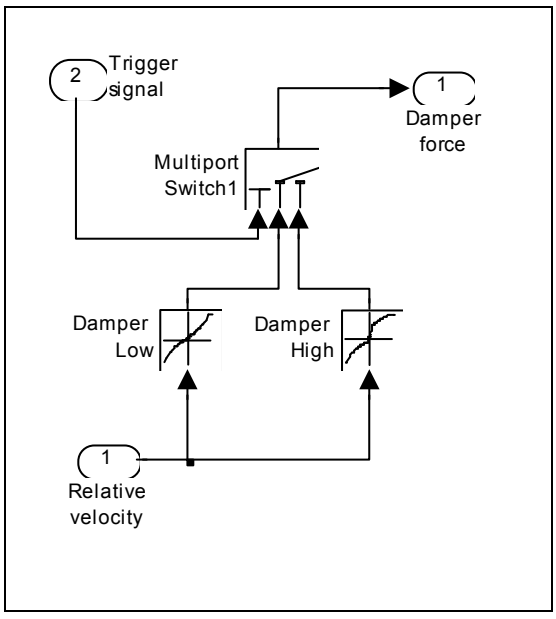


**Figure 3-3: Damper model**

From this figure it can be seen that both the high and low damper force are calculated continuously, but that only one of these signals are connected to the damper force output signal line at any time. More detail about the damper valve model can be found in paragraph 3.2.4.

### 3.2.3 Hydraulic flow model

The hydraulic flow was modelled as incompressible, inviscid flow. The elemental equations are derived from first principles and represent the system without the semi-active damper. A complete derivation of the hydraulic flow model is presented in Appendix C. Figure 3-4 shows the Simulink model of the hydraulic flow. The elements of the flow model are shown in blue, while the spring models are orange.

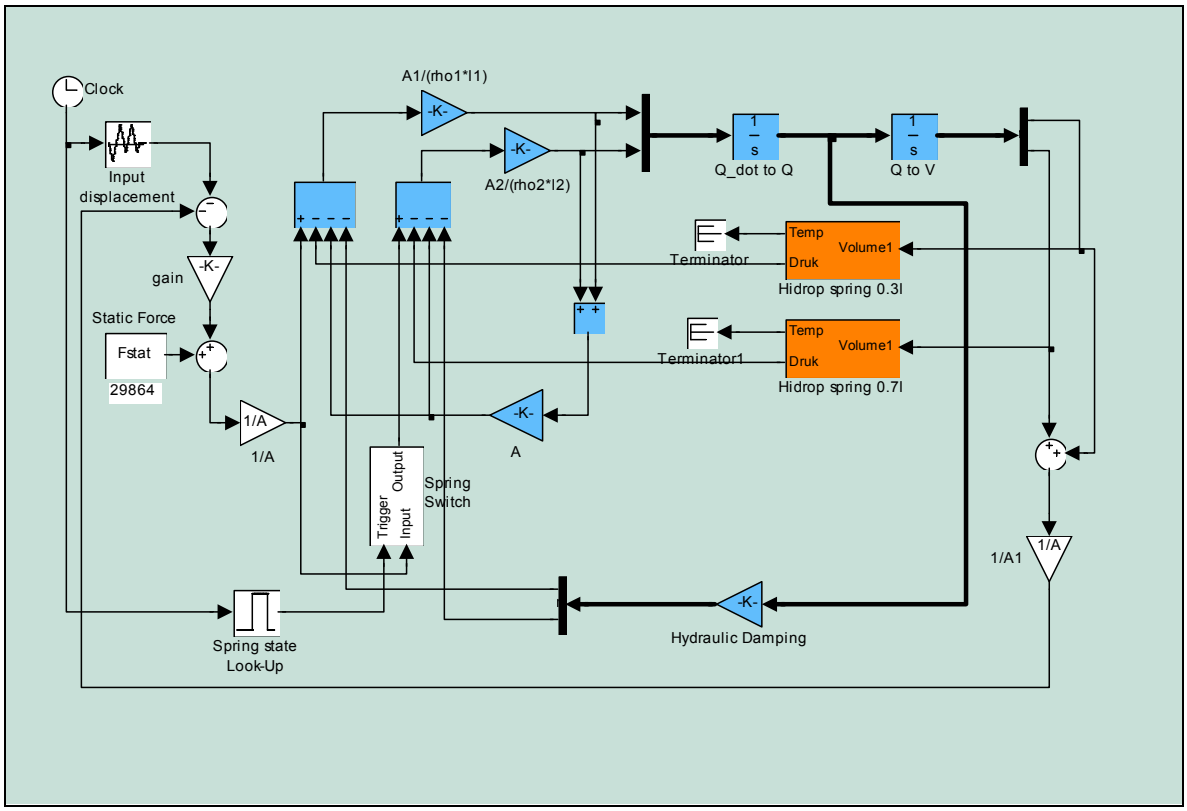


**Figure 3-4: Hydraulic flow model in Simulink**

From this figure it can be seen that a displacement feedback loop is used to control the input to the parallel hydro-pneumatic springs. This Simulink model determines the change in flow rate to each of the accumulators, which is then integrated twice to obtain the volume. The volumes are fed to the two spring models from which the pressure inside the two accumulators are calculated. Accumulator pressures are then fed back to the summer blocks in order to calculated the new change in flow rate based on the current accumulator pressure and the input signal (pressure).

Also visible in the Simulink model is a gain block called damping. This block was added in order to eliminate resonance between the two accumulators. In practice there are flow losses in the pipes that will damp out the flow exchange between the two accumulators. A constant value was assumed for the damping and was coupled to the flow rate, as is flow losses. The magnitude of the damping constant was determined through trial and error to eliminate high frequency pressure resonance.

### 3.2.4 Damper valve model

As mentioned previously, the damper valve model is based on a first order delay of the switching signal. The relative strut velocity determines the magnitude of the delay. The delay is calculated by evaluating a polynomial function representing the valve response time as a function of relative velocity. The coefficients of the polynomial function were determined by fitting a parabola to measured damper valve response times. Figure 3-5 shows the measured valve response times and the parabolic fit used in the Simulink model. A definition of valve response time can be found in paragraph 4.5.4 of Chapter 4.

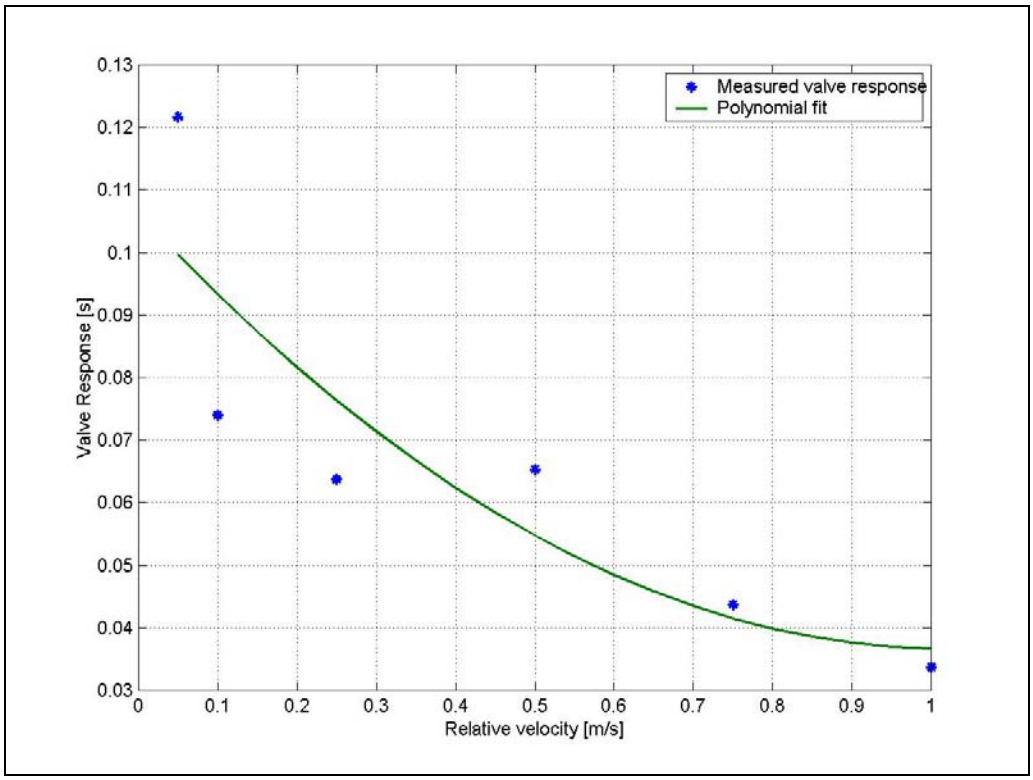


**Figure 3-5: Polynomial fit to measured damper valve response data**

Figure 3-6 indicates how this model is implemented in Simulink.

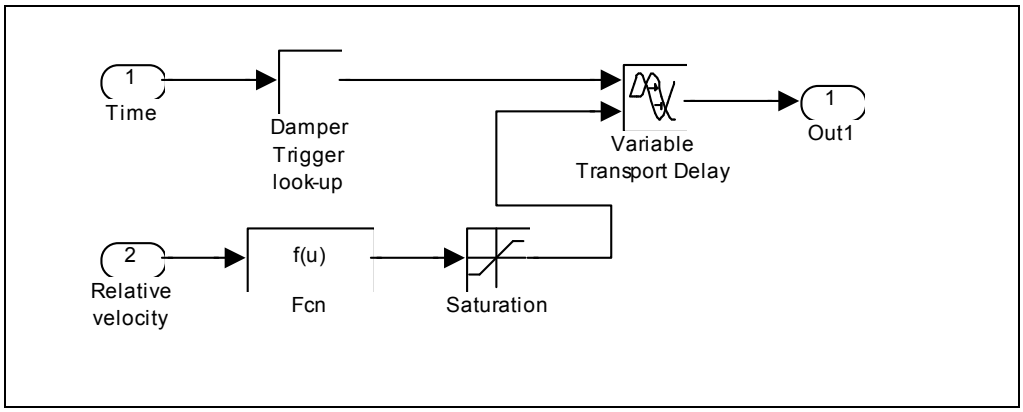


**Figure 3-6: Damper valve model**

In this figure the look-up table for determining the damper state, the function for calculating the response time, a saturation block and a variable transport delay block can be seen. The purpose of the saturation block is to ensure that only realistic delay values are passed to the variable transport delay block.

### 3.2.5 Spring valve model

The spring valve model not only incorporates the valve response of the spring valve, but also forms an integral part of the dual spring model. Since the flow rate and volume of each spring is fed back to the model, the flow rate to the isolated accumulator has to be zero. The accumulator volume therefore has to remain constant when the accumulator is disconnected from the hydraulic system. This was achieved by including a spring valve switching module displayed in Figure 3-7. From this figure it can be seen that when the valve is “open” or “off”, the input is directly connected to the output. When the valve is “closed” or “on” the last input value is maintained at the output. The spring valve switch therefore maintains a constant pressure inside the accumulator that is isolated from the rest of the hydraulic circuit.

The spring valve response was incorporated in the same way as the damper valve response. In the case of the spring valve a linear curve is fitted to the measured response data, as can be seen in Figure 3-8. The valve response of the spring valve is supplied as response time versus force difference. The force difference can also be interpreted as a pressure difference in the two accumulators. When the valve is open, the pressure difference is small and the delay is a maximum (approximately 130$ms$).

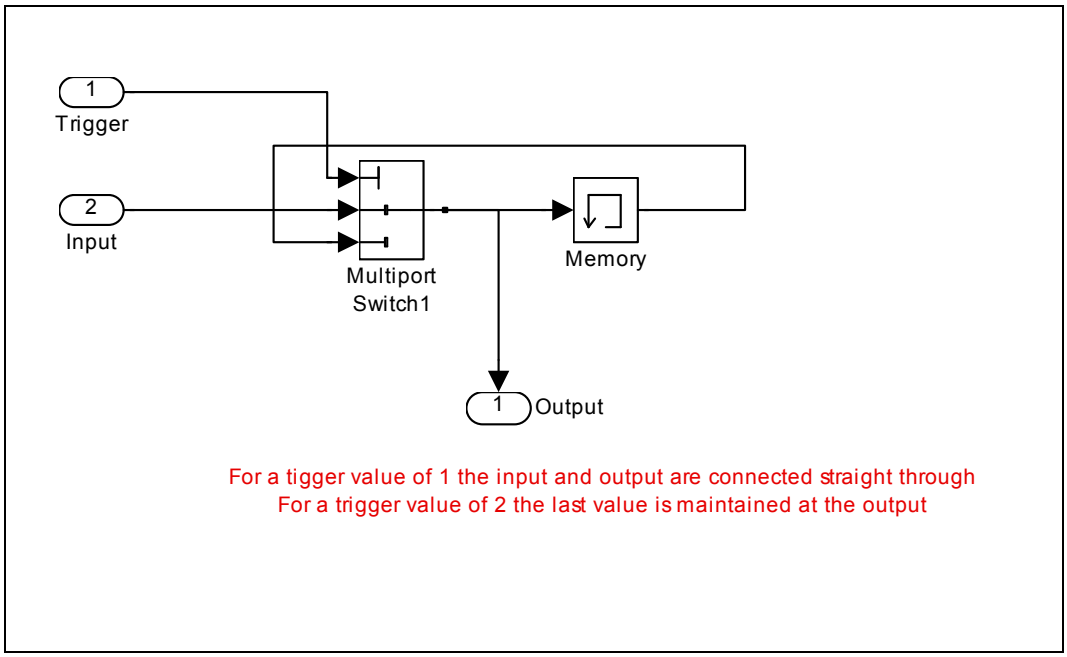


**Figure 3-7: Spring valve switching module**

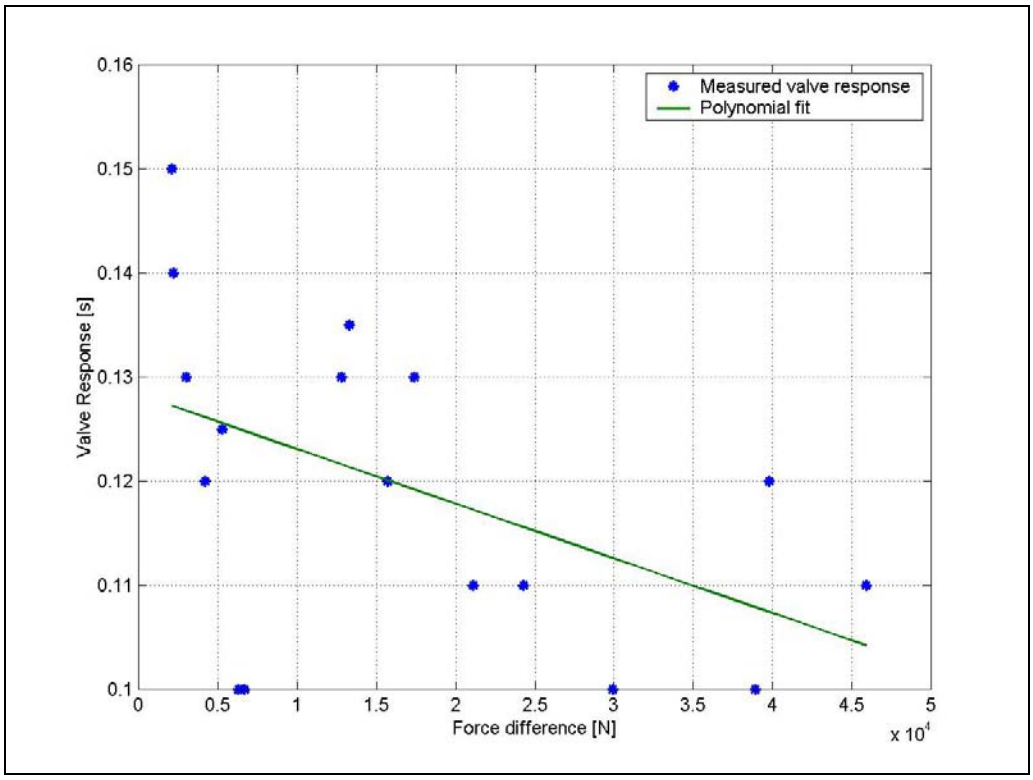


**Figure 3-8: Linear fit to measured spring valve response data**

Figure 3-9 indicates the spring valve model. From this figure, it can be seen that a look-up table is used to determine the required spring state from the recorded data and that the pressure difference is used to calculate the delay time. The absolute value of the pressure difference is used to eliminate negative response times. The pressure difference is converted to a force

difference. The force difference is then used to determine the valve response time from the linear fit to measured data. A saturation block is included to ensure that realistic valve response times are always fed to the variable transport delay block.

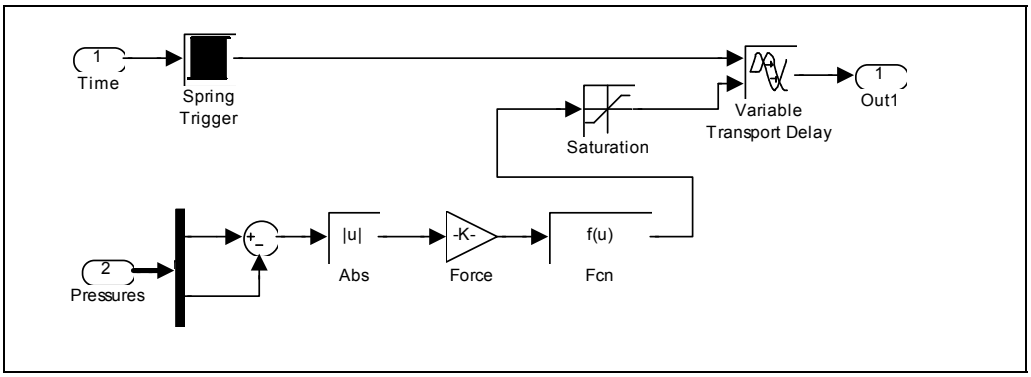


**Figure 3-9: Spring valve model**

In both the damper and spring valve models, the response delay value is multiplied by 0,5. The reason for this is that the valve response time is defined as the time for the force to rise from 5% to 95% of its final value. The delay therefore has to be only half of this value, since the valve is switched half way between the initial and final time. Figure 3-10 indicates that in practice the valve does not switch immediately, but that the valve was modelled as switching instantaneously, halfway between the start and end time.

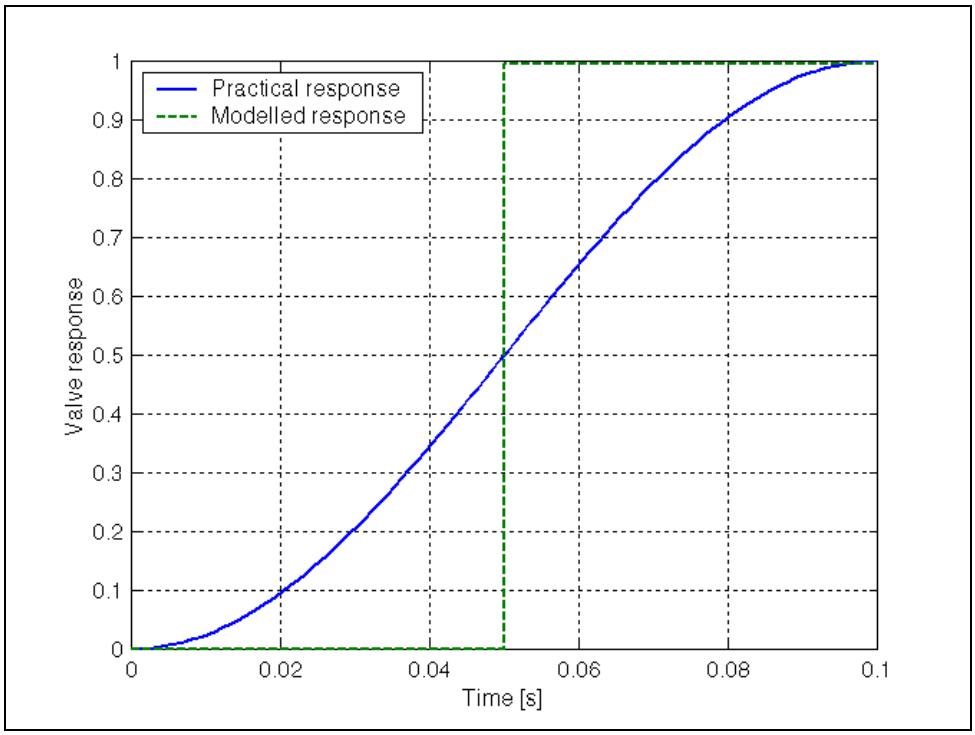


**Figure 3-10: Modelling the response delay**

## 3.3 Sub-model integration

The various mathematical sub-models were integrated into a single Matlab/Simulink model. Figure 3-11 shows the complete Simulink model used for the SDOF simulations. From this figure, it can be seen that the mathematical sub-models were included as sub-systems in the Simulink model in order to reduce the complexity of the main model.

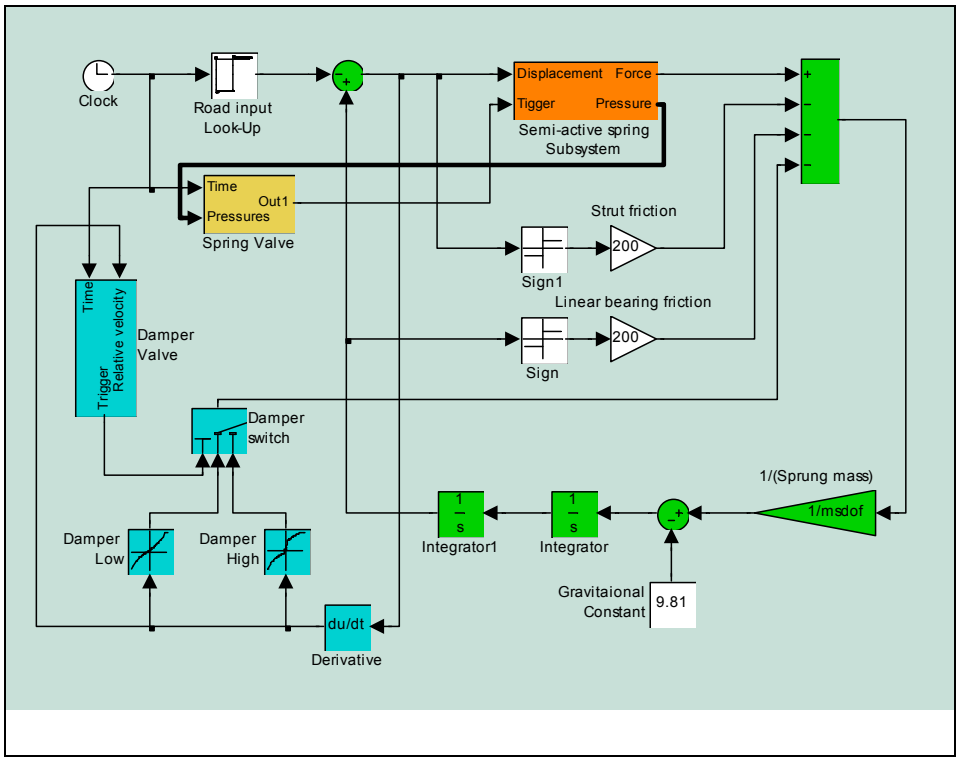


**Figure 3-11: SDOF Simulink model**

The main SDOF model therefore contains the semi-active damper and valve model (Cyan), the semi-active spring valve model (Yellow), the two spring models contained in the semi-active spring sub-system (Orange), as well as the SDOF sprung mass differential equation (Green). Friction in the linear bearings for the sprung mass, as well as in the strut is also included in the model. The friction was modelled as dry friction with a peak value of 200N. This value was determined through trial and error. The input to this model is the road displacement and the valve switching signals.

## 3.4 Alternative mathematical model

For basic 2D and 3D vehicle dynamics simulations, a complex mathematical model such as the real gas thermal time constant model discussed in the preceding paragraphs might contain too much detail. A basic anelastic model is therefore included in this chapter as an alternative to the

more complex model. Figure 3-12 shows a schematic representation of the anleastic model. From this figure, it can be seen that the anelastic model consists of a spring in parallel with a spring and damper, which is in series. Through inspection it is possible to see that the basic spring stiffness is supplied by spring k2, while the hysteresis loop will be produced by the series spring and damper combination.

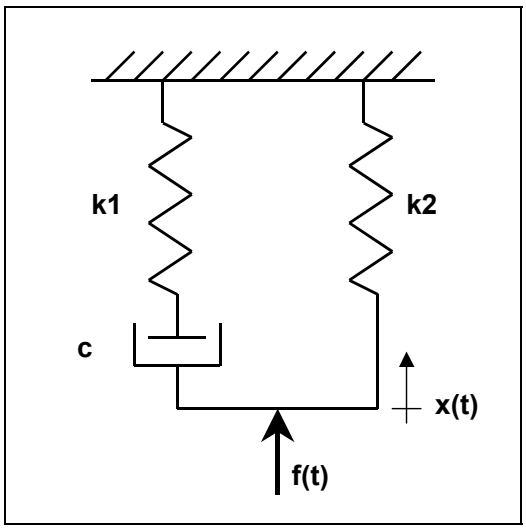


**Figure 3-12: Anelastic model for modelling heat transfer in accumulators**

Although linear spring and damper characteristics in this model also produce a hysteresis loop, the characteristics are not progressive, as with a hydro-pneumatic spring. It was therefore decided to use a polytropic process to model the main spring. Since the volume and pressure of the accumulators are known, the one unknown parameter (for the main spring) is the polytropic constant. In order not to over complicate the model, linear characteristics were assumed for the series elements. Equation 3-4 shows the formula used to calculate the spring force ($F$) as a function of displacement ($x$).

$$F = \frac{kA}{(xA)^n} \tag{3-4}$$

with

$F$ - Spring force [$N$]

$k$ - Constant (function of static volume and pressure)

$A$ - Accumulator floating piston area [$m^2$]

$x$ - Floating piston displacement [$m$]

n - Polytropic exponent

During the process of determining the values of k1 and c, it was found that for the accumulators used in this study, with a thermal time constant of approximately 6*s*, the thermal damping is negligible for frequencies of interest in vehicle dynamics studies. The polytropic constant is however a function of excitation frequency and amplitude, therefore the characterisation real gas model discussed in paragraph 3.2.1 was used to determine the polytropic exponents. Figure 3-13 shows a graph in linear and log scale of the polytropic exponent determined in this way. For this "characterisation", the values for k1 and c were kept constant at 3e3*N/m* and 2.5e3*Ns/m*, however it should be possible to neglect the series spring and damper altogether, since there is very little thermal damping present at the frequencies indicated in Figure 3-13.

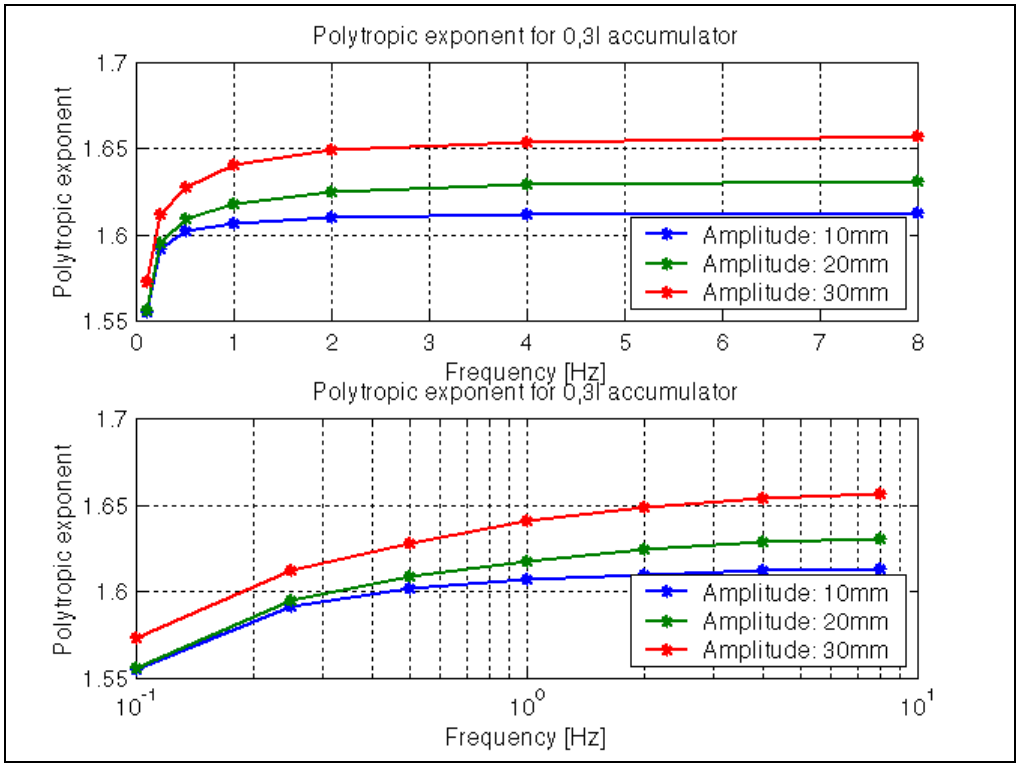


**Figure 3-13: Polytropic exponent as a function of excitation frequency and amplitude**

Table 3-1 contains several figures, which compares the force vs. displacement characteristic of the real gas thermal time constant and anelastic model. Three excitation frequencies, namely 0.25Hz, 1.0Hz and 4.0Hz are shown for excitation amplitudes of 10mm, 20mm and 30mm. From this table, it can be seen that the hysteresis loop is only really visible for an excitation frequency of 0.25Hz, which is below any rigid body or wheel hop natural frequencies found on wheeled vehicles. It is therefore valid to disregard thermal damping when modelling the hydro-pneumatic spring.

**Table 3-1: Comparison between Real gas and Anelastic model**

| | 10mm | 20mm | 30mm |
|---|---|---|---|
| **0.25*Hz*** | 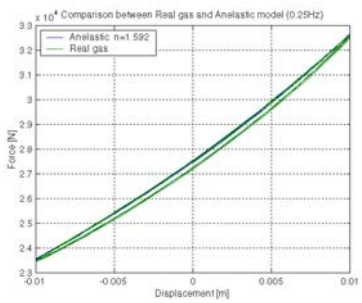 | 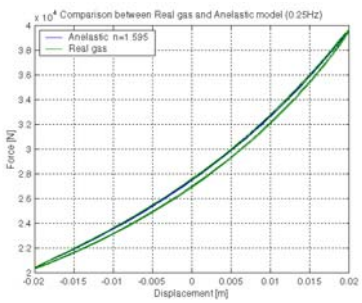 | 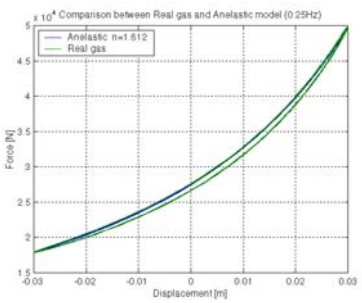 |
| **1.0*Hz*** | 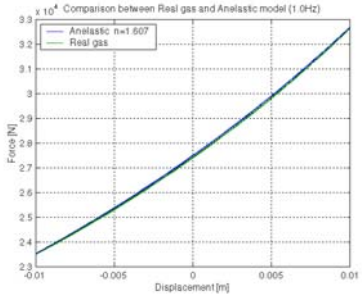 | 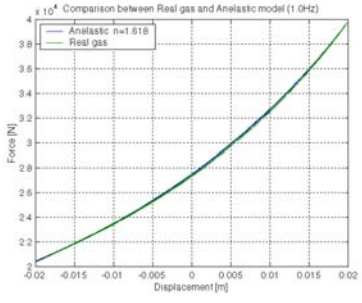 | 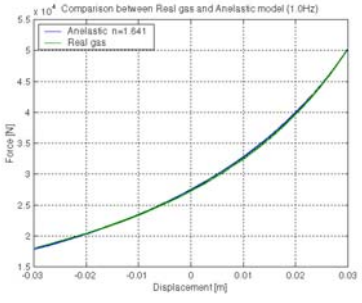 |
| **4.0*Hz*** | 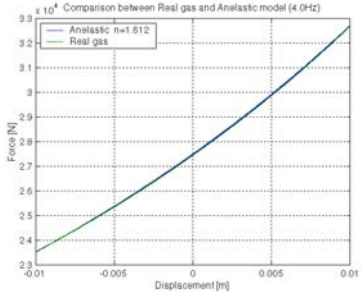 | 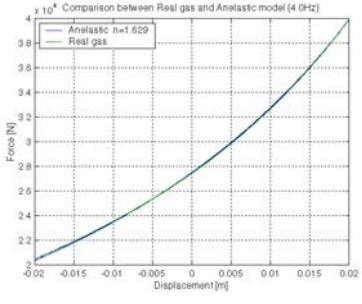 | 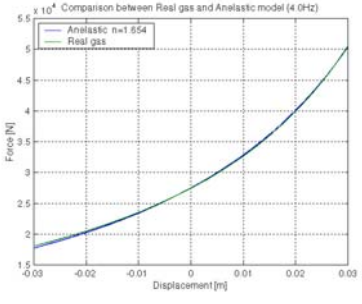 |

Although the Anelastic model was not evaluated in the semi-active spring, it should be quite easy to generate a semi-active spring model based on a mechanical model using force balance. Figure 3-14 shows a schematic layout of such a configuration. The displacement of spring k1 can be selectively held fixed, making it the accumulator that is being closed of by the valve, while the beam ensures that equal force (pressure) is exerted by both springs. It is recommended that the semi-active anelastic model be further investigated and thoroughly correlated with measured data.

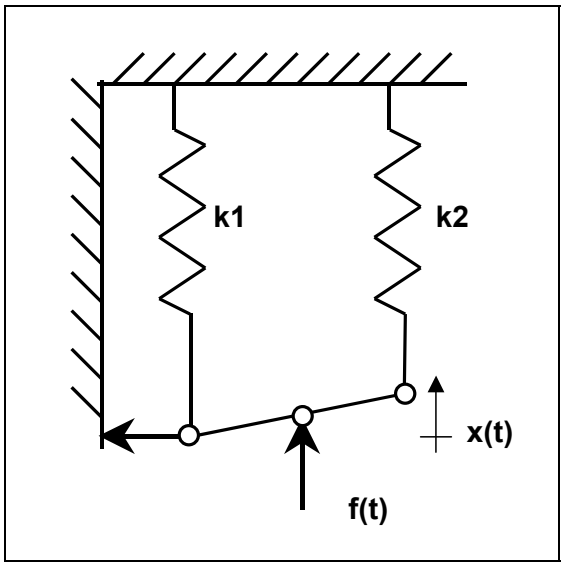


**Figure 3-14: Semi-active anelastic spring model**

## 3.5 Simulations

As mentioned previously, all the simulations were performed using Matlab/Simulink. The ODE45 (Fourth order Runge-Kutta) numerical integration algorithm was used for all simulations and an error tolerance of $1e^{-6}$ was prescribed. A 333*MHz* Pentium II computer with 64*Mb* RAM was used to solve the mathematical models. The CPU times for the full SDOF model were between 5 and 10 minutes for approximately 10s of real time input. The anelastic model runs in a matter of seconds for a simulation time of 100*s*.

## 3.6 Closing

Sub-systems such as the damper, spring, valve etc. are modelled as separate sub-systems and then combined to form the main model. This approach reduces the main model complexity and simplifies the debugging process. The models consist of previously developed models (hydro-

pneumatic spring), look-up tables (damper), empirical models (valve models) and models derived from first principles (hydraulic flow models).

**********

# 4 EXPERIMENTAL WORK

## 4.1 Preamble

In this chapter, the experimental work is presented. The experimental work can be divided into two stages, namely characterisation tests and single degree of freedom tests. The test setup, test equipment and characterisation procedures for both these stages are discussed in this chapter. Where deemed necessary, some background information is supplied, in order to elucidate the characterisation process. The test results are presented in graphical and tabular format.

In the following paragraphs, firstly the test setup is discussed, with reference to the hardware, software and test equipment. Secondly, the characterisation of the spring, damper and valves are discussed. After that, the single degree of freedom tests are discussed and finally some closing remarks are made. All the test results are supplied in Appendix D.

## 4.2 Test setup

### 4.2.1 Experimental setup

Two experimental setups were used, one for the component characterisations (springs, damper and valves) and another one for the single degree of freedom tests. In both cases, a 160*kN* Schenck hydraulic actuator was used to supply the desired input. Figure 4-1 shows schematically the characterisation test setup.

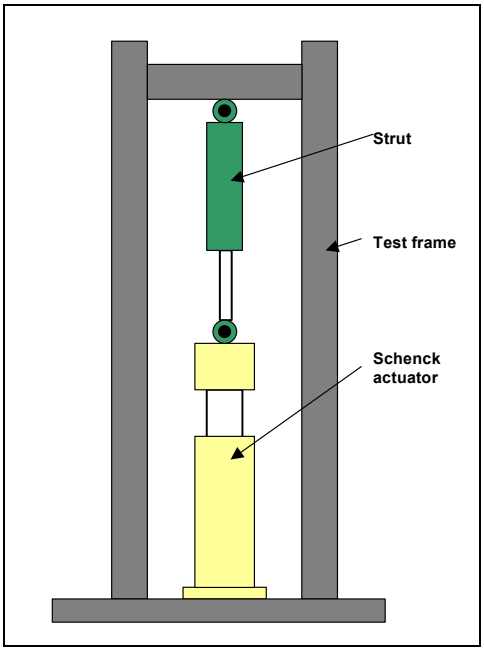


**Figure 4-1: Characterisation test setup**

The top of the strut was fixed to the rigid test frame with a locating pin, while the bottom mounting was fixed to the hydraulic actuator. Spherical rod ends were used, in order to eliminate any bending moments on the strut. In this setup, the required relative strut displacement is generated by vertical actuator motion.

For the single degree of freedom tests, a separate test frame was build. Figure 4-2 shows a photograph of the single degree of freedom test setup.

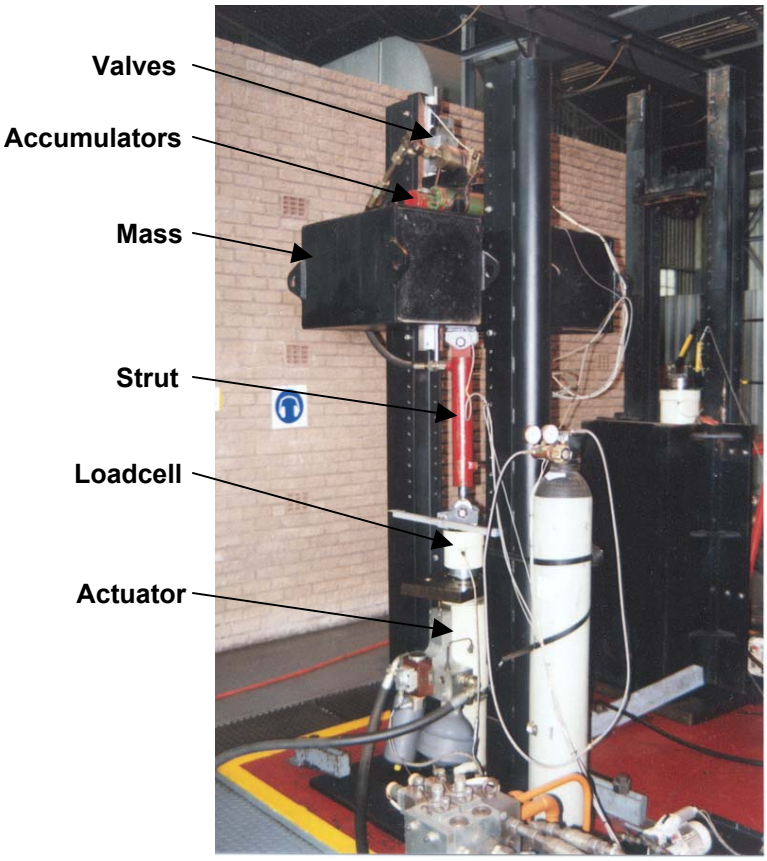


**Figure 4-2: Single degree of freedom test setup**

A lead mass of approximately 3 tons was used to simulate the sprung mass of a vehicle, since a static wheel load of between 2,5 tons and 3 tons are common for military off-road vehicles. The test frame was equipped with a set of linear bearings, guiding the sprung mass, which was supported by the lower mounting on the Schenck actuator. Also visible in the photograph is the nitrogen cylinder used to fill the accumulators. The accumulators, damper and valves were secured on top of the lead mass (see Figure 4-3). The test frame was securely fixed to the test floor, to ensure that the SDOF setup does not fall over.

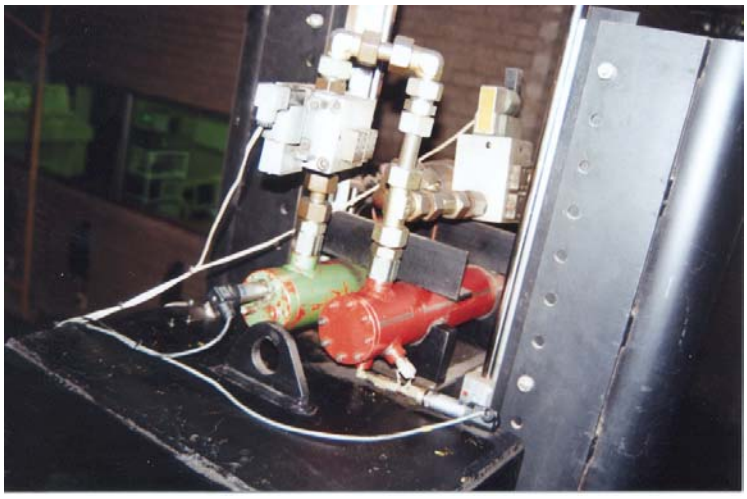

**Figure 4-3: Accumulators, damper and valves secured on top of sprung mass**

### 4.2.2 Instrumentation, control and data acquisition

The Schenck actuator has a PID controller, which controls the actuator to follow a desired input signal. A built in Schenck signal generator can be used to supply sinusoidal, square and triangular signals. A sinusoidal input signal was use to characterise the spring and the damper. An external control signal can also be supplied to the Schenck controller. This feature was used to determine the valve response times, where it was necessary to construct a custom displacement signal, which is synchronised with the valve switching signal. A 486 personal computer with a Burr-Brown D/A card was used to supply the desired input signal.

A separate 486 personal computer with a Burr-Brown A/D card was used to record the signals from the test equipment. Table 4-1 indicates the parameters, as well as the measuring equipment.

**Table 4-1: Test equipment (component characterisation)**

| No. | Parameter | Instrument |
|---|---|---|
| 1 | Actuator displacement | Schenck PFM LVDT |
| 2 | Actuator force | Schenck 160kN PM-Rn loadcell |
| 3 | Pressure in 0,3*l* accumulator (see Figure 4-5) | Wika 40*MPa* pressure sensor |
| 4 | Pressure in 0,7*l* accumulator (see Figure 4-5) | Wika 40*MPa* pressure sensor |

For the single degree of freedom tests, some additional parameters were measured. Table 4-2 supplies a list of parameters and measuring equipment used for the single degree of freedom tests.

**Table 4-2: Test equipment (single degree of freedom tests)**

| No. | Parameter | Instrument |
|---|---|---|
| 1 | Actuator displacement | Schenck PFM LVDT |
| 2 | Actuator force | Schenck 160*kN* PM-Rn loadcell |
| 3 | Relative displacement (see Figure 4-4) | Penny & Giles linear potentiometer |
| 4 | Sprung mass acceleration | VTI Hamlin A050AA 5*g* accelerometer |
| 5 | Pressure in 0,3*l* accumulator (see Figure 4-5) | Wika 40*MPa* pressure sensor |
| 6 | Pressure in 0,7*l* accumulator (see Figure 4-5) | Wika 40*MPa* pressure sensor |

**Figure 4-4: Linear potentiometer measuring relative strut displacement**

**Figure 4-5: 40*MPa* pressure sensor measuring accumulator pressure**

## 4.3 Hydro-pneumatic spring characterisation

In this section the characteristics of the semi-active hydro-pneumatic spring is discussed. The physical attributes and characterisation procedures are also outlined.

### 4.3.1 Physical attributes

There are many different types of hydro-pneumatic springs, but the basic difference lies in the way the gas and the oil is separated. Some hydro-pneumatic springs have a rubber bladder separating the gas and the working fluid, while others have a floating piston. Both the hydro-

pneumatic springs considered in this study are of the floating piston type. Figure 4-6 shows a schematic drawing of the floating piston accumulator.

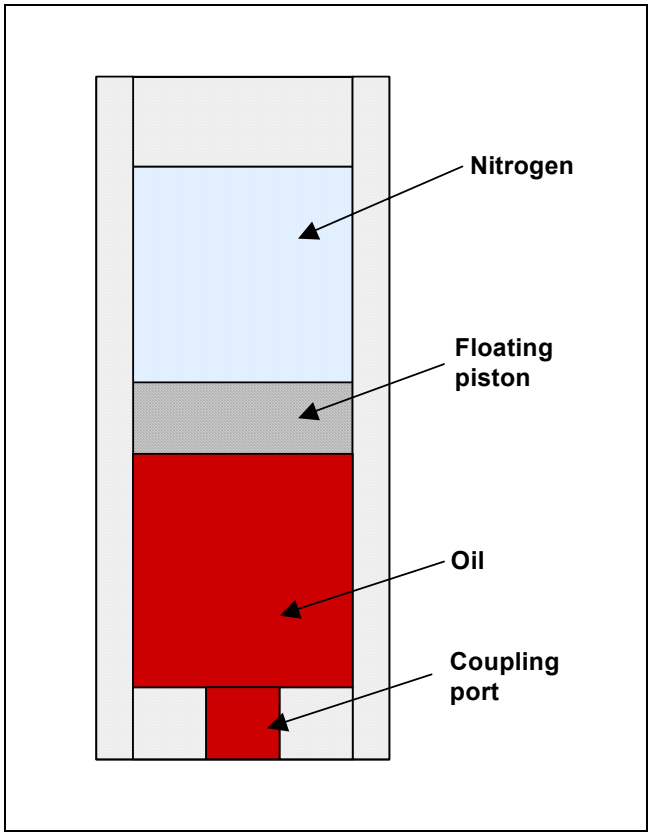


**Figure 4-6: Floating piston hydraulic accumulator**

The static volumes of the two accumulators are 0,3*l* and 0,7*l* respectively. When the valve is open the combined volume of the two accumulators is 1,0*l* and when the valve is closed only the 0,3*l* accumulator is connected with the single acting cylinder.

Nitrogen gas was chosen as springing medium. The reasons for using Nitrogen are:

- Nitrogen is widely used in accumulators and hydro-pneumatic springs.
- Properties of Nitrogen are well documented.
- Nitrogen is an inert gas.

### 4.3.2 Characterisation procedure

For the hydro-pneumatic spring characterisation the first experimental setup described in paragraph 4.2.1 was used. The two stages of the semi-active hydro-pneumatic spring were characterised by subjecting the strut to a sinusoidal displacement, of varying frequency. The

excitation speed is defined as the piston speed when moving through the static position. The excitation speed is therefor a function of the excitation frequency and the excitation amplitude. The amplitude of the signal was approximately 100*mm*. Figure 4-7 indicates the two spring characteristics for an excitation speed of 0.01*m/s*. From this figure, it can be seen that two very different spring characteristics were achieved.

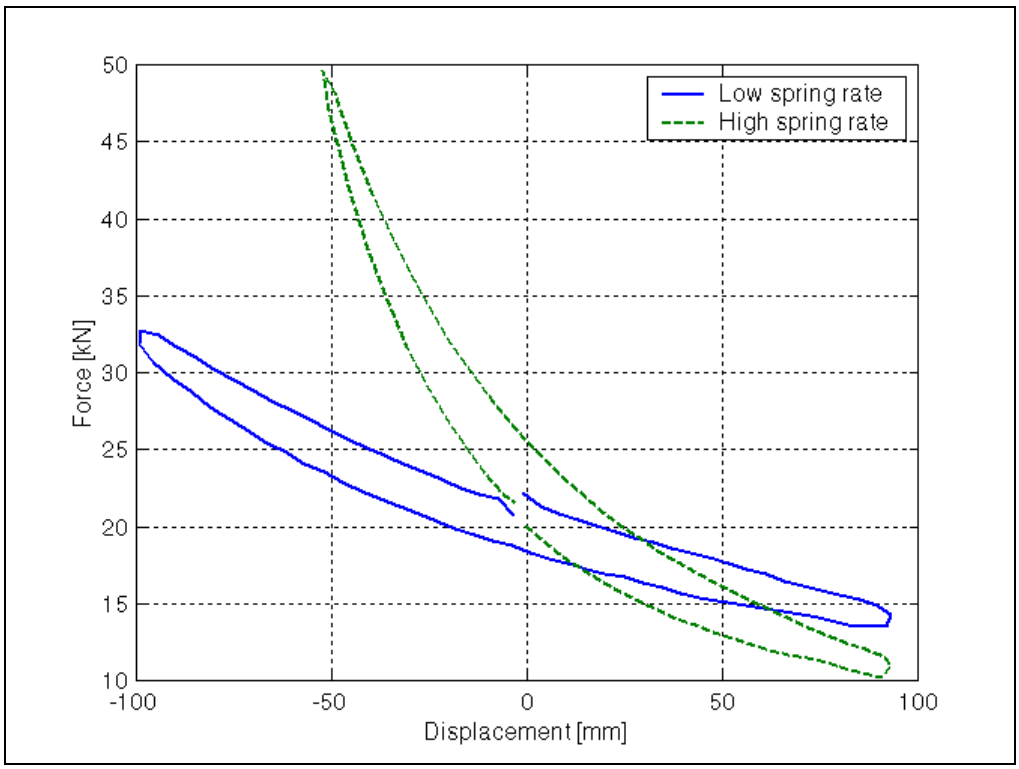


**Figure 4-7: Semi-active spring characteristics (0.01*m/s*)**

## 4.4 Hydraulic damper characterisation

In this paragraph, the methodology for determining the damping force versus velocity relationship of the semi-active damper is discussed. A description of the hardware, as well as the characterisation procedure is supplied.

### 4.4.1 Physical attributes

As explained previously, the low damper state is achieved by short circuiting the damper with a bypass valve. The characteristics of the valve will be discussed in more detail in paragraph 4.5. The damper pack used in the semi-active damper assembly is the same as found in a Ratel damper. No modifications were made to the damper characteristics and the damper pack was

built into a custom made damper housing. The Ratel damper has non-linear damping characteristic, which is achieved by a system of orifices, sealing washers and Belville springs.

Unlike a conventional translational damper, which acts directly on relative suspension motion, this damper was mounted statically between the strut and the hydro-pneumatic springs (see Figure 1-10 in Chapter 1). The damping force is therefor supplied by resistance to fluid flow through the damper pack.

### 4.4.2 Characterisation procedure

The damper characteristics of the two-state damper were determined by subjecting the strut to a sinusoidal displacement input. The actuator force was recorded when the strut travels through the static position, where the velocity is almost constant and a maximum. In order to determine only the damper force, the spring force was subtracted form the total force (actuator force). The spring force was calculated from the accumulator pressure and the cylinder area. From these measurements, the force versus velocity relationship of the damper could be determined.

Figure 4-8 shows the measured damper characteristics for both the “on” and “off” states. From this figure it can be seen that the “off” characteristic for velocities above $0.25 m/s$ is approximately half that of the “on” state, in the compression direction (negative velocity). It can also be seen that the damper force, in the rebound direction, shows an almost constant damping force at high velocities. This is because during rebound motion the driving force behind the hydraulic fluid is the accumulator pressure and in the compression direction, the single acting strut cylinder. Rebound damping can therefore not be made too high, since cavitation may occur at high velocities.

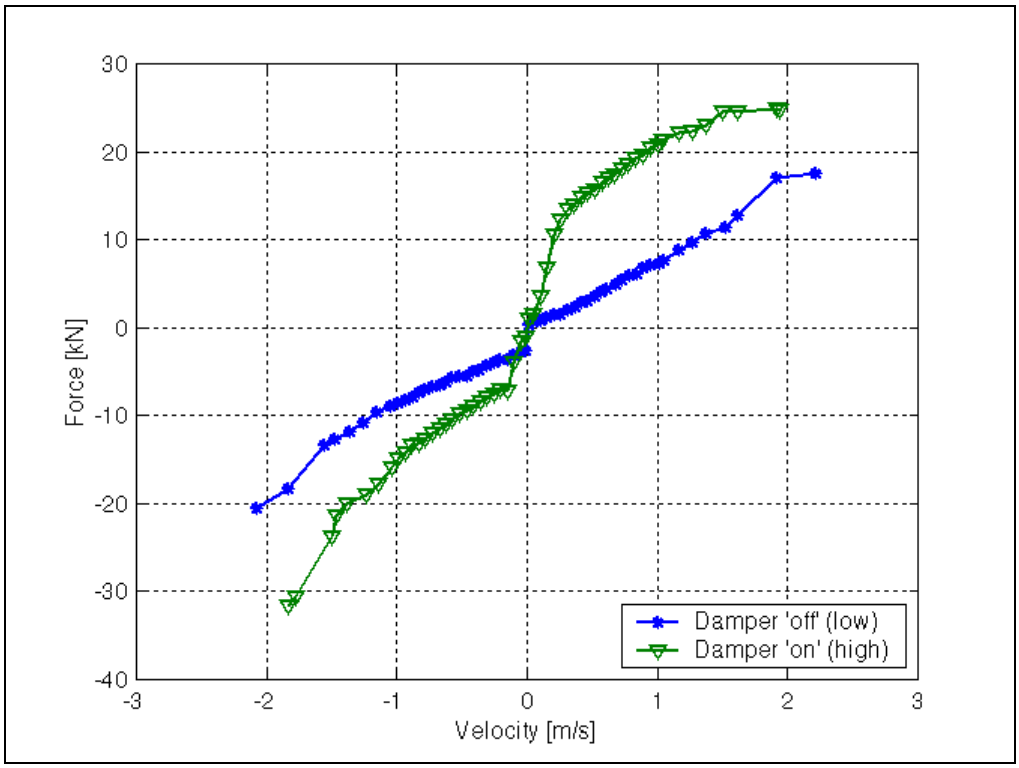


**Figure 4-8: Two stage damper characteristics**

## 4.5 Hydraulic valve

In this section, the type of hydraulic valve used in the experimental spring/damper unit is discussed. The working principle, characterisation procedure and response times are supplied in the following paragraphs.

### 4.5.1 Valve type and working principle

Regular solenoid valves are limited by the amount of flow they can handle. Semi-active dampers for large off-road vehicles have very large flow requirements, because of the large size of the dampers. In order to accommodate the high flow rates (up to 1000*l/min*), a logic element type valve was used.

According to DIN24342 the correct name for this type of valve is a "2-Way Cartridge Valve", but for simplicity the valve will be referred to as a hydraulic valve. The basic element is a 2/2 way valve i.e. a valve with 2 service ports and 2 operating positions, namely "open" and "closed". The logic element status is determined by the force balance on the valve poppet. From Figure 4-9, it can be seen that the pressure from the two service ports A & B, the control port X and the closing spring (3) acts on the valve poppet (2).

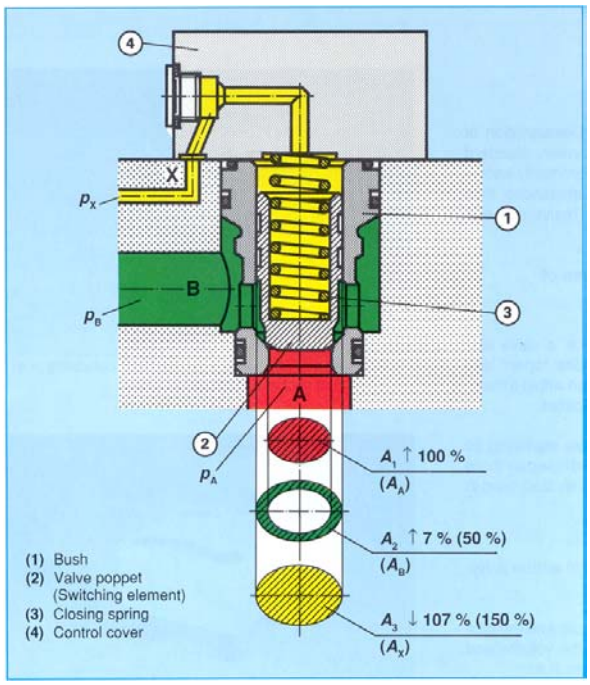


**Figure 4-9: 2-Way Cartridge Valve sectional drawing**

The control port pressure is switched by a Mannesman Rexroth WSE3, 3-way solenoid spool valve. The solenoid valve connects either a high- or a low-pressure line, supplied by an arrangement of one-way valves, to the control port. The control pressure determines the direction of the resultant force on the valve poppet, causing it to either open or close.

### 4.5.2 Valve response times

Valve response times were determined by subjecting the strut to a triangular displacement input resulting in constant velocity regions between turning points. The valves were then switched on and off in both the compression and rebound directions at different speeds. Valve response time is defined as the difference between the trigger signal and the time at which the force reaches 95% of its final value. This includes the initial delay and the rise time of the hydraulic valve, as described in by Nell (1993).

As was mentioned in paragraph 4.5.1, the valve state is dependant on the pressure balance on the valve poppet and therefore the valve switching times are a function of the pressure difference between the two service ports.

Figure 4-10 indicates the response times of the semi-active spring valve, as a function of force difference. The force difference is based on the pressure difference over the valve. The valve response times for the semi-active spring varies between 170*ms* at low difference in force (or

pressure) to 70*ms* at high difference in force (or pressure). It can also be seen that valve response times decrease as the pressure difference increase.

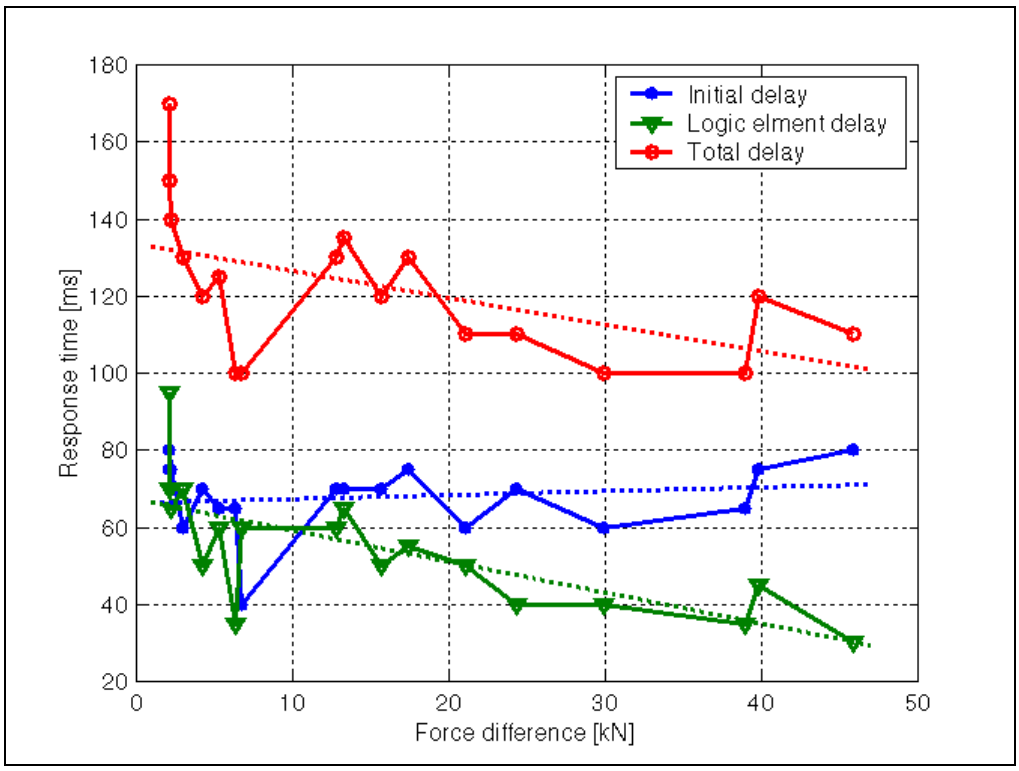


**Figure 4-10: Valve response times for semi-active spring valve (on to off)**

The valve response times for the semi-active damper valve decreases as the relative velocity increases. This is because an increase in velocity results in a higher differential pressure, which causes the valve to open or close quicker. Valve response times ranges from 145*ms* at low relative velocities to 40*ms* at high relative velocities. Figure 4-11 shows the valve response times for the semi-active damper valve, as a function of relative strut speed. The values indicated in this figure represent the average response time from the "off" condition to the "on" condition for both tension and compression motion.

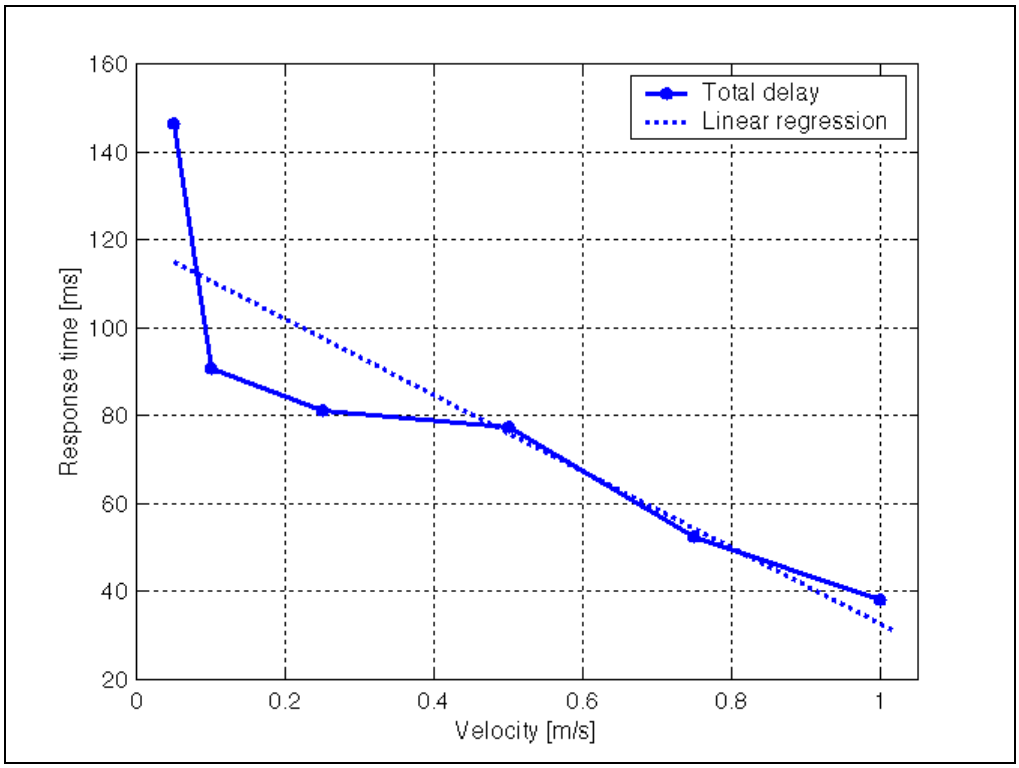


**Figure 4-11: Valve response times for semi-active damper valve (off to on)**

Although the valve response times are slow at low relative velocities, it is fast enough at higher velocities where fast response times are needed. Over severe off-road terrains where the wheel travel is large, the valve response times are faster.

## 4.6 Single degree of freedom testing

Several single degree of freedom tests were performed to evaluate the characteristics and performance of the semi-active spring/damper system. Step response, random input response, sine sweeps, as well as a novel ride height adjustment feature were evaluated. The single degree of freedom test setup, as explained in paragraph 4.2.1, was used for the tests described in the following paragraphs.

### 4.6.1 Step response

The purpose of the step response tests is to evaluate the spring and damper performance potential. The tests were done by subjecting the system to a step displacement input of 43*mm*. The sprung mass displacement, for different spring and damper combinations, are shown in Figure 4-12. From this figure, it can be seen that for the spring “on” condition an effective

natural frequency of approximately 1,5*Hz* is achieved. For the spring "off" state, the natural frequency is in the region of 1*Hz*.

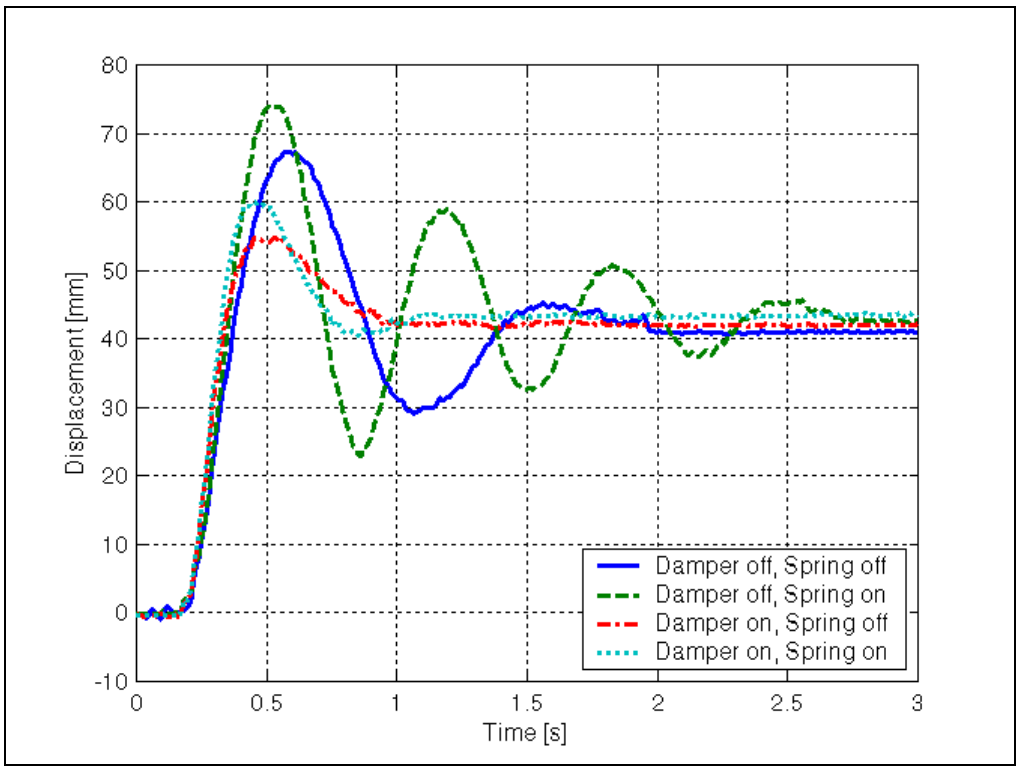


**Figure 4-12: Step response of the sprung mass for different spring and damper combinations**

The response for the two cases where the damper is in the "off" state indicates that the system is under damped. For the damper "on" state, the motion is damped out within one cycle.

The single degree of freedom test results indicate that good on-road, as well as off-road behavior is possible by selecting the appropriate spring and damper settings. A more detailed set of step response test results are supplied in section D.1 in Appendix D.

### 4.6.2 Random input response (Belgian paving)

Random input response tests were performed to evaluate some existing semi-active damper control strategies, as well as to quantify the difference in sprung mass acceleration for the two spring settings. The same control strategy used for the semi-active damper was tested for a semi-active spring strategy. The reason for applying the damper strategies directly to the spring is that the same principle holds, namely the spring setting that would minimize sprung mass acceleration is chosen.

The Belgian paving track at Gerotek Vehicle test facility was chosen as a representative random road input. The track is 100*m* long and consists of randomly packed cobblestones. The Belgian paving has a roughness coefficient of $2*10^{-5}$ and a terrain index of 2. No provision was made for including the effect of the tyre, since the purpose of the tests was only to do relative performance comparisons.

Figure 4-13 displays the sprung mass acceleration for different spring settings over the Belgian paving track. In both cases, the damper was in the passive "on" state. From the figure, it can be seen that the vibration levels for the spring "off" state is much lower than for the spring "on" state.

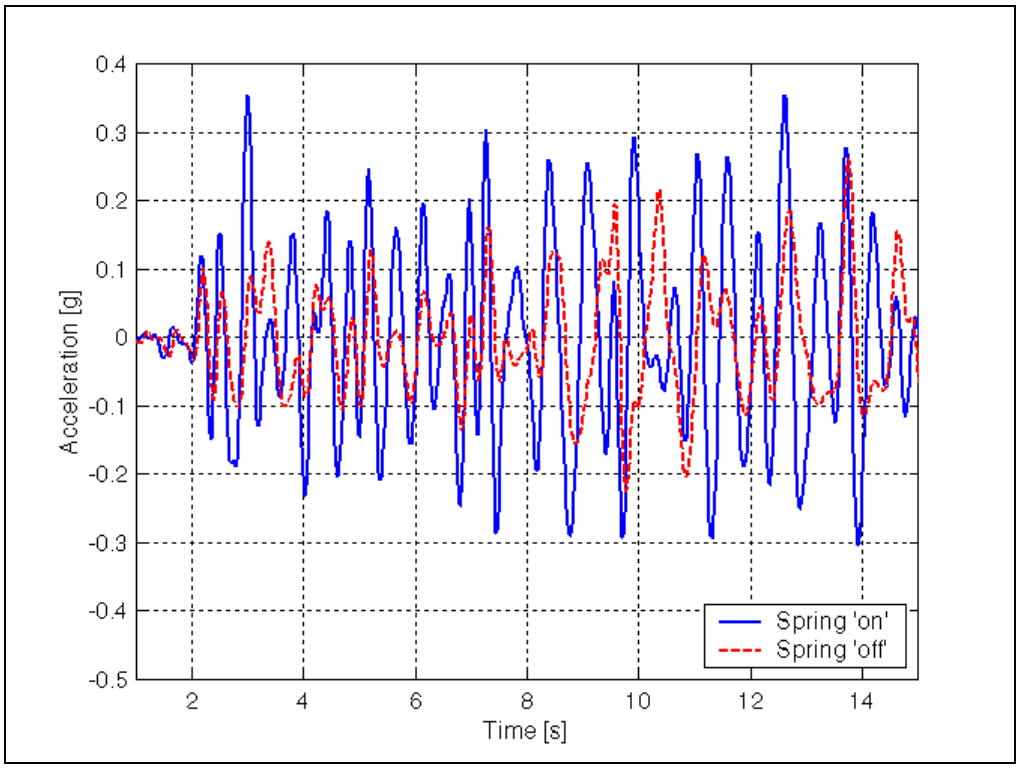


**Figure 4-13: Sprung mass acceleration for different spring settings over the Belgian paving**

The RMS acceleration for the spring "off" state is 0,72$m/s^2$ and for the "on" state 1,36$m/s^2$. An improvement of 47% was therefore achieved by a using different spring characteristics.

In Figure 4-14, the sprung mass acceleration for the damper "on" and the damper semi-active is displayed. In both cases, the spring was set to the passive "off" state. The semi-active control strategy of Karnopp (Barak 1989) was implemented for controlling the damper. From the figure, it is evident that much lower acceleration levels were experienced when the damper is controlled semi-actively.

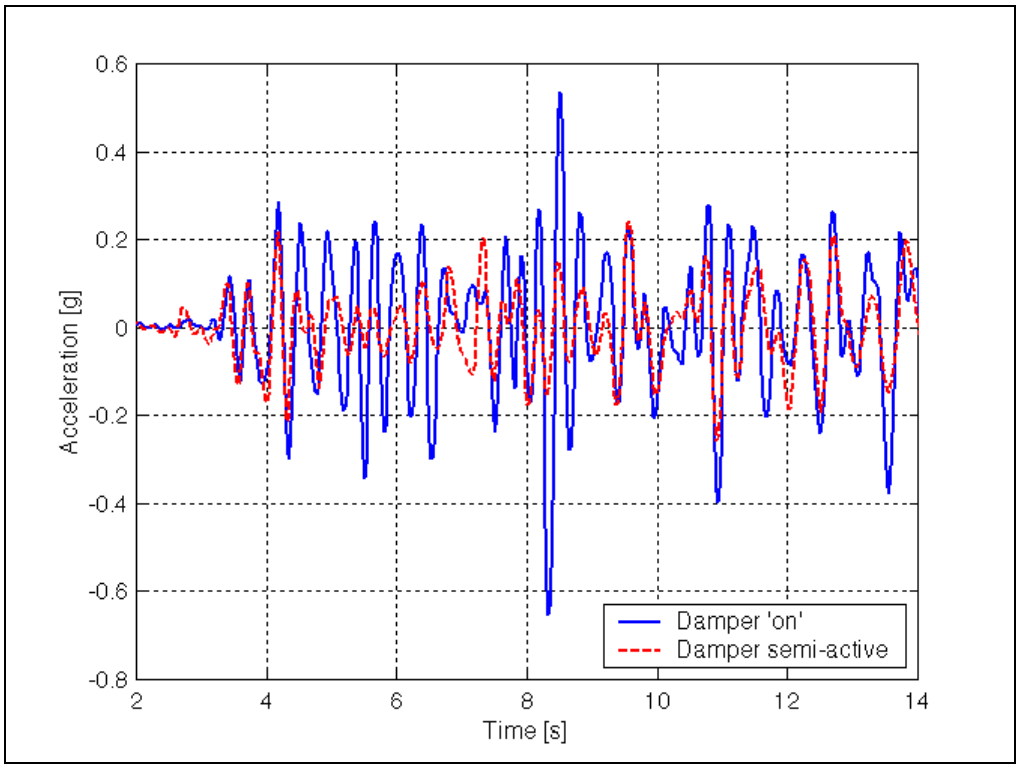


**Figure 4-14: Sprung mass acceleration for the damper "on" setting and damper semi-active**

The RMS acceleration for the passive "on" state is $1{,}48 m/s^2$ and for the semi-active case $0{,}83 m/s^2$. An improvement of 44%, in vertical acceleration levels was therefore achieved by controlling the damper semi-actively.

The results for different spring and damper combinations are supplied in section D.2 in Appendix D.

### 4.6.3 Sine sweep

A sine sweep experiment was performed to determine the properties of the system in the frequency domain. The results of these tests are supplied in section D.3 in Appendix D. Figure 4-15 shows the transmissibility of the spring/damper system for different configurations. The definition of the configurations can be found in Appendix D. From this figure, it can be seen that all the configurations show a resonance between $1Hz$ and $2Hz$. It is also clear that the spring "off" damper "off" configuration offers the best vibration isolation at higher frequencies, while spring "on" and damper "off" resulted in severe resonance, which caused the test to abort due to high actuator force (refer to Figure D-24).

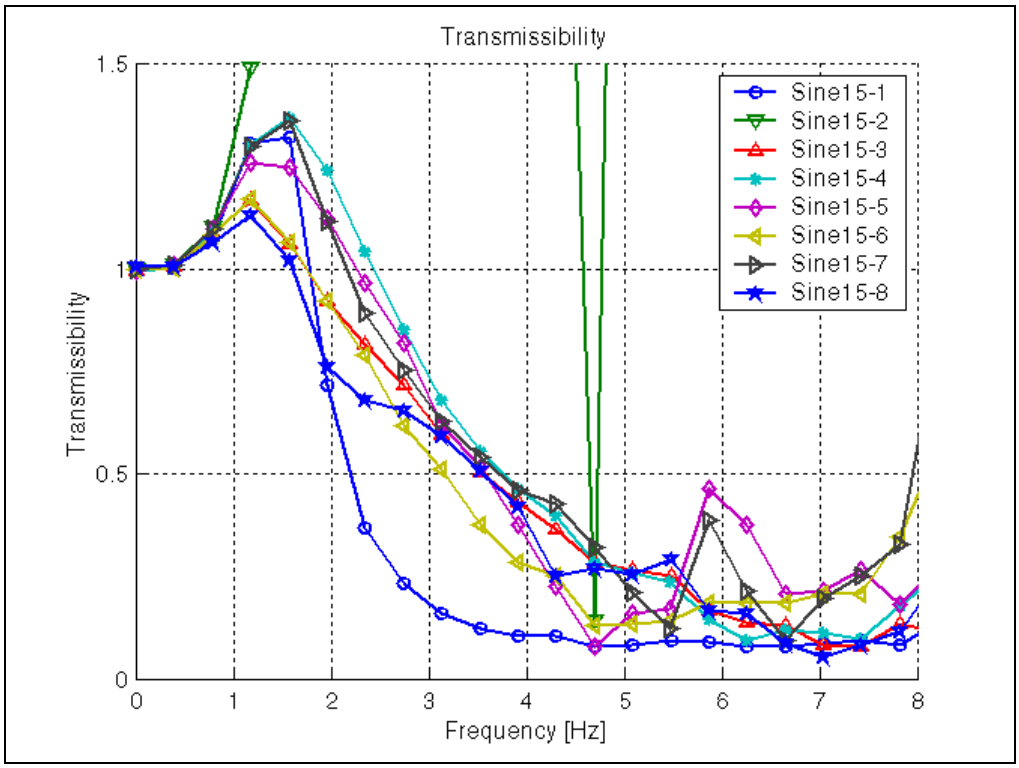


**Figure 4-15: Transmissibility of spring/damper for different configurations**

Although the spring/damper system is non-linear and FRF's (Frequency Response Functions) are theoretically meaningless, the transmissibility graph from the sine sweep test report on an actual operating condition, which gives some insight into the behavior of the system.

### 4.6.4 Ride height adjustment

The ride height of vehicles fitted with hydro-pneumatic suspensions can be easily adjusted by adding or removing hydraulic fluid from the system. A lower ride height results in reduced body roll, lower center of gravity, a more stable firing platform and a lower silhouette. The ride height can also be increased when a greater ground clearance is needed.

Ride height adjustments are usually achieved by making use of an external power source, such as an engine driven hydraulic pump. A control system then regulates the amount of hydraulic fluid in the system with a network of pipes and valves. The Swiss Mowag Piranah III is an example of a vehicle fitted with such a system (refer to Chapter 2).

The semi-active hydro-pneumatic spring/damper system investigated in this study has the added advantage of being able to adjust the ride height without using an external pump. Referring to Figure 1-10 in Chapter 1, the ride height adjustment works as follows:

When valve (6) is closed, the hydraulic fluid in the accumulator (2) is effectively removed from the system. By opening and closing the valve at the right moment an amount of hydraulic fluid can be stored in accumulator (2), thus varying the ride height. To decrease ride height, valve (6) is kept closed and only opened when the pressure in accumulator (3) is higher than in accumulator (2). This is done until the pressure in accumulator (2) reaches a predetermined value corresponding to a specific reduction in ride height. To increase the ride height, valve (6) is only opened when the pressure in accumulator (2) is higher than in accumulator (3).

The control strategy for changing ride height works well for big suspension inputs, but not very well when accumulator pressure fluctuates rapidly (high frequency suspension inputs). This problem can be solved by specifying a dead band for which the valve is not allowed to switch keeping the valve from oscillating between the "on" and the "off" state.

Figure 4-16 shows the result of the ride height adjustment control algorithm. The vehicle ride height was increased by 25*mm* within a period of 20 seconds while driving over the Belgian paving track at 20*km/h*.

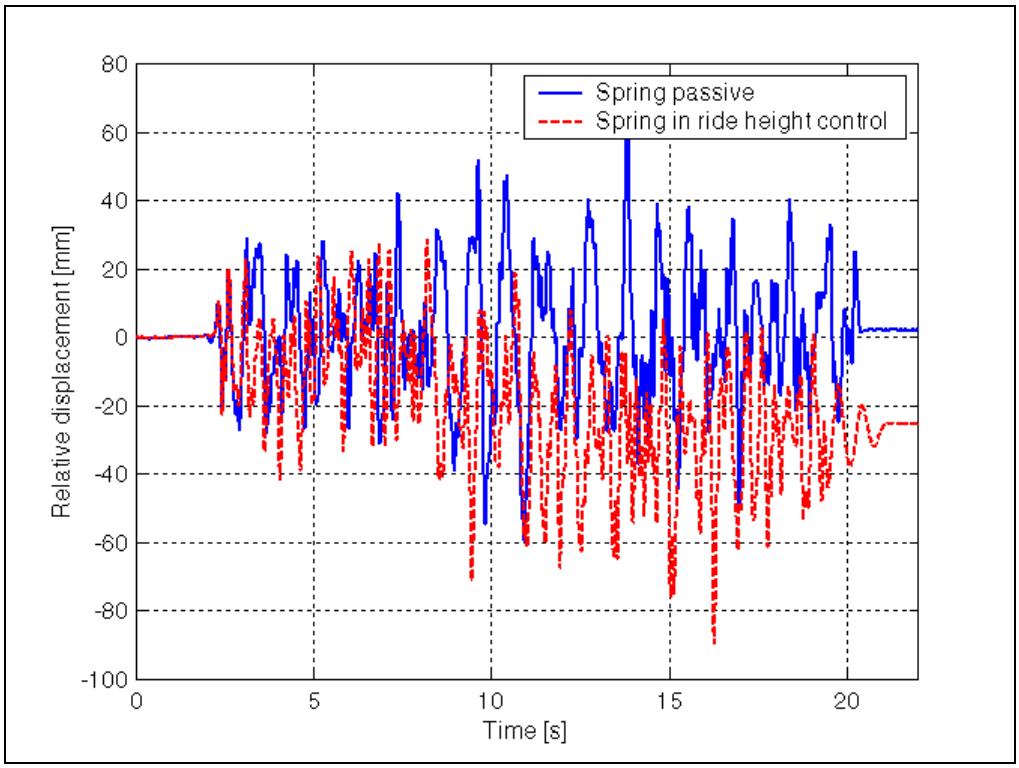


**Figure 4-16: Ride height adjustment for driving over the Belgian paving track**

## 4.7 Closing

The characteristics discussed in this chapter are first order test results to quantify the properties and performance potential of the semi-active spring/damper system. More detailed characterisation of the different elements is possible, but for the purpose of this study, the data presented in this chapter is sufficient to adequately characterise the system.

**********

# 5 MATHEMATICAL MODEL VALIDATION

## 5.1 Preamble

In this chapter, the mathematical model proposed in Chapter 3 is correlated with the experimental results discussed in Chapter 4. The mathematical model is validated with quantitative, as well as qualitative results. The reason for performing quantitative, as well as qualitative comparisons is that for the basic strut characteristics, the absolute forces and displacements are important, while for the SDOF simulations over a random terrain, peak, mean, or RMS values are important. The purpose of comparing the measured and simulated values is not only to determine the accuracy of the simulation model, but also to determine the deficiencies of the simulation model.

The mathematical model validation is discussed under two headings, namely basic strut modelling and SDOF modelling. The reason for treating the validation as two separate parts is that for the basic strut model the relative displacement signal was provided by the Schenck actuator, while for the SDOF model the sprung mass dynamics are also taken into account.

Since the ultimate goal of developing the mathematical model is to integrate it into a full multi-body 3D vehicle simulation (not part of this study), the signals recorded during the experimental tests are used as inputs to the simulation models. These signals include the actuator displacement signal, as well as the damper valve and spring valve switching signals. The recorded signals are used for the following reasons:

- Only the mathematical model is validated and not the control strategies (programming thereof), sensors and data acquisitioning equipment.
- To ensure repeatability (input signals stay constant i.e. not a function of model behaviour)

All the correlation results are supplied in graphical form in Appendix E.

## 5.2 Basic strut model validation

The basic strut configuration consists of the suspension strut, actuated by the Schenck hydropuls in a rigid characterisation frame (see Figure 4-1). The Schenck displacement signals, as well as the valve switching signals recorded during the experimental characterisations are used in the simulations.

### 5.2.1 Passive characteristics

The passive spring characteristics are validated by comparing the P-V diagrams of the measured and simulation results. By passive, it is implied that none of the valves are switched during the characterisation and only one state of the spring/damper unit is tested. Two simulations, one for each spring setting, were performed. The passive characterisations verify the correct working of the hydro-pneumatic spring model, as well as the "steady state" operation of the hydraulic flow model. Figure 5-1 indicates the correlation for the passive spring states.

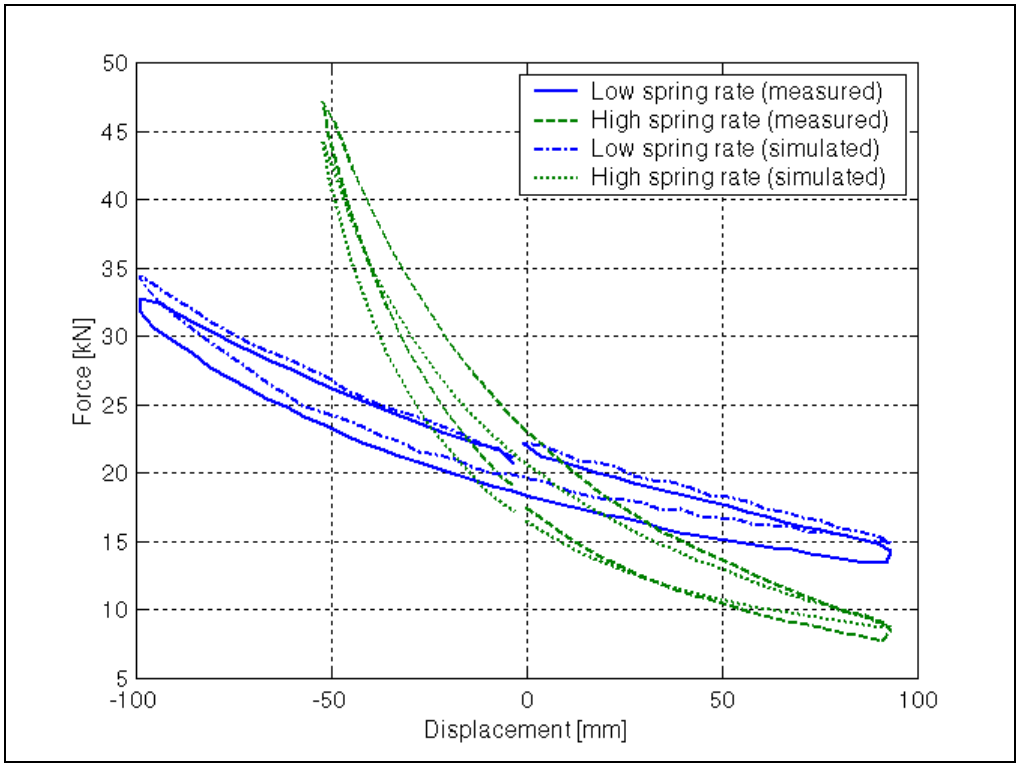


**Figure 5-1: Passive spring characteristic validation (0.01*m/s*)**

From this figure, it can be seen that good correlation is obtained for the passive spring states. Both the low spring (spring "off") and high spring (spring "on") characteristics are in good agreement with the measured data. This data is confirmed by the results obtained by Els (1993). It is evident that the passive spring behaviour can be predicted with high precision and that results similar to that predicted by Els (1993) are obtained.

### 5.2.2 Workspace tests

In order to determine the workspace of the strut and to validate the spring valve switching, the valve is opened and closed during a series of compression and extension strokes. This was done

at excitation speeds of 0.001*m/s*, 0.01*m/s* and 0.1*m/s*. A relative strut displacement (peak-to-peak) of 200*mm* was used, while the spring valve was switched selectively in order to achieve both low and high spring characteristics. The displacement and switching signal used for the characterisation at 0.001*m/s* (nearly isothermal) is shown in Figure 5-2.

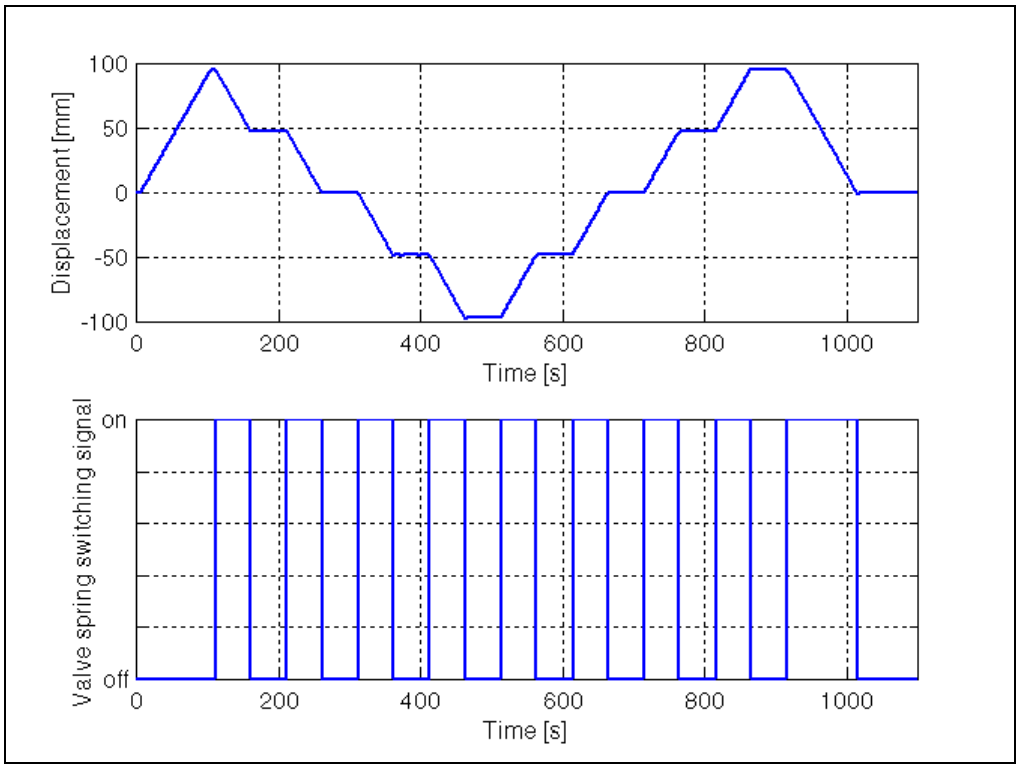


**Figure 5-2: Workspace characterisation**

From this figure, it can be seen that the displacement and switching signal is constructed so that the strut is first extended (positive displacement) and then compressed on the high characteristics for a quarter of the stroke. The spring valve is opened and the strut remains static for a few seconds. After the waiting period, the valve is again closed and another quarter compression stroke is performed. This process is continued, until a maximum stroke of approximately 100*mm* is reached. The strut is extended in the same way as it was compressed, until a rebound displacement of 100*mm* is reached. The strut is then returned to the static position.

The input signals shown in Figure 5-2 is used as input to the simulation model. The damper is not included in this model, since the characterisation configuration did not have a damper present. The result of this series of compression and rebound movements are displayed in Figure 5-3 and Figure 5-4.

Figure 5-3 indicates the force versus time results for the simulation, as described above, while Figure 5-4 indicates the force versus displacement results. From these two figures, it can be seen that good correlation was obtained between measured and simulated data for the low speed characterisations. The results of the simulations at 0.01*m/s* and 0.1*m/s* are supplied in Appendix E.

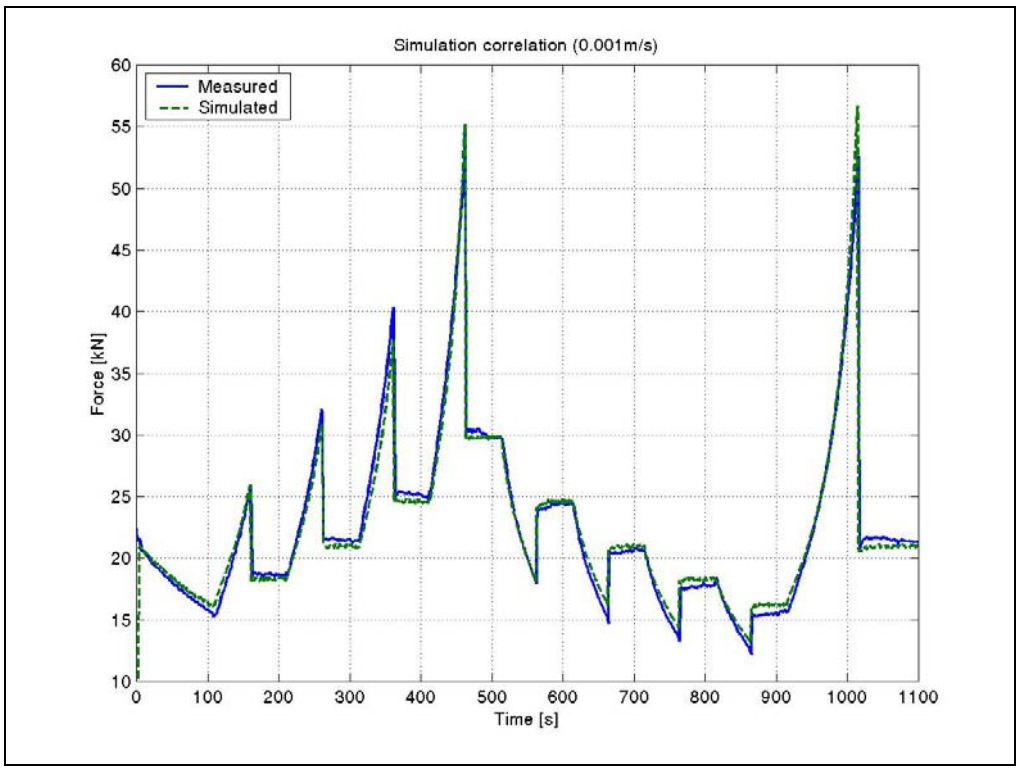


**Figure 5-3: Force versus time correlation (0.001*m/s*)**

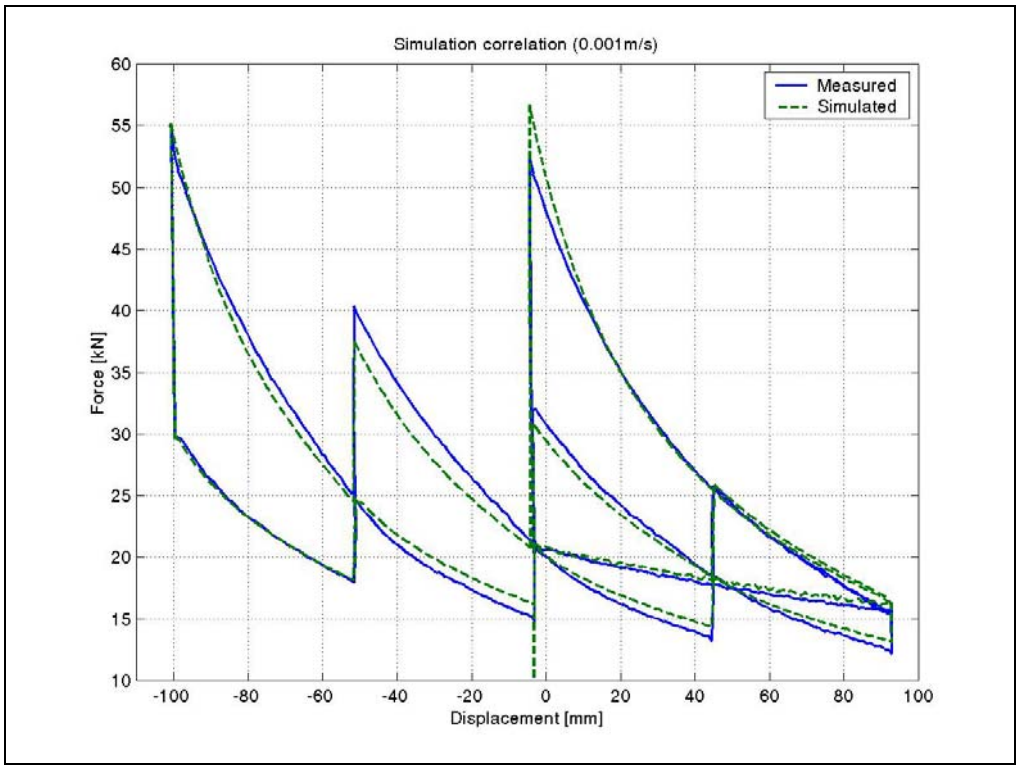


**Figure 5-4: Force versus displacement correlation (0.001*m/s*)**

From the figures presented in section E.1 of Appendix E, it can be seen that the correlation was not as good at the higher excitation speeds, as it was at the lower speeds. This may be attributed to the fact that flow losses and friction were nor modelled in detail.

## 5.3 SDOF model validation

For the single degree of freedom simulations, the complete spring-mass-damper system was modelled and compared with the measured results. The relative strut displacement was used as comparison criteria, since this parameter could easily be measured and does not present filtering and resonance problems, as do accelerometers. As explained previously, the measured actuator displacement and valve switching signals were used as input to the mathematical model.

Three types of tests were performed on the SDOF setup, namely step response, random input response and a sine sweep. The correlation results of these three simulations will be discussed in the following paragraphs.

### 5.3.1 Step response

The step response of a SDOF system gives and indication of the natural frequency and damping behaviour of the system, therefore the step response correlation indicates whether the dynamic properties (spring stiffness, SDOF mass, damping force etc.) of the model are accurate.

For the step response simulations, the basic SDOF model is used, with the measured Schenck displacement as input. Figure 5-5 indicates the measured actuator displacement that was used in the step response SDOF simulations. From this figure, it can be seen that the actuator supplied a step input of approximately 30*mm*. The actuator overshoot is also clearly visible in this figure.

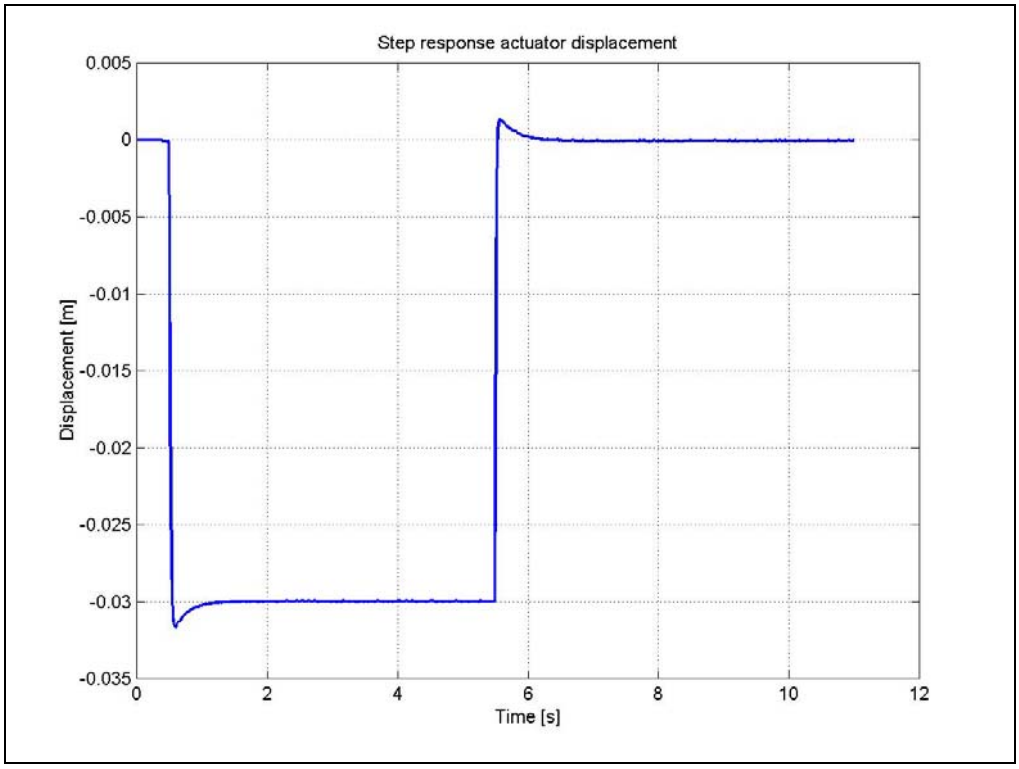


**Figure 5-5: Measured actuator displacement used for SDOF simulations**

Figure 5-6 indicates the recorded and simulated relative displacement step response of the strut unit in the passive state with both spring and damper off.

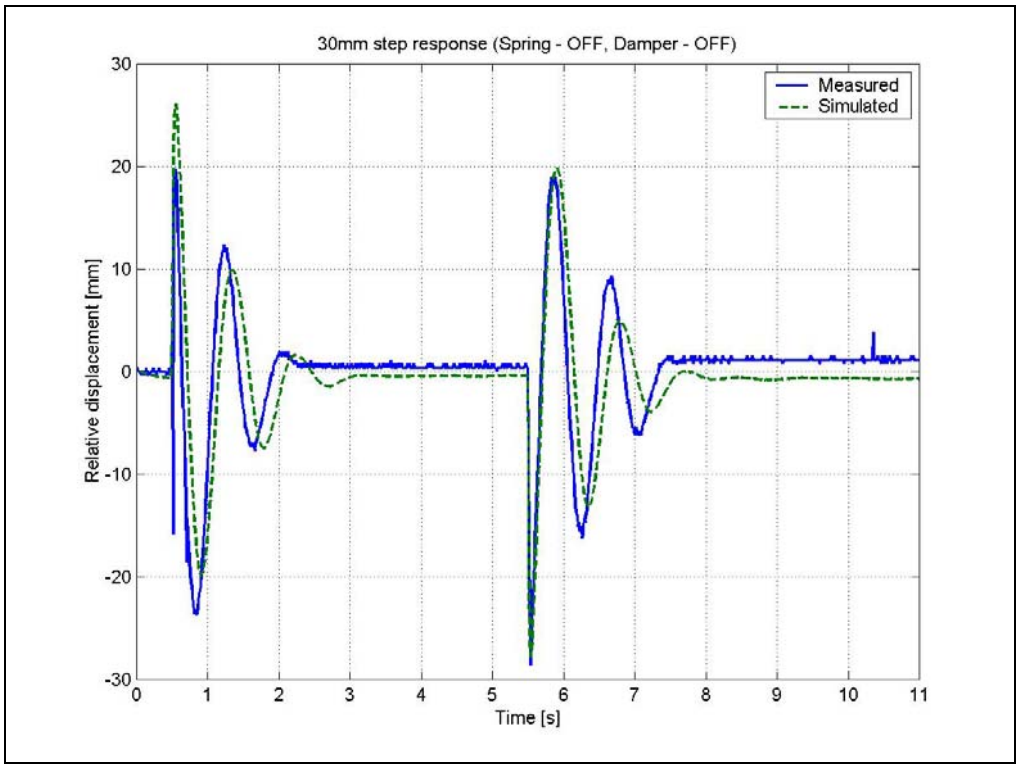


**Figure 5-6: 30*mm* step response (Spring – OFF, Damper – OFF)**

From Figure 5-6 it can be seen that the correlation between measured and simulated data is good and that the model is able to predict the amplitude, as well as phase response to the step input with reasonable accuracy. Both spring and damper was in the OFF state for this test, thereby indicating the passive response.

The correlation for different combinations of spring and damper settings and input amplitudes are supplied in section E.2 of Appendix E. From Figures E-8 to E-16 it can be see that good correlation was achieved for various combinations of spring and damper settings and that reasonable correlation was obtained with the damper controlled according to the strategy of Karnopp (Nell 1993) (Figure E-12).

### 5.3.2 Random input response

For the random input response simulations, the recorded Schenck displacement signal was used as input to the simulation model. The input signal represents the left hand lane of the Belgian paving track at the Gerotek Vehicle Testing Facility. The Belgian paving track is a 100*m* long cobble stone paving and can be used as a realistic random input for off-road vehicles. Figure 5-7 indicates the vertical displacement versus time at a vehicle speed of 25km/h over the Belgian paving track (left lane).

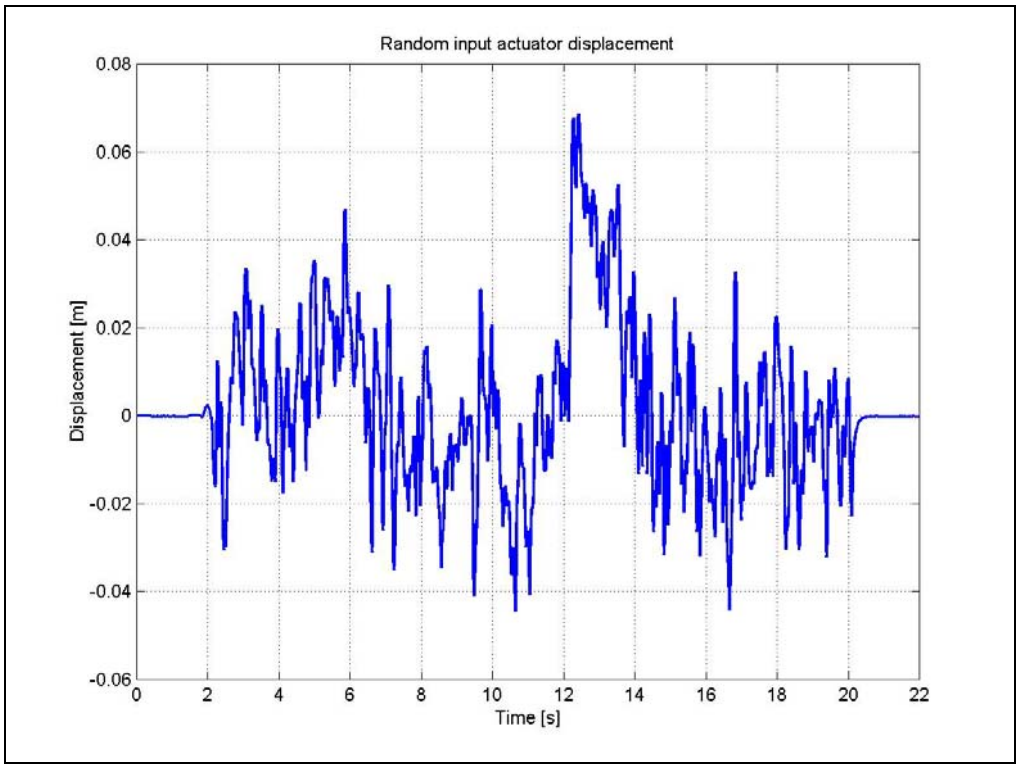


**Figure 5-7: Random input actuator displacement (Belgian paving - left lane)**

Figure 5-9 indicates the correlation between measured and simulated values for the random input (Belgian paving - Figure 5-8 shows the PSD of this track). From this figure, it can be seen that the correlation was good and that the simulated peak displacement is higher than what was measured. A possible reason for this is that not all the losses are accounted for in the simulation model.

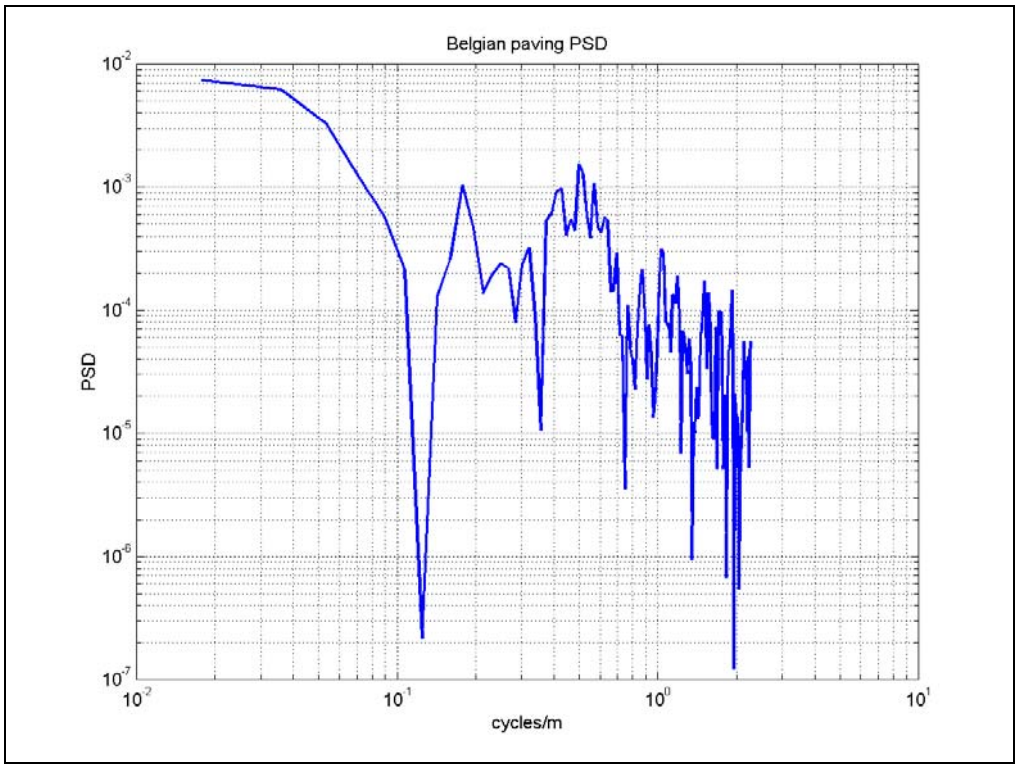


**Figure 5-8: PSD of Belgian paving track (left lane)**

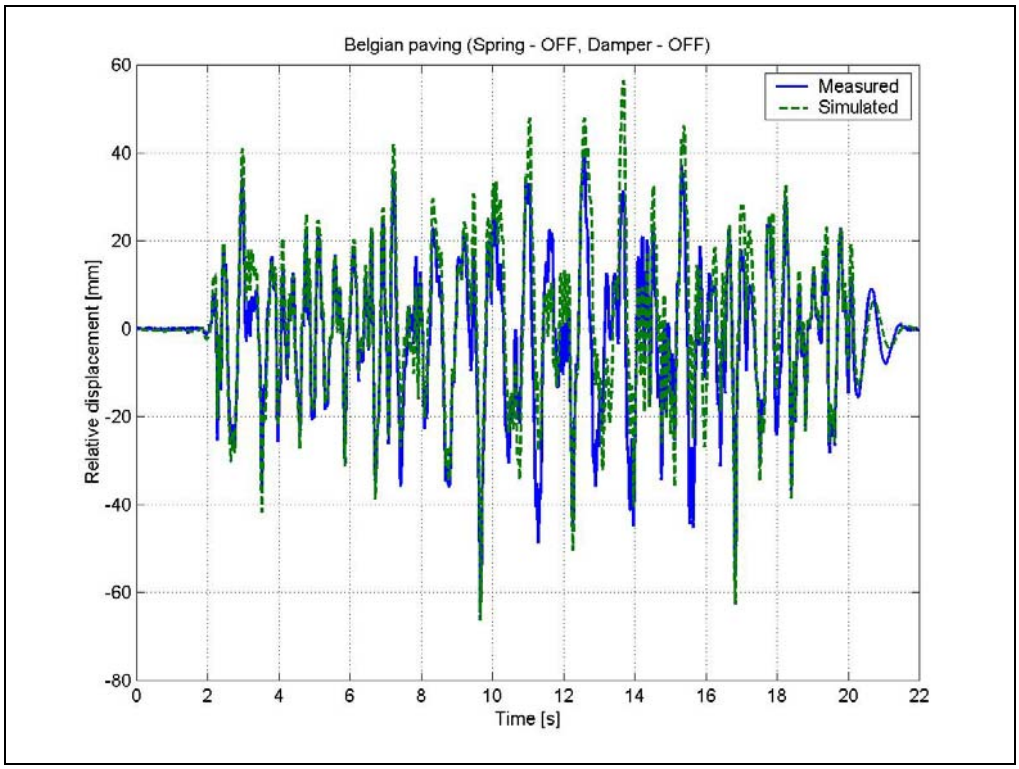


**Figure 5-9: Correlation over Belgian paving (Spring – OFF, Damper – OFF)**

Figures E-17 to E-26 indicate the random input correlation for some other spring and damper settings. Figure 5-10 shows the summary of statistical correlation between measured and simulated results. The configurations are defined in Table 5-1.

**Table 5-1: Spring/damper configuration for random input tests**

| Configuration no. | Figure no. | Spring state | Damper state |
|---|---|---|---|
| 1 | Figure E-17 | OFF | OFF |
| 2 | Figure E-18 | ON | OFF |
| 3 | Figure E-19 | OFF | ON |
| 4 | Figure E-20 | ON | ON |
| 5 | Figure E-21 | ON | Karnopp |
| 6 | Figure E-22 | OFF | Karnopp |
| 7 | Figure E-23 | ON | Hölscher & Huang |
| 8 | Figure E-24 | OFF | Hölscher & Huang |
| 9 | Figure E-25 | Karnopp | Karnopp |
| 10 | Figure E-26 | Height adjustment | OFF |

From Figure 5-10, it can be seen that good correlation was obtained, except for configuration 10 (Spring - height adjustment, Damper - OFF). Additional statistical information can be found in Figures E-27 and E-28.

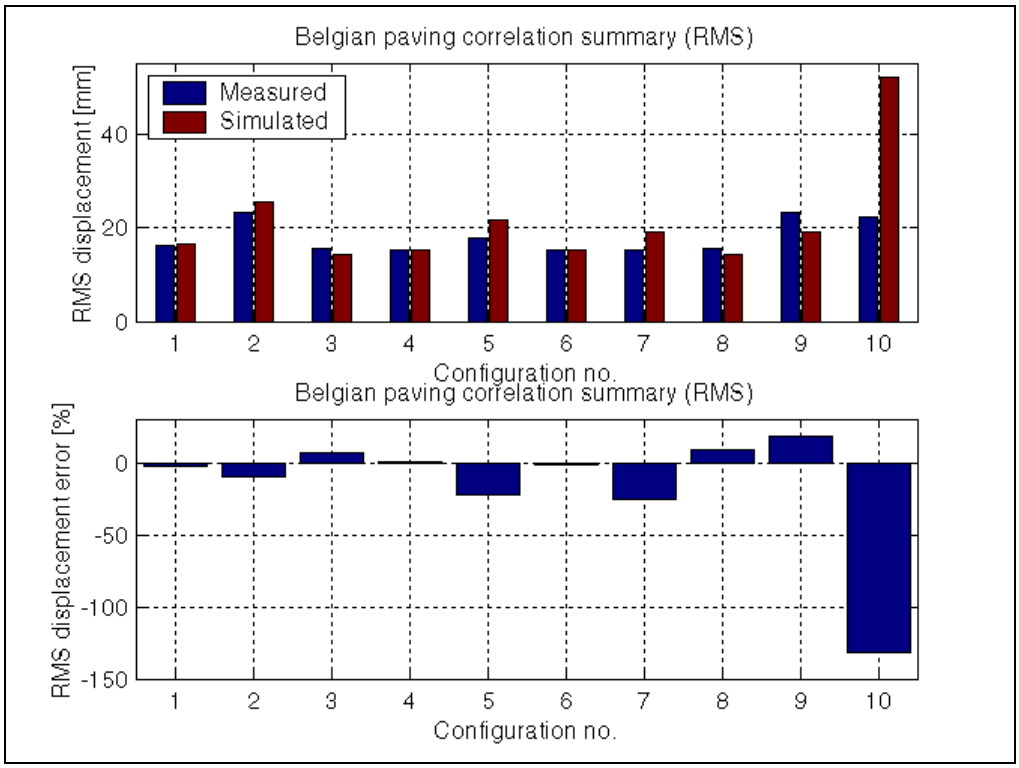


**Figure 5-10: Belgian paving correlation summary (RMS)**

### 5.3.3 Sine sweep

Although it is not valid to determine the frequency response of the strut with a sine sweep input since the system is highly non-linear, the sine sweep gives an indication of the system's natural frequency for a certain excitation amplitude. Sine sweep tests were therefore performed not to characterise the system in the frequency domain, but to determine whether the mathematical model is be able to reproduce the response to a sine sweep input.

A 78*s* sine sweep signal was used with a frequency content between 0,1*Hz* and 15*Hz*. The sine sweep input signal can be seen in Figure E-29 in Appendix E. Figure 5-11 indicates the sine sweep response for the spring in the "OFF" sate and the damper in the "ON" state. From this figure, it can be seen that the relative displacement decreases with an increase in frequency. This is because the damper characteristic in rebound is higher than in compression. This is a typical tendency of a wheeled vehicle damper. From Figure 5-11, it can be seen that the simulation model is able to reproduce this type of behaviour. More detailed results are supplied in Appendix E.

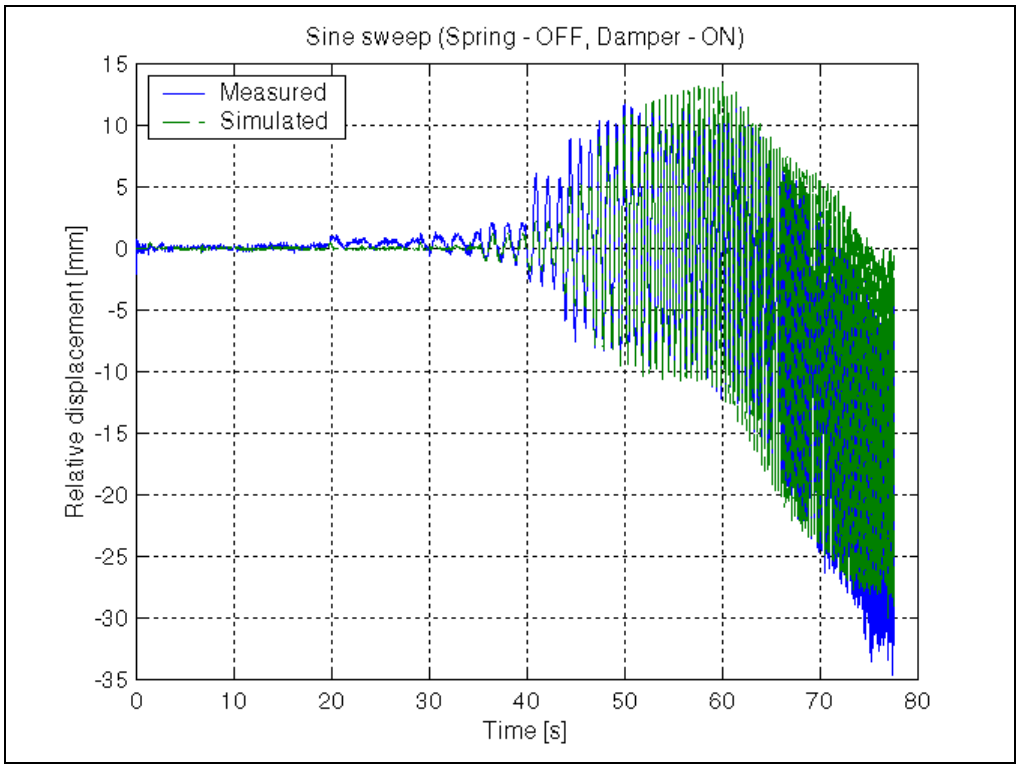


**Figure 5-11: Sine sweep correlation (Spring - OFF, Damper - ON)**

In order to determine whether the simulation model provides an accurate representation of the strut in the frequency domain, the transmissibility between the input displacement and the sprung mass response for the measured, as well as the simulated data was determined (see Figures E-38 to E-45). Figure 5-12 indicates the transmissibility for both the spring and damper in the "OFF" state. Also supplied in this figure is the coherence between the two displacement signals, giving an indication of the level of confidence in the transmissibility. From this figure, it can be seen that the coherence (for measured and simulated) is high below 10*Hz*. The transmissibility graph indicates that the simulated data has a higher transmissibility in the region of resonance, but that the region of resonance is the same for measured and simulated data.

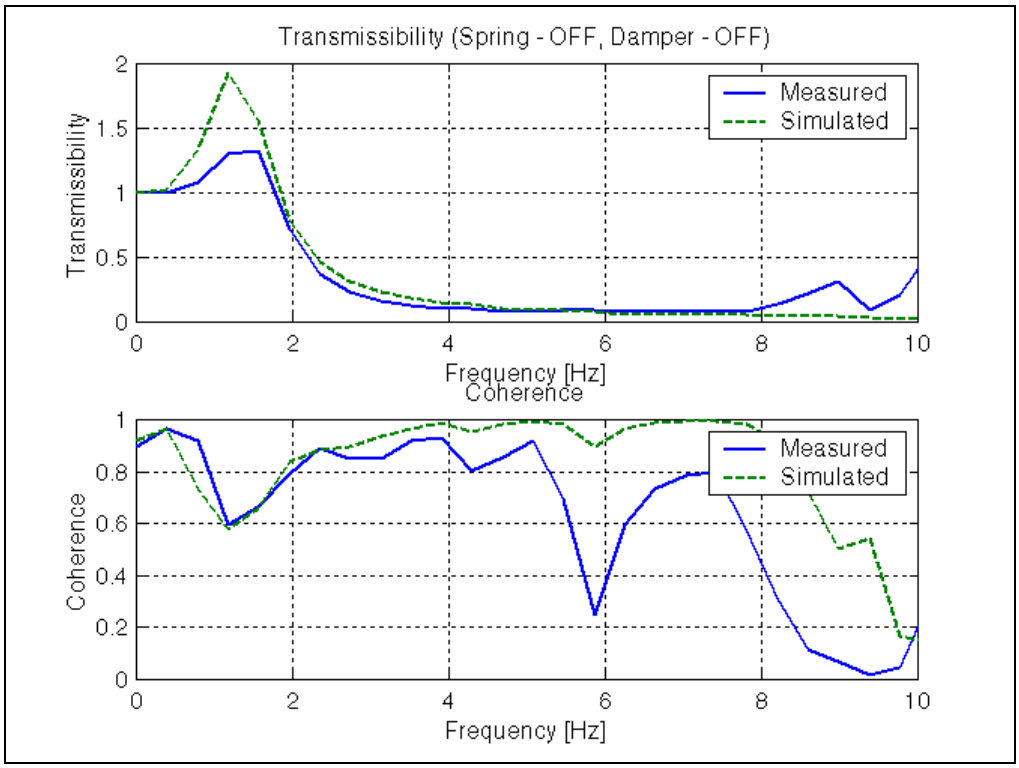


**Figure 5-12: Transmissibility (Spring - OFF, Damper - OFF)**

## 5.4 Closing

In conclusion, it can be said that the current mathematical model provides an adequate representation of the semi-active hydro-pneumatic spring/damper system. In the preceding paragraphs, it was illustrated that the mathematical model is able to predict the force versus displacement characteristics of the strut for different excitation frequencies.

For the SDOF modelling, good correlation was obtained for the step response, random input response, as well as the sine sweep simulations. Although the correlation for the time domain response of the random input simulations is not very good in all cases, the statistical correlation (RMS) was good. It is also illustrated that the simulation model is able to predicted phenomenon such as suspension squat at high frequencies, due to the unsymmetrical damper characteristics. Discrepancies between measured and simulated results can be attributed to amongst others gas leaks in the experimental units, unaccounted effects such as bearing friction, hydraulic damping effects in the pipes and valve response uncertainty.

The current model can be further refined by introducing a more sophisticated valve model to better simulate the strut at higher excitation frequencies. The solving time of this mathematical

model is sufficiently fast (5-10 minutes of CPU time for 10*s* real time on a Pentium II 333*MHz* computer), in order to be incorporated into a full 3D, multi wheeled vehicle model.

# 6 CONCLUSIONS AND RECOMMENDATIONS

## 6.1 Preamble

In this chapter, a brief summary will be provided followed by conclusions and recommendations. The primary comments in the conclusions and recommendations are focussed on the mathematical modelling of the semi-active spring/damper, while the secondary comments are general observations about the system.

Examples of semi-active damper rig tests, as well as full-scale vehicle tests were developed locally and internationally by various organisations. Locally semi-active damper systems were mainly evaluated on large military off-road vehicles. For this study, an existing semi-active spring/damper system was analysed and the characteristics of the suspension system is supplied in this document. No examples of a semi-active spring/damper system like the one discussed in this document could be found in the literature. Conceptual suspension layouts utilising two or more hydro-pneumatic springs were found, however no test or simulations results were presented by the authors.

Most of the high mobility military vehicles make use of hydro-pneumatic suspensions and some of them are fitted with ride height adjustment systems. Although hydro-pneumatic suspensions are more expensive than conventional suspension elements, they are popular because of their non-linear characteristics, compact structure and other features such as ride height control and lockout.

Five ways of mathematically modelling a hydro-pneumatic spring were discussed in Chapter 2. The different methods imply varying levels of complexity, of which the real gas thermal time constant method would be classified as the most complex and the polytropic and ideal gas approach the least complex. The anelastic model was found to be a possible way of simulating the thermal behaviour of a hydropneumatic spring, since it is mathematically similar to the thermal time constant model. The hydro-pneumatic spring in this study was modelled with the real gas thermal time constant approach proposed by Els (1993), while the semi-active damper part was modelled using interpolation in look-up tables. Both the hydraulic valves were modelled by a first order delay, as a function of relative pressure across the valve, while the hydraulic flow model was constructed from first principles, making use of conservation of mass principles. The mathematical models of the semi-active hydro-pneumatic spring, the semi-active hydraulic damper and the hydraulic flow were successfully integrated into a single model. All the mathematical models were programmed in Matlab/Simulink and measured displacement and

valve switching signals were used to drive the mathematical model to compare it with measured data.

Sine sweep tests were performed at a fixed excitation amplitude from 0*Hz* to 15*Hz*, therefore it was not possible to comment on the validity of the frequency response of the spring/damper system. As part of the experimental tests, a ride height adjustment scheme was evaluated, which does not require any external power source and only remove hydraulic fluid from the system when one of the accumulators is isolated. Discrepancies between measured and simulated results can be attributed to amongst others gas leaks in the experimental units, unaccounted effects such as bearing friction and modelled hydraulic damping effects in the pipes.

## 6.2 Conclusions

The following *primary* conclusions can be made from this study:

- *Acceptable correlation was obtained between the mathematical model and the experimental results.*

  Analysis results from the simulation model were correlated with measured data from the experimental setup. These correlations included the passive characteristics, the workspace test, step response, random input response and sine sweep tests. Good correlation was obtained for the characterisation simulations, while the correlation for the workspace test was good at low excitation frequencies only.

  In most cases, good correlation was obtained for the step response simulations in terms of absolute measures, such as relative strut displacement. For the random input simulations the absolute correlations was not good, however the statistical, i.e. RMS correlations were in general very good.

  Good correlation was also obtained for the sine sweep simulations and the model was able to predict phenomenon such as suspension squat for the damper “on” spring “off” condition.

  Transmissibility graphs indicated that the mathematical model was able to predict the resonance frequency fairly well, however the peak values did not correspond very well.

- *The anelastic model proved to be the most promising in terms of simplicity, computational efficiency and programming effort.*

  As an alternative way of modelling the hydro-pneumatic spring, an anelastic model making use of a polytropic main spring was compared to the real gas thermal time constant spring model. It was found that the hysteresis loop seen in the hydro-pneumatic spring characteristic is only encountered at very low excitation frequencies (below the vehicle body natural frequencies) and that the anelastic model was able to match the real gas thermal time constant model predictions for steady state conditions at higher excitation frequencies. Although the real gas thermal time constant model yielded good results in general, it is too complicated for first order vehicle dynamics simulations.

The following *secondary* conclusions can be made from this study:

- From the background in Chapter 1 and the literature overview in Chapter 2, it is clear that a lot of research has been done in the field of semi-active suspension systems. Most of this work was done on semi-active dampers, although a few studies were also performed on frequency dependent springs and springs with variable spring rates.

- Physical tests revealed that for the four operating conditions of the spring/damper system, very different SDOF responses could be expected. The test results showed that the spring/damper system can supply spring and damper characteristics associated with good ride comfort, as well as good handling in a single package. For good ride comfort the hydro-pneumatic spring can be set to the soft state, while controlling the damper semi-actively and for good handling both the spring and damper can be set to the hard state.

- Measured valve response times between 180*ms* and 40*ms* for the spring and damper valves did not seem to be too slow for semi-active control, although a faster response would enable more precise control, especially of the unsprung mass.

## 6.3 Recommendations

The following *primary* recommendation can be made:

- *The anelastic model seems to be a viable alternative to the more complicated real gas thermal time constant model and should be investigated in more detail.*

For full 3D dynamic vehicle models, the real gas thermal time constant will be adding complexity to the model that might not contribute significantly to the fidelity of the vehicle model. Using an anelastic model should result in good overall vehicle response, without too much complexity. A non-linear anelastic model can easily be constructed by making use of a polytropic process and the polytropic constant can either be determined through experimental tests, or by making use of the real gas thermal time constant model, as was done in this study.

The following *secondary* recommendations can be made:

- Since a lot a research has been done on semi-active dampers and not much on semi-active springs, it is recommended that a dedicated semi-active spring control strategy be developed and tested. The reason for this is that a spring is a displacement dependent force element, while a damper is a velocity dependent element. Switching from the "on" state to the "off" state during cornering might unsettle the vehicle.

- Most semi-active control strategies only cater for improving either ride comfort or handling, therefore it would be worthwhile to develop a control strategy for the spring/damper that is able to handle most driving conditions. A combination of reaction driven (react to suspension inputs) and input driven (react to driver inputs, i.e. throttle, brake and steering) control can be followed.

- The possibility of ride height control by selectively opening and closing the spring valve should also be further investigated and a control strategy developed.

- The experimental setup worked well for the tests conducted in this study, but can be modified to include the tyre, in order to be more representative of an actual vehicle application. Including the tyre in the test setup would add higher frequency dynamics at approximately the wheel hop frequency, which would increase the demand on the bandwidth of the semi-active control strategies and the valve response times.

- An unknown factor in the single degree of freedom test setup used in this study is the frictional losses in the linear bearings of the sprung mass. Misalignment of the bearings might account for substantial losses, which are not easily determinable. A hardware-in-the-loop (HIL) test setup might be more useful for performing single degree of freedom simulations and for expanding the dynamic model. In a HIL simulation, frictional losses

and other effects such as a tyre can be added and their influence on the results can be quantified.

- Pilot operated logic element valves are used to channel the hydraulic fluid in the spring/damper system. These valves perform well at high pressure differences, but are slow at low pressure differences. A project investigating alternative hydraulic valves, which are both fast acting and permit high flow rates would be a useful for improving the bandwidth of the current system.

- Since standard components were used in the construction of the spring/damper unit, a packaging exercise would be required, in order to determine the optimal layout of accumulators and pipes in a vehicle set.

**********

# REFERENCES

Abd El-Tawwab, A M 1997. Twin-Accumulator Suspension System. ***SAE Technical paper no. 970384.*** Warrendale: Society of Automotive Engineers.

Barak, P 1989. Design and evaluation of an adjustable automobile suspension. ***SAE Technical paper no. 890089.*** Warrendale: Society of Automotive Engineers.

***CAR Magazine*** July 1989. Adaptive Suspension, 101-102. Cape Town: Ramsay, Son & Parker.

Chance, B K 1984. 1984 Continental Mark VII/Lincoln Continental Electronically-Controlled Air Suspension (EAS) System. ***SAE Technical paper no. 840342***. Warrendale: Society of Automotive Engineers.

Cooper, H W & Goldfrank, J C 1967. B-W-R Constants and New Correlations. ***Hydrocarbon Processing*** 46(12), 141-146.

Els, P S 1993. Die Hitteprobleem op Hidropneumatiese Veer-en-Demperstelsels. MEng thesis. University of Pretoria, Pretoria.

Els, P S & Giliomee C L 1998. The development History of Semi-active Dampers in South Africa. ***Wheels & Tracks Symposium '98,*** Royal Military College of Science. Shrivenham: Cranfield University.

Els P S & Grobbelaar B 1999. Heat transfer effects on hydropneumatic suspension systems. ***Journal of Terramechanics*** 36, 197-205. Warrendale: Pergamon.

Félez, J & Vera, C 1987. Bond Graph Assisted Models for Hydro-Pneumatic Suspensions in Crane Vehicles. ***Vehicle System Dynamics*** 16, 313-332. Amsterdam: Swets & Zeitlinger.

Hilmes, R 1982. Dreissig Jahre Kampfpanzerentwicklung (1950-1980). ***Soldat und Technik*** 6, 324-329. Germany.

Hirose, M et al 1988. Toyota Electronic Modulated Air Suspension System for the 1986 Soarer. ***IEEE Transactions on industrial Electronics*** 35(2), 193-200.

Hohl G H 1986. Torsion-bar springs and damping systems of tracked combat vehicles. ***Journal of Terramechanics*** 22(4). Warrendale: Pergamon.

Horton D N L & Crolla D A 1986. Theoretical Analysis of a Semi-Active Suspension Fitted to an Off-Road Vehicle. ***Vehicle System Dynamics*** 15, 351-372. Amsterdam: Swets & Zeitlinger.

Hrovat, D & Margolis, D L 1981. An experimental comparison between semi-active and passive suspension for air-cushion vehicles. ***International Journal of Vehicle Design*** 2(3). Great Britain: Inderscience Enterpises.

Karnopp, D & Heess, G 1991. Electronically Controllable Vehicle Suspension. ***Vehicle System Dynamics*** 20, 207-217. Amsterdam: Swets & Zeitlinger.

Meller, T 1987. Self-Energizing Hydropneumatic Levelling System. ***SAE Technical paper no. 780052.*** Warrendale: Society of Automotive Engineers.

Miller, L R & Nobles, C M 1988. The design and development of a semi-active suspension for a military tank. ***SAE Technical paper no. 881133.*** Warrendale: Society of Automotive Engineers.

Moulton, A E & Best, A 1979. Hydragas Suspension. ***SAE Technical paper no. 790374.*** Warrendale: Society of Automotive Engineers.

Moulton, A E & Best A 1980. Hydragas Suspension**.** ***SAE Technical paper no. 790374***. Warrendale: Society of Automotive Engineers.

Nell, S 1990. Literatuurstudie: Gevorderde Suspensiestelsels. ***Reumech Ermetek dokument nr. 0102748-0629-001***. Boksburg.

Nell, S 1991. Teoretiese- en Rekenaar- evaluering van Semi-Aktiewe Dempers. ***Reumech Ermetek dokument nr. 0114659-0679-001***. Boksburg.

Nell, S 1993. 'n Algemene Strategie vir die beheer van Semi-aktiewe Dempers in 'n Voertuigsuspensiestelsel. PhD thesis. University of Pretoria, Pretoria.

Nell, S & Steyn, J L 1994. Experimental Evaluation of an Unsophisticated Two State Semi-Active Damper. ***Journal of Terramechanics*** 31(4), 227-238. Warrendale: Pergamon.

Otis, D R & Pourmovahed, A 1985. An Algorithm for Computing Nonflow Gas Processes in Gas Springs and Hydropneumatic Accumulators. ***Journal of Dynamic Systems, Measurement, and Control*** 107, 93-96.

Pourmovahed, A & Otis, D R 1984. Effects of Thermal Damping on the Dynamic Response of a Hydraulic Motor-Accumulator System. ***Journal of Dynamic Systems, Measurement, and Control*** 106, 21-26.

Pourmovahed, A & Otis, D R 1990. An Experimental Thermal Time-Constant Correlation for Hydraulic Accumulators. ***Journal of Dynamic Systems, Measurement, and Control*** 112, 116-121.

Rakheja, S & Sankar, S 1985. Vibration and Shock Isolation Performance of a Semi-Active "On-Off" Damper. ***Journal of Dynamic Systems, Measurement, and Control*** 107, 398-403.

Salemka, R M & Beck, R R 1975. Feasibility Analysis and Evaluation of an Adaptive Tracked Vehicle Suspension and Control System. ***Technical Report no. 11893 (LL-146),*** US Army Tank Automotive Command. Michigan.

Soltis, M W 1987. 1987 Thunderbird Turbo Coupe Programmed Ride Control (PRC) Suspension. ***SAE Technical paper no. 870540***. Warrendale: Society of Automotive Engineers.

***TACOM Technical report no. 12072,*** 1975. Investigation of fluidically controlled suspension systems for tracked vehicles. Michigan.

Van Wylen, G J & Sonntag, R E 1985. ***Fundamentals of Classical Thermodynamics.*** 3rd edition, SI Version. Singapore: John Wiley & Sons.

Yokoya, Y et al 1984. Toyota Electronic Modulated Suspension (TEMS) System for the 1983 Soarer. ***SAE Technical paper 840341.*** Warrendale: Society of Automotive Engineers.

# APPENDIX A: HYDRO-PNEUMATIC SUSPENSIONS

## A.1 Hydrolastic / Hydragas (Moulton & Best 1979, 1980)

The Hydrolastic suspension system is one of the first interconnected suspensions. This suspension made use a rubber for the springing medium, with a fluid interconnection. The Hydragas suspension is the product of a 15-year evolution of the Hydrolastic suspension. The Hydragas suspension makes use of Nitrogen gas instead of rubber and a fluid interconnection. Figure A-1 shows the Hydragas suspension unit.

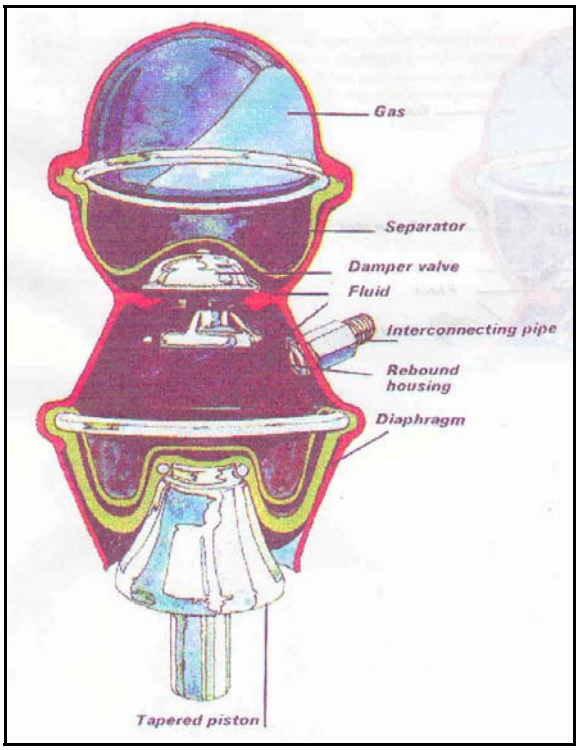


**Figure A-1: Hydragas suspension unit**

The reason for interconnecting the front and the rear suspension is to reduce the pitch frequency. More detail on interconnected suspensions is available in (Moulton & Best 1980).

## A.2 Cadillac Gage Textron

Cadillac Gage Textron has a large range of hydro-pneumatic suspension units. Presented here are some of their products. The 6K unit (see Figure A-2) unit is designed for light AFV's and can be fitted to vehicles such as the M2/M3 Bradley and the USMC's AAV7A1 armoured amphibious assault vehicle.

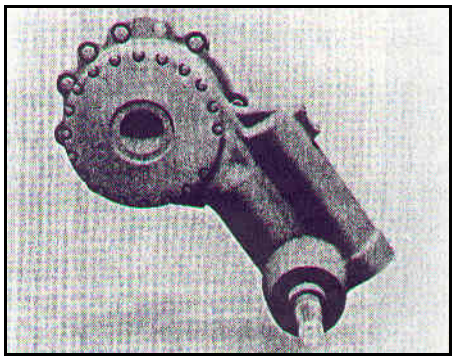

**Figure A-2: 6K in-arm suspension**

The 10K unit (see Figure A-3) can be fitted to AFV's such as the M48, M60, Centurion and the T-series MBT.

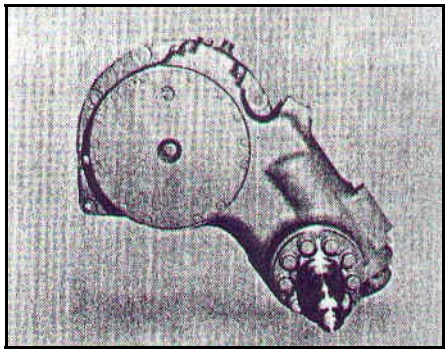

**Figure A-3: 10K in-arm suspension**

The 14K unit (see Figure A-4) is designed for installation on heavier MBT's such as the M1A1 and Leopard 2.

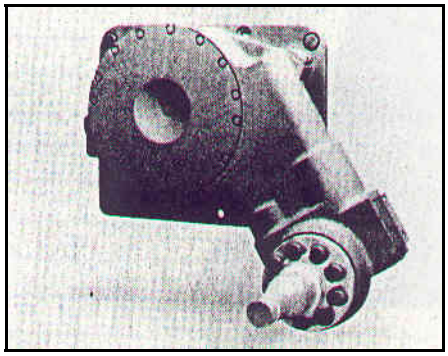

**Figure A-4: 14K in-arm suspension**

## A.3 Citroen Xantia Activa

The Citroen Xantia Activa employs the Hydractive suspension system. This system was recently upgraded with active roll control. Figure A-5 shows a photograph of the Citroen Xantia Activa.


**Figure A-5: Citroen Xantia Activa**

The working principle of the active roll control is illustrated in Figure A-6.

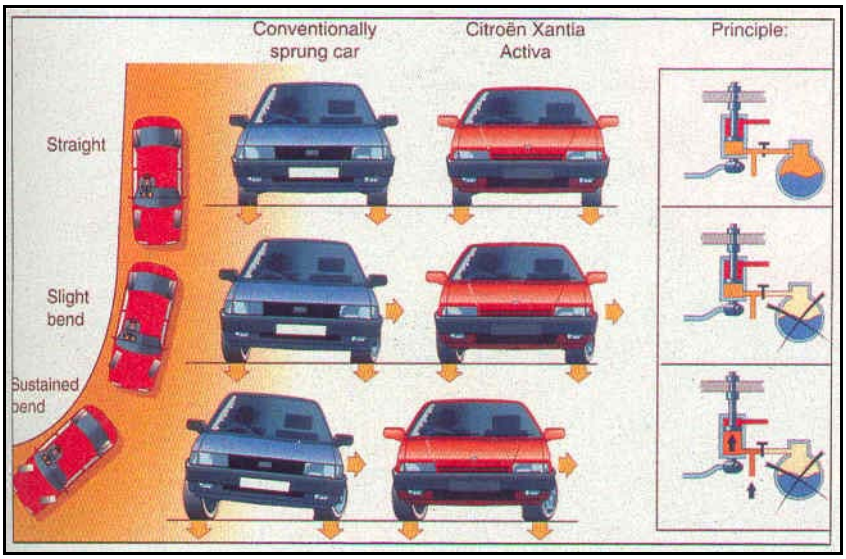


**Figure A-6: Citroen's active roll control**

## A.4 Hydrostrut (Horstman Defence Systems)

The hydrostrut is manufactured by Horstman Defence Systems in the UK. This strut is a telescopic unit, which combines a nitrogen gas spring and a hydraulic oil damper in a single unit.

**Figure A-7: Airlog Hydrostrut**

The gas and the oil are separated by a floating piston, as can be seen in Figure A-8.

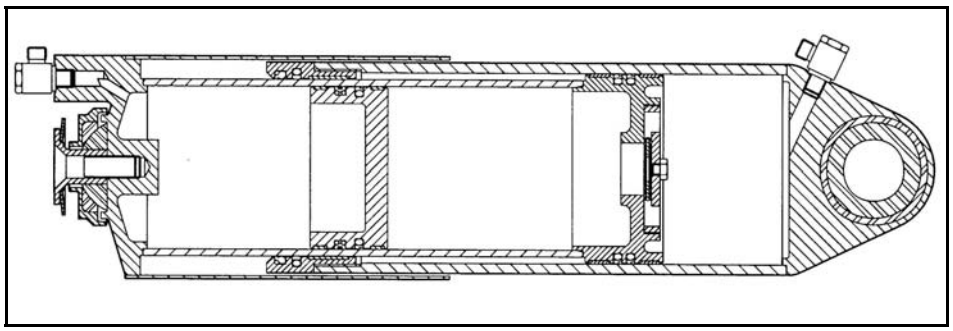

**Figure A-8: Hydrostrut cut through**

The hydrostut can also be equipped with additional features for increasing vehicle mobility. These includes variable ride height control (changing the amount of oil), load compensation (changing the amount of gas), suspension lock-out and roll and pitch compensation (interconnected struts).

## A.5 SAMM, subsidiary company of Peugeot

SAMM produces various type of hydro-pneumatic suspensions, mainly for the military market. The following products are available:

### a.) On-arm linear (translational) strut (for AFV and ATV)

- Vehicle weight: 10 to 30 ton
- Wheel travel: 330*mm*
- Natural frequency: 1*Hz*
- Damping factor: 0.4

- Maximum pressure: 420*bar*
- Weight: 25*kg*

### b.) Twin cylinder (for MBT)

- Vehicle weight: 50 ton
- Wheel travel: -125*mm*, +300*mm*, 425*mm* total
- Natural frequency: 0.9*Hz*
- Maximum pressure: 900*bar* (225*bar* nominal)
- Weight: 250*kg*

### c.) Mac Pherson (for wheeled vehicles)

- Static force per element: 25*kN*
- Maximum force: 110*kN*
- Static pressure: 50*bar*
- Maximum pressure: 220*bar*
- Total stroke: 280*mm*

## A.6 Teledyne Hydro-pneumatic Suspension System (HSS)

The Teledyne HSS was developed for use initially in military tracked vehicles. This suspension unit can be retrofitted to the Centurion, M60 and M48. Figure A-9 shows a cut through of the Teledyne HSS unit. From this figure, it can be seen that the damper valve is separated from the spring unit and that a floating piston arrangement is used. This suspension unit is successfully implemented on several military vehicles.

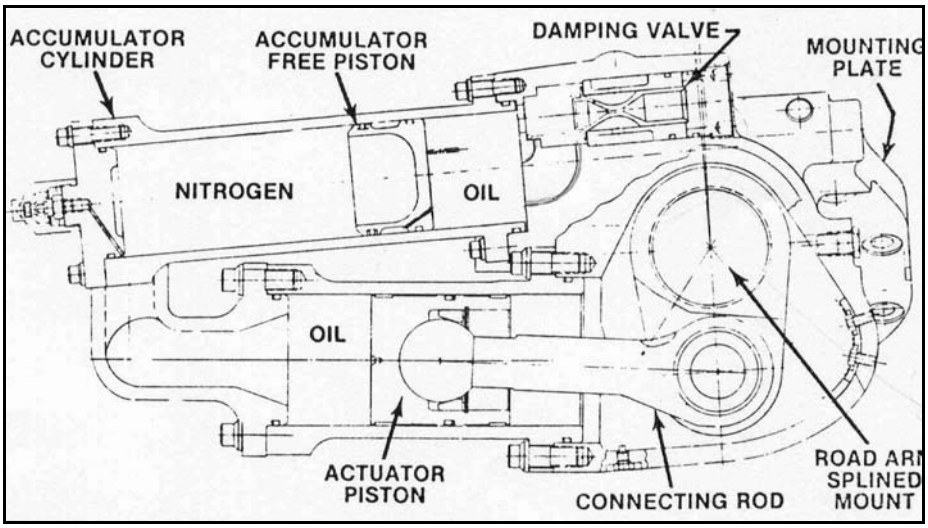


**Figure A-9: Teledyne HSS unit**

# APPENDIX B: M-FILES AND SIMULINK MODELS

## B.1 Simulink models

The strut characterisation and SDOF simulink models are supplied in this section. Table B-1 lists the figure numbers and Simulink model descriptions.

**Table B-1: Simulink sub-systems**

| Figure no. | Simulink model description |
|---|---|
| Figure B-1 | Characterisation main Simulink model |
| Figure B-2 | SDOF main Simulink model |
| Figure B-3 | SDOF spring sub-system |
| Figure B-4 | 0,3*l* Hydro-pneumatic spring sub-system |
| Figure B-5 | 0,3*l* BWR sub-system |
| Figure B-6 | 0,3*l* $C_v$ sub-system |
| Figure B-7 | 0,3*l* Specific volume sub-system |
| Figure B-8 | 0,3*l* Temperature differential equation |
| Figure B-9 | 0,3*l* Sub-system |
| Figure B-10 | 0,7*l* Hydro-pneumatic spring sub-system |
| Figure B-11 | 0,7*l* BWR sub-system |
| Figure B-12 | 0,7*l* $C_v$ sub-system |
| Figure B-13 | 0,7*l* Specific volume sub-system |
| Figure B-14 | 0,7*l* Temperature differential equation sub-system |
| Figure B-15 | 0,7l Sub-system |
| Figure B-16 | Spring trigger sub-system |
| Figure B-17 | Spring valve model sub-system |
| Figure B-18 | Damper valve model sub-system |

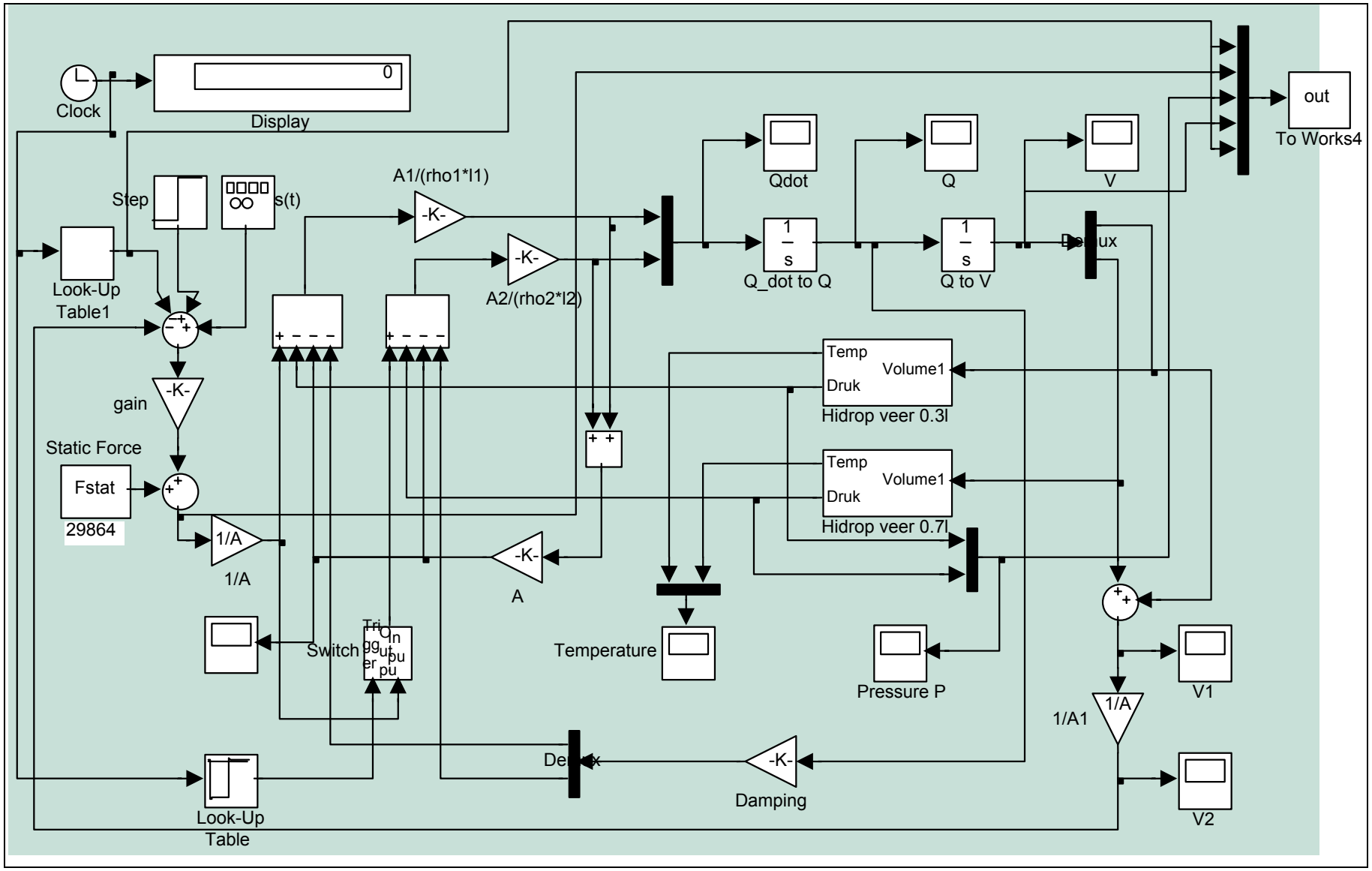


**Figure B-1: Characterisation main Simulink model**

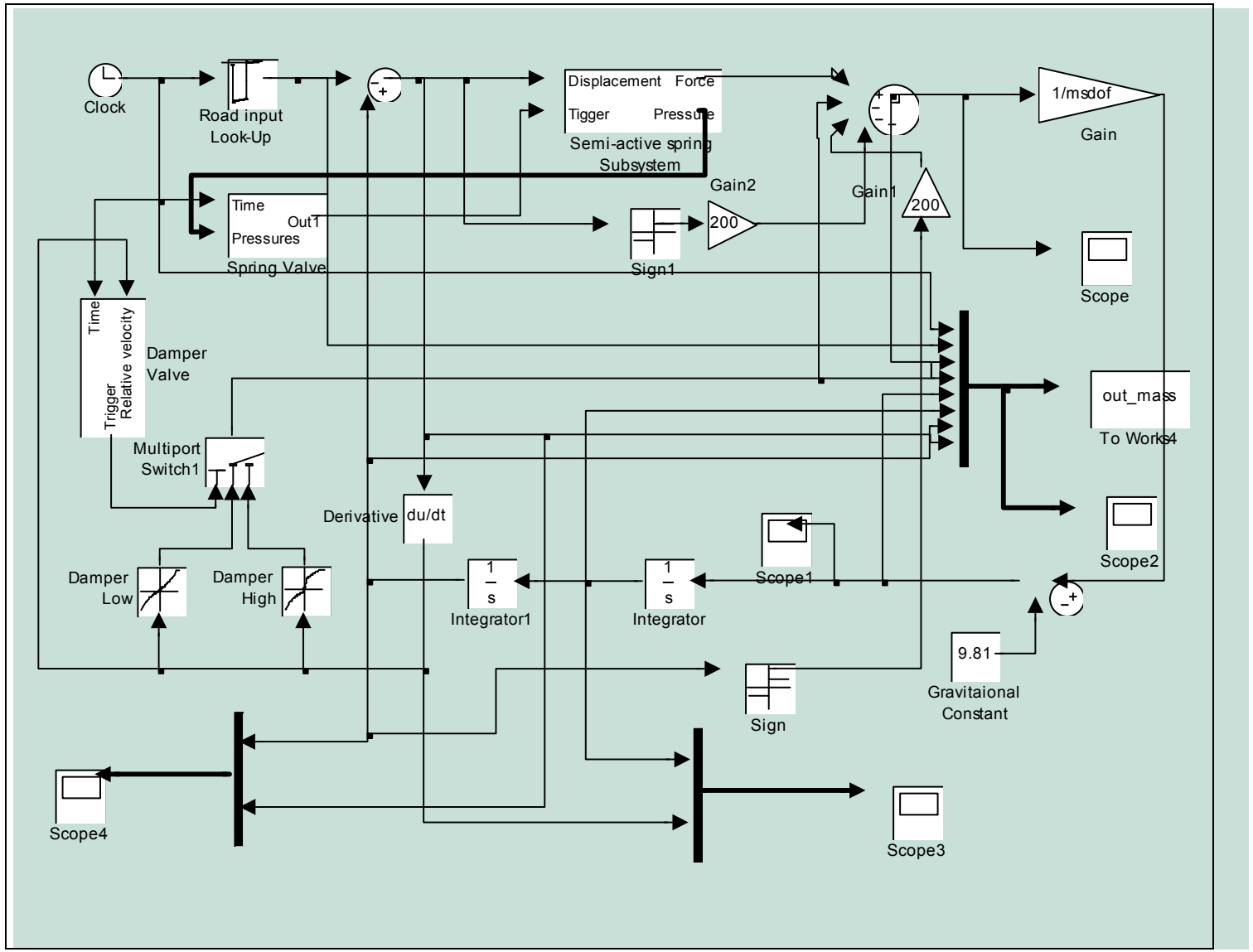


**Figure B-2: SDOF main Simulink model**

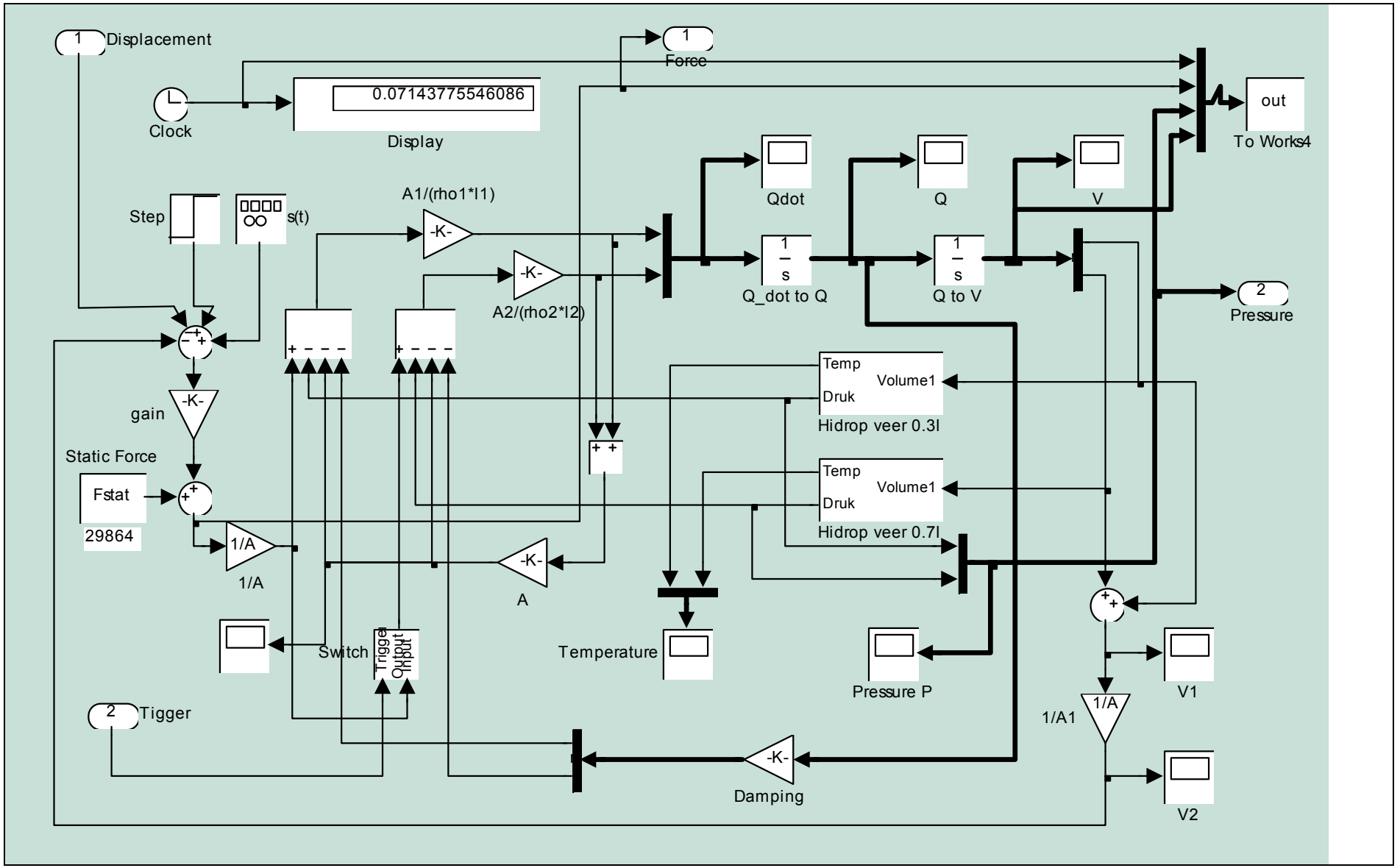


**Figure B-3: SDOF spring sub-system**

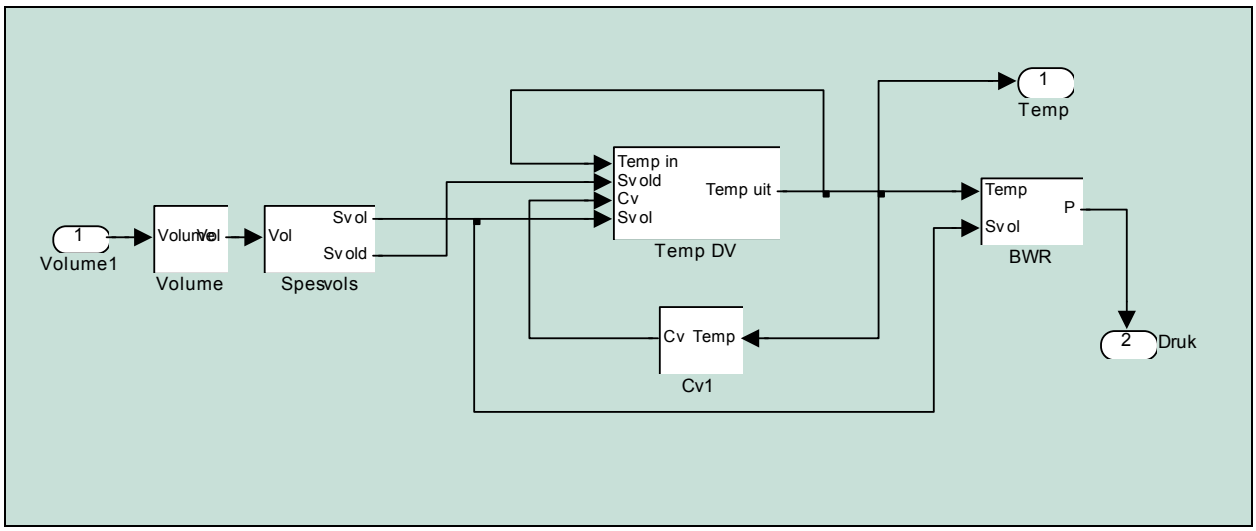


**Figure B-4: 0,3/ Hydro-pneumatic spring sub-system**

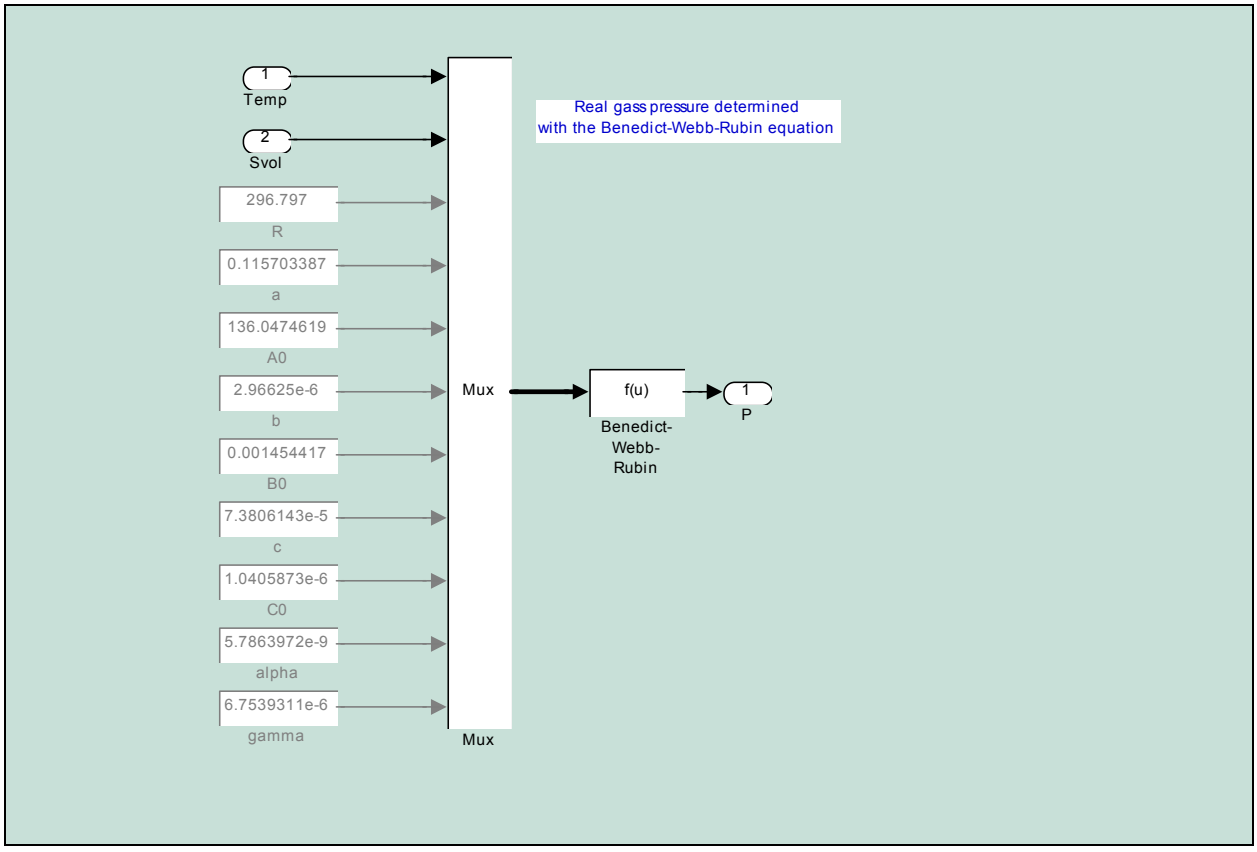


**Figure B-5: 0,3/ BWR sub-system**

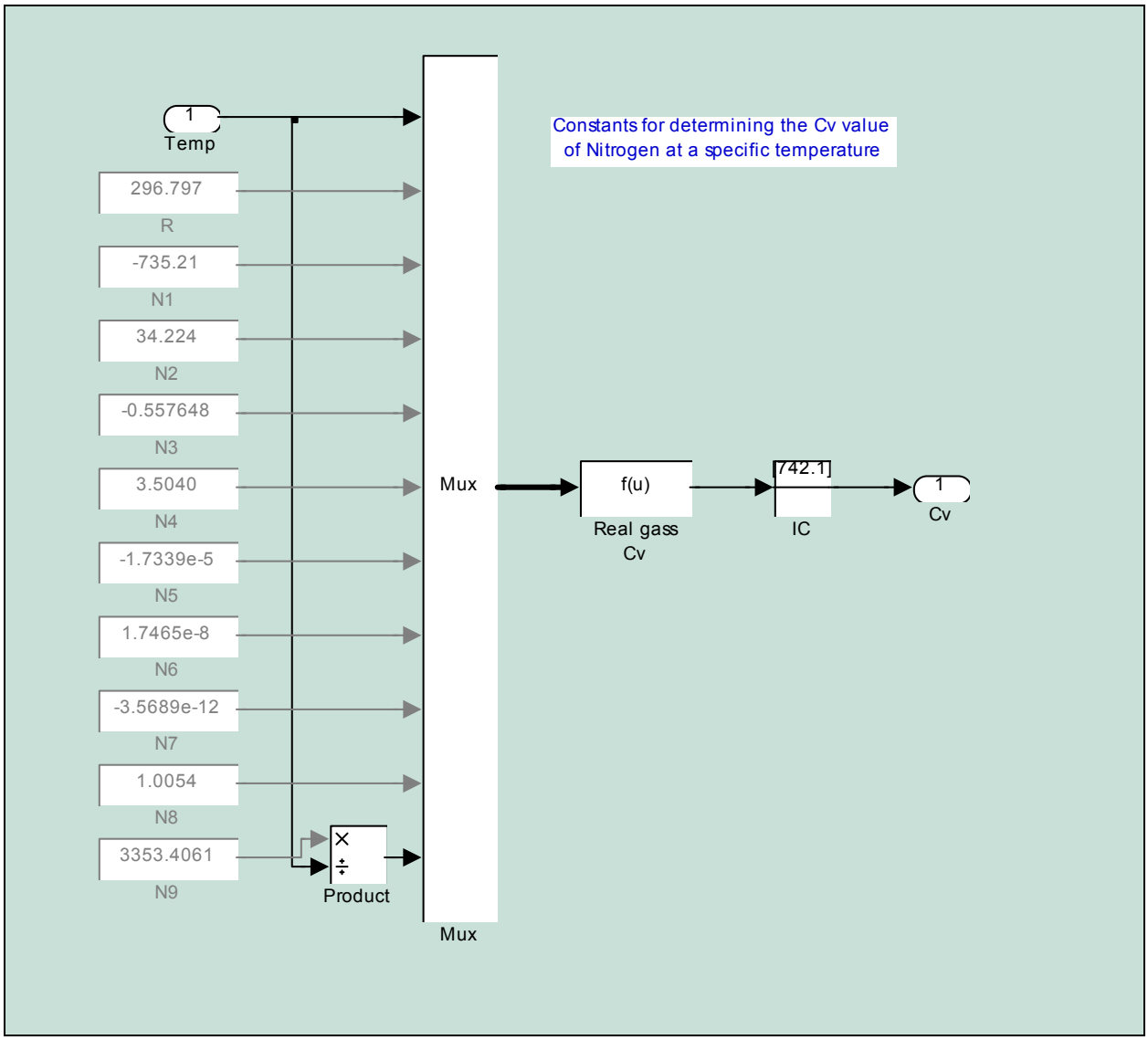


**Figure B-6: 0,3/ $C_v$ sub-system**

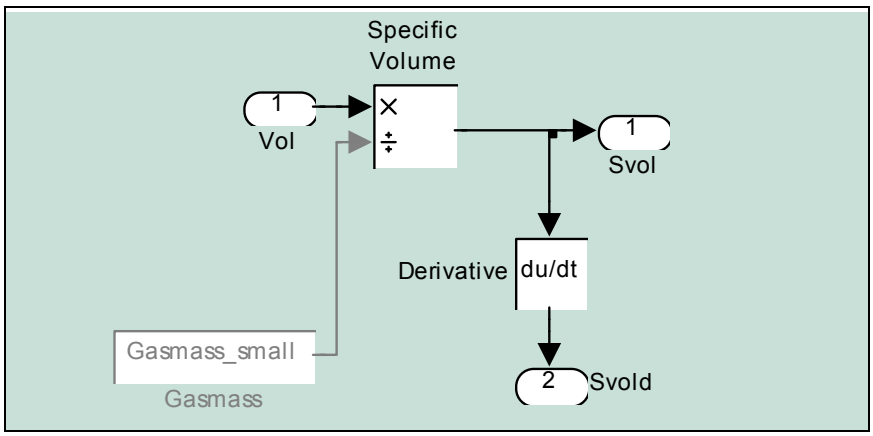


**Figure B-7: 0,3/ Specific volume sub-system**

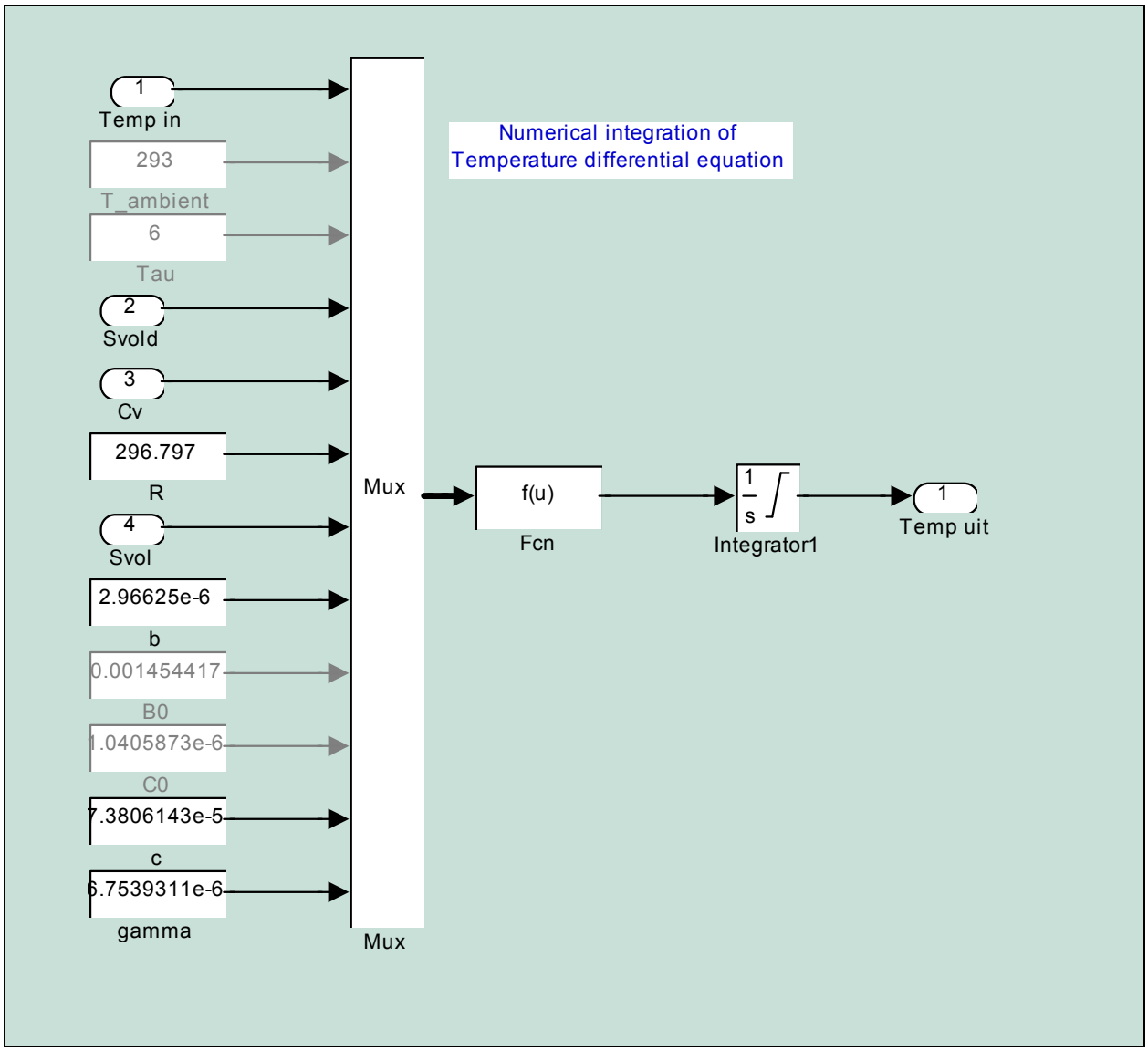


**Figure B-8: 0,3/ Temperature differential equation**

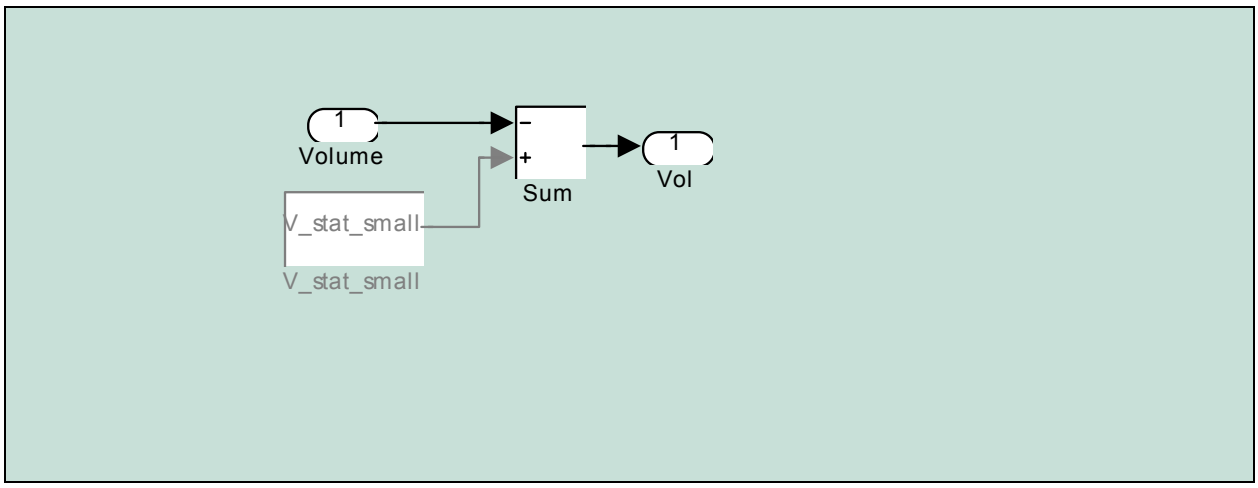


**Figure B-9: 0,3/ Sub-system**

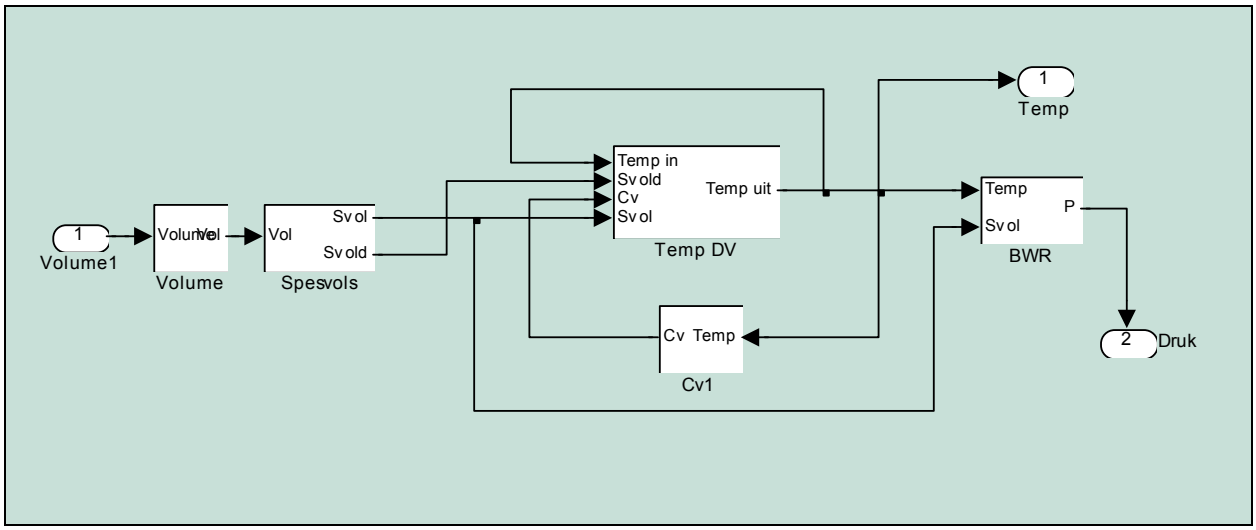


**Figure B-10: 0,7/ Hydro-pneumatic spring sub-system**

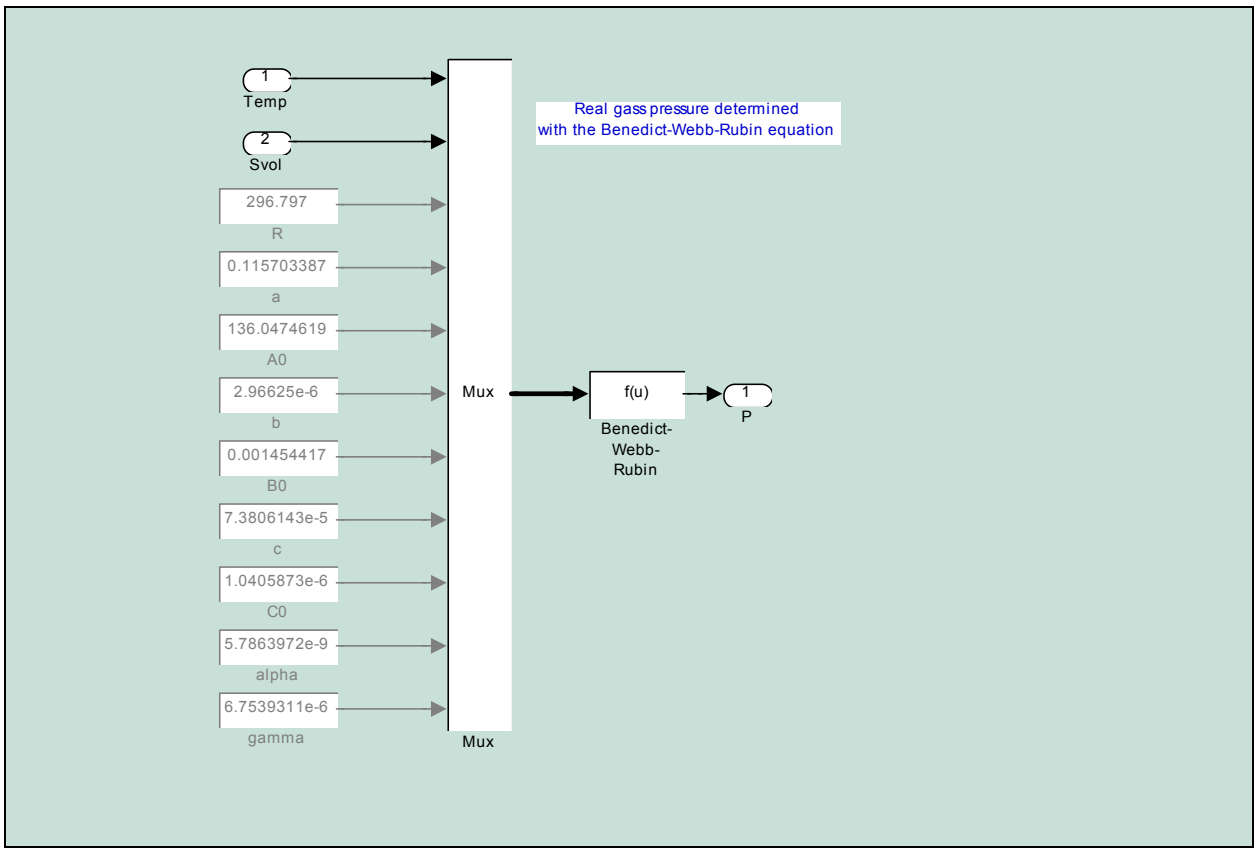


**Figure B-11: 0,7/ BWR sub-system**

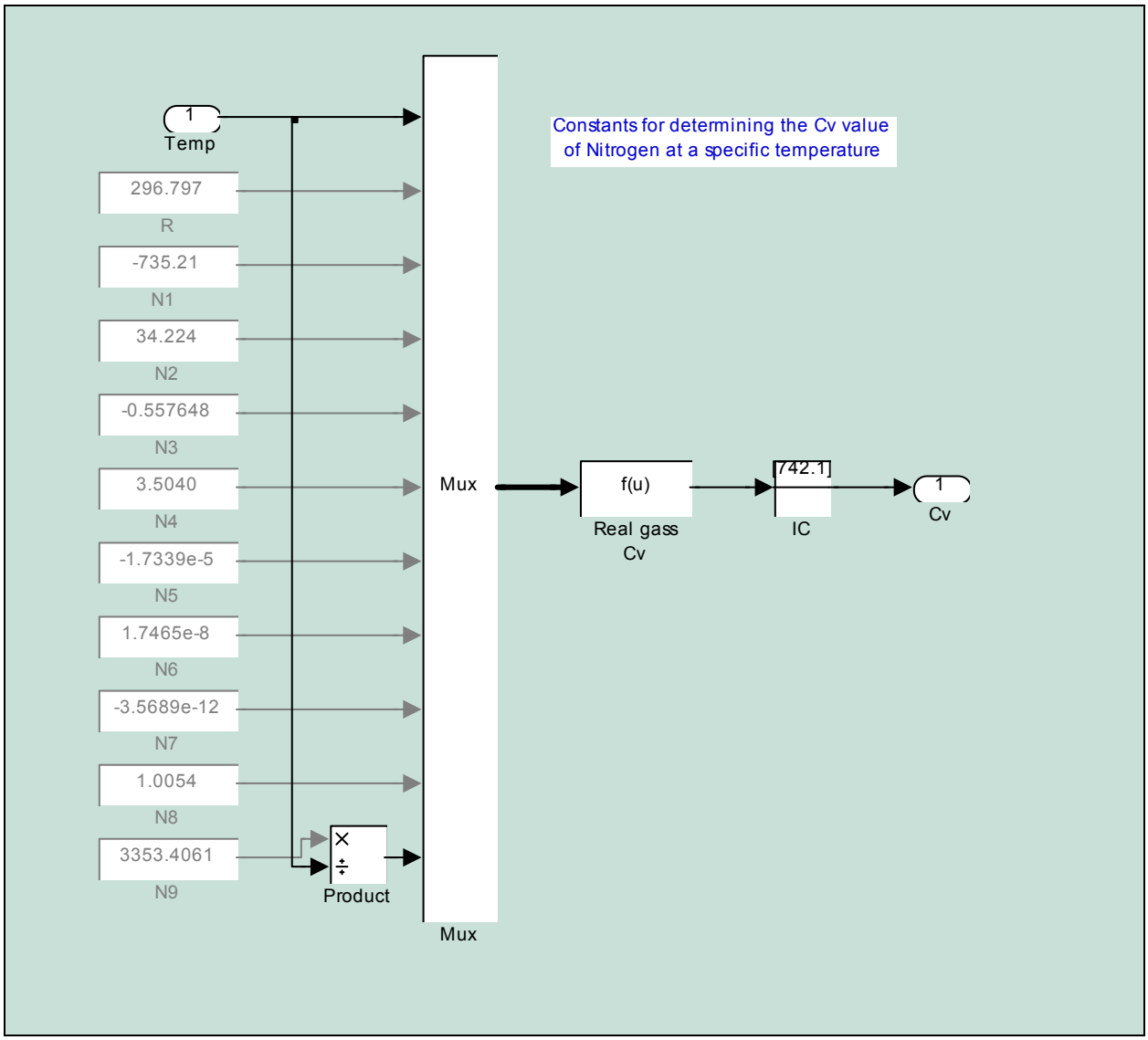


**Figure B-12: 0,7/ $C_v$ sub-system**

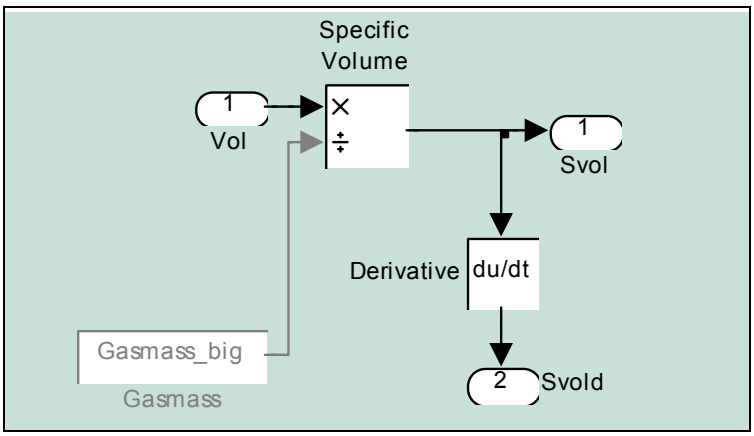


**Figure B-13: 0,7/ Specific volume sub-system**

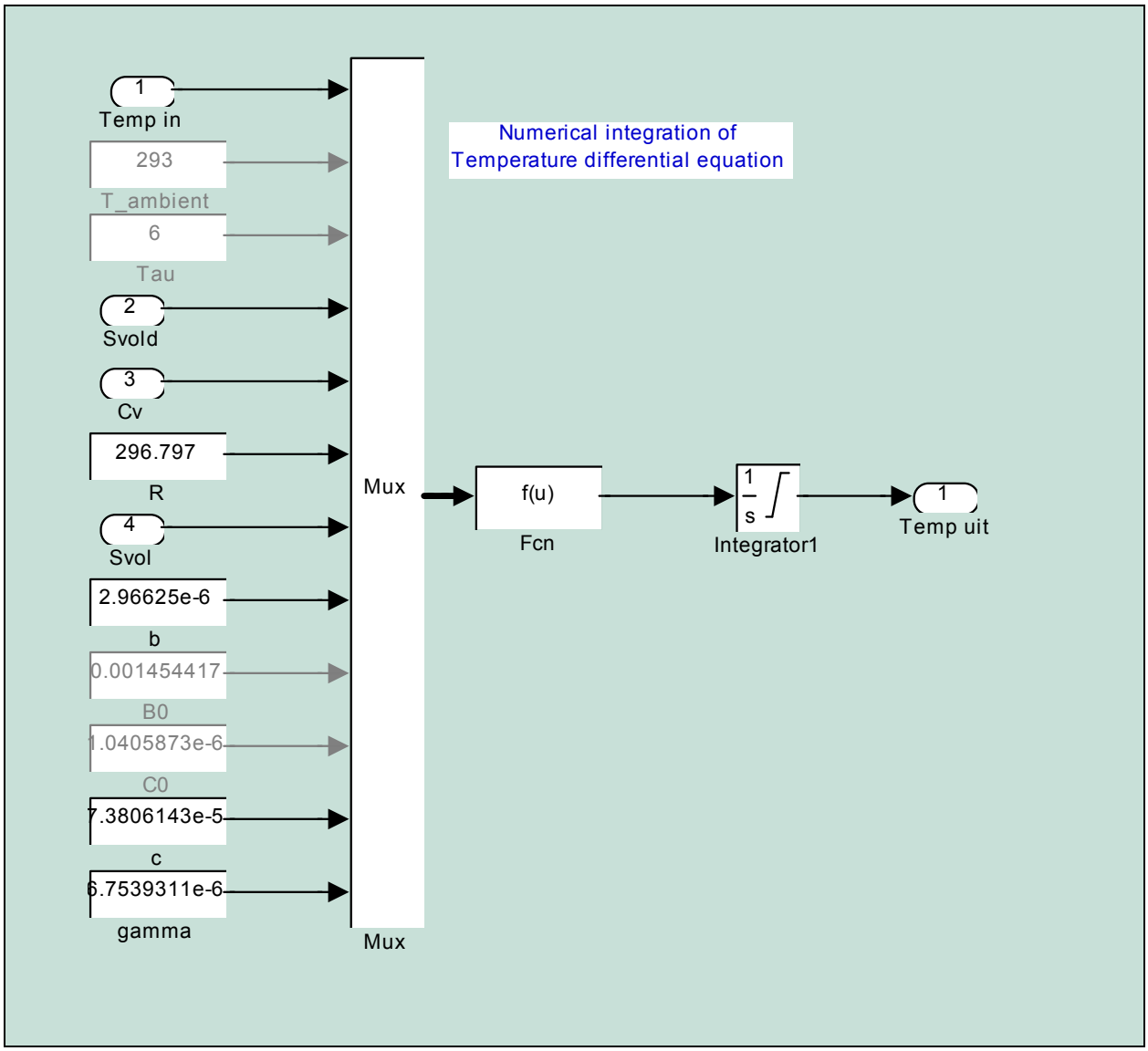


**Figure B-14: 0,7*l* Temperature differential equation sub-system**

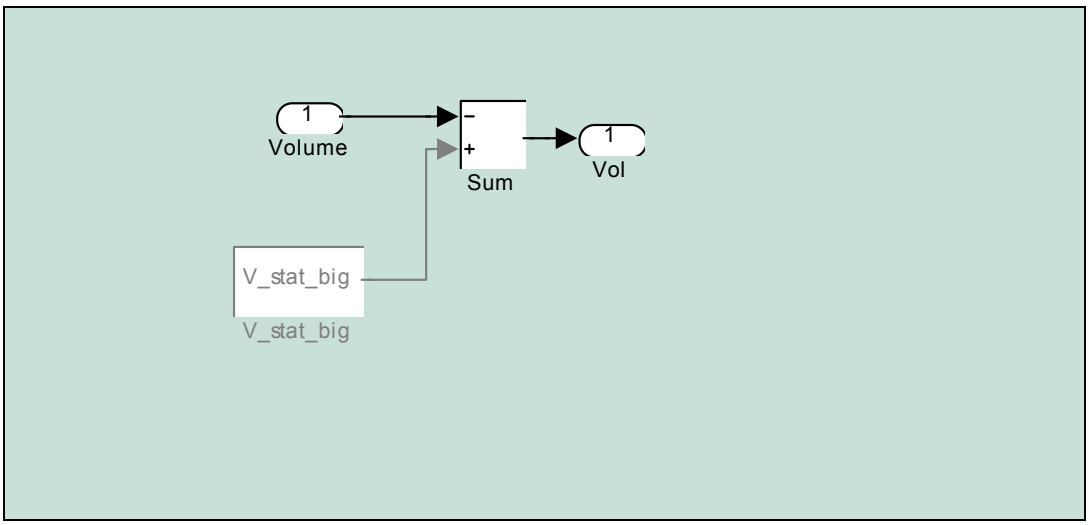


**Figure B-15: 0,7l Sub-system**

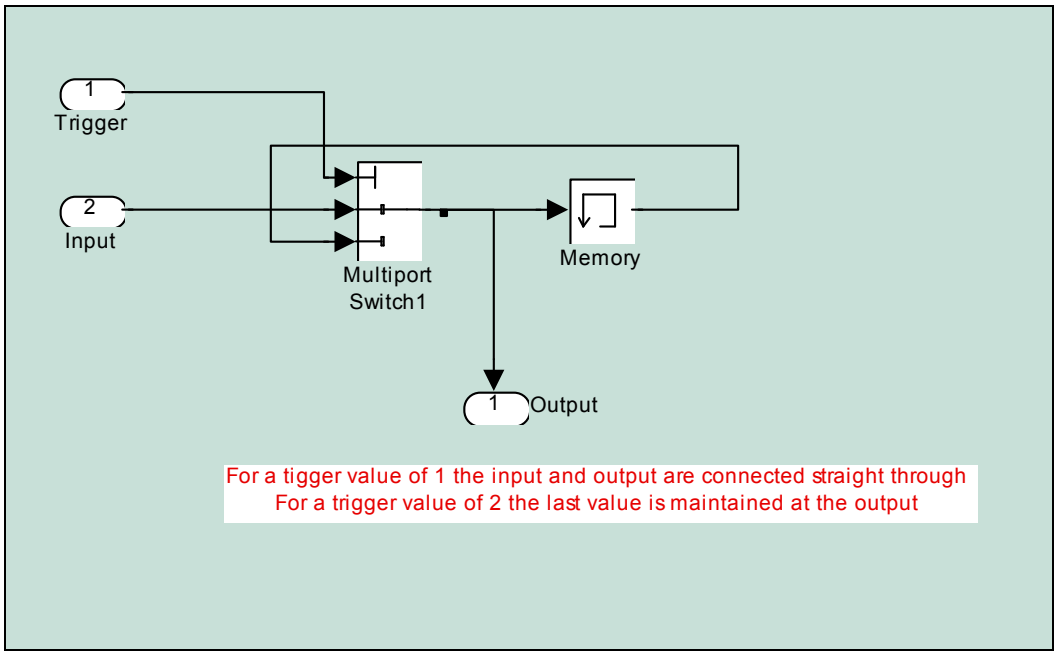


**Figure B-16: Spring trigger sub-system**

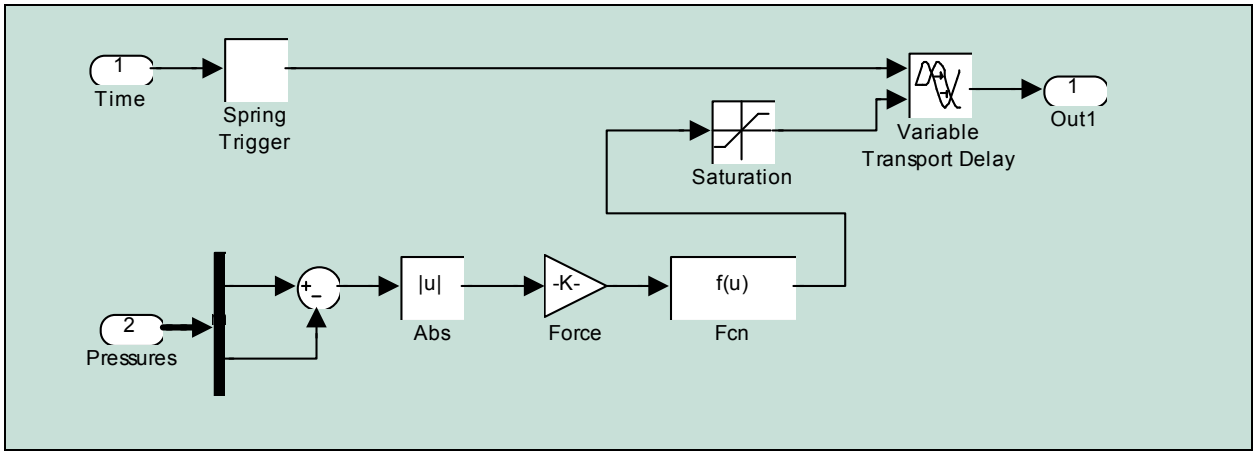


**Figure B-17: Spring valve model sub-system**

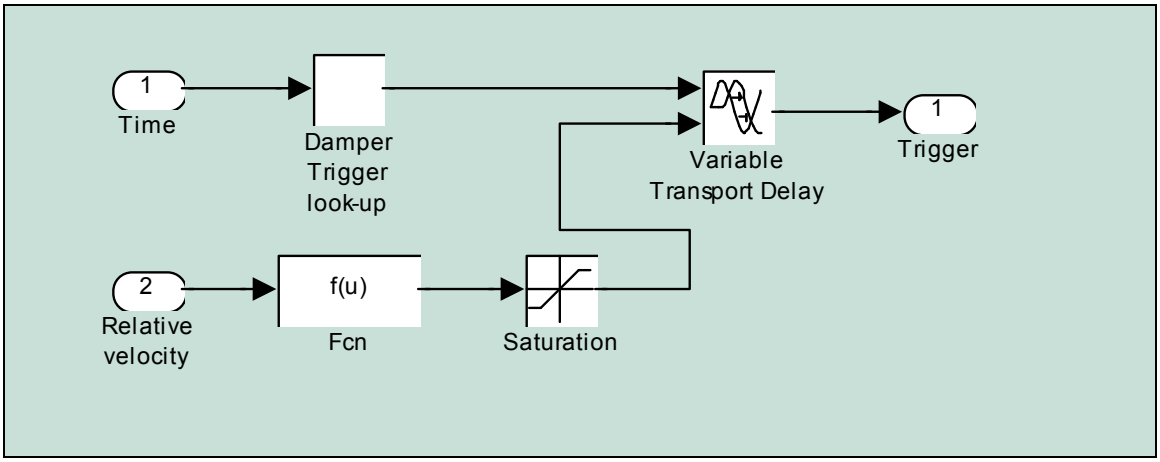


**Figure B-18: Damper valve model sub-system**

## B.2 M-files

Two m-files were used in conjunction with the characterisation simulations (hidropsim.m) and the SDOF simulation (sdofsim.m). Numerous other m-files were also used to reduce measured and simulated data. The two m-files hidropsim.m and sdofsim.m are supplied below.

### Hidropsim.m

```
% hidropsim.m
% 12/08/2000

clear all
close all

tic
%=== LOPIE KONSTANTES ===
load in_sig    %tfin = 1100
load in_sig2   %tfin = 110
load in_sig3   %tfin = 11
load karakteristieke.txt

%sinusvormige verplasing
in_sig4 = [karakteristieke(:,1) (-karakteristieke(:,2)/5)+2 karakteristieke(:,4)/1000];
q = find(in_sig4(:,2) <= 1.6);
w = find(in_sig4(:,2) >= 1.6);
in_sig4(q,2) = 1;
in_sig4(w,2) = 2;
in_sig4(1,2) = 1;

input_signal = in_sig4;
tfin = max(input_signal(:,1));
sample_time = .01;
%Fstat = 29864 - 8000 - 8000;
Fstat = 000;
Pstat = 6330000;
Tstat = 293;
%V_stat_small = 0.000365; %0.000345 vir in_sig en in_sig2
V_stat_small = 0.00033;      %0.00032 vir in_sig4
V_stat_big = 0.0007;          %0.00069 vir in_sig en in_sig2 0.0007 vir in_sig4
Gasmass_small = gasmassa([Pstat,V_stat_small,Tstat]);
Gasmass_big = gasmassa([Pstat,V_stat_big,Tstat]);
%=== LOPIE KONSTANTES ===

%=== MODEL KONSTANTES ===
rho0 = 917;
rho1 = 917;
rho2 = 917;
rho = 917;
l0 = .3;
l1 = .3;
l2 = .3;
m = 10;
A = pi/4*(.065^2); %Piston area
A0 = pi/4*(.0245^2); %Pyp0 area
A1 = pi/4*(.0245^2);   %Pyp1 area
A2 = pi/4*(.0245^2);   %Pyp2 area
n = 1.4;
k1 = (1.35*9000000*(pi/4*.063^2)^2)/(.0003);
k2 = (1.35*9000000*(pi/4*.063^2)^2)/(.0007);
k1 = k1/(pi/4*.063^2)^2;
k2 = k2/(pi/4*.063^2)^2;
%=== MODEL KONSTANTES ===

%=== SIMULASIE ===
sim('chris1_1');
%=== SIMULASIE ===

%=== VERWERK RESULTATE ===
cd gemeet
load klepres4.txt
cd ..
```

```
t = linspace(0,length(klepres4(:,1)),length(klepres4(:,1)));

%plot(t,-klepres4(:,2),t,-klepres4(:,1)+25,out(:,1),out(:,2)/1000);
out([1 2 3],2) = 0;
karakteristieke(85:168,3) = karakteristieke(85:168,3)+2.5;
plot(karakteristieke(:,4),-karakteristieke(:,3),out(:,7)*1000,out(:,2)/1000);
grid on
zoom on
%=== VERWERK RESULTATE ===
toc
```

## SDOFsim.m

```
% SDOFsim.m
% 12/08/2000

clear all
close all

tic
%=== LOPIE KONSTANTES ===
load dempkar
dempkar(:,2) = dempkar(:,2) * 1000;
dempkar(:,4) = dempkar(:,4) * 1000;

plot(dempkar(:,1),dempkar(:,2),'*',dempkar(:,3),dempkar(:,4),'*')
hold on
dempkar(:,2) = dempkar(:,2)-dempkar(:,1)*745.3;
dempkar(1:28,2) = dempkar(1:28,2)+2500;
dempkar(:,2) = dempkar(:,2)*1;
dempkar(:,4) = dempkar(:,4)*1;
plot(dempkar(:,1),dempkar(:,2),'*r',dempkar(:,3),dempkar(:,4),'*y')
grid on
zoom on

filename = {'trp30_1','trp30_2','trp30_3','trp30_4','trp30_5','trp30_6','trp30_7','trp30_8',...
      'belg1','belg2','belg3','belg4','belg5','belg6','belg7','belg8','belg9','belg10',...
      'sin15_1','sin15_2','sin15_3','sin15_4','sin15_5','sin15_6','sin15_7','sin15_8',...
      'trp60_1','trp60_2','trp60_3','trp60_4'};
% TRAP30 1 - 8
% BELG 9 - 18
% SINE 19 - 26
% TRAP60 27 - 30

for i = 1:30
   i
   cd gemeet
   switch i
   case 1
      load trp30_1.txt
      file = trp30_1;
   case 2
      load trp30_2.txt
      file = trp30_2;
   case 3
      load trp30_3.txt
      file = trp30_3;
   case 4
      load trp30_4.txt
      file = trp30_4;
   case 5
      load trp30_5.txt
      file = trp30_5;
   case 6
      load trp30_6.txt
      file = trp30_6;
   case 7
      load trp30_7.txt
      file = trp30_7;
   case 8
      load trp30_8.txt
      file = trp30_8;
   case 9
```

```
      load belg1.txt
      file = belg1;
   case 10
      load belg2.txt
      file = belg2;
   case 11
      load belg3.txt
      file = belg3;
   case 12
      load belg4.txt
      file = belg4;
   case 13
      load belg5.txt
      file = belg5;
   case 14
      load belg6.txt
      file = belg6;
   case 15
      load belg7.txt
      file = belg7;
   case 16
      load belg8.txt
      file = belg8;
   case 17
      load belg9.txt
      file = belg9;
   case 18
      load belg10.txt
      file = belg10;
   case 19
      load sin15_1.txt
      file = sin15_1;
   case 20
      load sin15_2.txt
      file = sin15_2;
   case 21
      load sin15_3.txt
      file = sin15_3;
   case 22
      load sin15_4.txt
      file = sin15_4;
   case 23
      load sin15_5.txt
      file = sin15_5;
   case 24
      load sin15_6.txt
      file = sin15_6;
   case 25
      load sin15_7.txt
      file = sin15_7;
   case 26
      load sin15_8.txt
      file = sin15_8;
   case 27
      load trp60_1.txt
      file = trp60_1;
   case 28
      load trp60_2.txt
      file = trp60_2;
   case 29
      load trp60_3.txt
      file = trp60_3;
   case 30
      load trp60_4.txt
      file = trp60_4;
   end
cd ..

input_signal = [file(:,1) file(:,2)/1000 file(:,8)+1 file(:,9)+1];
input_signal(1:40,4) = ones(40,1);
input_signal(1:40,2) = zeros(40,1);

figure(2)
%plot(input_signal(:,1),input_signal(:,2:4));
plot(input_signal(:,1),input_signal(:,2),'LineWidth',1.5);
zoom on
grid on
```

```
xlabel('Time [s]')
ylabel('Displacement [m]')
title('Step response actuator displacement')

tfin = max(file(:,1));
sample_time = .01;
%Fstat = 29864 - 8000 - 8000;
msdof = 3186;
Fstat = 000;
Pstat = 9420000;
Tstat = 293;
V_stat_small = 0.00035;    %0.000345 vir in_sig en in_sig2
V_stat_big = 0.0006;       %0.00069 vir in_sig en in_sig2
Gasmass_small = gasmassa([Pstat,V_stat_small,Tstat]);
Gasmass_big = gasmassa([Pstat,V_stat_big,Tstat]);
%=== LOPIE KONSTANTES ===

%=== MODEL KONSTANTES ===
rho0 = 917;
rho1 = 917;
rho2 = 917;
rho = 917;
l0 = .3;
l1 = .3;
l2 = .3;
m = 10;
A = pi/4*(.065^2); %Piston area
A0 = pi/4*(.0245^2); %Pyp0 area
A1 = pi/4*(.0245^2);   %Pyp1 area
A2 = pi/4*(.0245^2);   %Pyp2 area
n = 1.4;
k1 = (1.35*9000000*(pi/4*.063^2)^2)/(.0003);
k2 = (1.35*9000000*(pi/4*.063^2)^2)/(.0007);
k1 = k1/(pi/4*.063^2)^2;
k2 = k2/(pi/4*.063^2)^2;
%=== MODEL KONSTANTES ===

%=== SIMULASIE ===
%sim('chris2_2');
sim('chris2_4')
%=== SIMULASIE ===

%=== VERWERK RESULTATE ===
switch i
   case 1
      trp30_1_out = out_mass;
      save trp30_1_out trp30_1_out
   case 2
      trp30_2_out = out_mass;
      save trp30_2_out trp30_2_out
   case 3
      trp30_3_out = out_mass;
      save trp30_3_out trp30_3_out
   case 4
      trp30_4_out = out_mass;
      save trp30_4_out trp30_4_out
   case 5
      trp30_5_out = out_mass;
      save trp30_5_out trp30_5_out
   case 6
      trp30_6_out = out_mass;
      save trp30_6_out trp30_6_out
   case 7
      trp30_7_out = out_mass;
      save trp30_7_out trp30_7_out
   case 8
      trp30_8_out = out_mass;
      save trp30_8_out trp30_8_out
   case 9
      belg1_out = out_mass;
      save belg1_out belg1_out
   case 10
      belg2_out = out_mass;
      save belg2_out belg2_out
   case 11
      belg3_out = out_mass;
      save belg3_out belg3_out
```

```
   case 12
      belg4_out = out_mass;
      save belg4_out belg4_out
   case 13
      belg5_out = out_mass;
      save belg5_out belg5_out
   case 14
      belg6_out = out_mass;
      save belg6_out belg6_out
   case 15
      belg7_out = out_mass;
      save belg7_out belg7_out
   case 16
      belg8_out = out_mass;
      save belg8_out belg8_out
   case 17
      belg9_out = out_mass;
      save belg9_out belg9_out
   case 18
      belg10_out = out_mass;
      save belg10_out belg10_out
   case 19
      sin15_1_out = out_mass;
      save sin15_1_out sin15_1_out
   case 20
      sin15_2_out = out_mass;
      save sin15_2_out sin15_2_out
   case 21
      sin15_3_out = out_mass;
      save sin15_3_out sin15_3_out
   case 22
      sin15_4_out = out_mass;
      save sin15_4_out sin15_4_out
   case 23
      sin15_5_out = out_mass;
      save sin15_5_out sin15_5_out
   case 24
      sin15_6_out = out_mass;
      save sin15_6_out sin15_6_out
   case 25
      sin15_7_out = out_mass;
      save sin15_7_out sin15_7_out
   case 26
      sin15_8_out = out_mass;
      save sin15_8_out sin15_8_out
   case 27
      trp60_1_out = out_mass;
      save trp60_1_out trp60_1_out
   case 28
      trp60_2_out = out_mass;
      save trp60_2_out trp60_2_out
   case 29
      trp60_3_out = out_mass;
      save trp60_3_out trp60_3_out
   case 30
      trp60_4_out = out_mass;
      save trp60_4_out trp60_4_out
   end
%=== VERWERK RESULTATE ===
end
toc
```

# APPENDIX C: MATHEMATICAL FLOW MODEL

The derivation of the hydraulic flow model is supplied in this appendix.

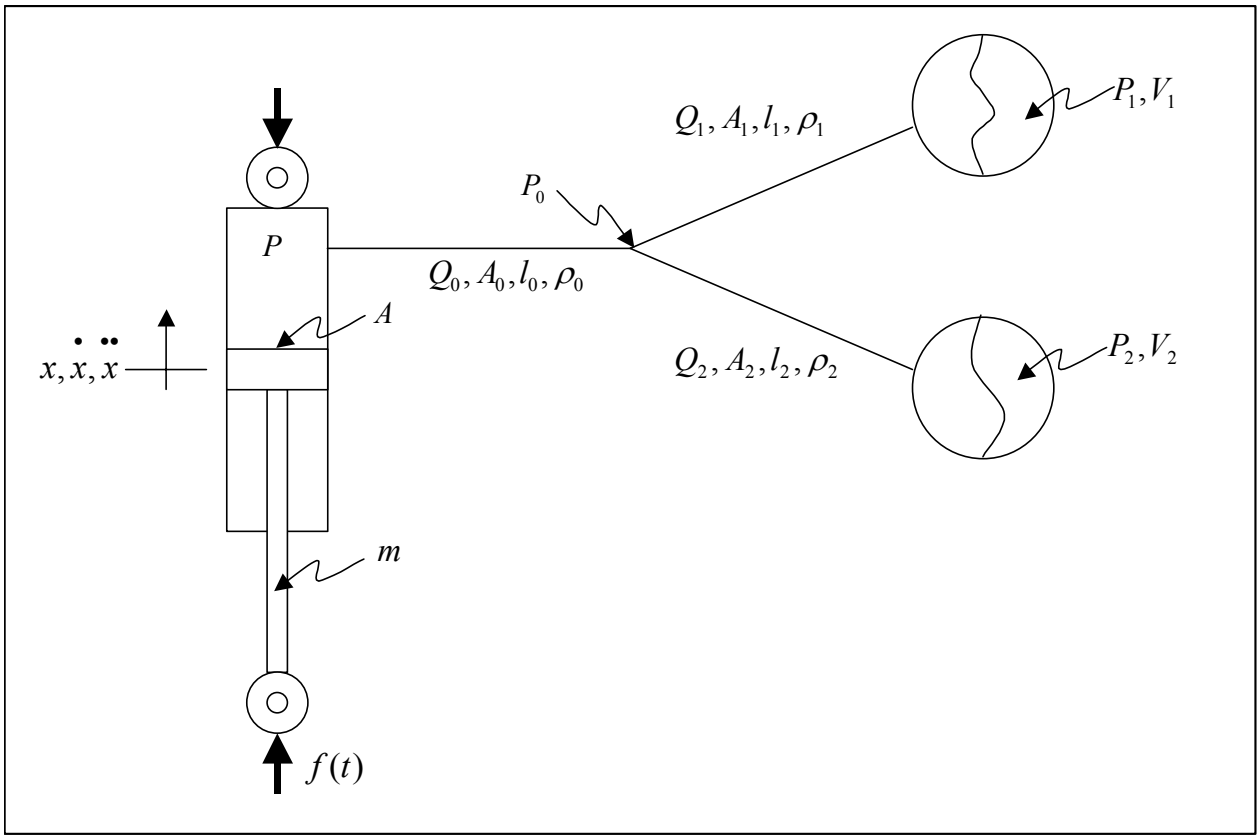


The following five states are defined:

$$x_1 = V_1$$
$$x_2 = V_2$$
$$x_3 = Q_0 = Q_1 + Q_2$$
$$x_4 = Q_1$$
$$x_5 = Q_2$$

therefore

$$\dot{x}_1 = \dot{V}_1 = Q_1 = x_4$$
$$\dot{x}_2 = \dot{V}_2 = Q_2 = x_5$$

The relationship between strut piston displacement and flow is:

$$A\dot{x} = Q_0 = Q_1 + Q_2$$

The force balance on the strut piston is as follows:

$$m\ddot{x} = f(t) - AP$$

but

$$\ddot{x} = \frac{\dot{Q}_0}{A} = \frac{1}{A}(\dot{Q}_1 + \dot{Q}_2)$$

therefore

$$\mathrm{m}/\mathrm{A}\,(\dot{Q}_1 + \dot{Q}_2) = f(t) - AP$$

$$\because \mathrm{m}/\mathrm{A}\,\dot{Q}_0 = f(t) - AP$$

Rearranging the above equation gives:

$$\mathrm{P} = \mathrm{f(t)}/\mathrm{A} - m/A^2\,\dot{Q}_0 \qquad \ldots(1)$$

Considering the oil in the pipes, the following equations can be written:

According to Newton's second law

$$\sum \mathrm{F} = \mathrm{m}\,\ddot{\mathrm{x}}$$

Therefore

$$\rho_0 l_0\,\dot{Q}_0 = A_0(P - P_0) \qquad \ldots(2)$$

$$\rho_1 l_1\,\dot{Q}_1 = A_1(P_0 - P_1) \qquad \ldots(3)$$

$$\rho_2 l_2\,\dot{Q}_2 = A_2(P_0 - P_2) \qquad \ldots(4)$$

Replace P in (2) with (1)

$$\rho_0 l_0\,\dot{Q}_0 = A_0\left(f(t)/A - m/A^2\,\dot{Q}_0 - P_0\right)$$

Rearranging the above equation gives:

$$P_0 = f(t)/A - \rho_0 l_0\,\dot{Q}_0/A_0 - m/A^2\,\dot{Q}_0$$

Substitute the above equation into equations (3) and (4)

From (3)

$$\rho_1 l_1 \dot{Q}_1 = A_1 \left( \rho_0 l_0 \dot{Q}_0 / A_0 + f(t)/A - m/A^2 \, \dot{Q}_0 - P_1 \right)$$

From (4)

$$\rho_2 l_2 \dot{Q}_2 = A_2 \left( \rho_0 l_0 \dot{Q}_0 / A_0 + f(t)/A - m/A^2 \, \dot{Q}_0 - P_2 \right)$$

Rearrange the above to two equations to isolate the flow terms:

Therefore:

$$\frac{\rho_1 l_1}{A_1} \dot{Q}_1 + \left( \frac{\rho_0 l_0}{A_0} + \frac{m}{A^2} \right) \dot{Q}_0 = \frac{f(t)}{A} - P_1$$

and

$$\frac{\rho_2 l_2}{A_2} \dot{Q}_2 + \left( \frac{\rho_0 l_0}{A_0} + \frac{m}{A^2} \right) \dot{Q}_0 = \frac{f(t)}{A} - P_2$$

These equations can be written in state-space format as follows:

$$\begin{bmatrix} 1 & 0 & 0 & 0 & 0 \\ 0 & 1 & 0 & 0 & 0 \\ 0 & 0 & \left( \frac{\rho_0 l_0}{A_0} + \frac{m}{A^2} \right) & \frac{\rho_1 l_1}{A_1} & 0 \\ 0 & 0 & \left( \frac{\rho_0 l_0}{A_0} + \frac{m}{A^2} \right) & 0 & \frac{\rho_2 l_2}{A_2} \\ 0 & 0 & 0 & 0 & 0 \end{bmatrix} \begin{bmatrix} \dot{V}_1 \\ \dot{V}_2 \\ \dot{Q}_0 \\ \dot{Q}_1 \\ \dot{Q}_2 \end{bmatrix} = \begin{bmatrix} 0 & 0 & 0 & 1 & 0 \\ 0 & 0 & 0 & 0 & 1 \\ 0 & 0 & 0 & 0 & 0 \\ 0 & 0 & 0 & 0 & 0 \\ 0 & 0 & 0 & 0 & 0 \end{bmatrix} \begin{bmatrix} V_1 \\ V_2 \\ Q_0 \\ Q_1 \\ Q_2 \end{bmatrix} + \begin{bmatrix} 0 \\ 0 \\ 1/A \\ 1/A \\ 0 \end{bmatrix} f(t) + \begin{bmatrix} 0 \\ 0 \\ P_1 \\ P_2 \\ 0 \end{bmatrix}$$

with the algebraic equation

$$Q_0 = Q_1 + Q_2$$

# APPENDIX D: TEST RESULTS

## D.1 Step response

The results for the step response tests are presented in this paragraph. The spring/damper configuration definitions are supplied in Table D-1.

**Table D-1: Spring/damper configuration for step response tests**

| Figure number | Input | Spring state | Damper state |
|---|---|---|---|
| Figure D-1 | 30mm step | OFF | OFF |
| Figure D-2 | 30mm step | ON | OFF |
| Figure D-3 | 30mm step | OFF | ON |
| Figure D-4 | 30mm step | ON | ON |
| Figure D-5 | 30mm step | ON | Karnopp |
| Figure D-6 | 30mm step | OFF | Karnopp |
| Figure D-7 | 30mm step | ON | Hölscher & Huang |
| Figure D-8 | 30mm step | Maximum strut force summary | |
| Figure D-10 | 30mm step | Maximum strut displacement summary | |
| Figure D-11 | 30mm step | Maximum sprung mass acceleration summary | |

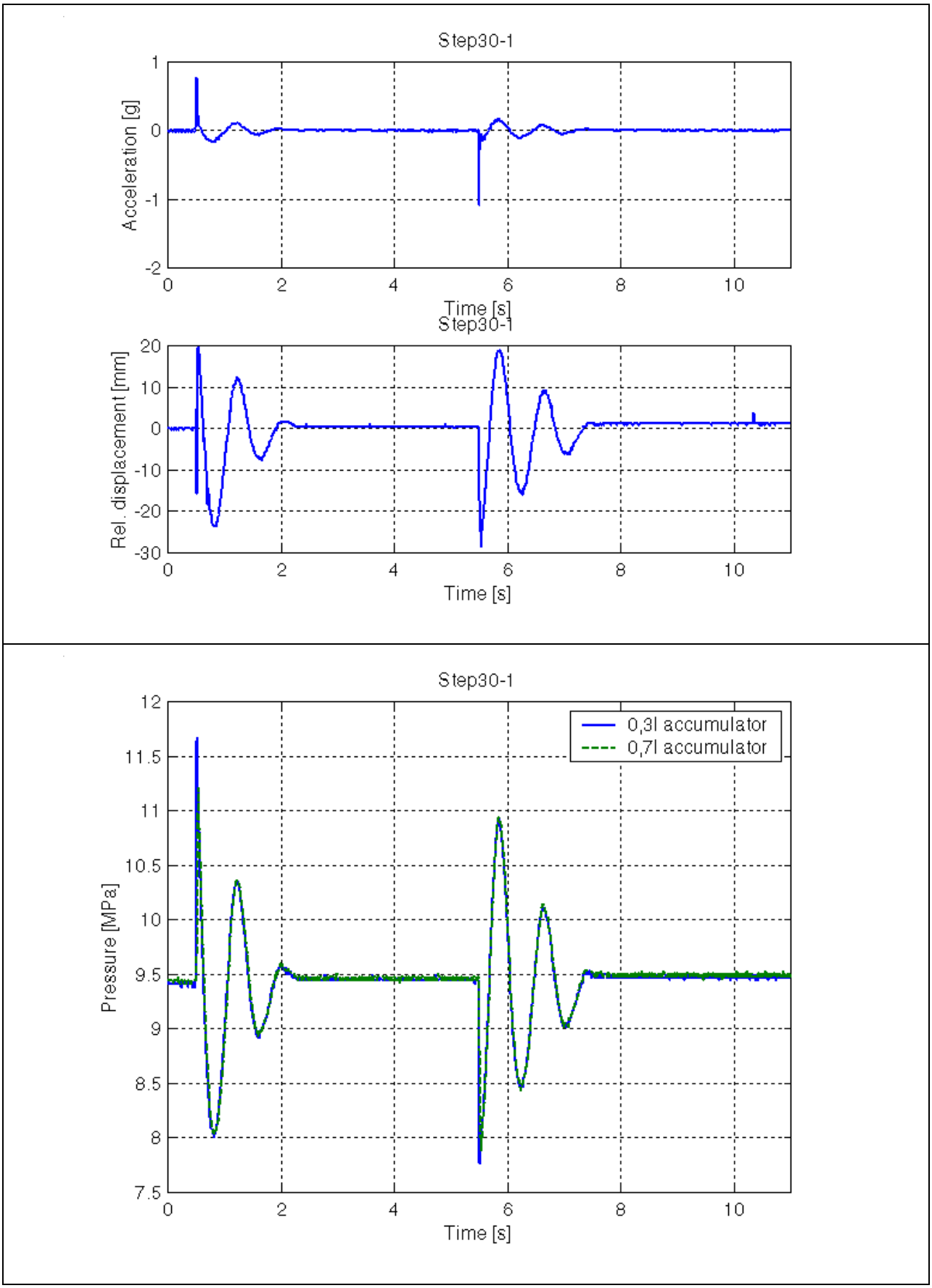


**Figure D-1: 30mm step response (Spring – OFF, Damper - OFF)**

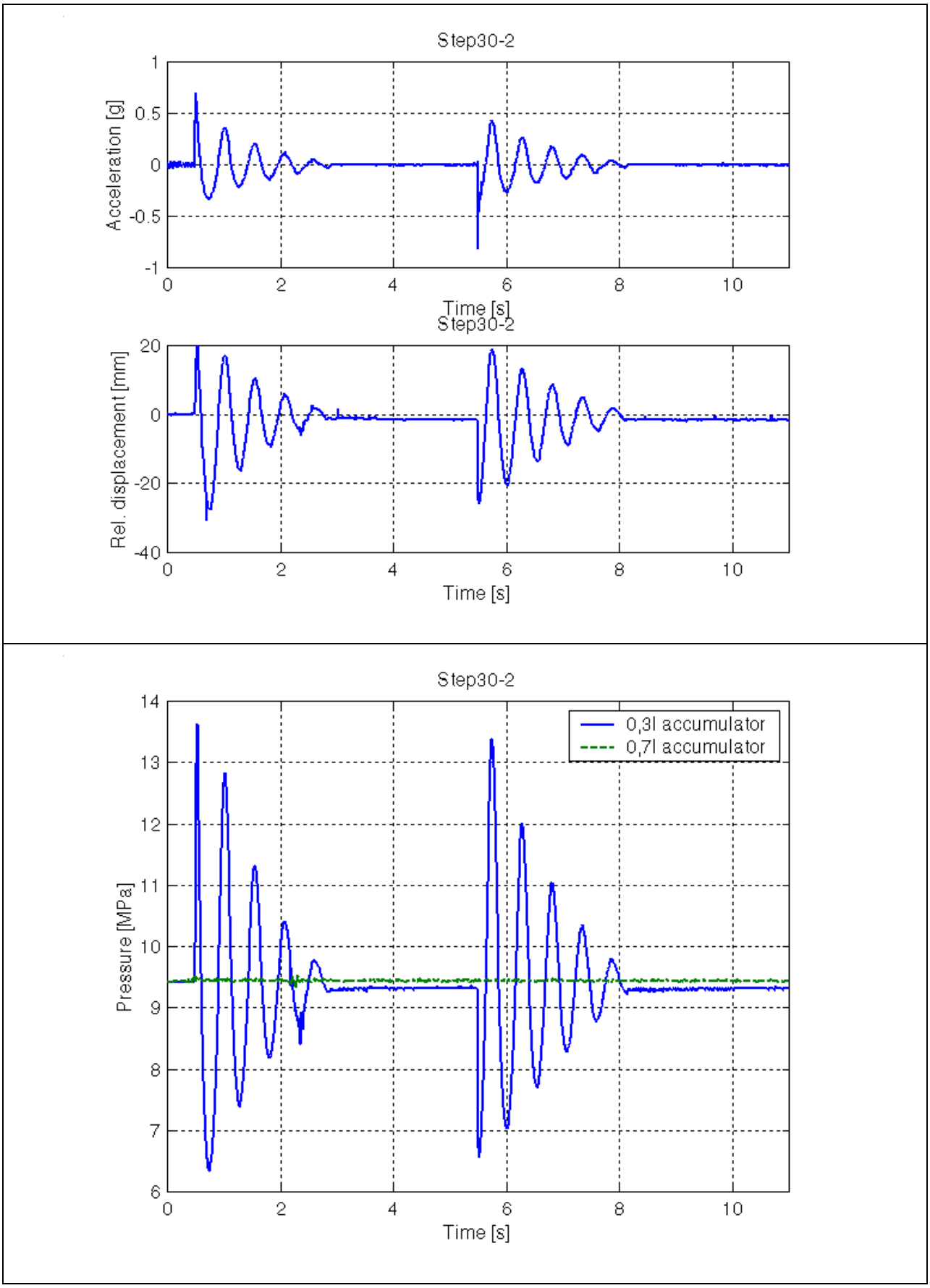


**Figure D-2: 30mm step response (Spring – ON, Damper - OFF)**

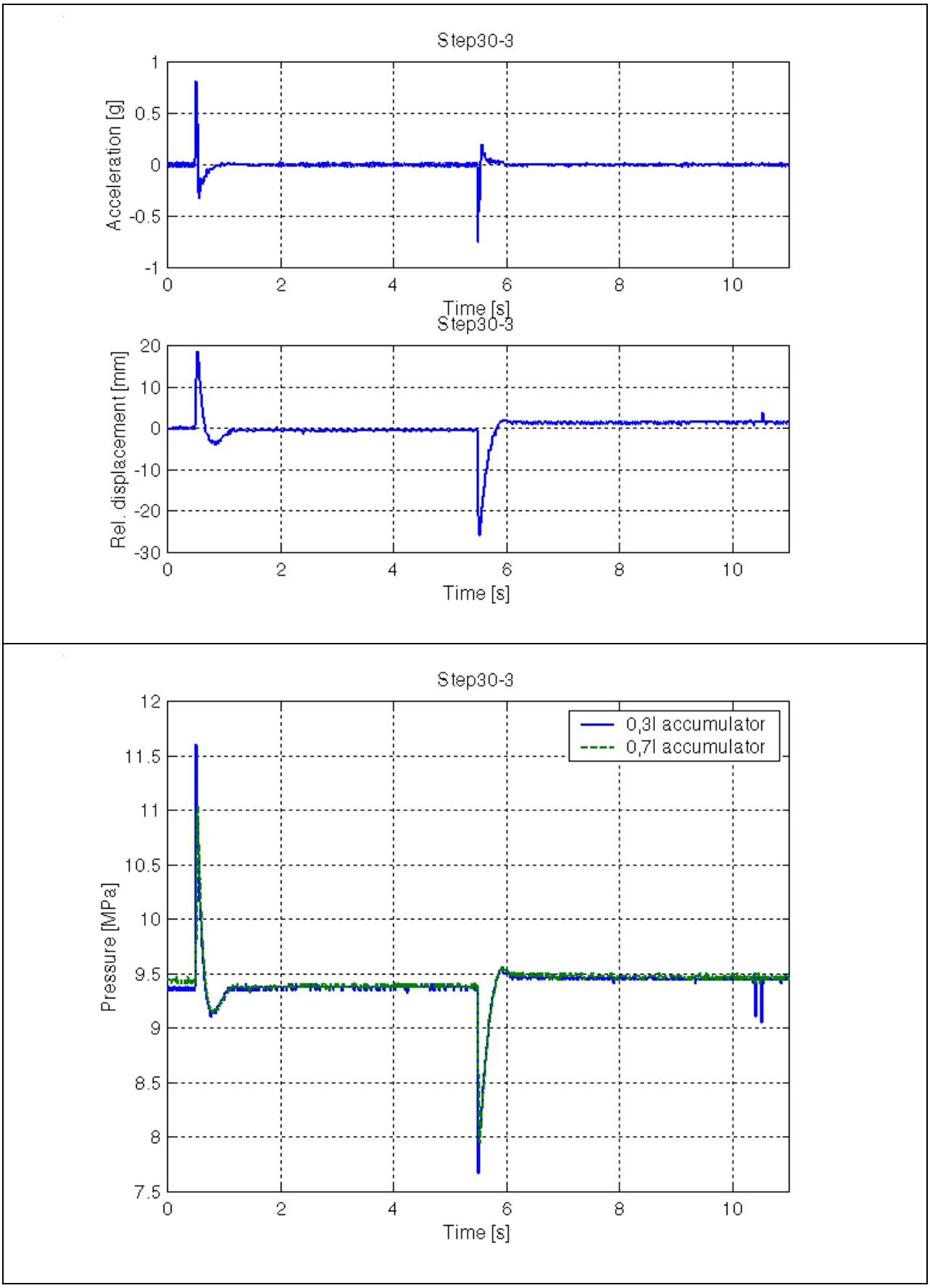


**Figure D-3: 30mm step response (Spring – OFF, Damper - ON)**

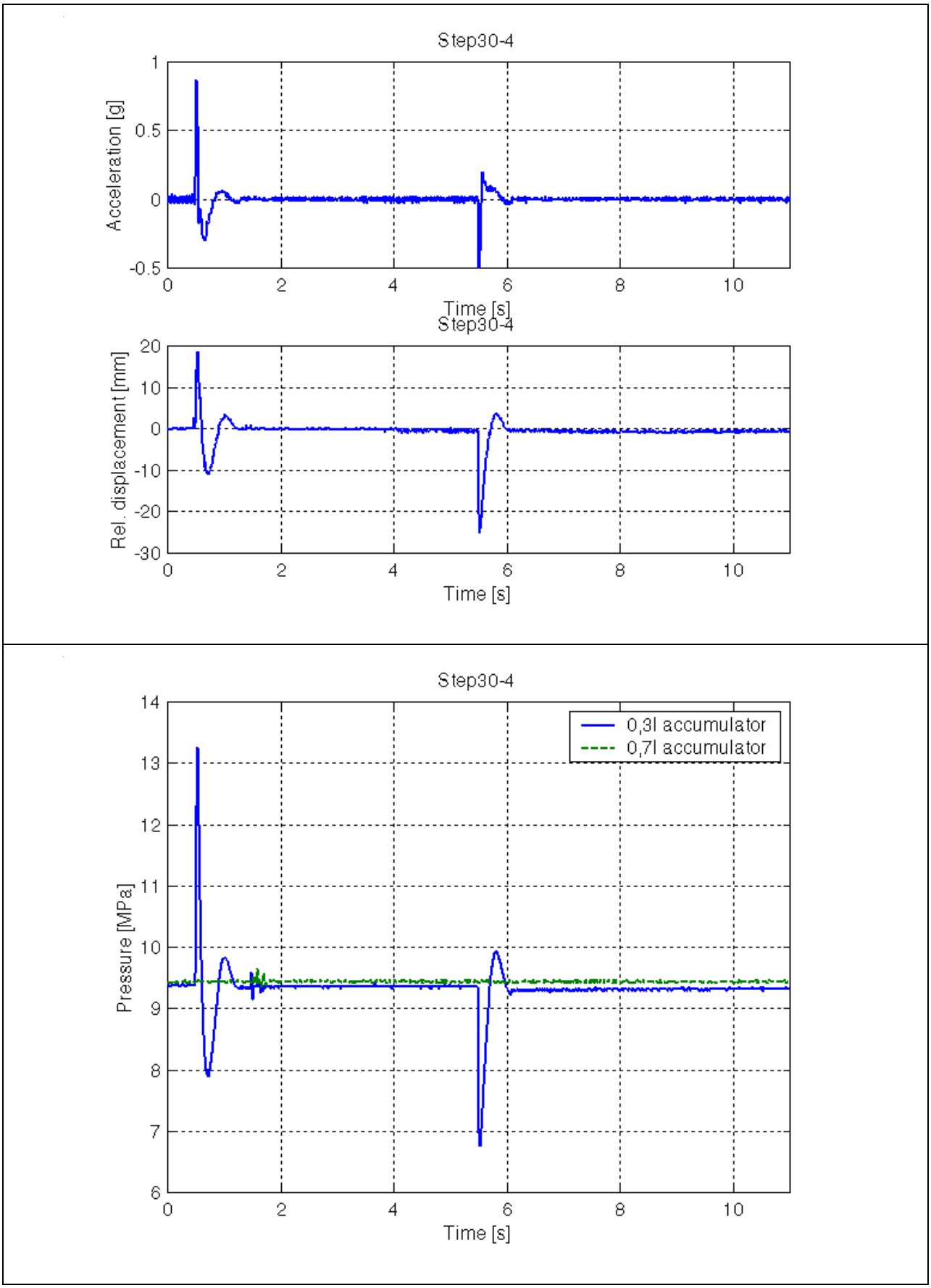


**Figure D-4: 30mm step response (Spring – ON, Damper - ON)**

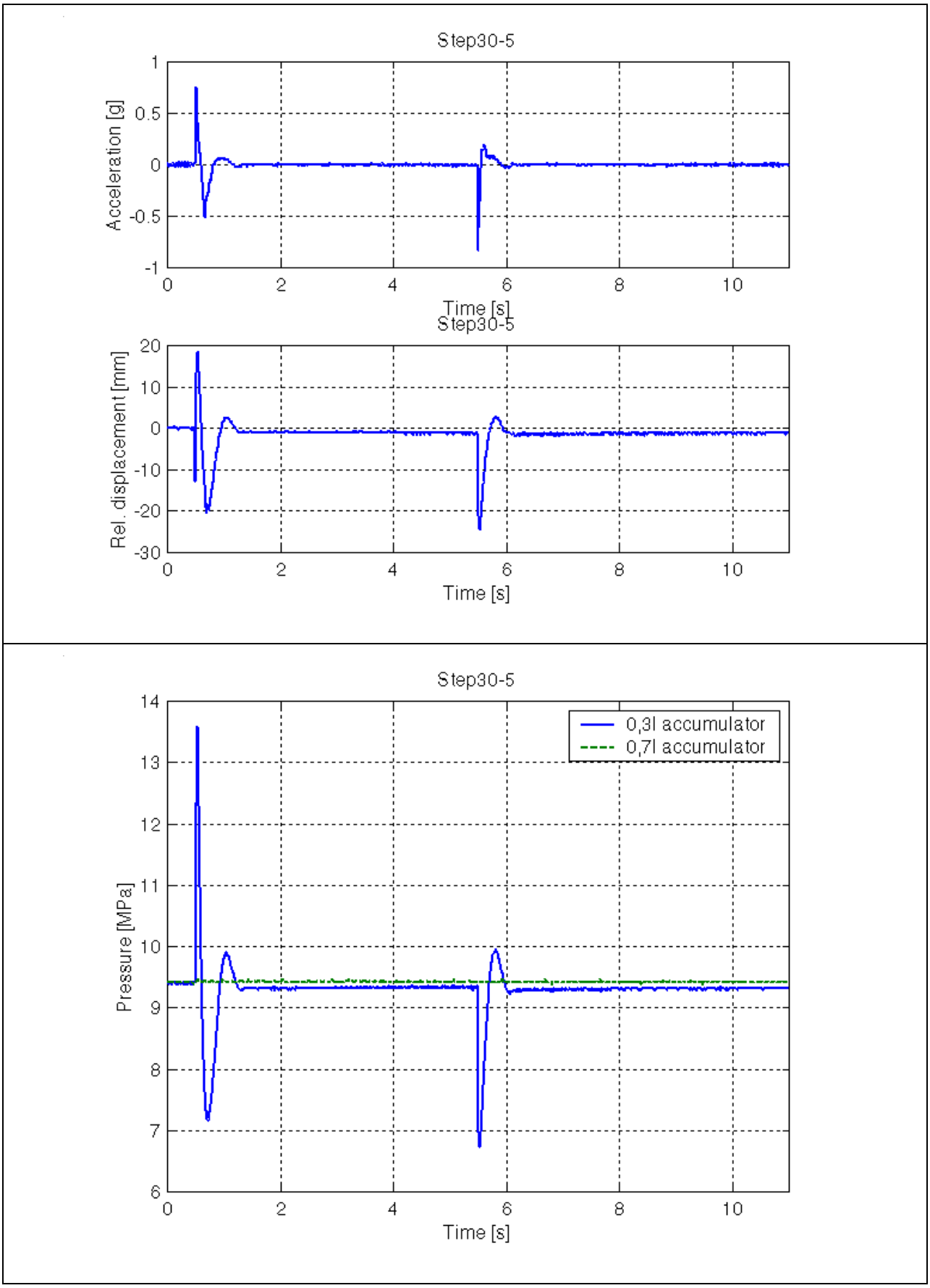


**Figure D-5: 30mm step response (Spring – ON, Damper - Karnopp)**

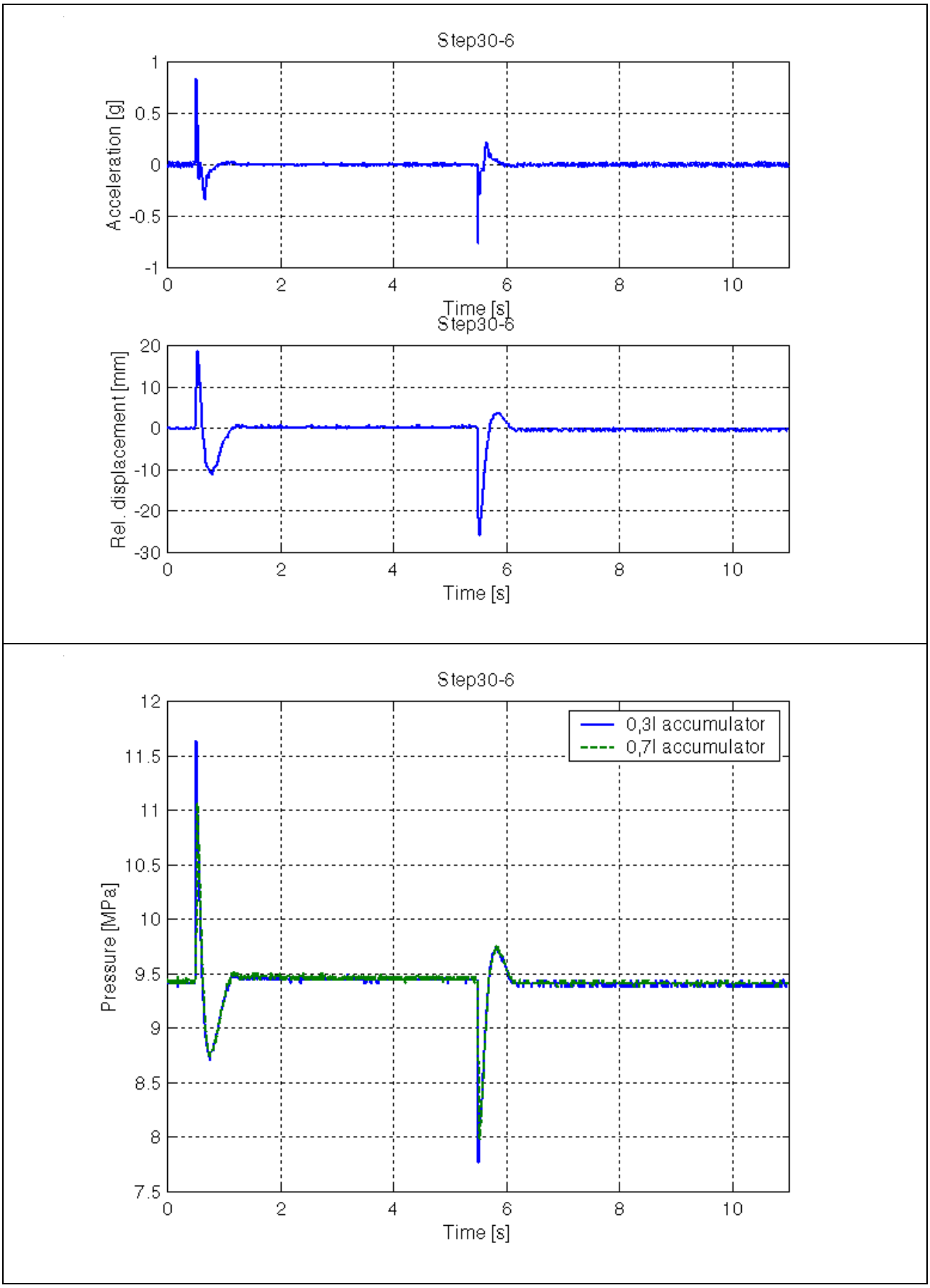


**Figure D-6: 30mm step response (Spring – OFF, Damper - Karnopp)**

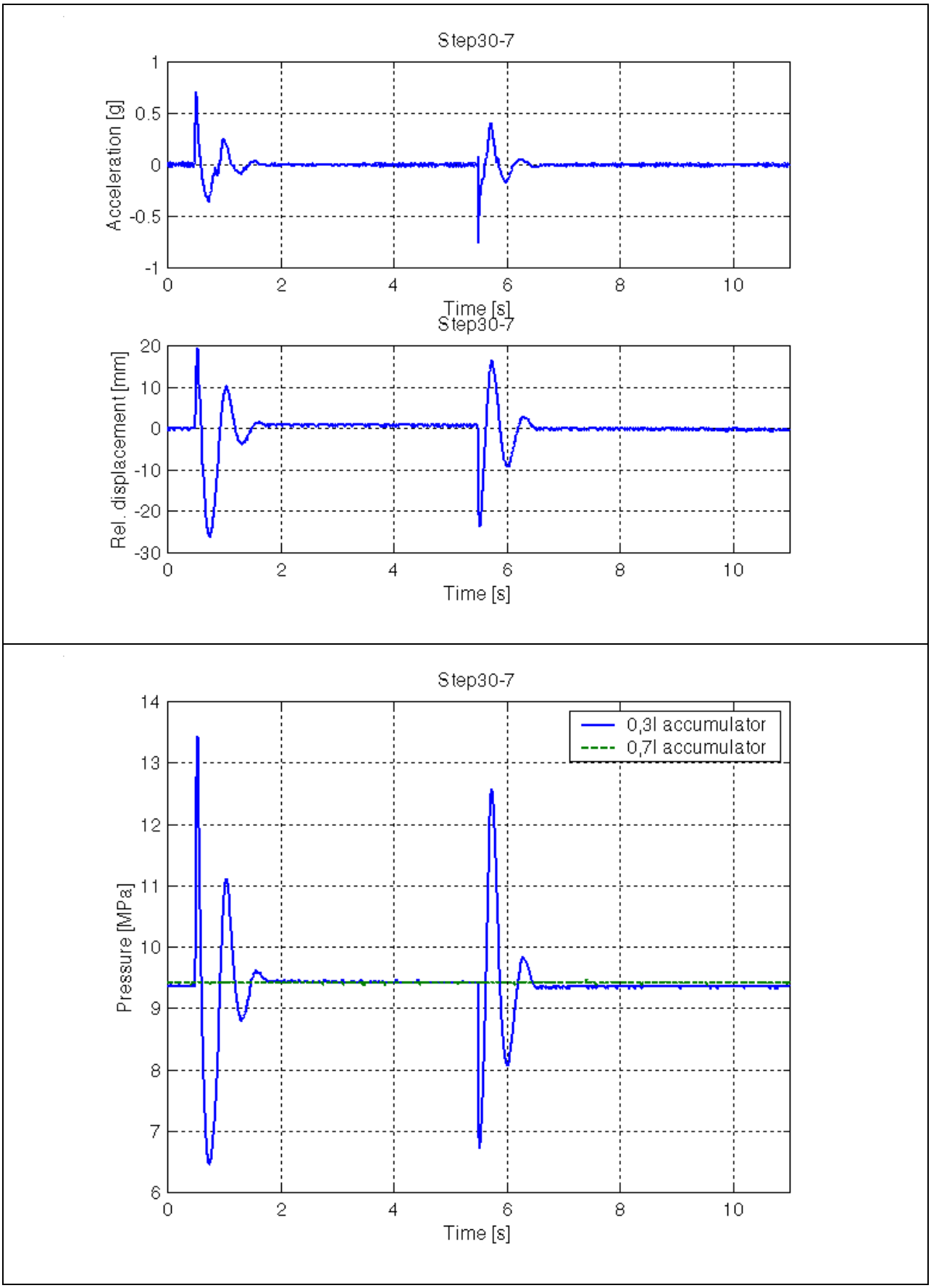


**Figure D-7: 30mm step response (Spring – ON, Damper – Hölscher & Huang)**

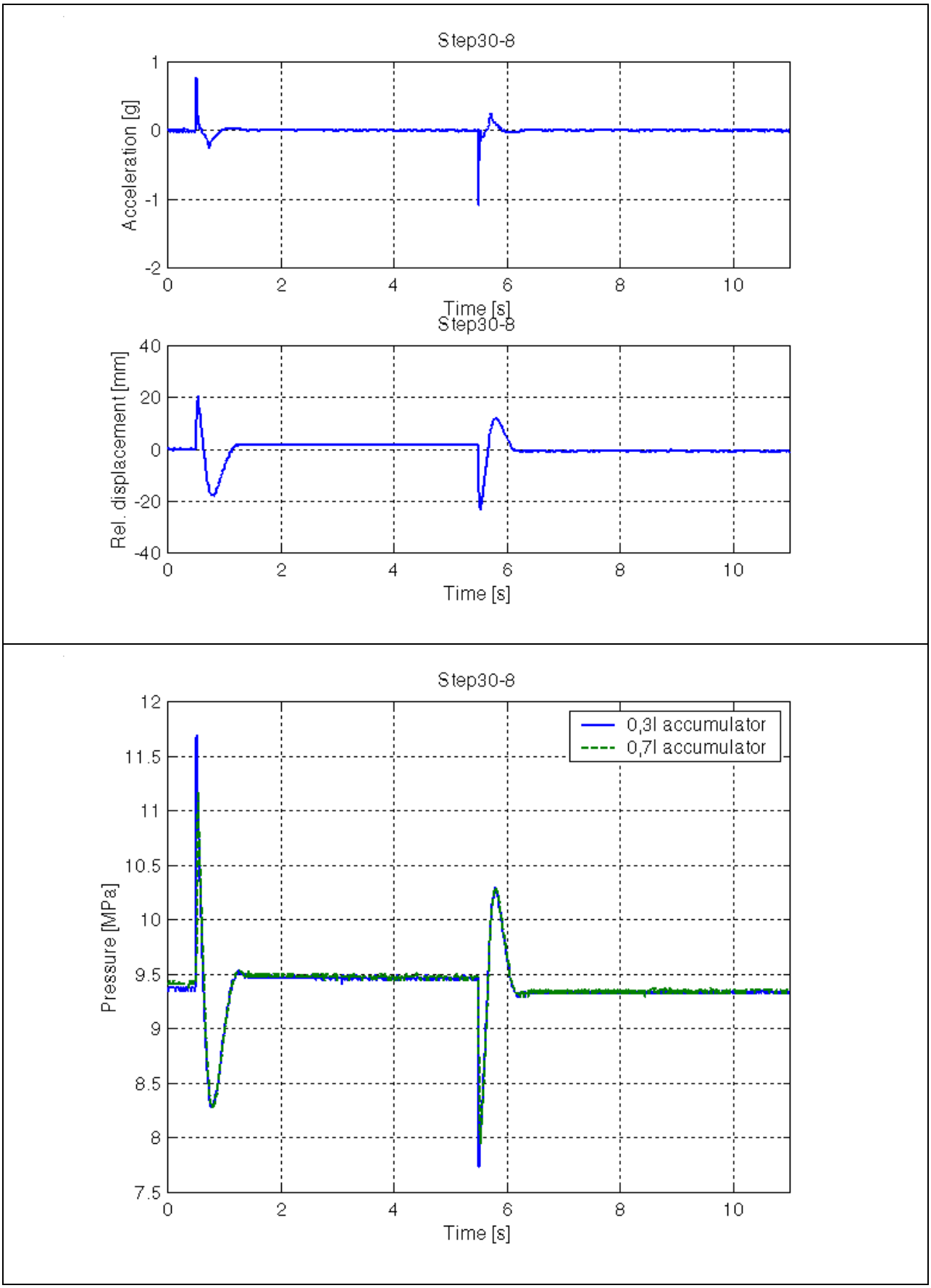


**Figure D-8: 30mm step response (Spring – OFF, Damper – Hölscher & Huang)**

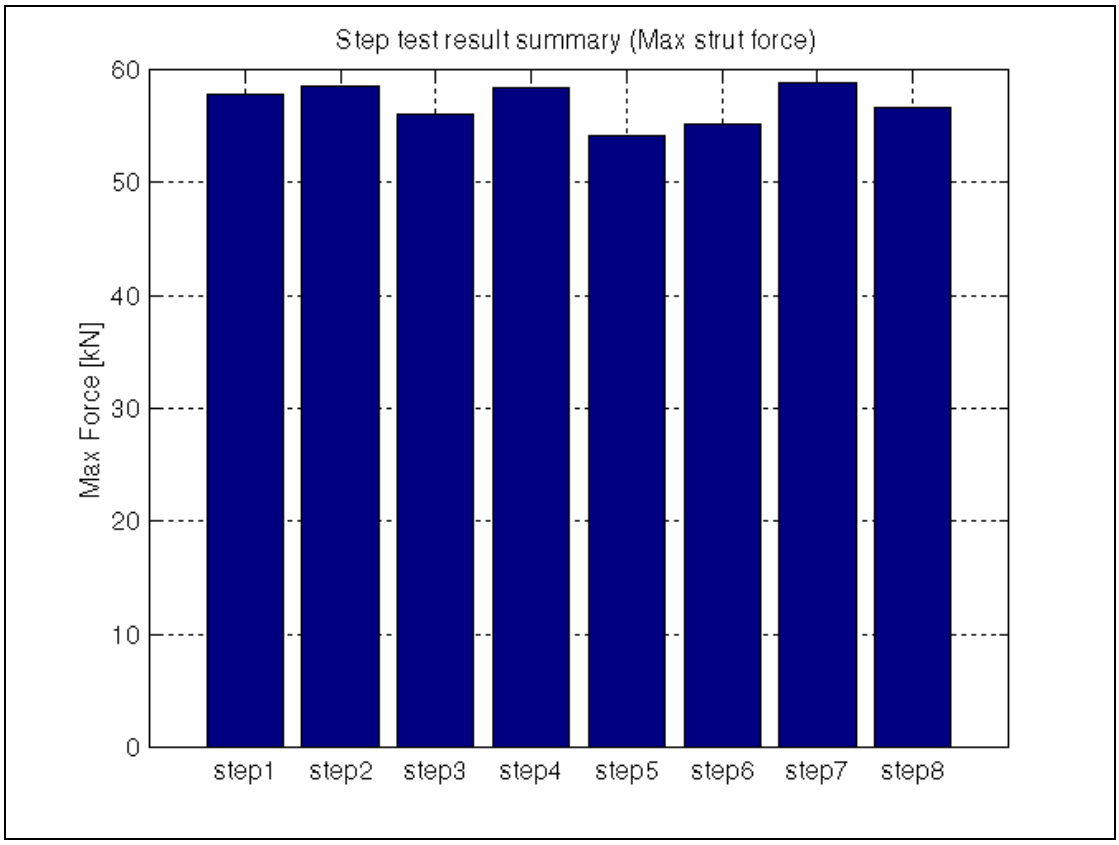


**Figure D-9: 60mm step response (Spring – OFF, Damper - OFF)**

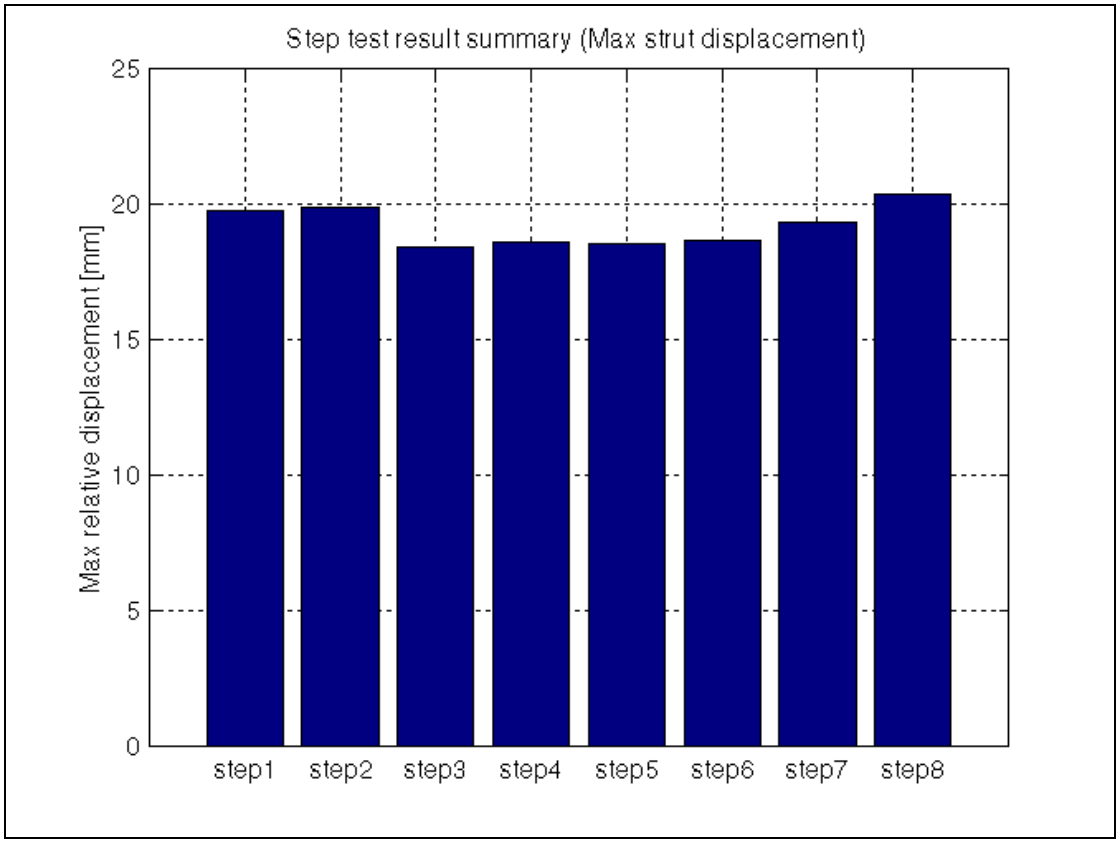


**Figure D-10: 60mm step response (Spring – OFF, Damper - OFF)**

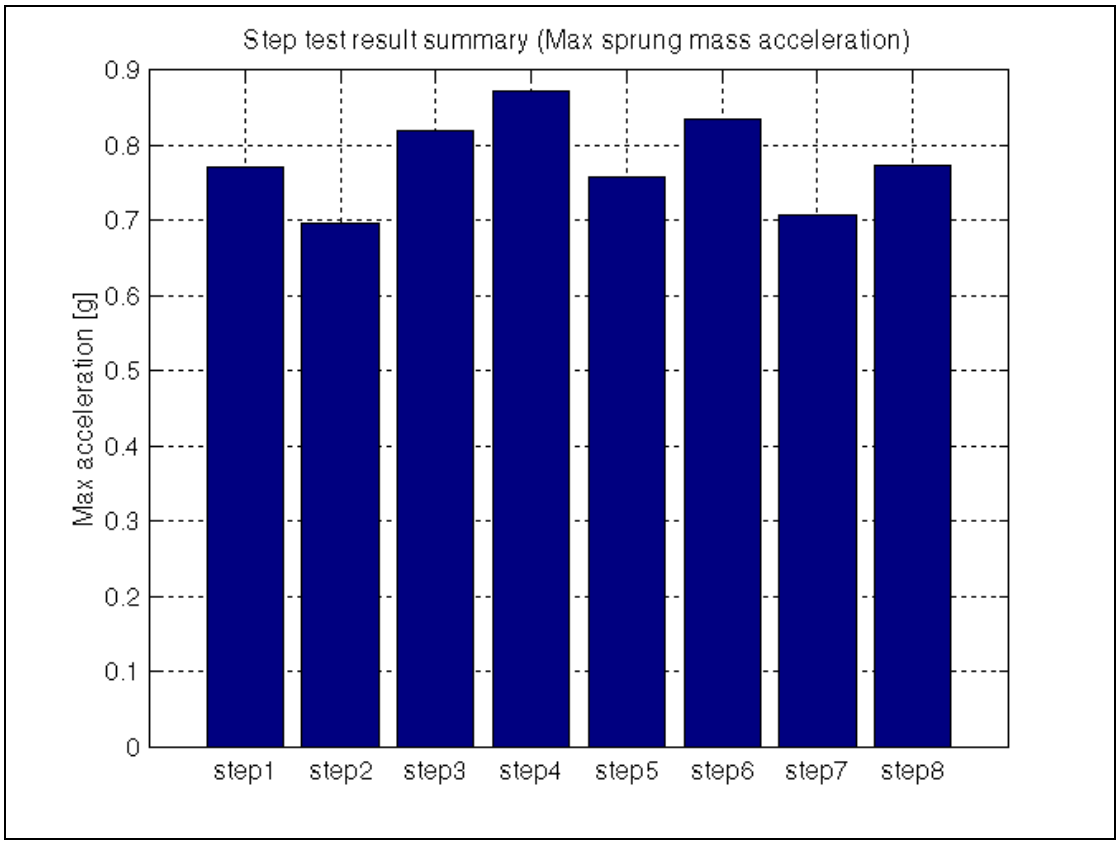


**Figure D-11: 60mm step response (Spring – OFF, Damper - OFF)**

## D.2 Belgian paving test results

For the random input response tests, the left-hand lane of the Belgian paving track at the Gerotek Vehicle Testing Facility was used. Different spring and damper settings were tested and the figures in this section indicate the test results. Table D-2 indicates the spring and damper setting for each of the graphs presented in this section.

**Table D-2: Spring/damper configuration for random input tests**

| Figure number | Input | Spring state | Damper state |
|---|---|---|---|
| Figure D-12 | Belgian paving | OFF | OFF |
| Figure D-13 | Belgian paving | ON | OFF |
| Figure D-14 | Belgian paving | OFF | ON |
| Figure D-15 | Belgian paving | ON | ON |
| Figure D-16 | Belgian paving | ON | Karnopp |
| Figure D-17 | Belgian paving | OFF | Karnopp |
| Figure D-18 | Belgian paving | ON | Hölscher & Huang |
| Figure D-19 | Belgian paving | OFF | Hölscher & Huang |
| Figure D-20 | Belgian paving | RMS strut force summary | |
| Figure D-21 | Belgian paving | RMS displacement summary | |
| Figure D-22 | Belgian paving | RMS sprung mass acceleration | |

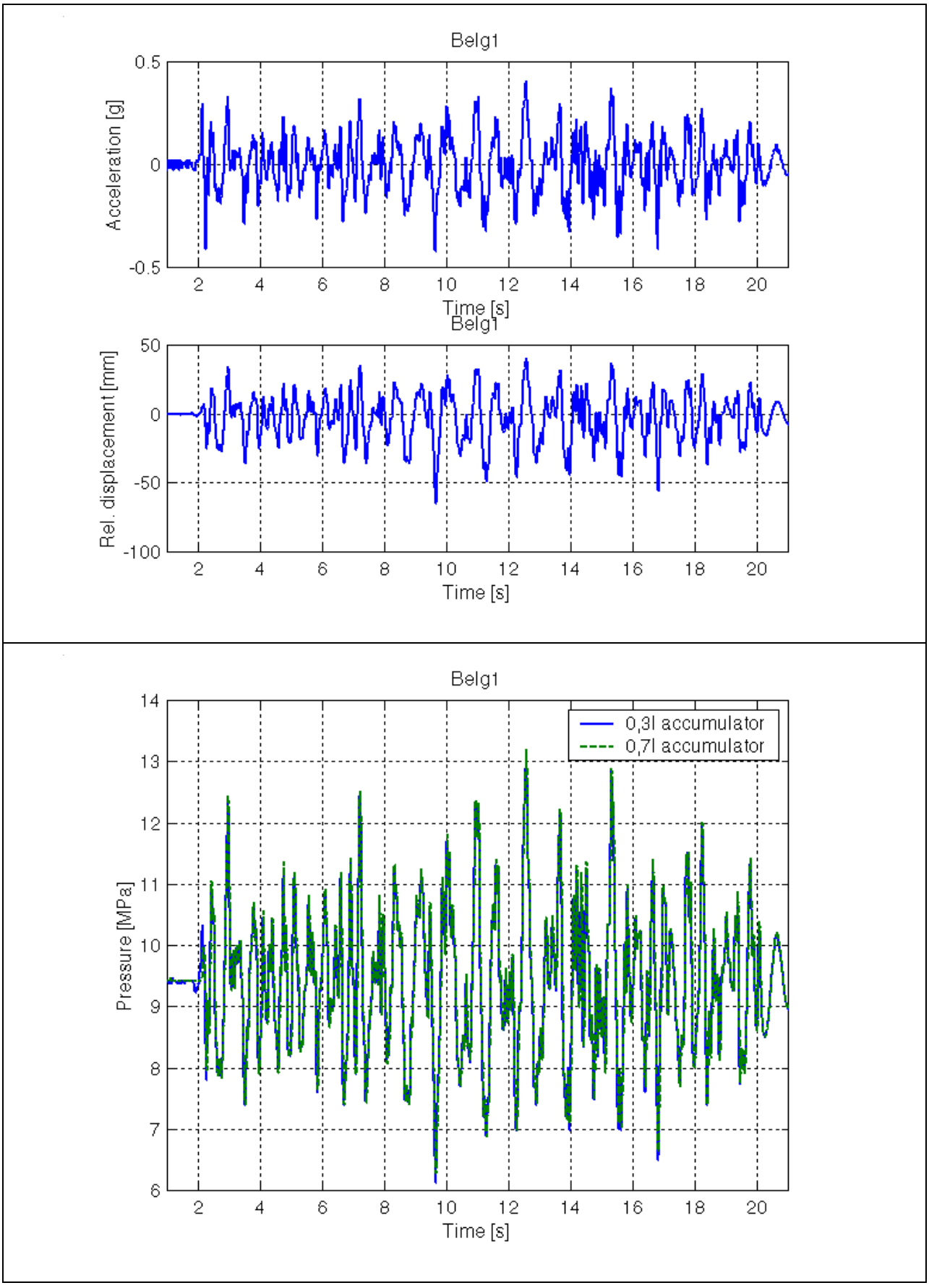


**Figure D-12: Random input test (Spring – OFF, Damper – ON)**

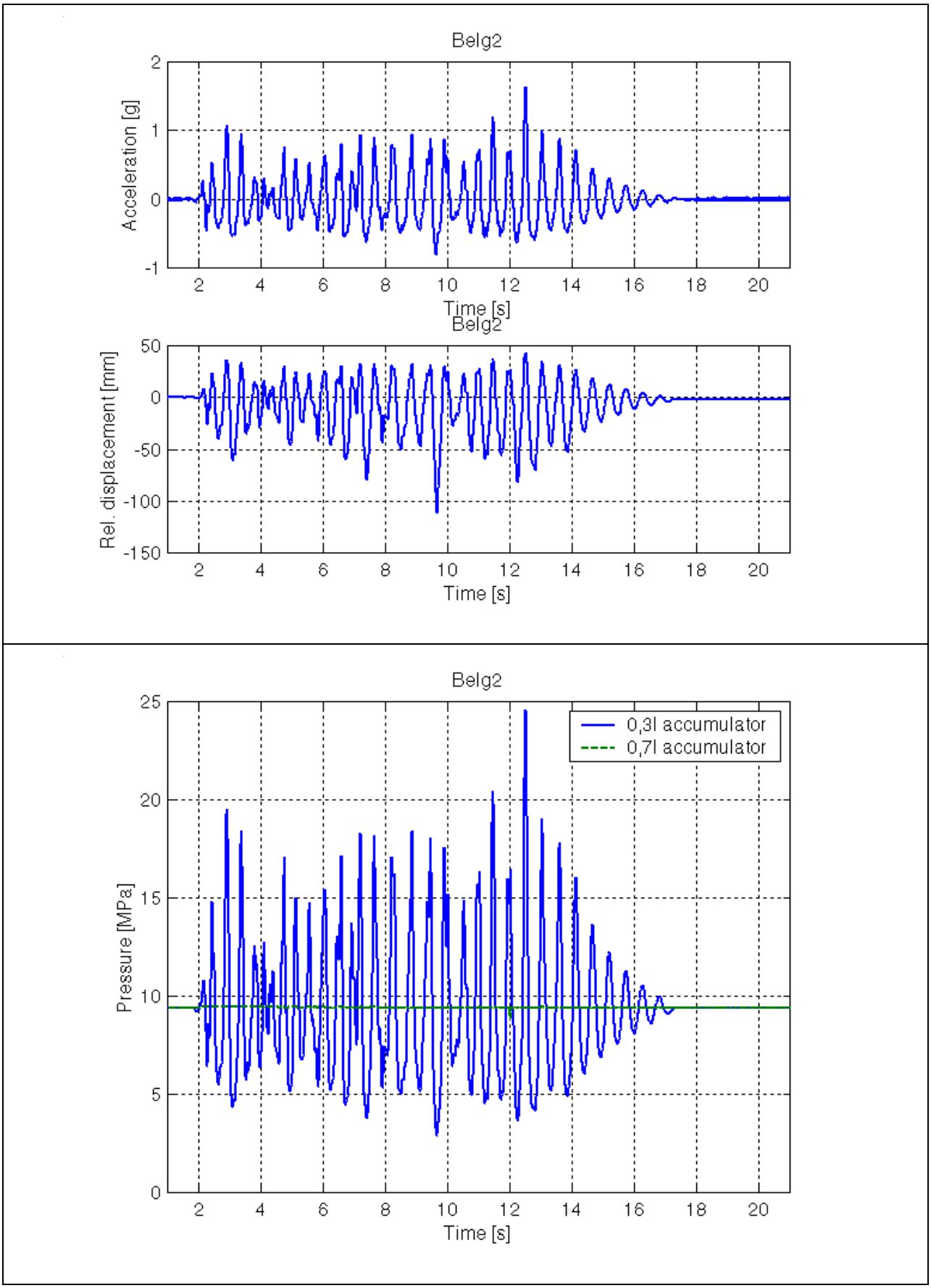


**Figure D-13: Random input test (Spring – ON, Damper – OFF)**

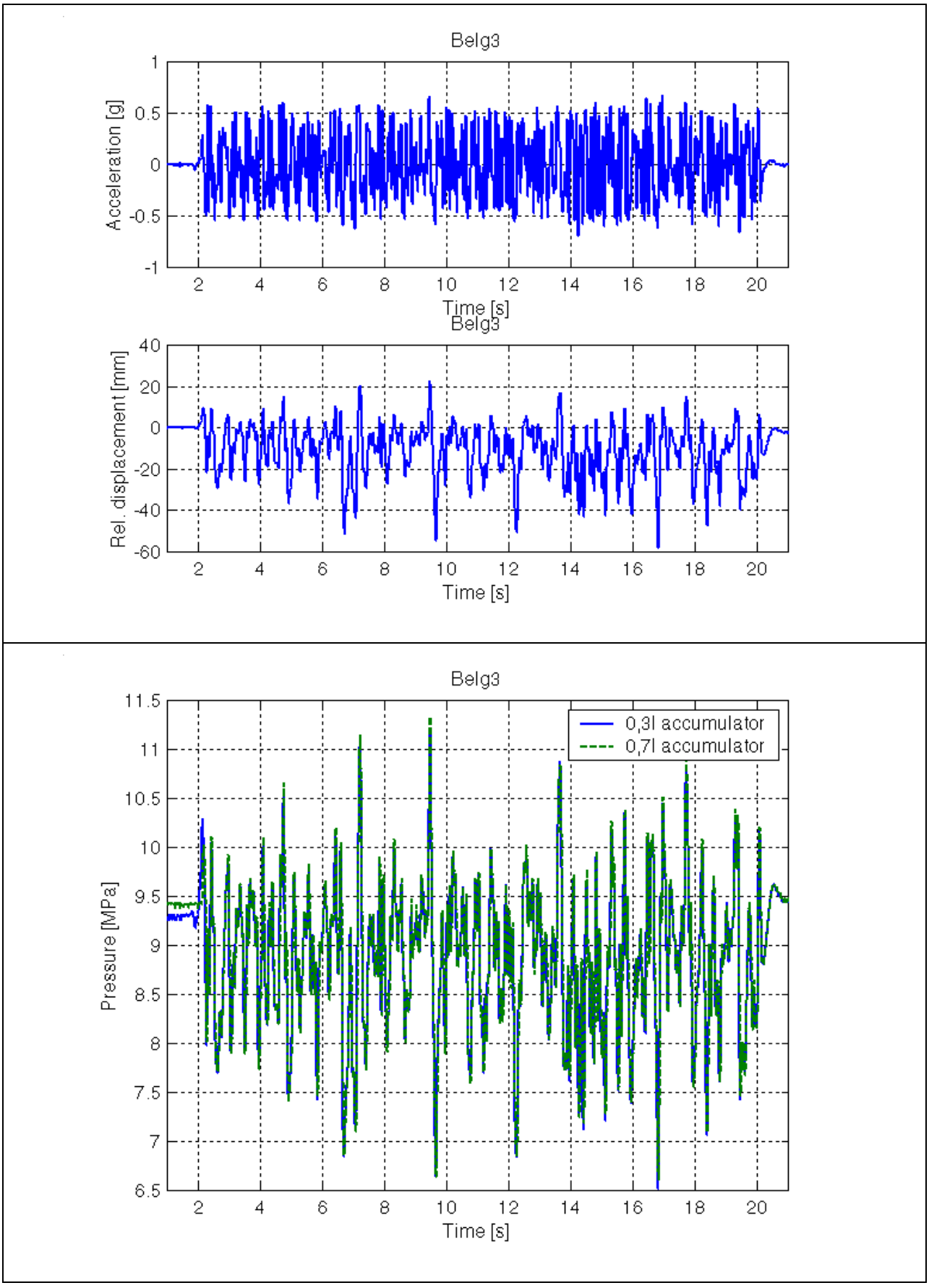


**Figure D-14: Random input test (Spring – OFF, Damper – ON)**

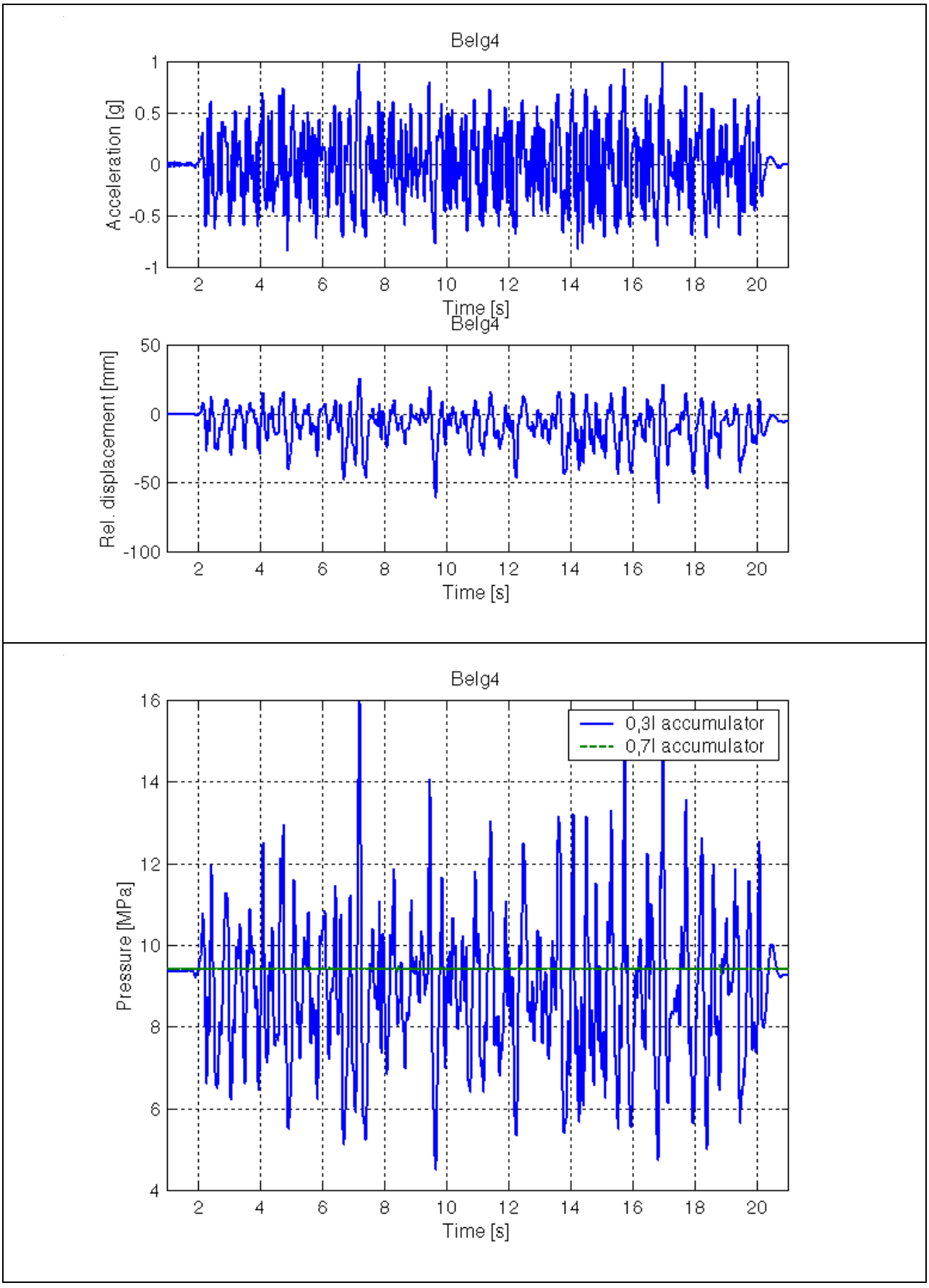


**Figure D-15: Random input test (Spring – ON, Damper – ON)**

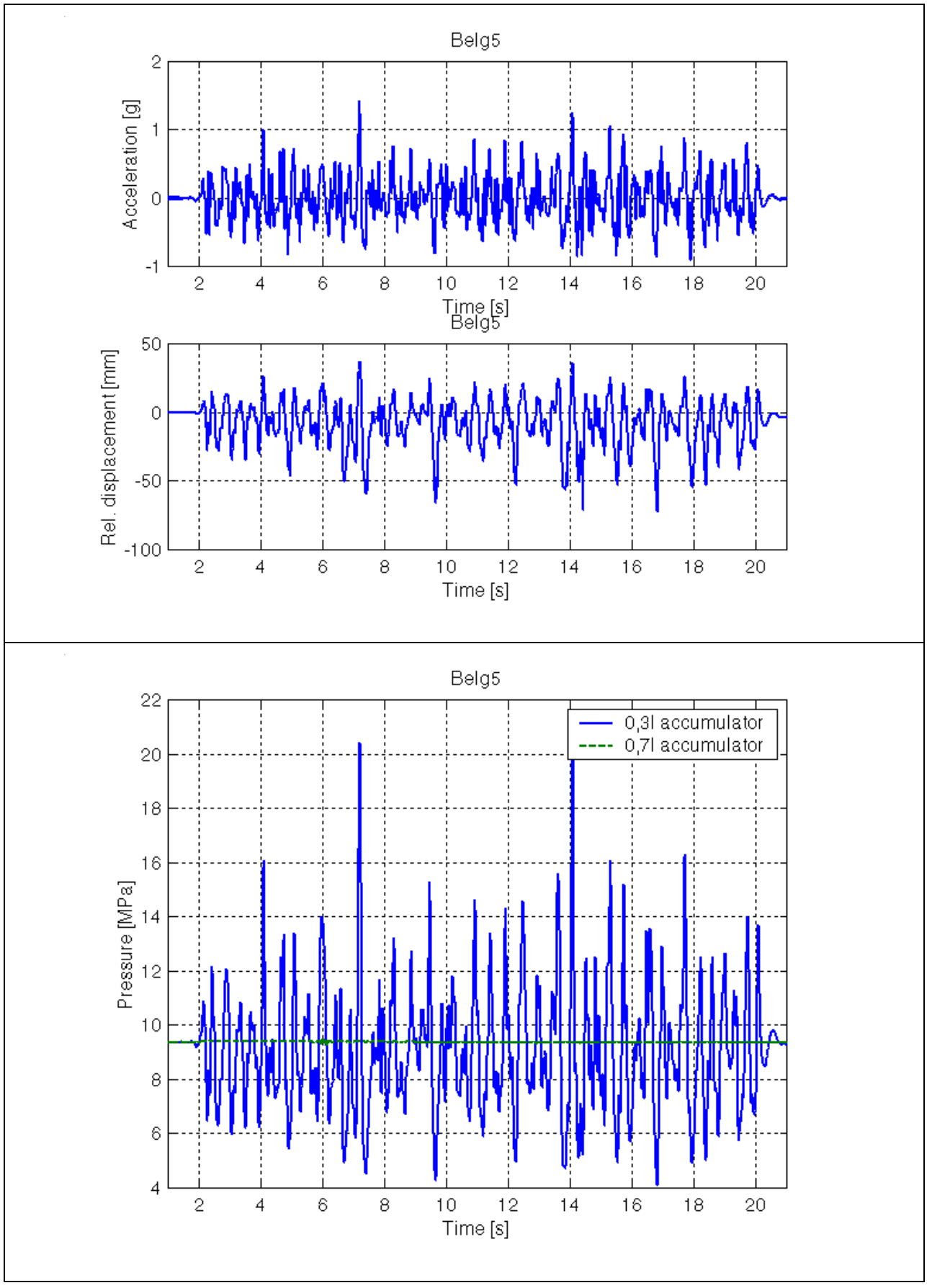


**Figure D-16: Random input test (Spring – ON, Damper – Karnopp)**

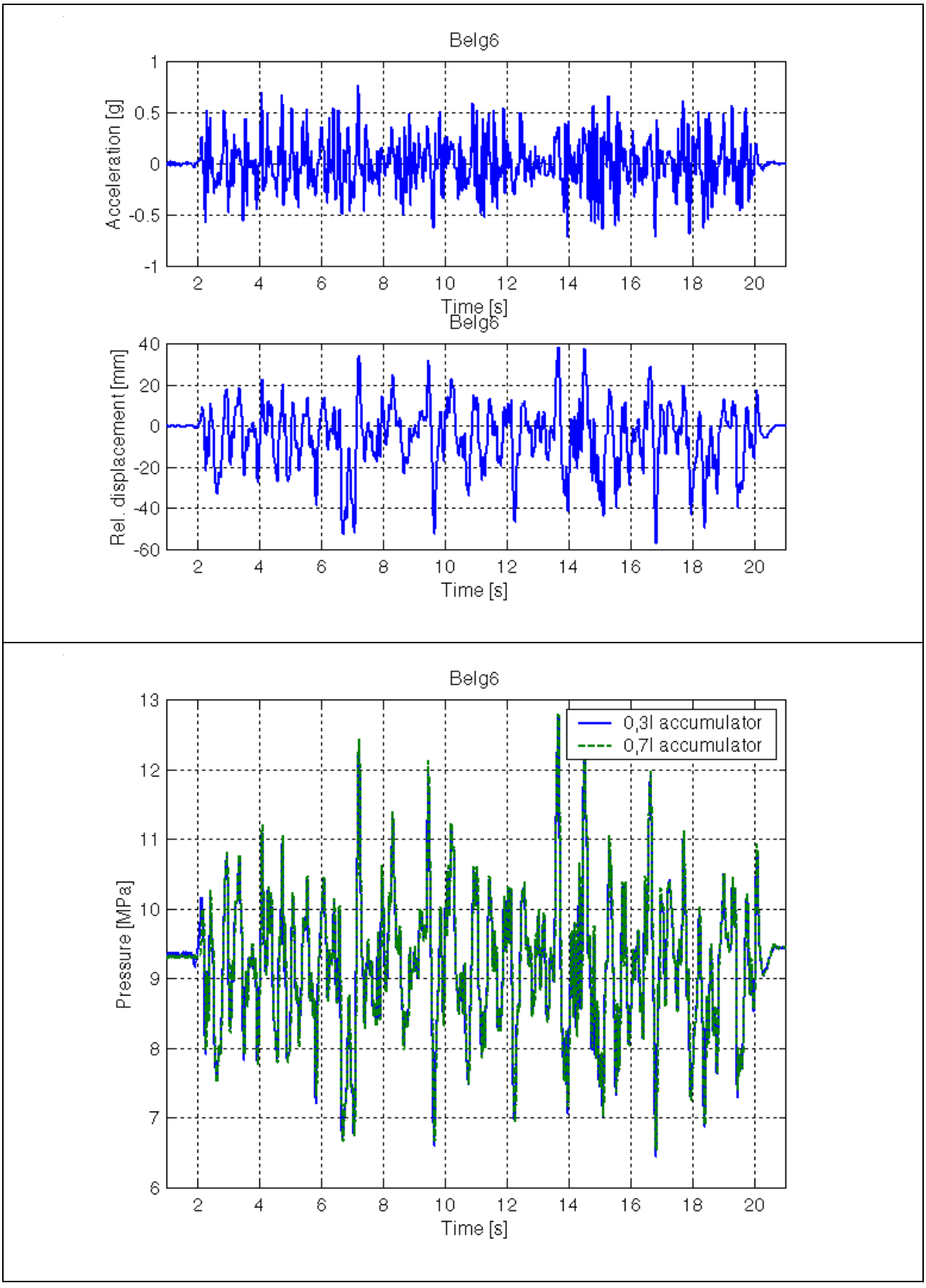


**Figure D-17: Random input test (Spring – OFF, Damper – Karnopp)**

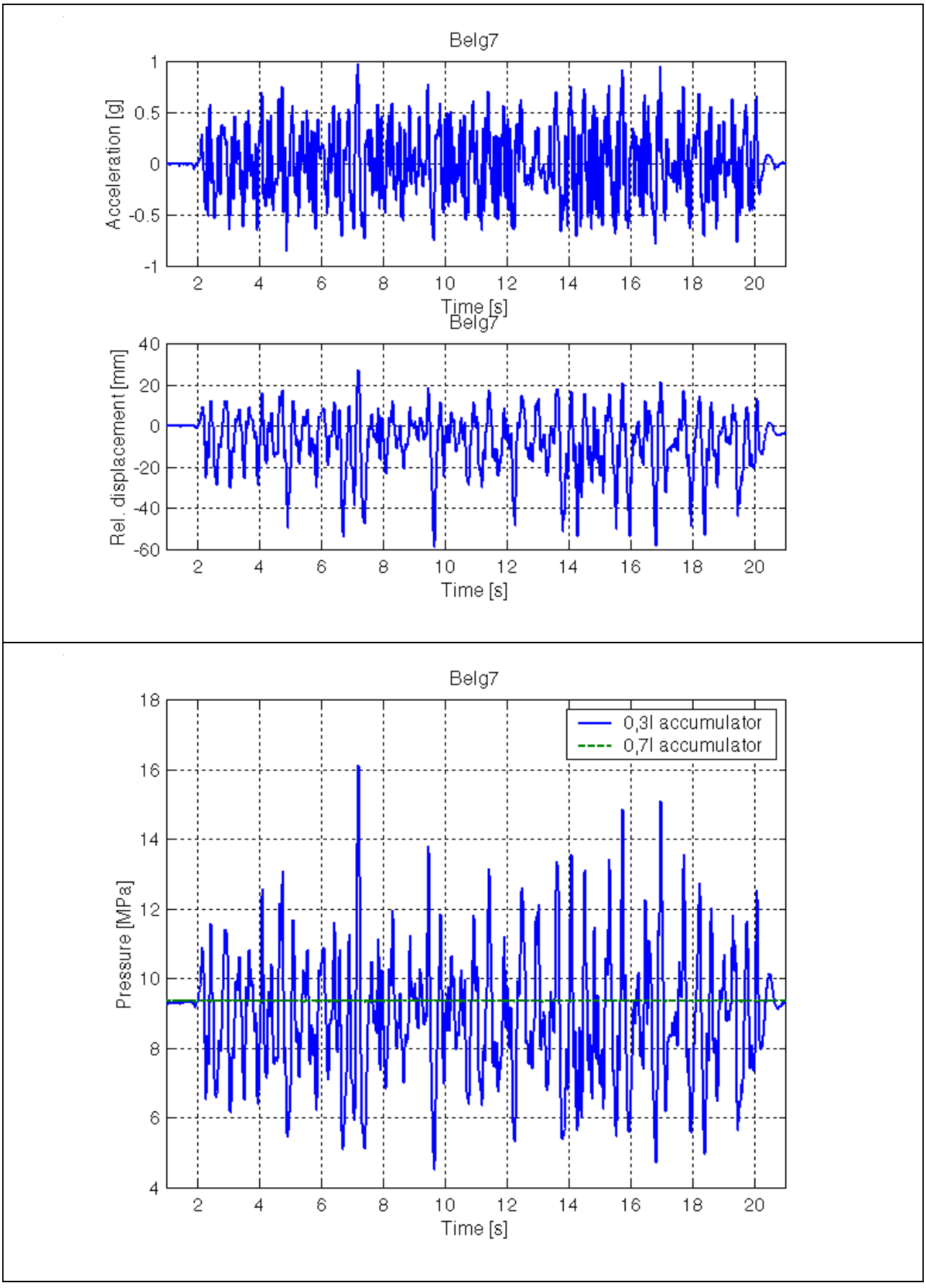


**Figure D-18: Random input test (Spring – ON, Damper – Hölscher & Huang)**

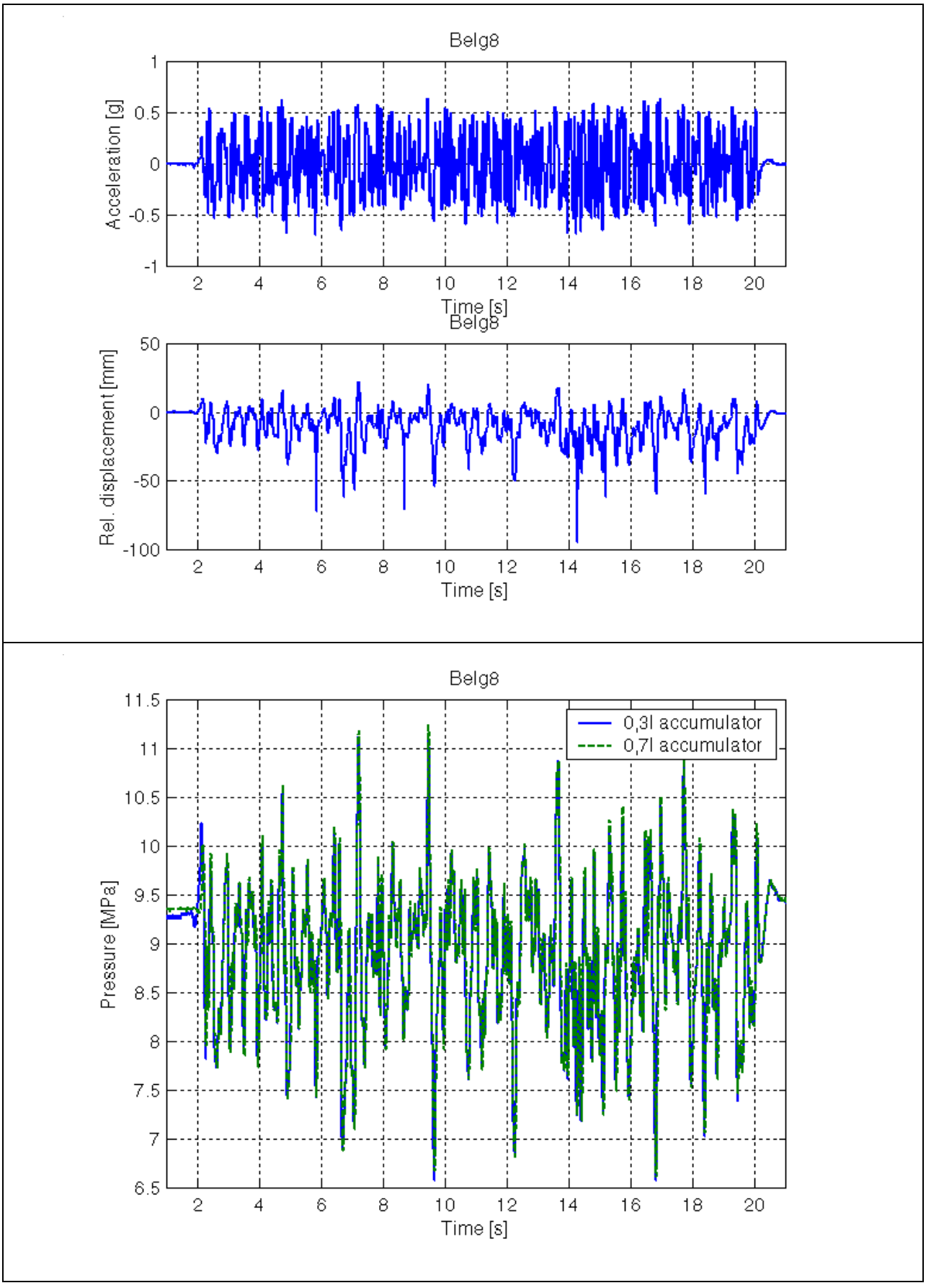


**Figure D-19: Random input test (Spring – OFF, Damper – Hölscher & Huang)**

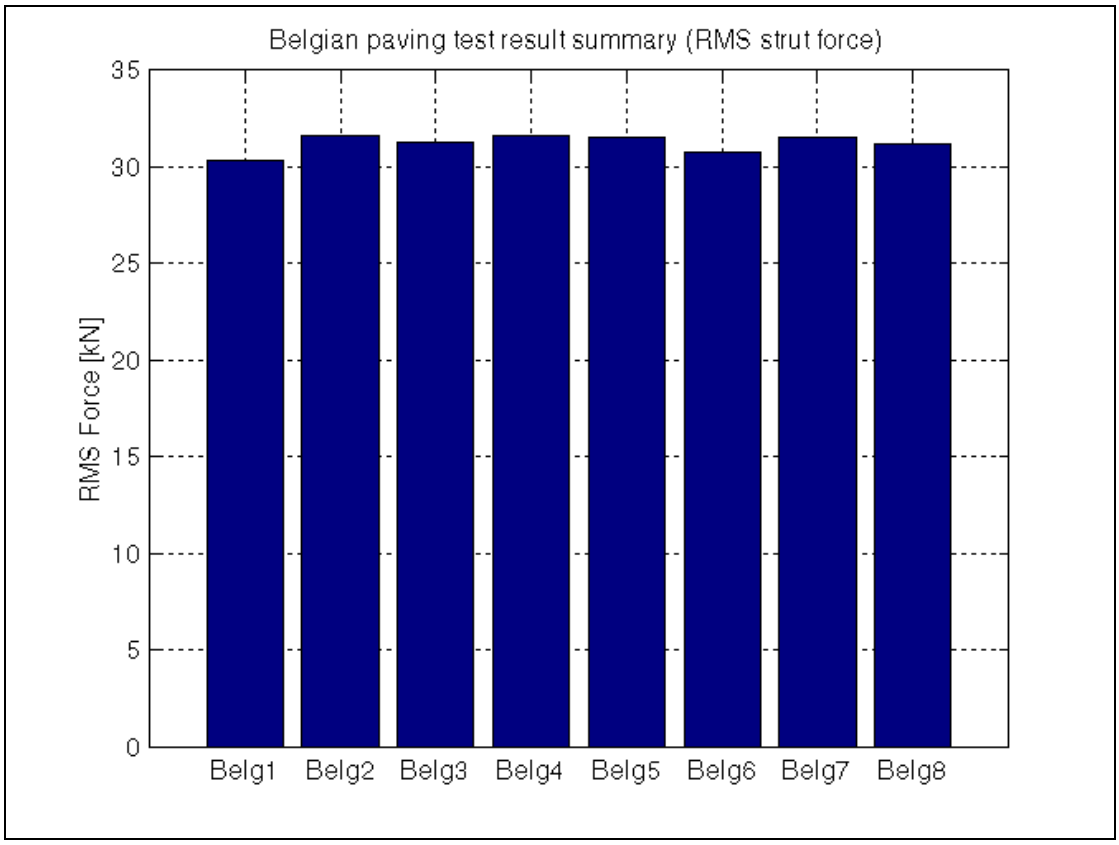


**Figure D-20: Random input test (Spring – Height adjustment, Damper – OFF)**

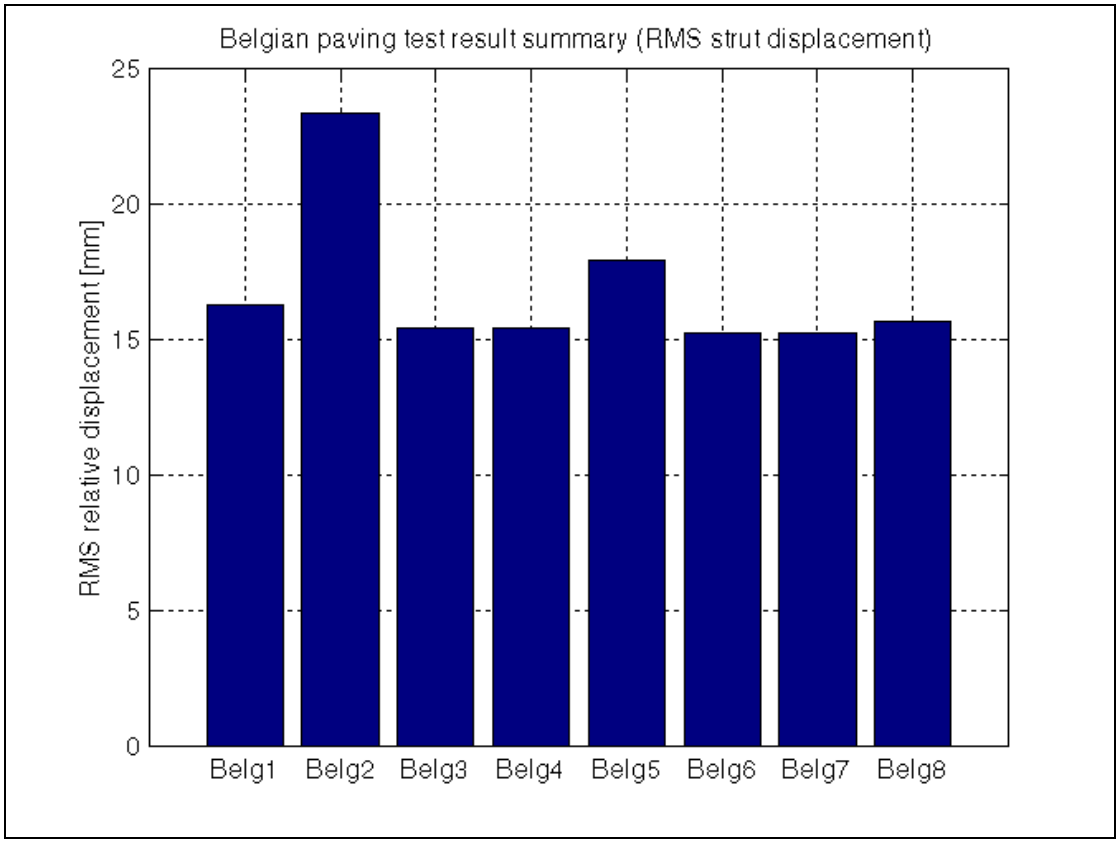


**Figure D-21: Random input test (Spring – Height adjustment, Damper – ON)**

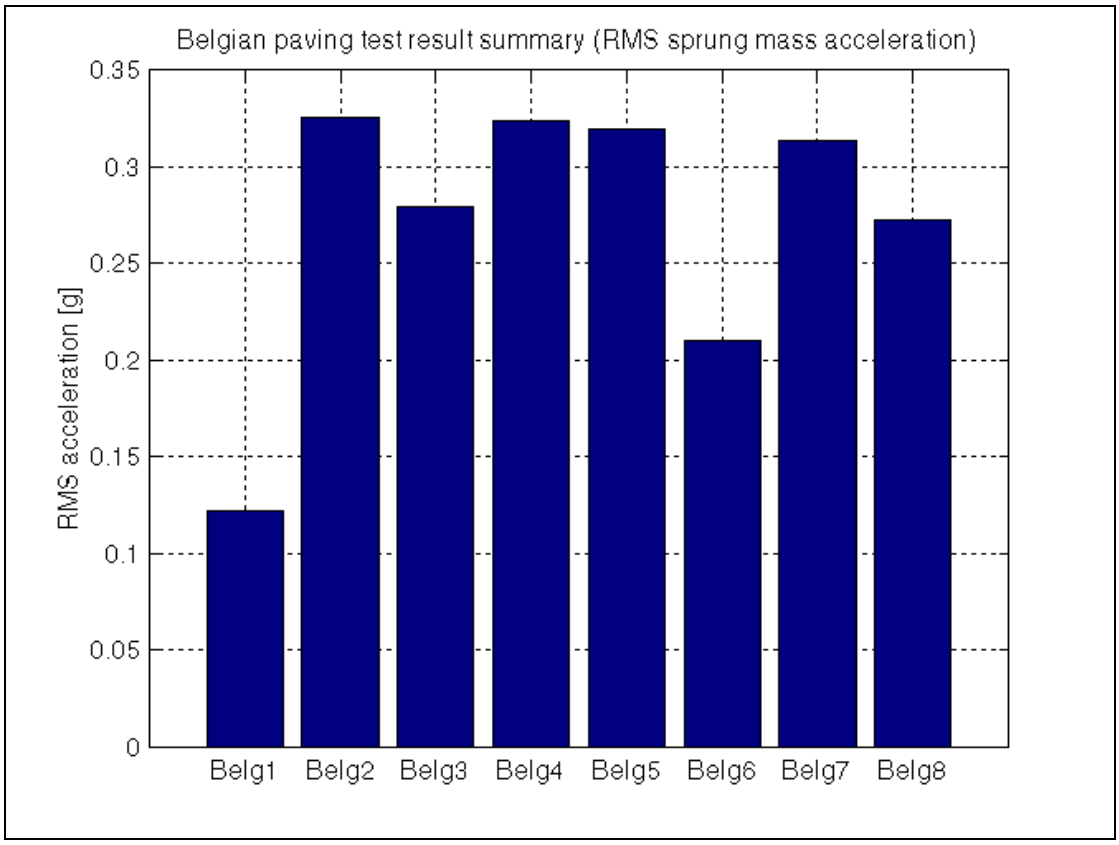


**Figure D-22: Belgian paving test summary (Minimum and maximum)**

## D.3 Sine sweep test results

For the sine sweep tests, a sine displacement input was supplied to the actuator. The sine wave had a constant amplitude of 15*mm*, while the frequency was linearly adjusted from 0.1*Hz* to 15*Hz* in 78*s*. Table D-3 supplies a list of figures and the corresponding spring and damper settings for different graphs. Figure D-31 shows an example of the measured actuator displacement, relative strut displacement, as well as the sprung mass displacement. From this figure, it is clear that the frequency response of the actuator is not sufficient to follow the input signal at the higher frequencies. Figure D-32 indicates the transmissibility of for the configurations listed in Table D-3.

**Table D-3: Spring/damper configuration for sine sweep tests**

| Figure number | Input | Spring state | Damper state | Filename |
|---|---|---|---|---|
| Figure D-23 | Sine sweep (15mm amplitude) | OFF | OFF | Sin15-1 |
| Figure D-24 | Sine sweep (15mm amplitude) | ON | OFF | Sin15-2 |
| Figure D-25 | Sine sweep (15mm amplitude) | OFF | ON | Sin15-3 |
| Figure D-26 | Sine sweep (15mm amplitude) | ON | ON | Sin15-4 |
| Figure D-27 | Sine sweep (15mm amplitude) | ON | Karnopp | Sin15-5 |
| Figure D-28 | Sine sweep (15mm amplitude) | OFF | Karnopp | Sin15-6 |
| Figure D-29 | Sine sweep (15mm amplitude) | ON | Holsher & Huang | Sin15-7 |
| Figure D-30 | Sine sweep (15mm amplitude) | OFF | Holsher & Huang | Sin15-8 |

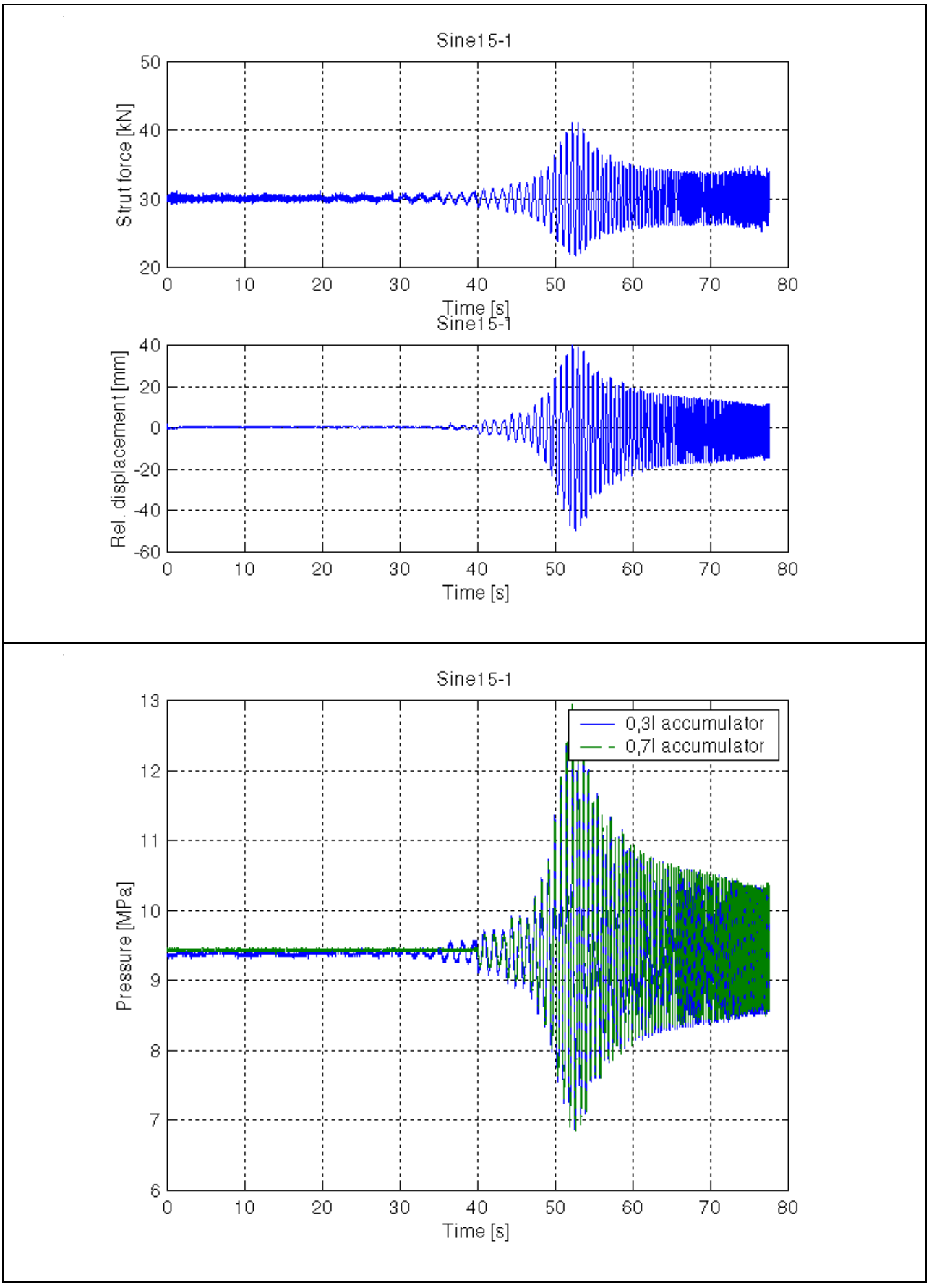


**Figure D-23: Sine sweep (Spring - OFF, Damper - OFF)**

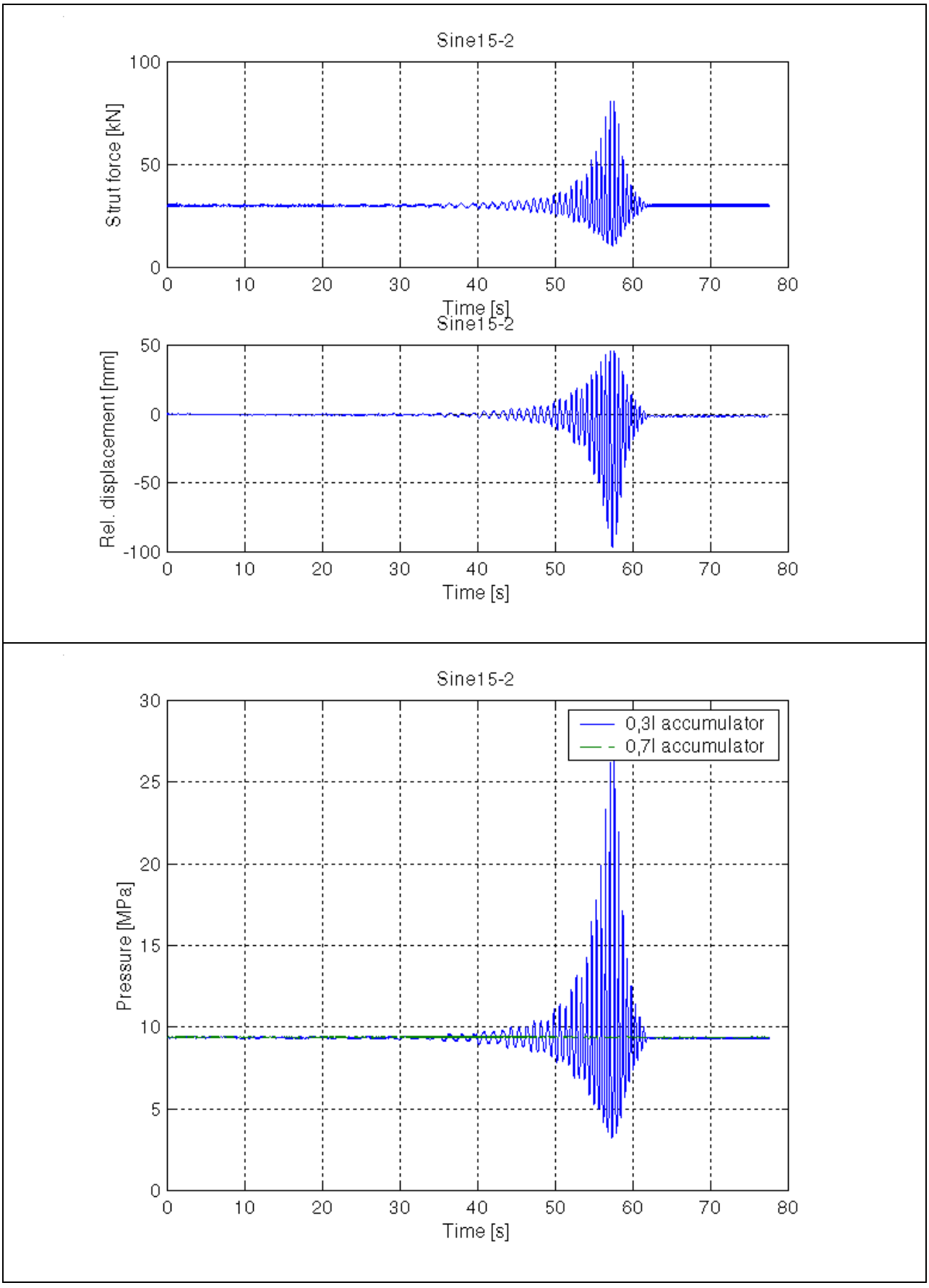


**Figure D-24: Sine sweep (Spring - ON, Damper - OFF)**

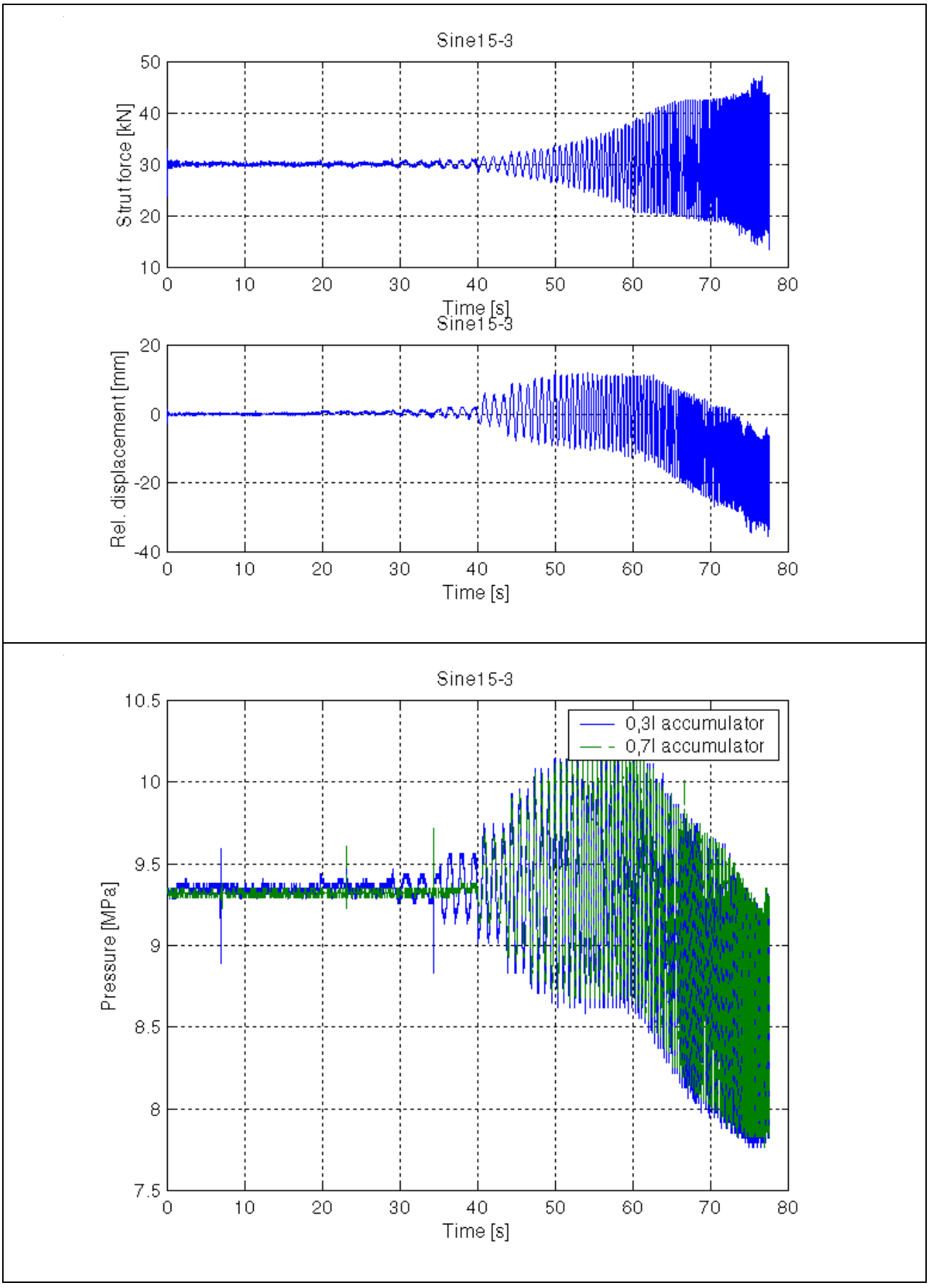


**Figure D-25: Sine sweep (Spring - OFF, Damper - ON)**

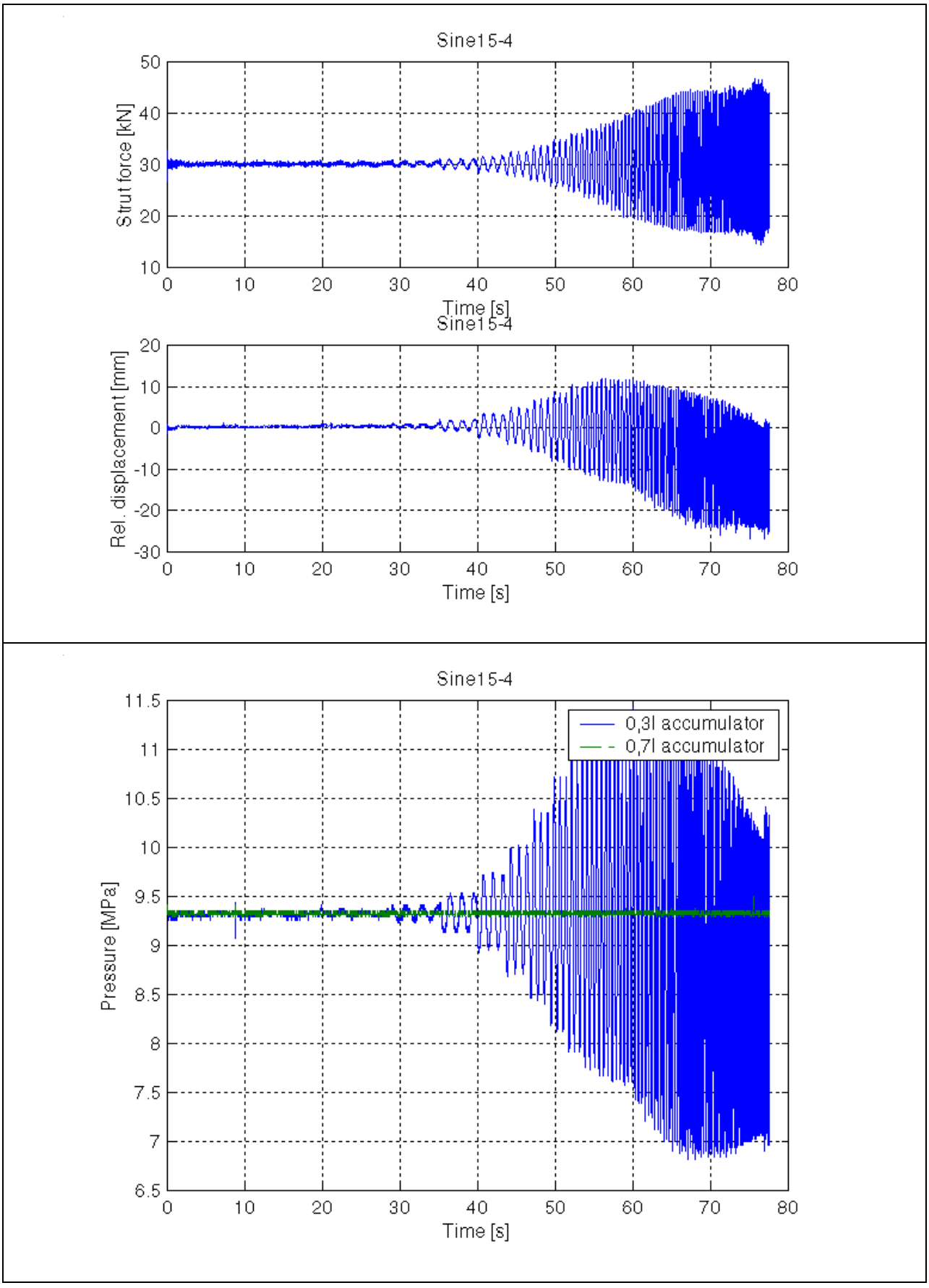


**Figure D-26: Sine sweep (Spring - ON, Damper - ON)**

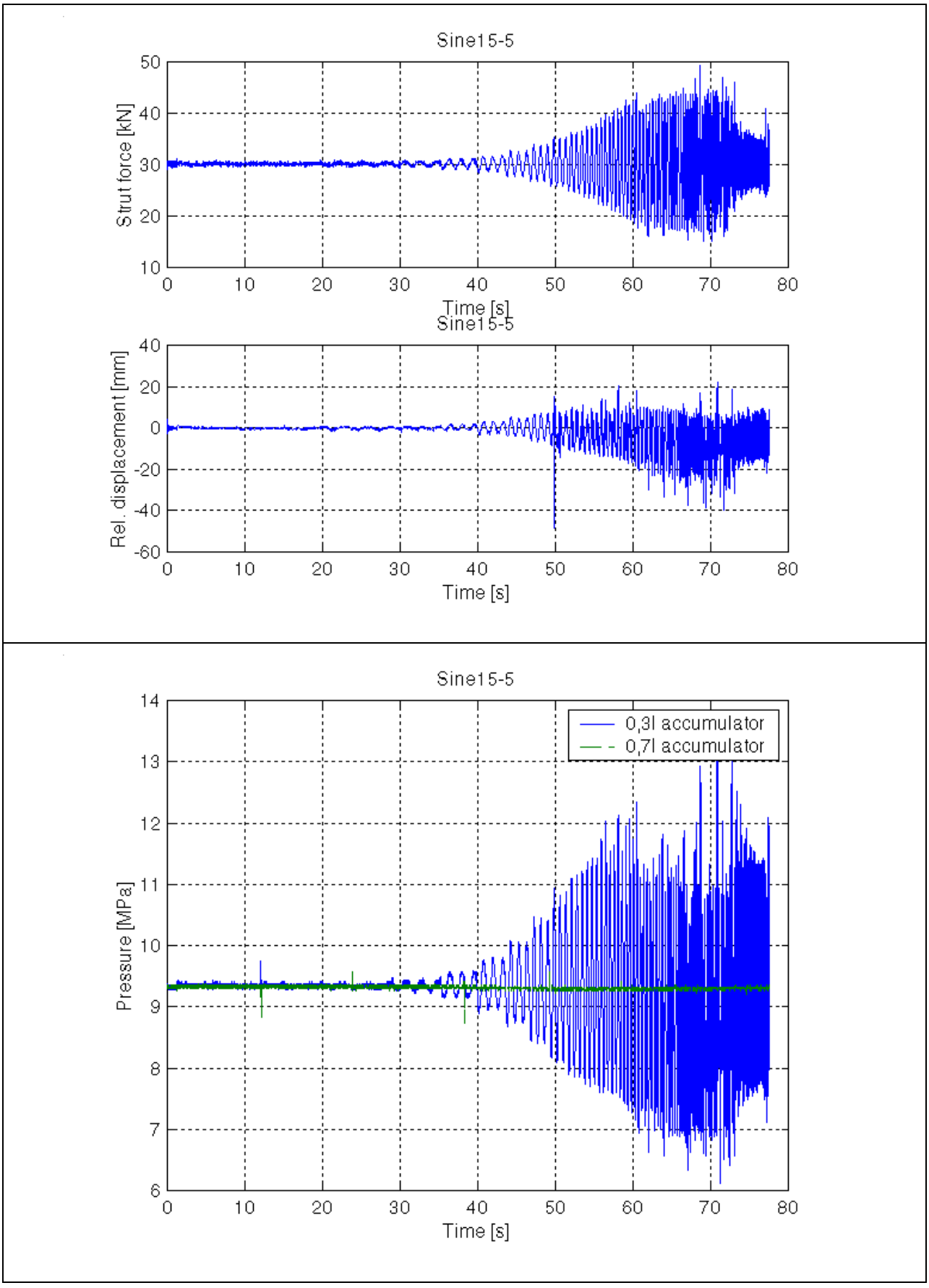


**Figure D-27: Sine sweep (Spring - ON, Damper - Karnopp)**

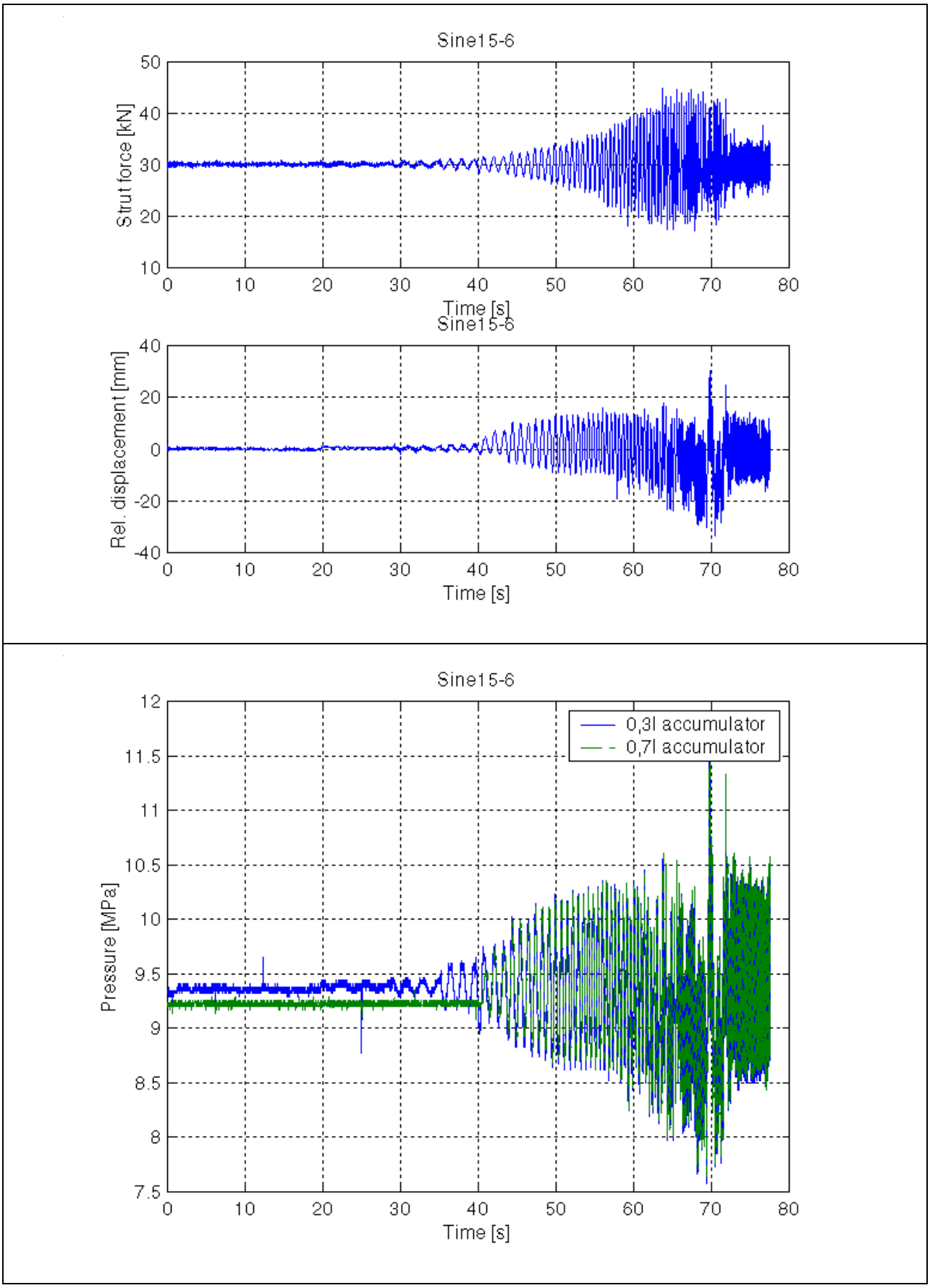


**Figure D-28: Sine sweep (Spring - OFF, Damper - Karnopp)**

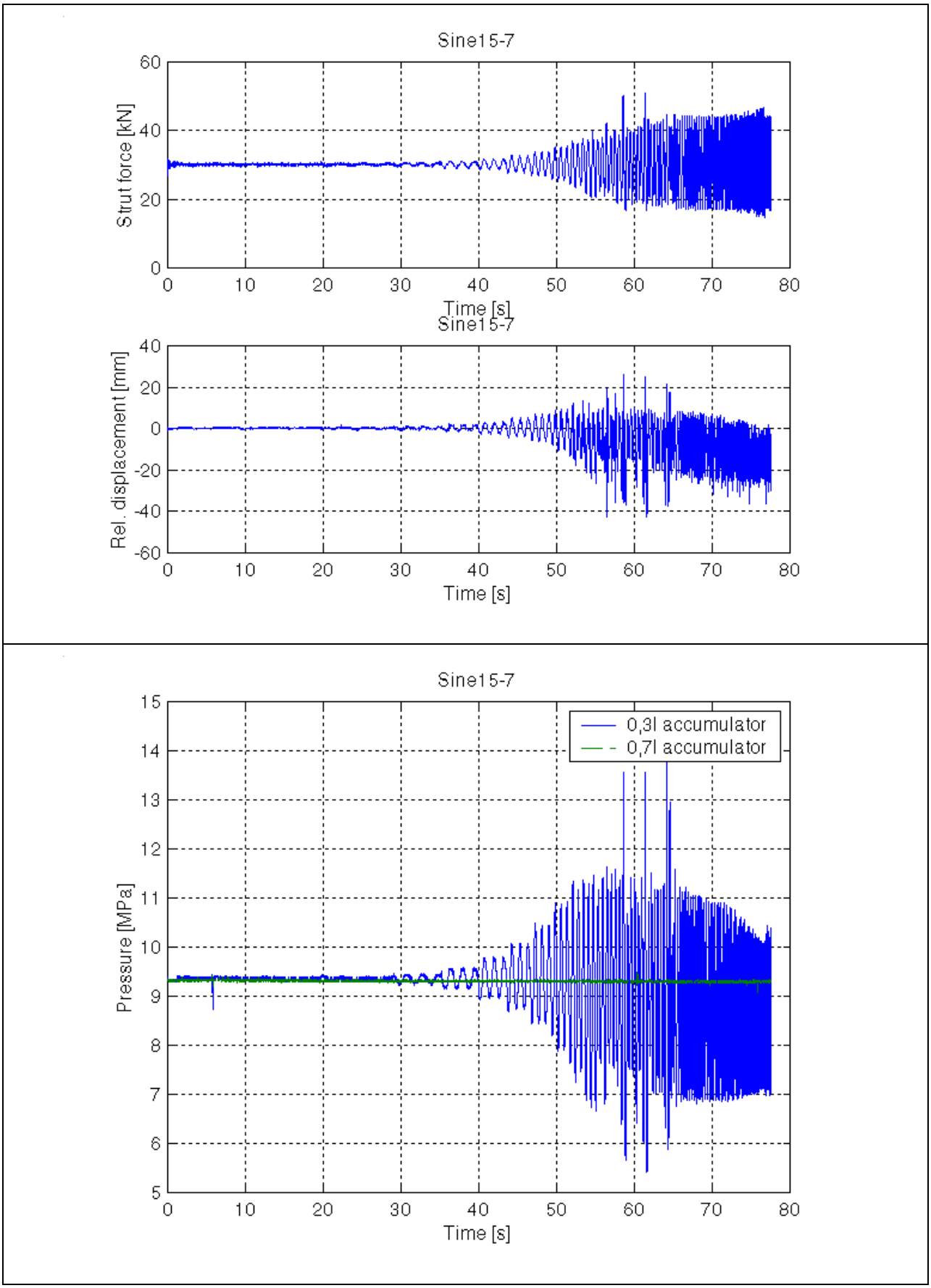


**Figure D-29: Sine sweep (Spring - ON, Damper - Hölscher & Huang)**

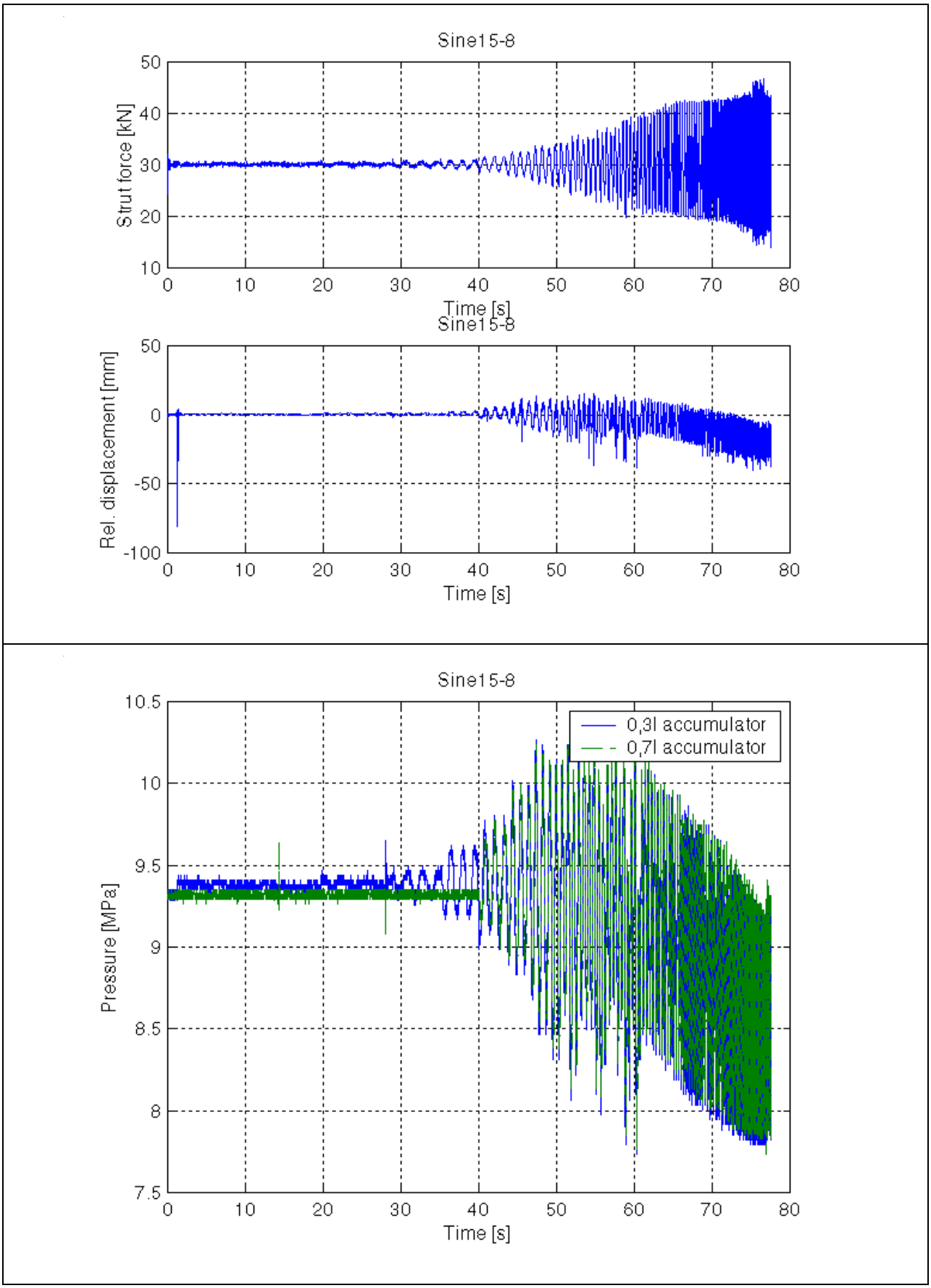


**Figure D-30: Sine sweep (Spring - OFF, Damper - Hölscher & Huang)**

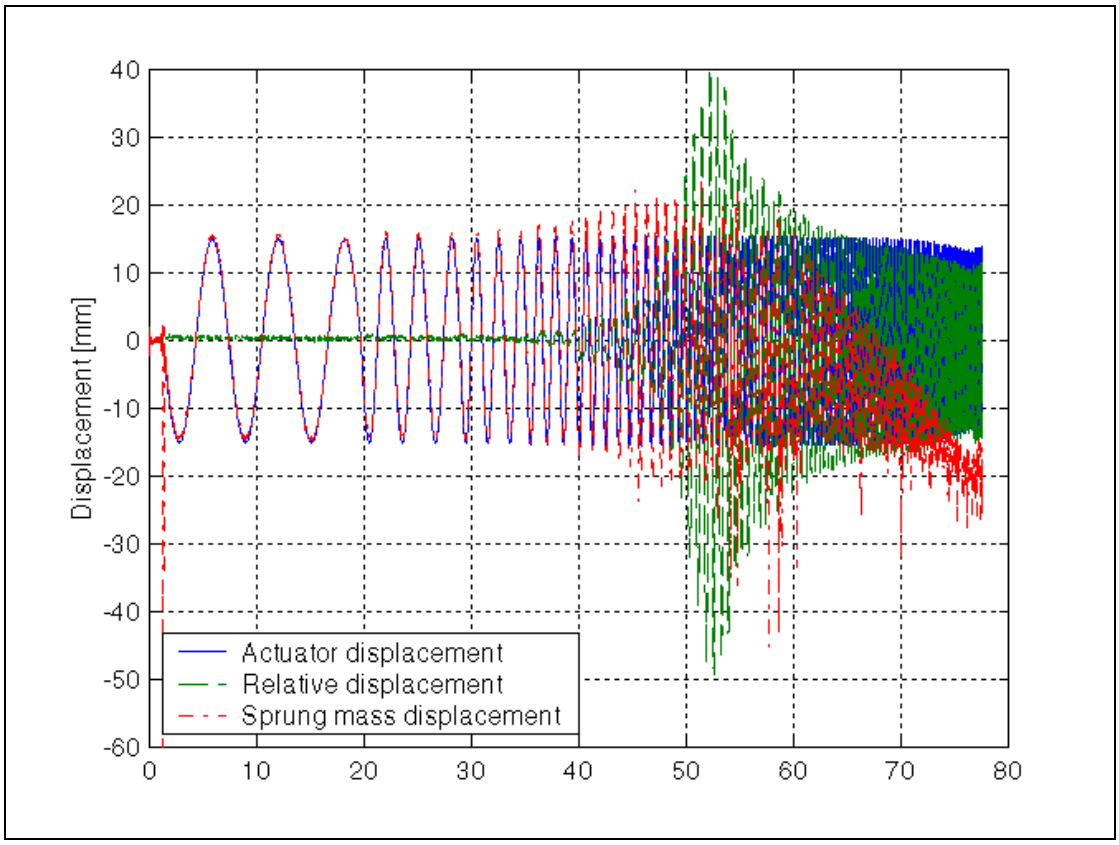


**Figure D-31: Transmissibility plot (Spring - OFF, Damper - OFF)**

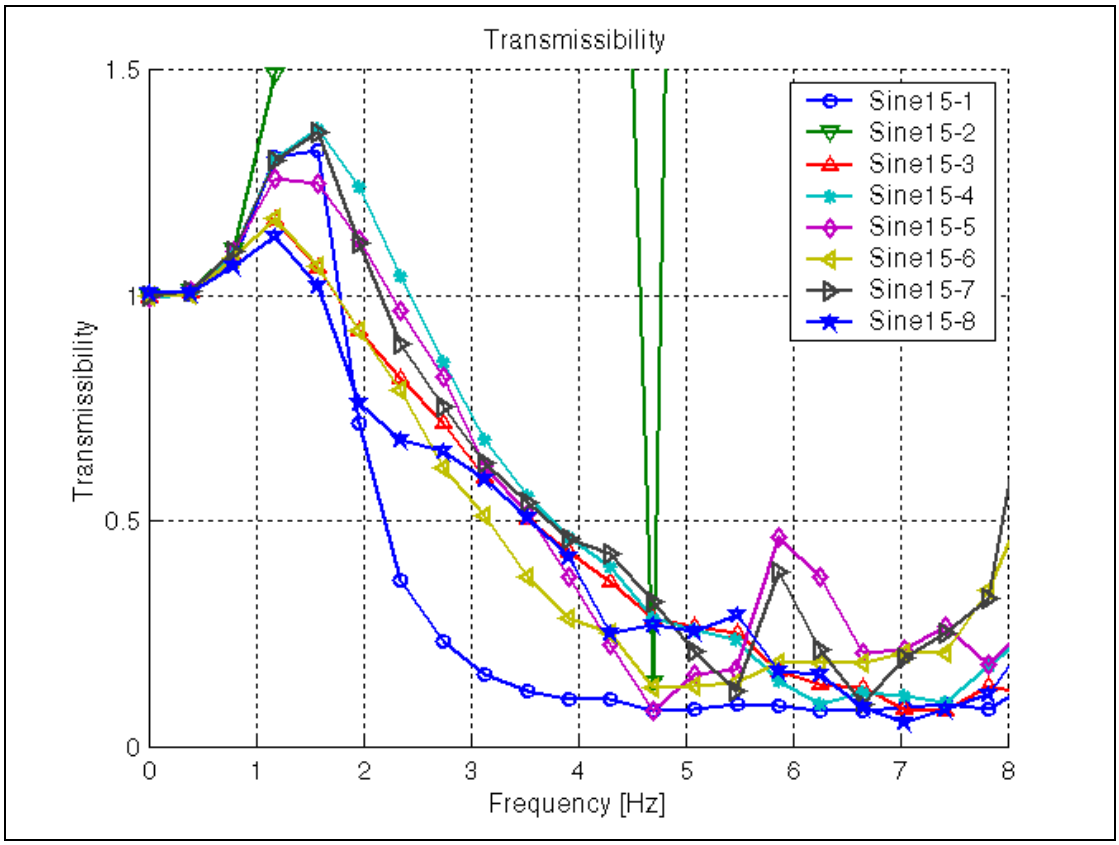


**Figure D-32: Transmissibility plot**

# APPENDIX E: CORRELATION RESULTS

## E.1 Workspace characterisations

For the workspace characterisations, the strut was subjected to a series of compression and extension displacements, while opening and closing the spring valve. During this stage of testing the suspension unit was not yet equipped with a damper and these tests were carried out in order to determine the workspace of the adjustable spring. Table E-1 indicates the spring and damper state, as well as the excitation speed.

**Table E-1: Spring/damper configuration for workspace characterisations**

| Figure number | Input | Spring state | Damper state | Excitation speed [*m/s*] |
|---|---|---|---|---|
| Figure E-2 and Figure E-3 | Figure E-1 | Figure E-1 | OFF | 0.001 |
| Figure E-4 and Figure E-5 | Figure E-1 | Figure E-1 | OFF | 0.01 |
| Figure E-6 and Figure E-7 | Figure E-1 | Figure E-1 | OFF | 0.1 |

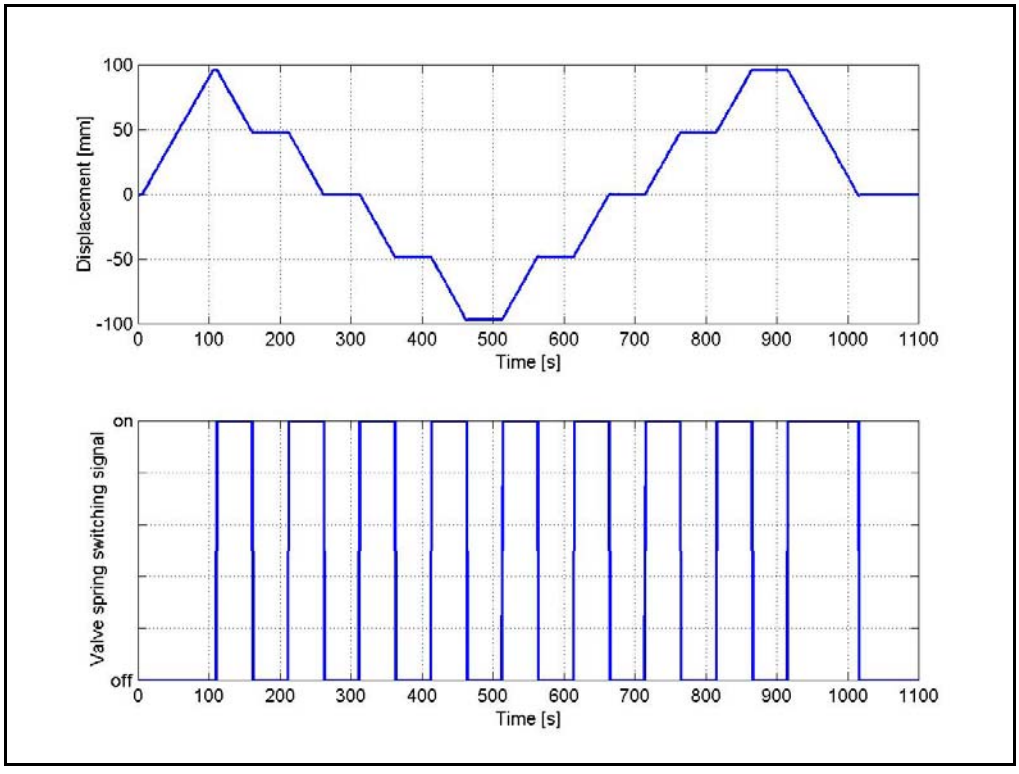


**Figure E-1: Input signal**

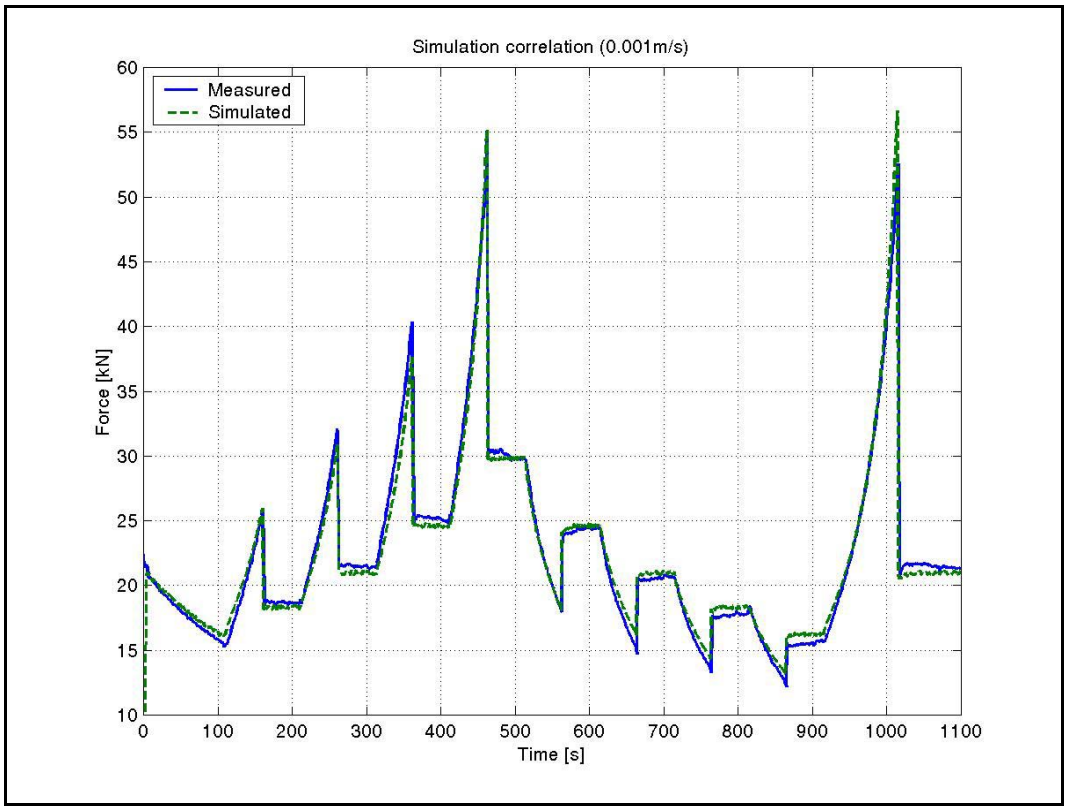


**Figure E-2: Simulation correlation at 0.001*m/s***

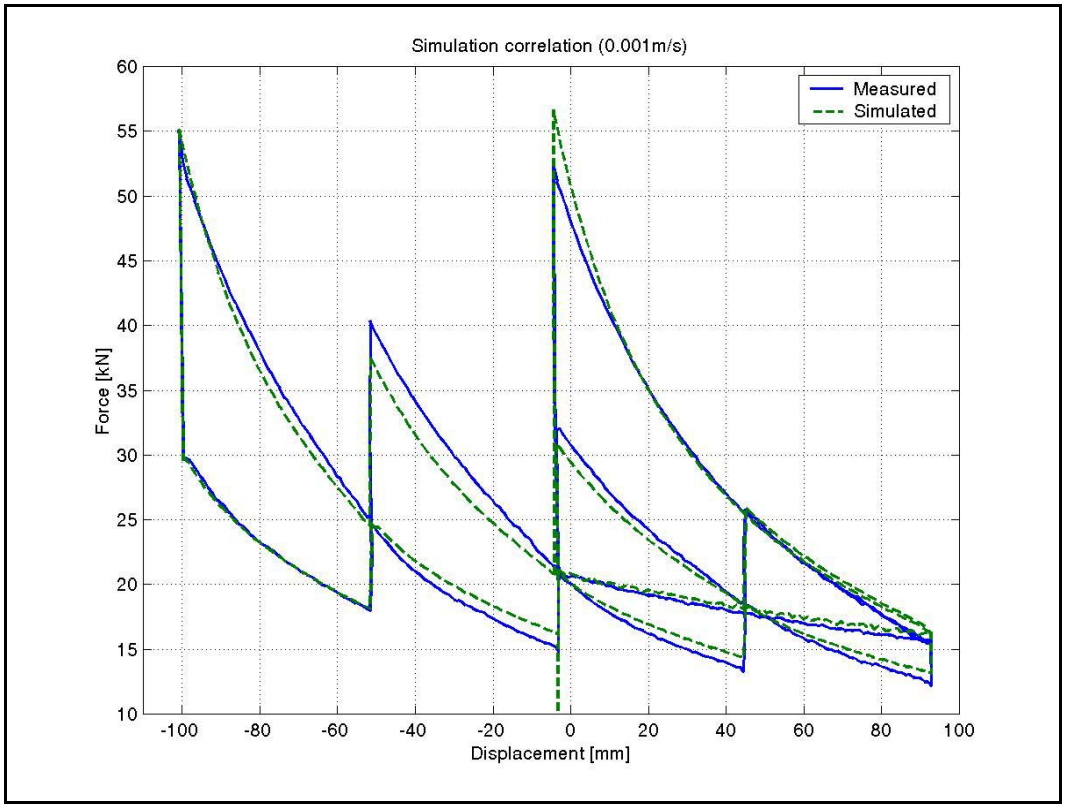


**Figure E-3: Simulation correlation at 0.001*m/s***

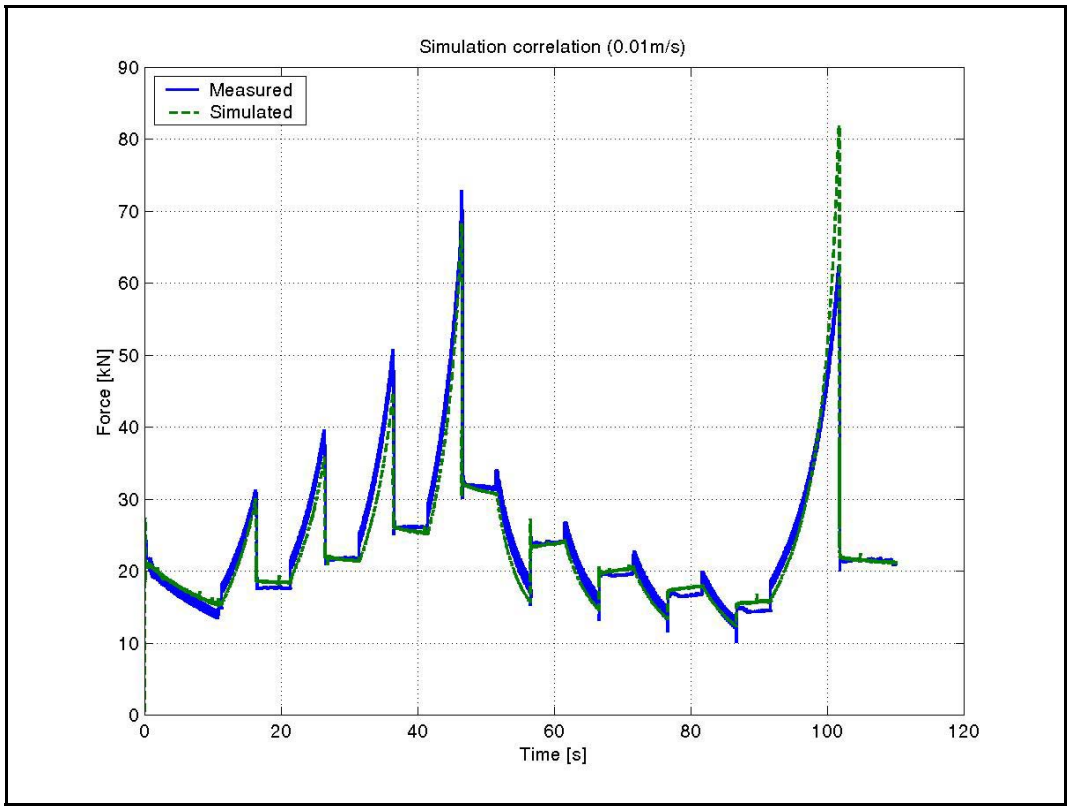


**Figure E-4: Simulation correlation at 0.01*m/s***

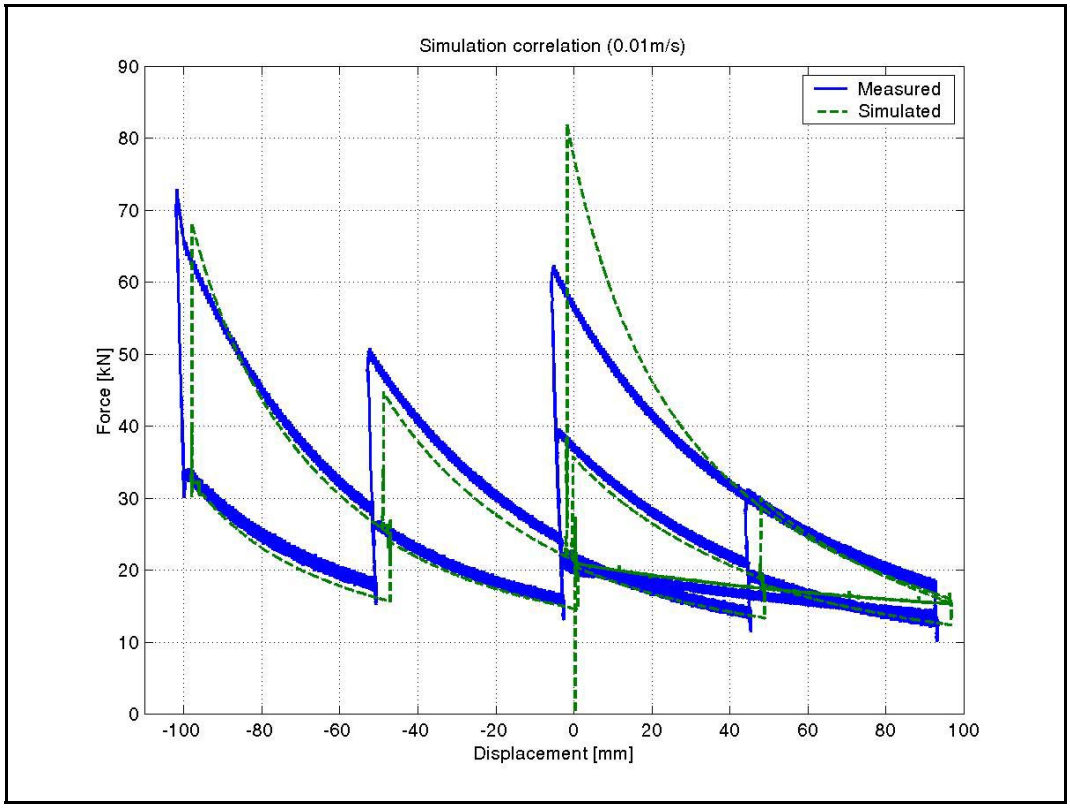


**Figure E-5: Simulation correlation at 0.01*m/s***

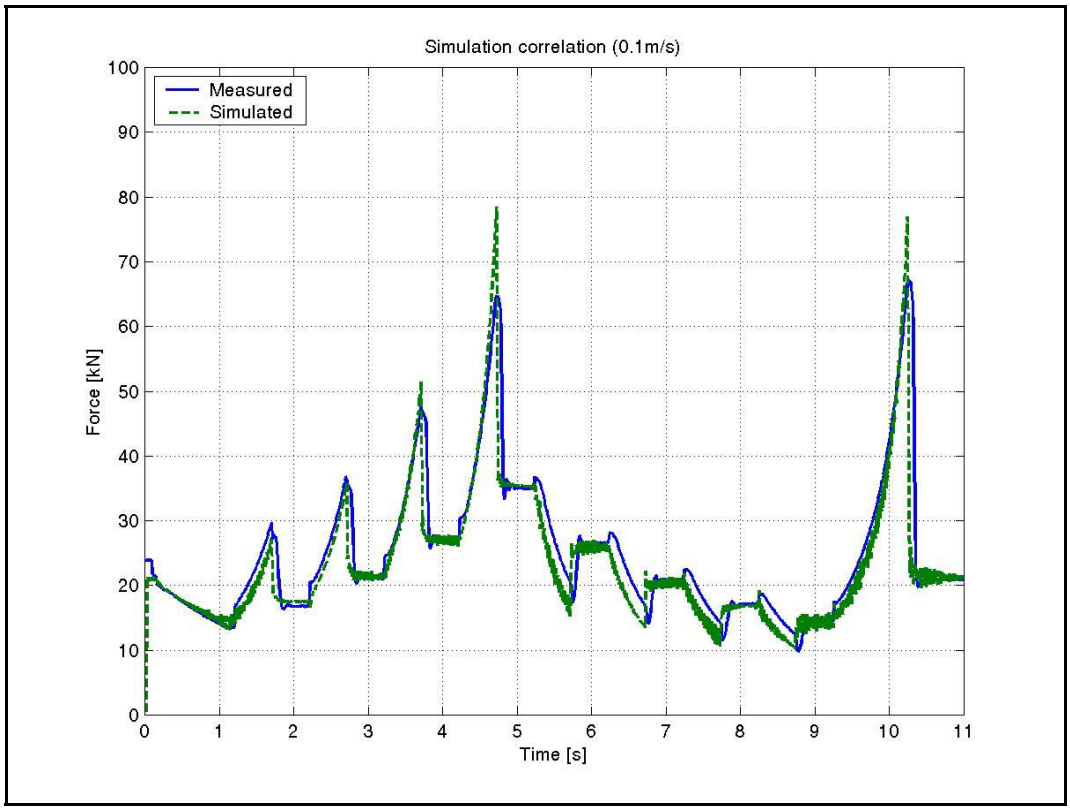


**Figure E-6: Simulation correlation at 0.1*m/s***

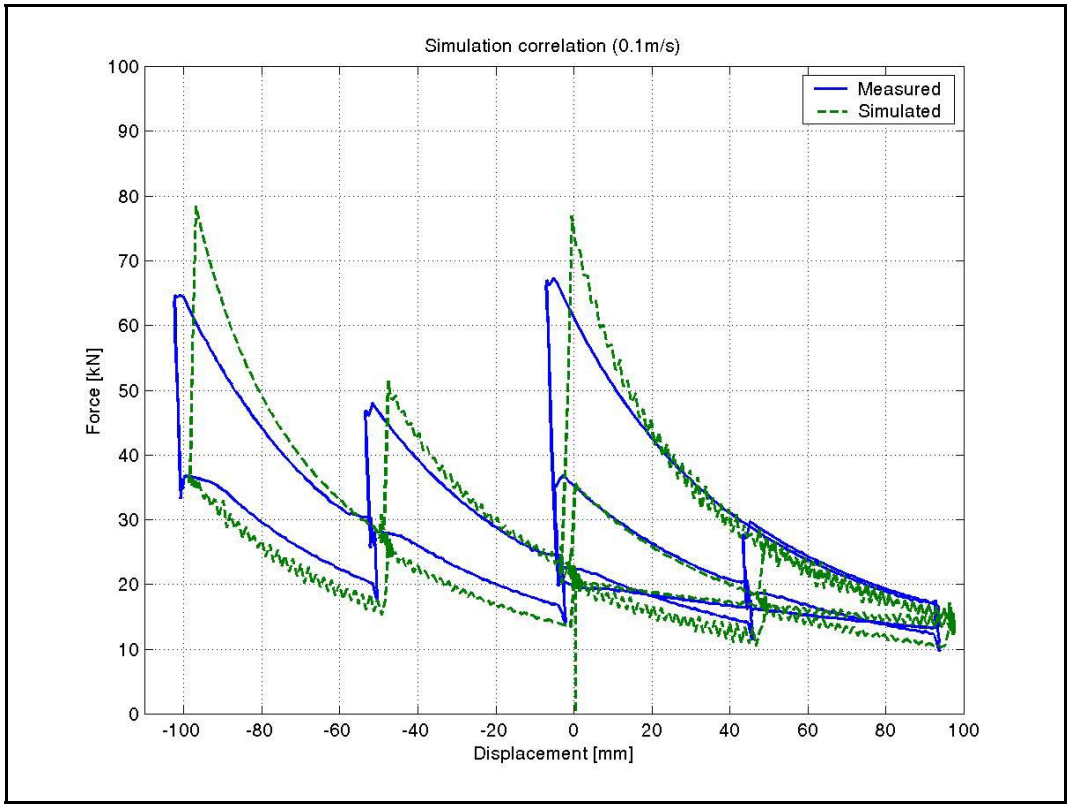


**Figure E-7: Simulation correlation at 0.1*m/s***

## E.2 Step response correlation

Three types of tests were performed on the SDOF setup, namely step response, random input response and sine sweep. This section contains the correlation between measured and simulated results for the step response tests. All the correlation graphs are of relative displacement.

**Table E-2: Spring/damper configuration for step response tests**

| Figure number | Input | Spring state | Damper state |
|---|---|---|---|
| Figure E-8 | 30*mm* step | OFF | OFF |
| Figure E-9 | 30*mm* step | ON | OFF |
| Figure E-10 | 30*mm* step | OFF | ON |
| Figure E-11 | 30*mm* step | ON | ON |
| Figure E-12 | 30*mm* step | ON | Karnopp |
| Figure E-13 | 30*mm* step | OFF | Karnopp |
| Figure E-14 | 30*mm* step | ON | Hölscher & Huang |
| Figure E-15 | 30*mm* step | OFF | Hölscher & Huang |
| Figure E-16 | 60*mm* step | OFF | OFF |

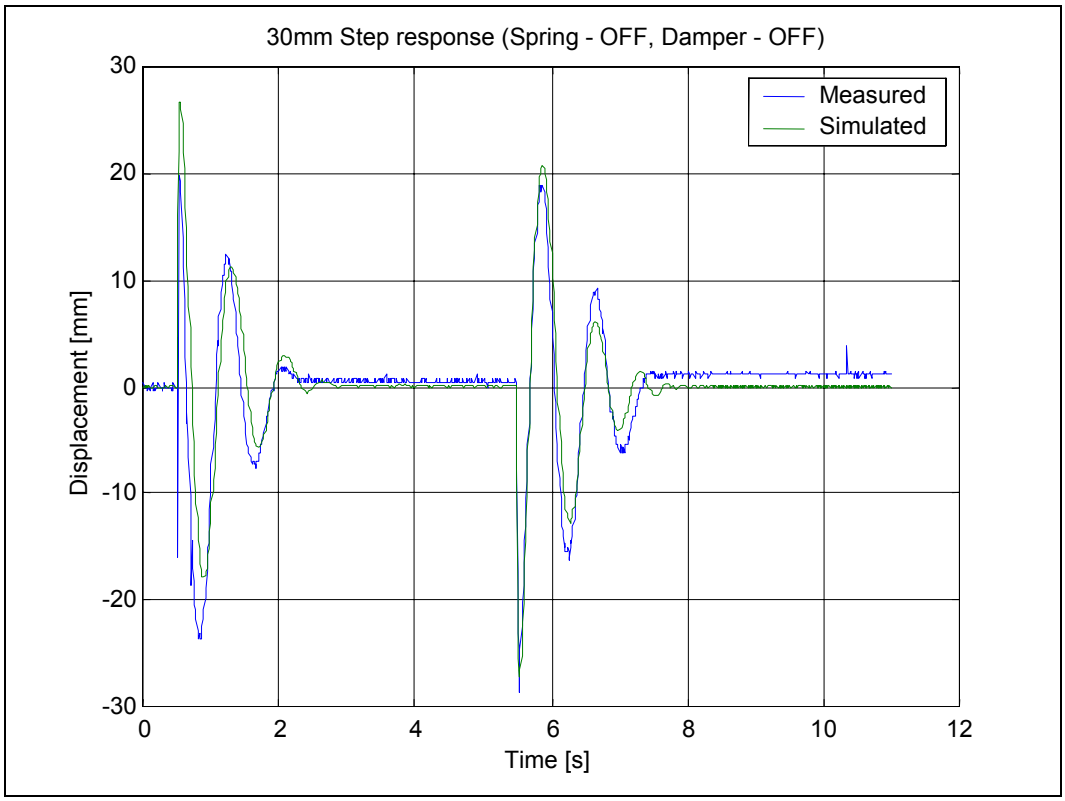


**Figure E-8: 30*mm* step response (Spring – OFF, Damper - OFF)**

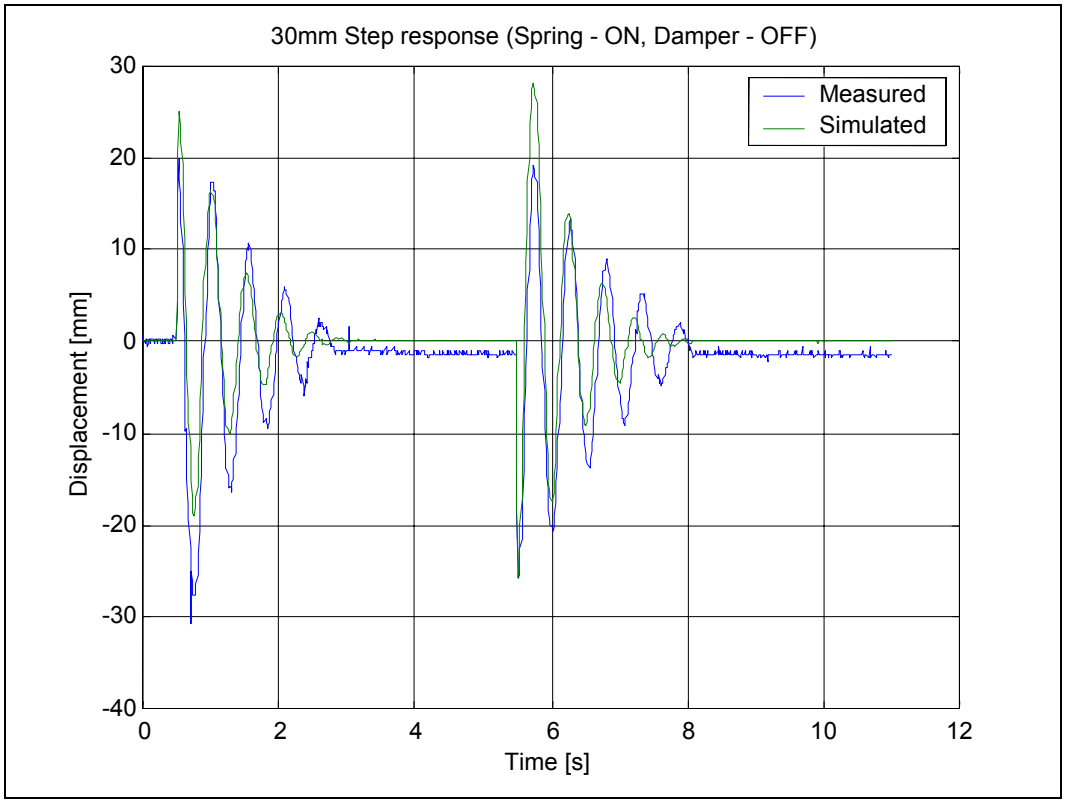


**Figure E-9: 30*mm* step response (Spring – ON, Damper - OFF)**

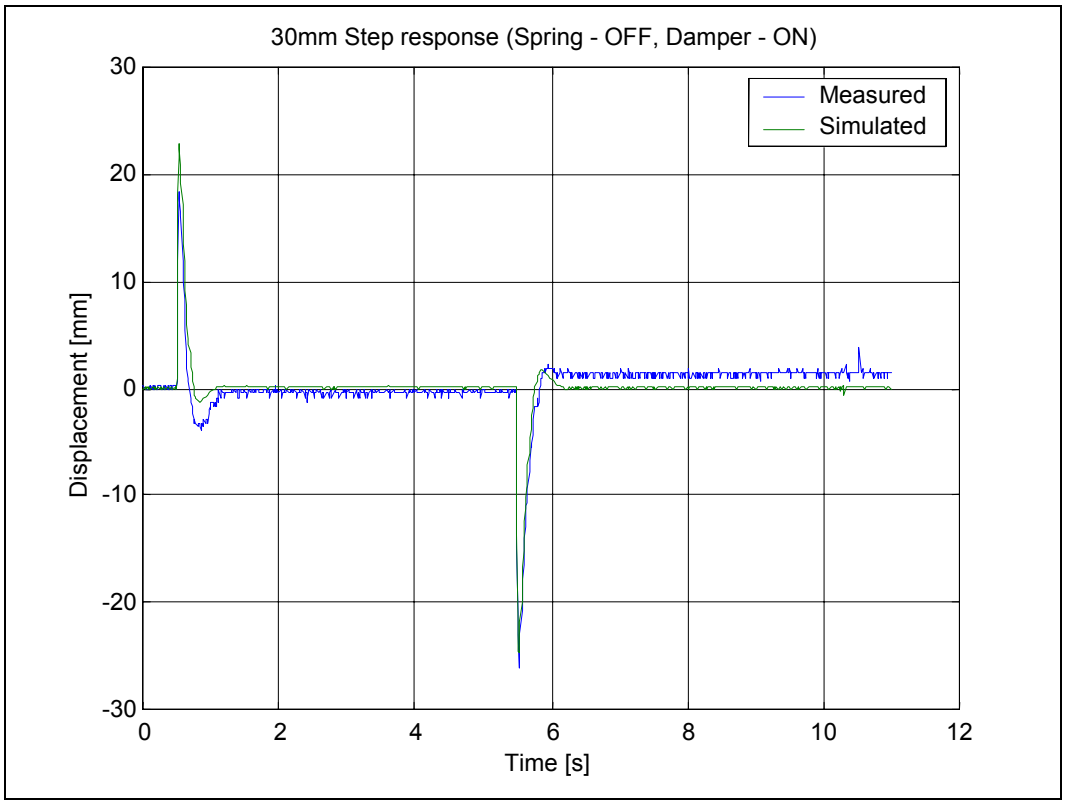


**Figure E-10: 30*mm* step response (Spring – OFF, Damper - ON)**

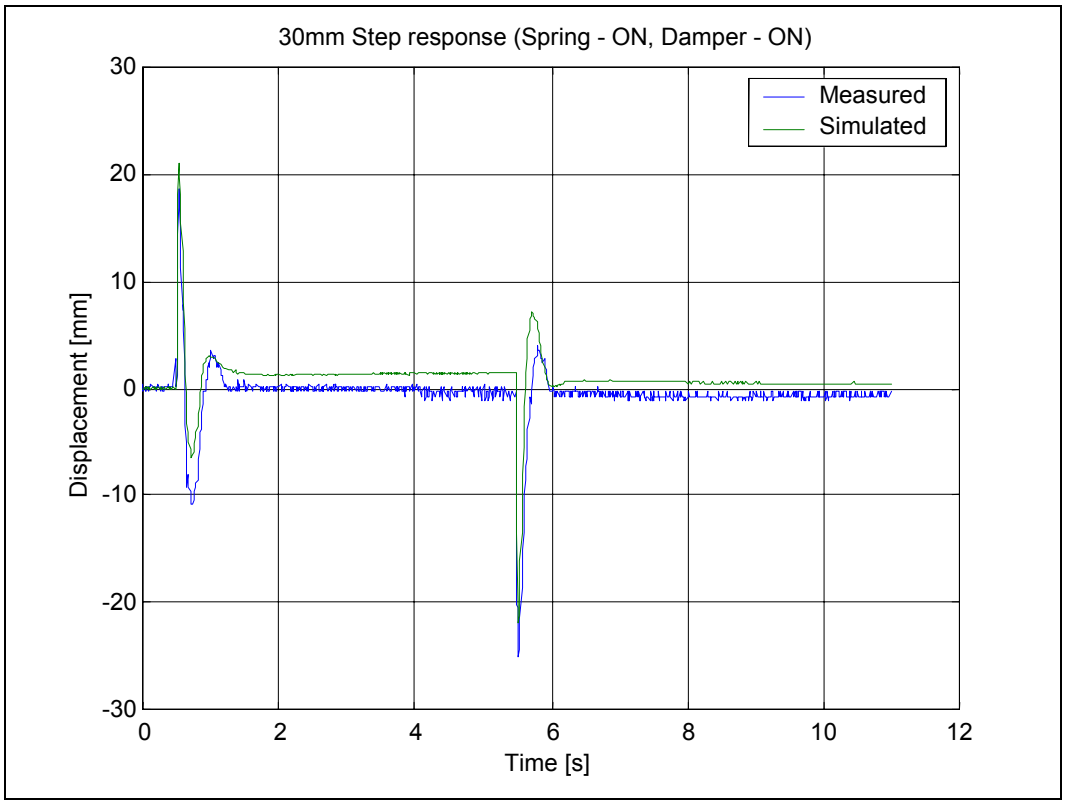


**Figure E-11: 30*mm* step response (Spring – ON, Damper - ON)**

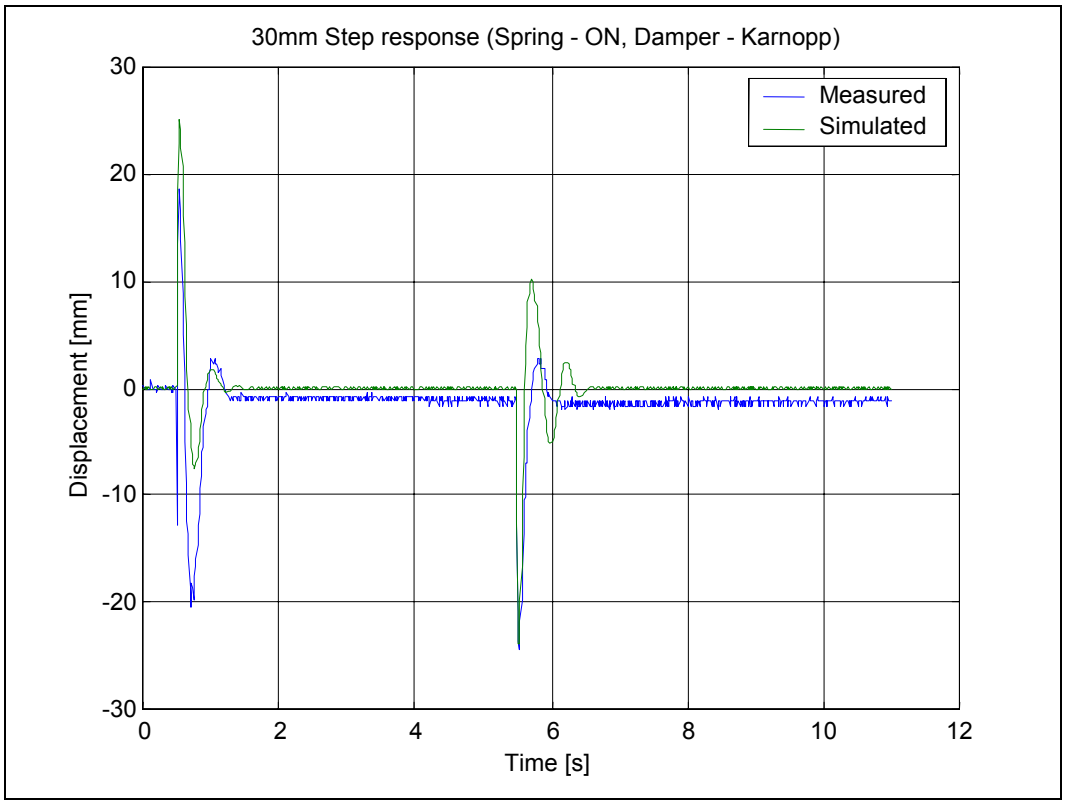


**Figure E-12: 30*mm* step response (Spring – ON, Damper - Karnopp)**

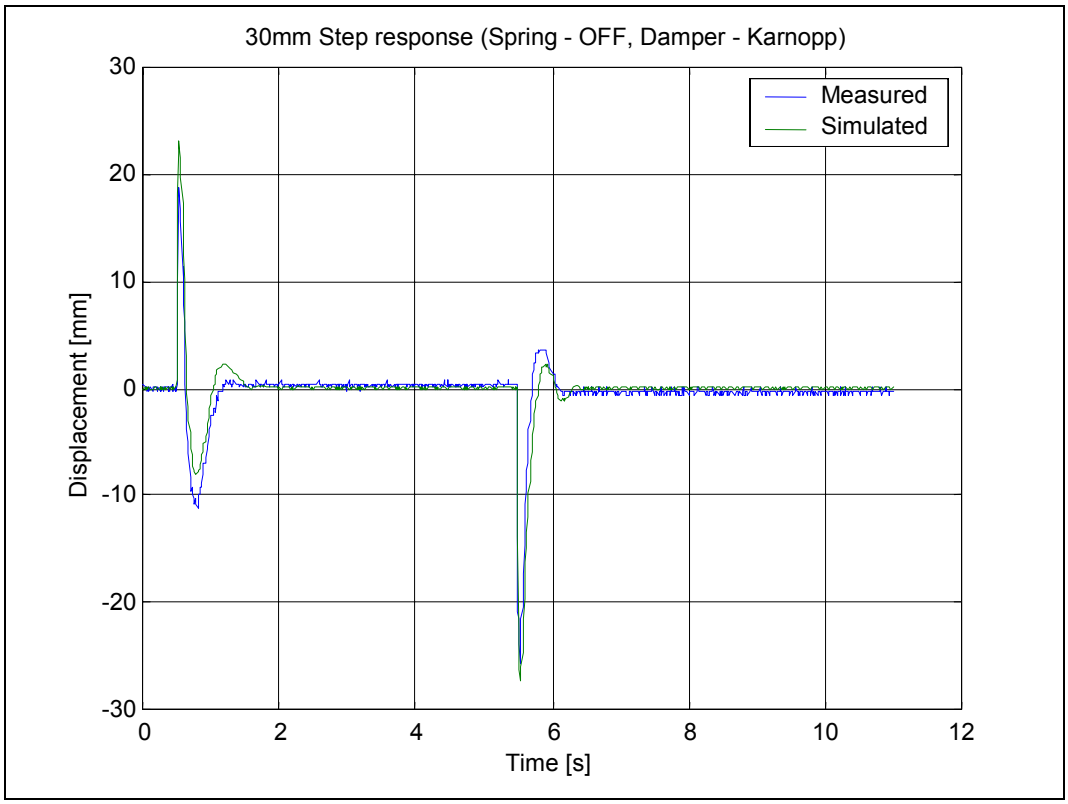


**Figure E-13: 30*mm* step response (Spring – OFF, Damper - Karnopp)**

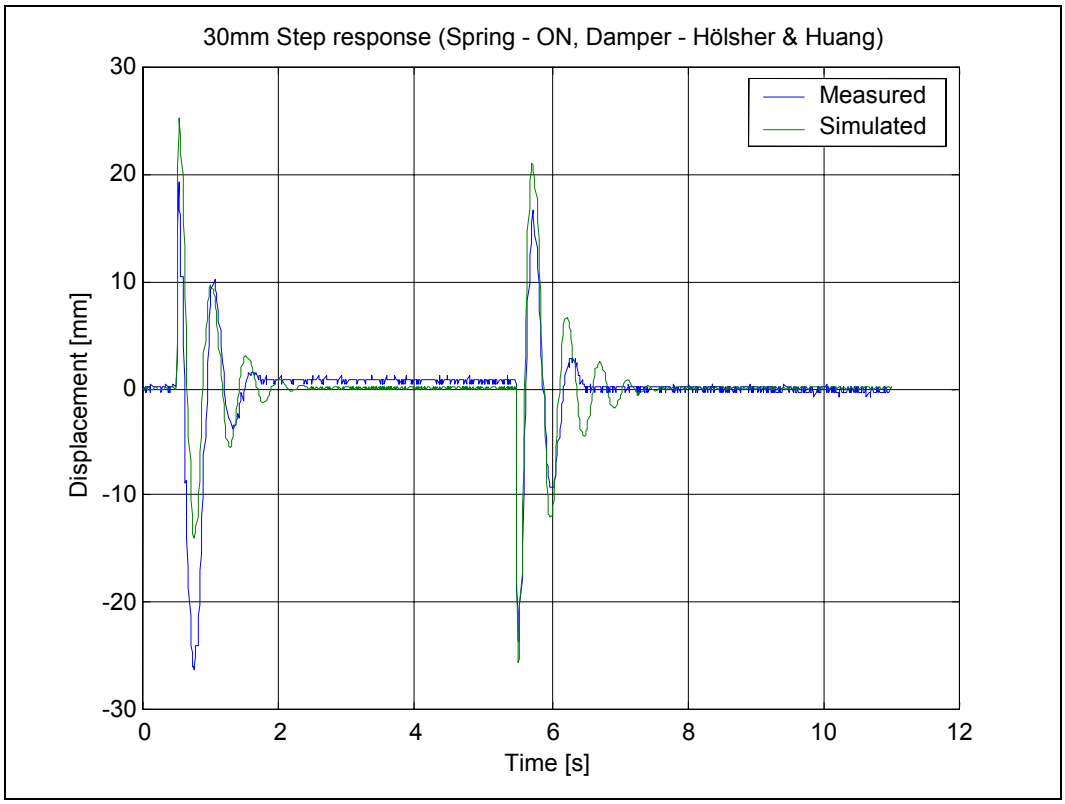


**Figure E-14: 30*mm* step response (Spring – ON, Damper – Hölscher & Huang)**

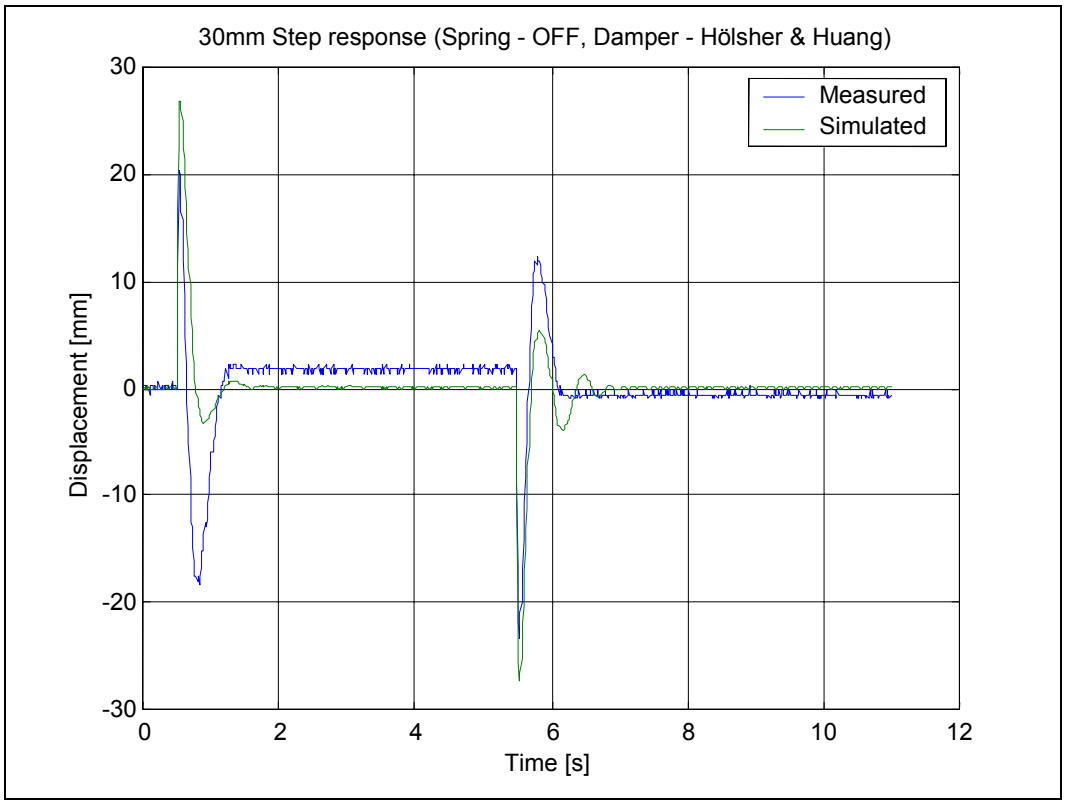


**Figure E-15: 30*mm* step response (Spring – OFF, Damper – Hölscher & Huang)**

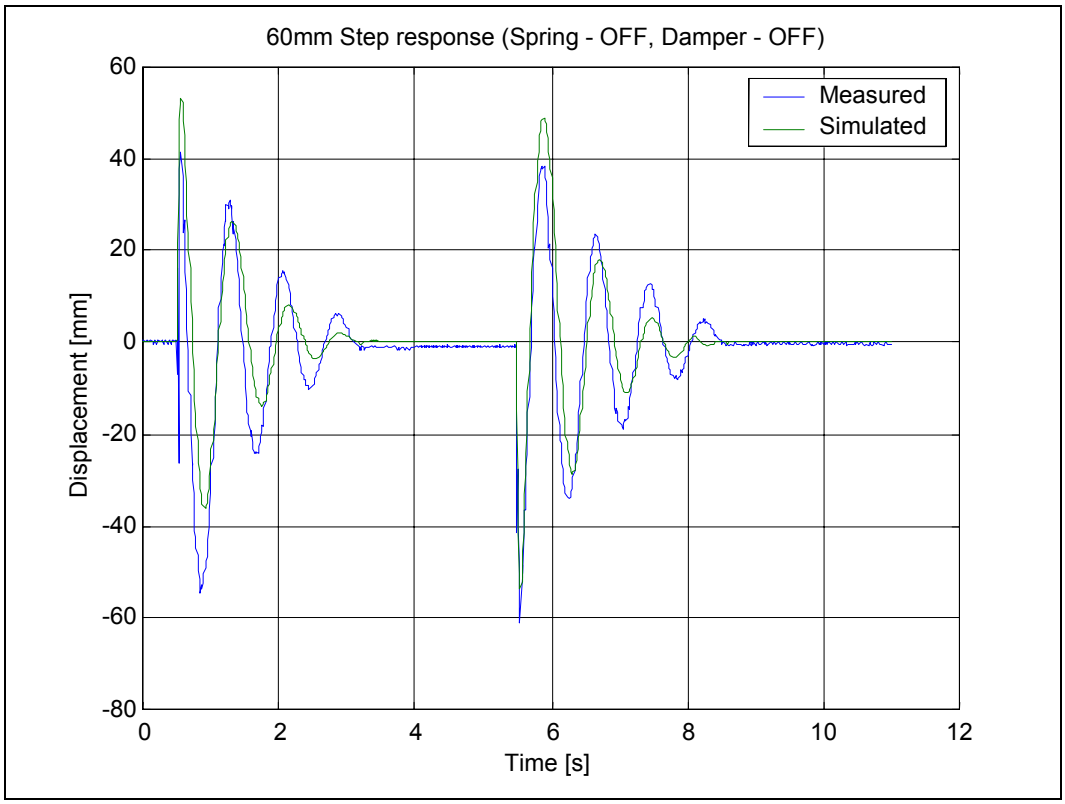


**Figure E-16: 60*mm* step response (Spring – OFF, Damper - OFF)**

## E.3 Random input response correlation

For the random input response tests, the left-hand lane of the Belgian paving track at the Gerotek Vehicle Testing Facility was used. Different spring and damper settings were tested and the figures in this section indicate the correlation obtained between measured and simulated results. Table E-3 indicates the spring and damper setting for each of the graphs presented in this section.

**Table E-3: Spring/damper configuration for random input tests**

| Configuration no. | Figure number | Input | Spring state | Damper state |
|---|---|---|---|---|
| 1 | Figure E-17 | Belgian paving | OFF | OFF |
| 2 | Figure E-18 | Belgian paving | ON | OFF |
| 3 | Figure E-19 | Belgian paving | OFF | ON |
| 4 | Figure E-20 | Belgian paving | ON | ON |
| 5 | Figure E-21 | Belgian paving | ON | Karnopp |
| 6 | Figure E-22 | Belgian paving | OFF | Karnopp |
| 7 | Figure E-23 | Belgian paving | ON | Hölscher & Huang |
| 8 | Figure E-24 | Belgian paving | OFF | Hölscher & Huang |
| 9 | Figure E-25 | Belgian paving | Karnopp | Karnopp |
| 10 | Figure E-26 | Belgian paving | Height adjustment | OFF |
| - | Figure E-27 | Belgian paving | Minimum and maximum results summary | |
| - | Figure E-28 | Belgian paving | RMS results summary | |

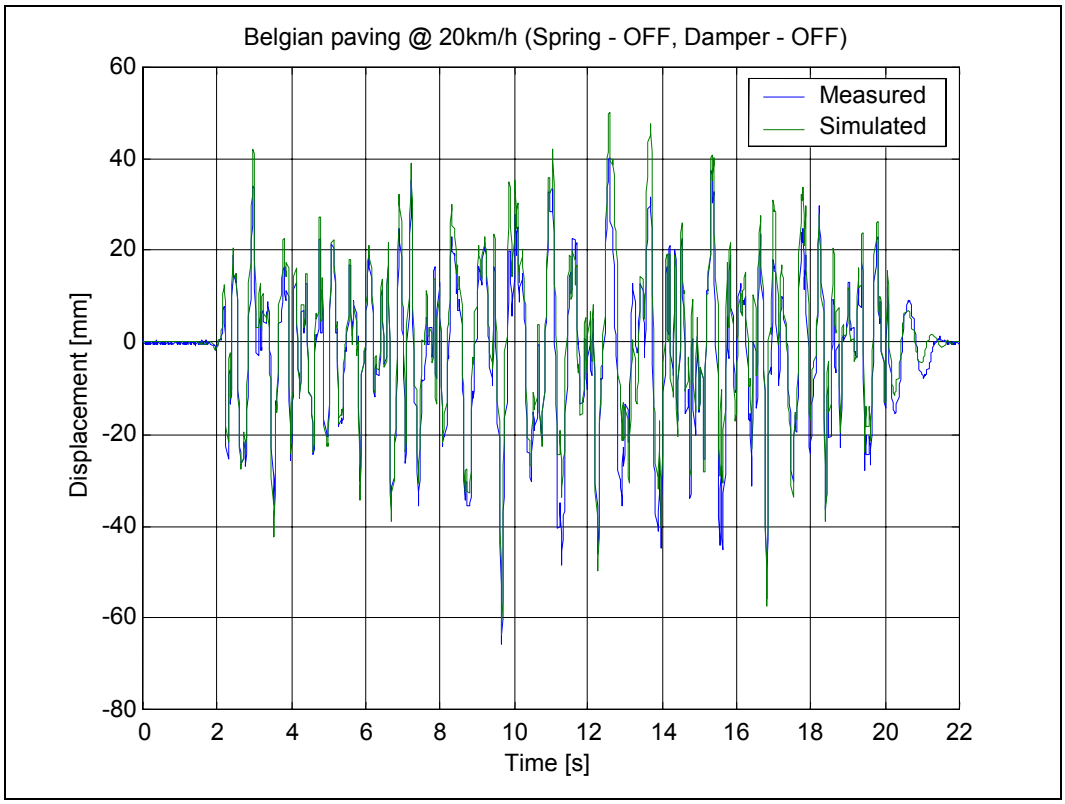


**Figure E-17: Random input correlation (Spring – OFF, Damper – ON)**

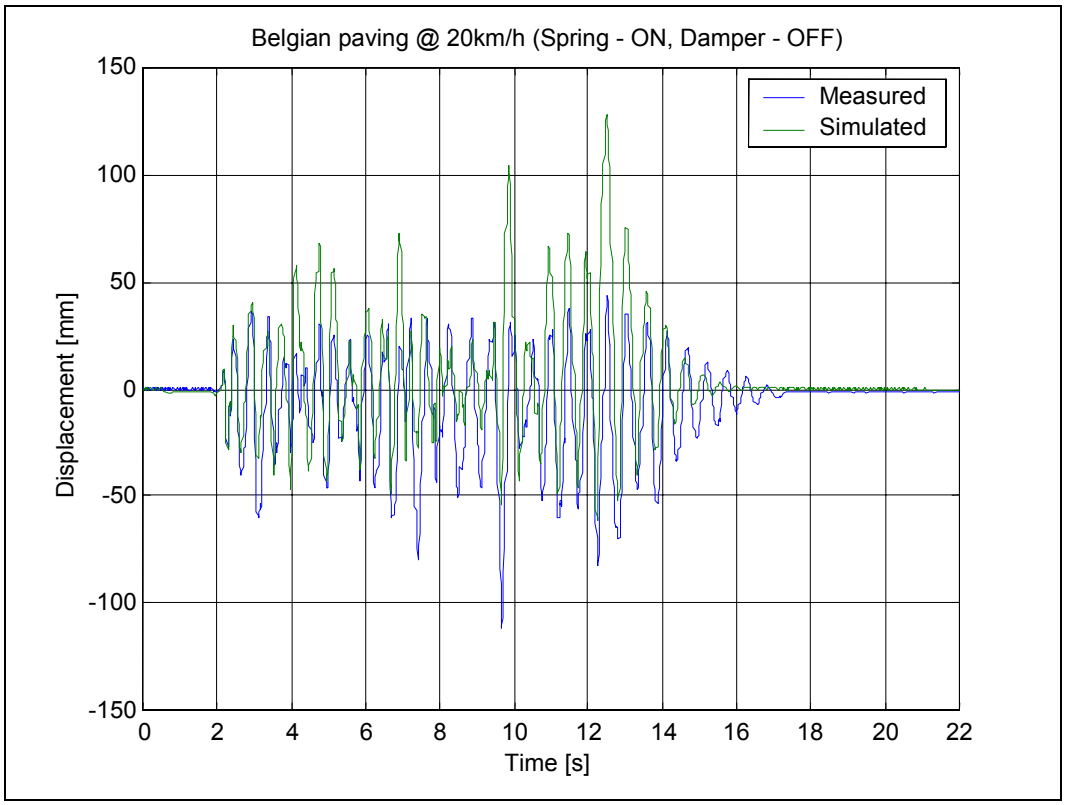


**Figure E-18: Random input correlation (Spring – ON, Damper – OFF)**

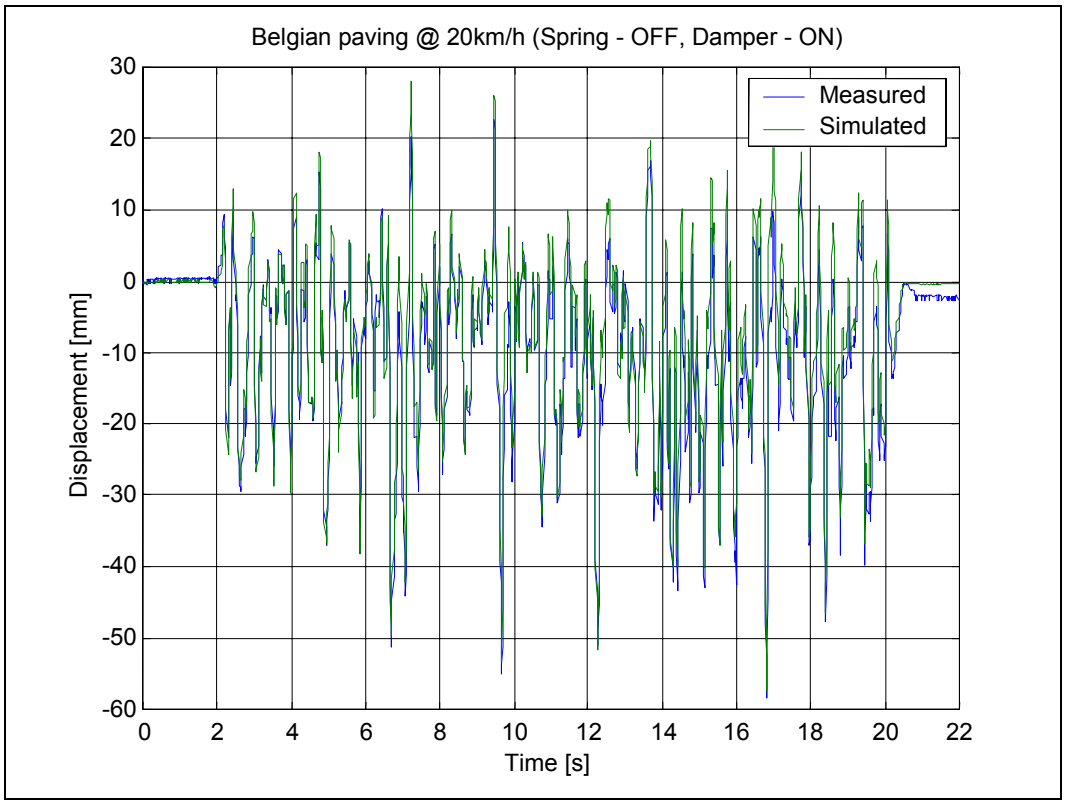


**Figure E-19: Random input correlation (Spring – OFF, Damper – ON)**

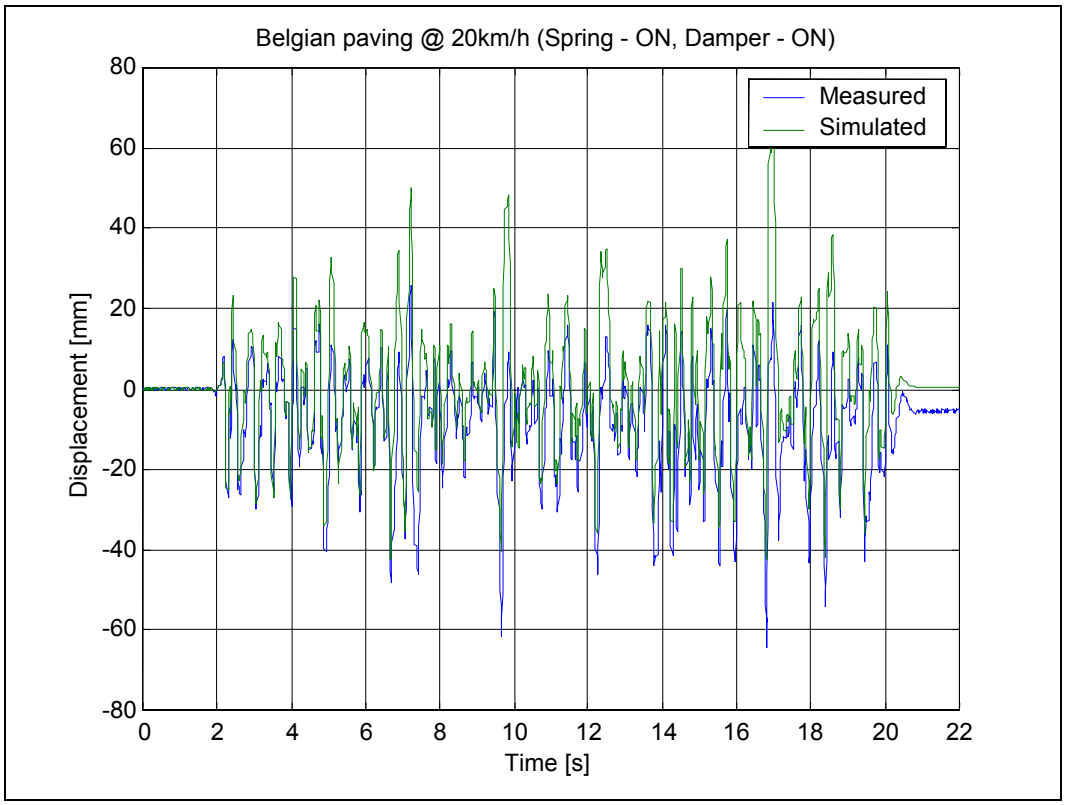


**Figure E-20: Random input correlation (Spring – ON, Damper – ON)**

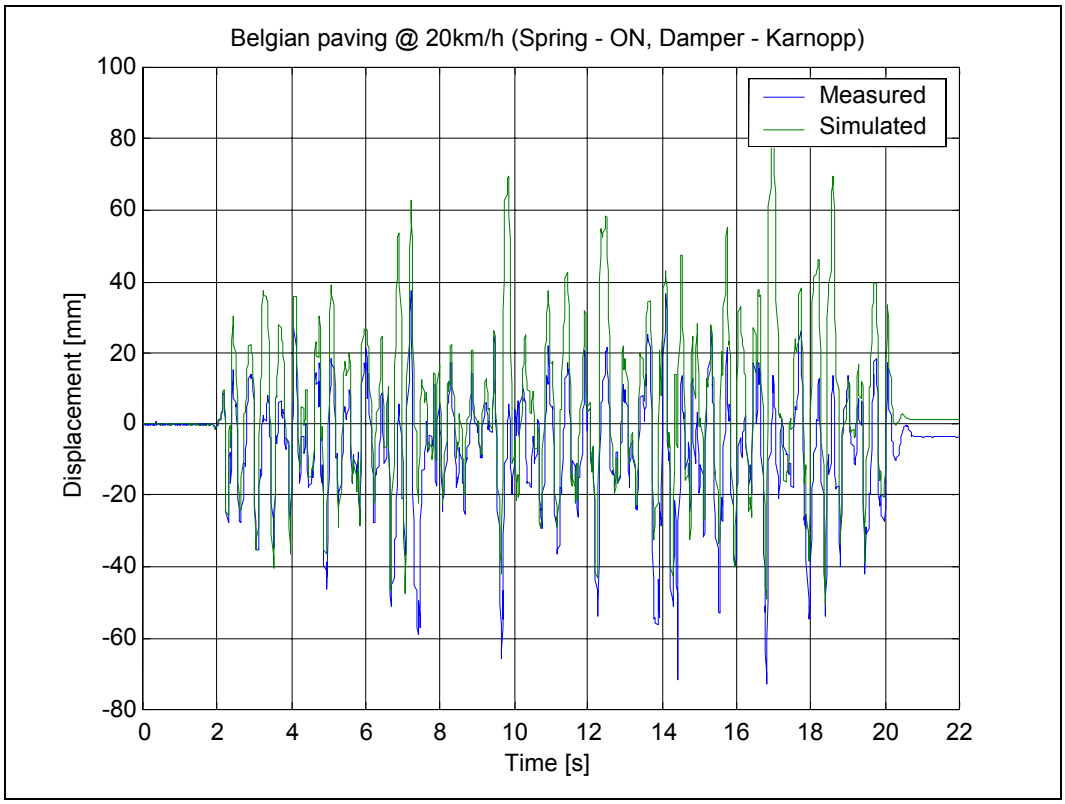


**Figure E-21: Random input correlation (Spring – ON, Damper – Karnopp)**

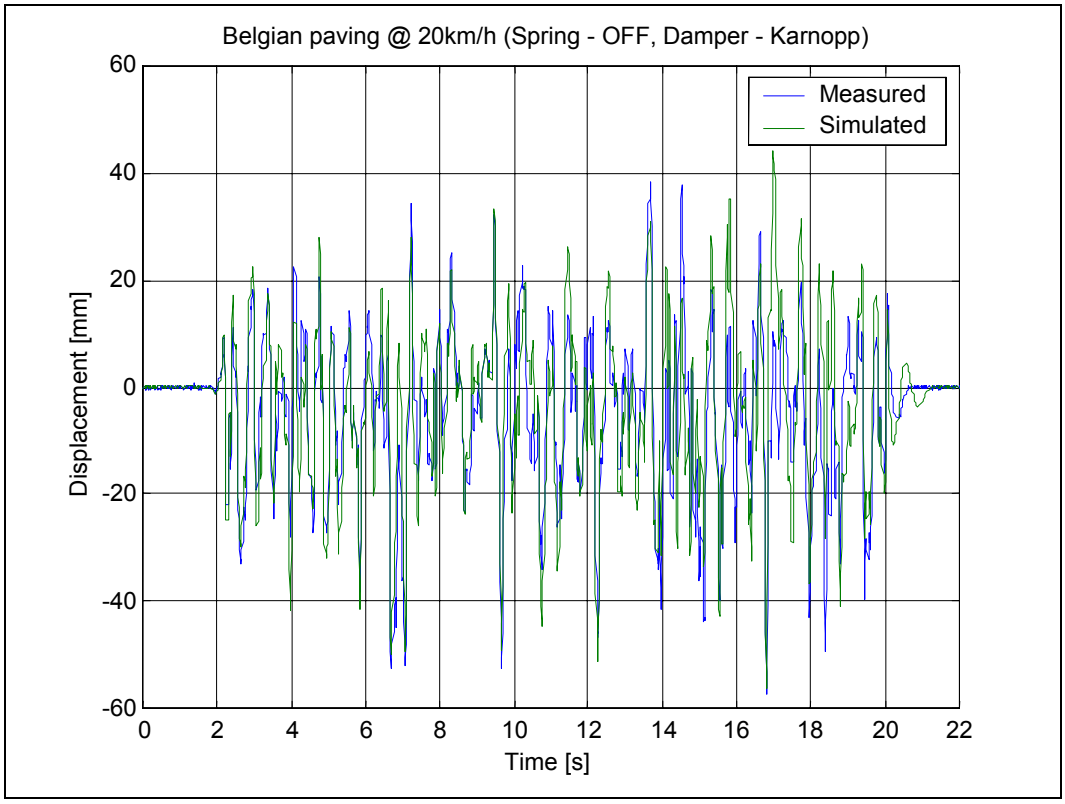


**Figure E-22: Random input correlation (Spring – OFF, Damper – Karnopp)**

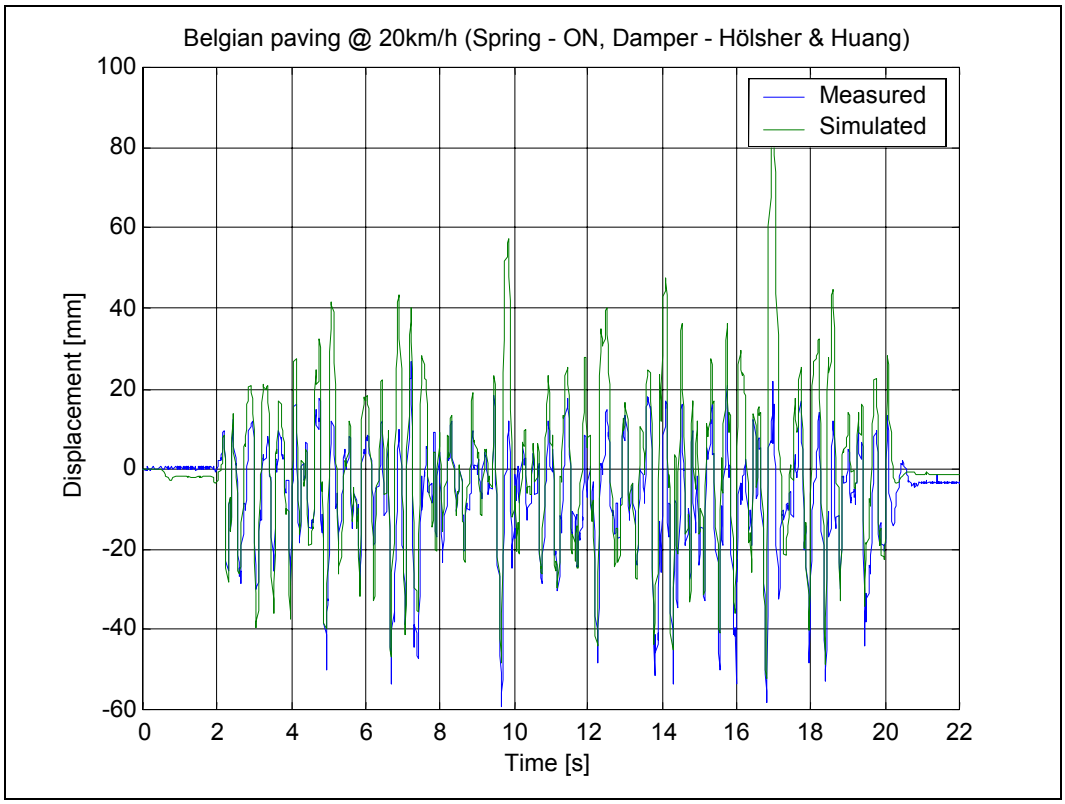


**Figure E-23: Random input correlation (Spring – ON, Damper – Hölscher & Huang)**

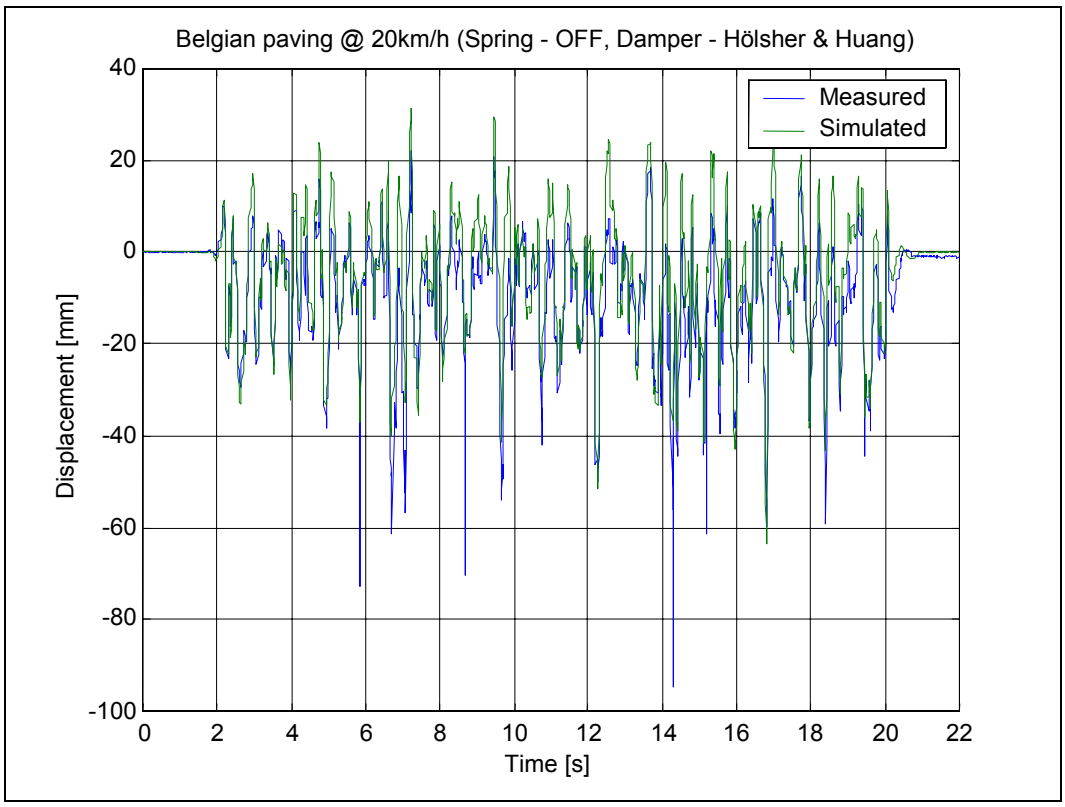


**Figure E-24: Random input correlation (Spring – OFF, Damper – Hölscher & Huang)**

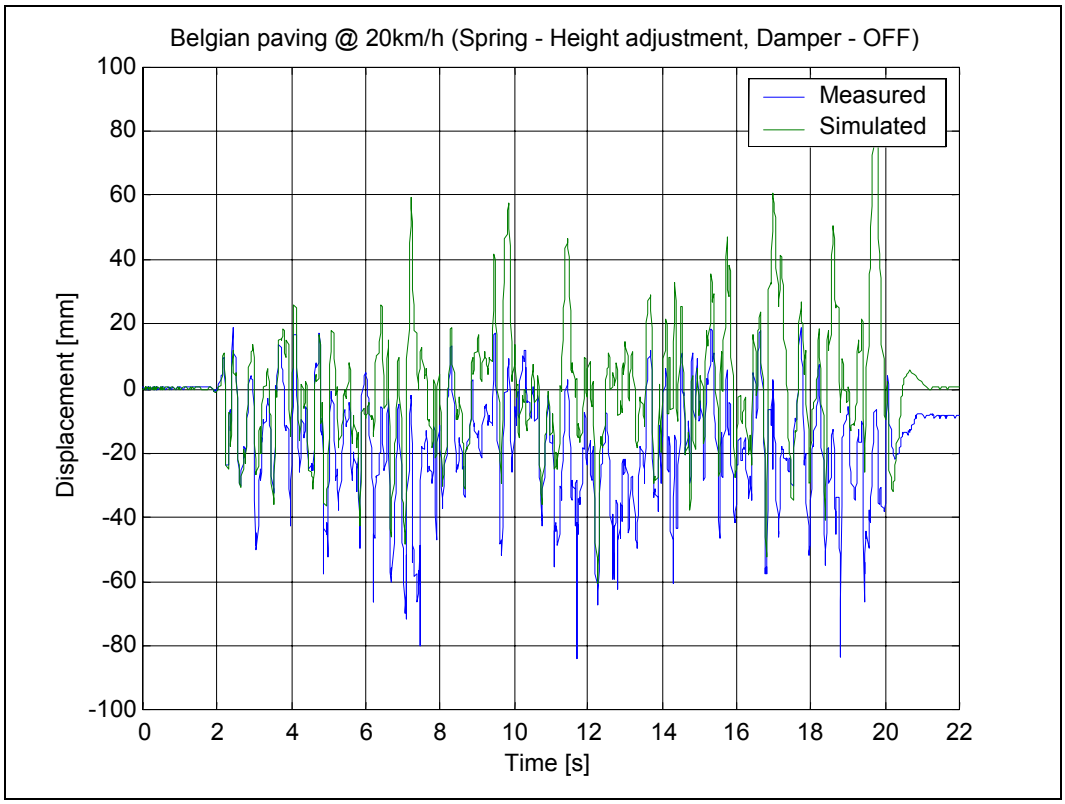


**Figure E-25: Random input correlation (Spring – Height adjustment, Damper – OFF)**

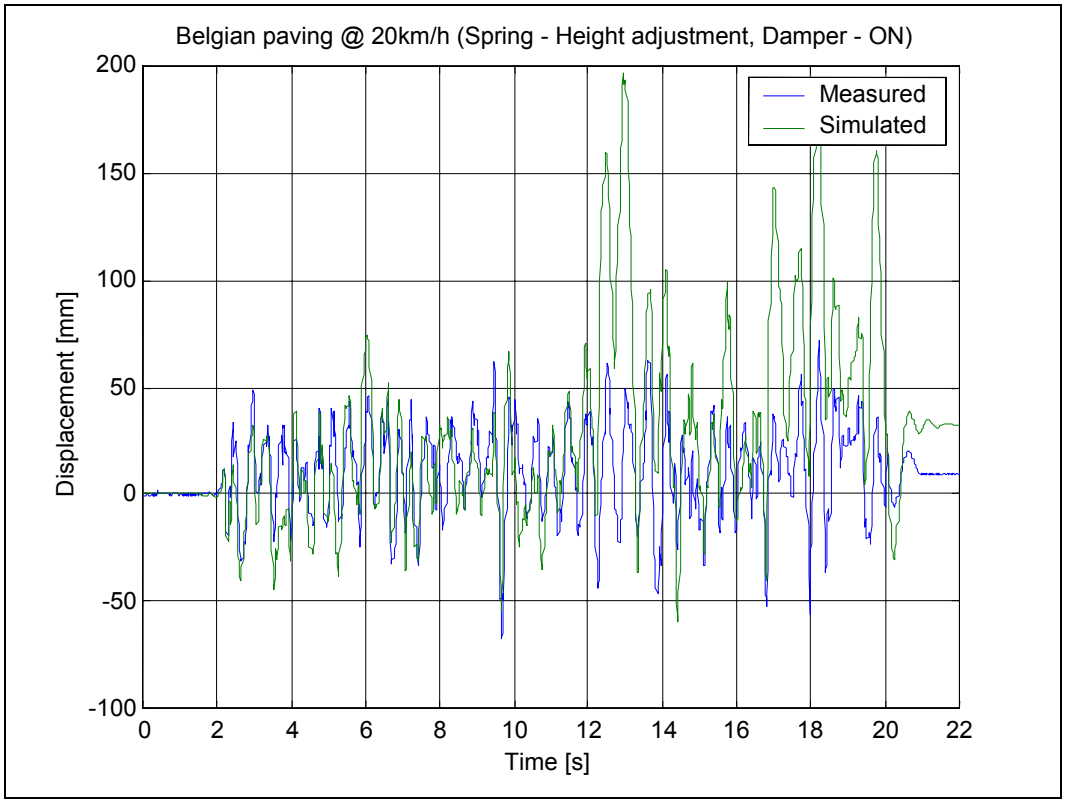


**Figure E-26: Random input correlation (Spring – Height adjustment, Damper – ON)**

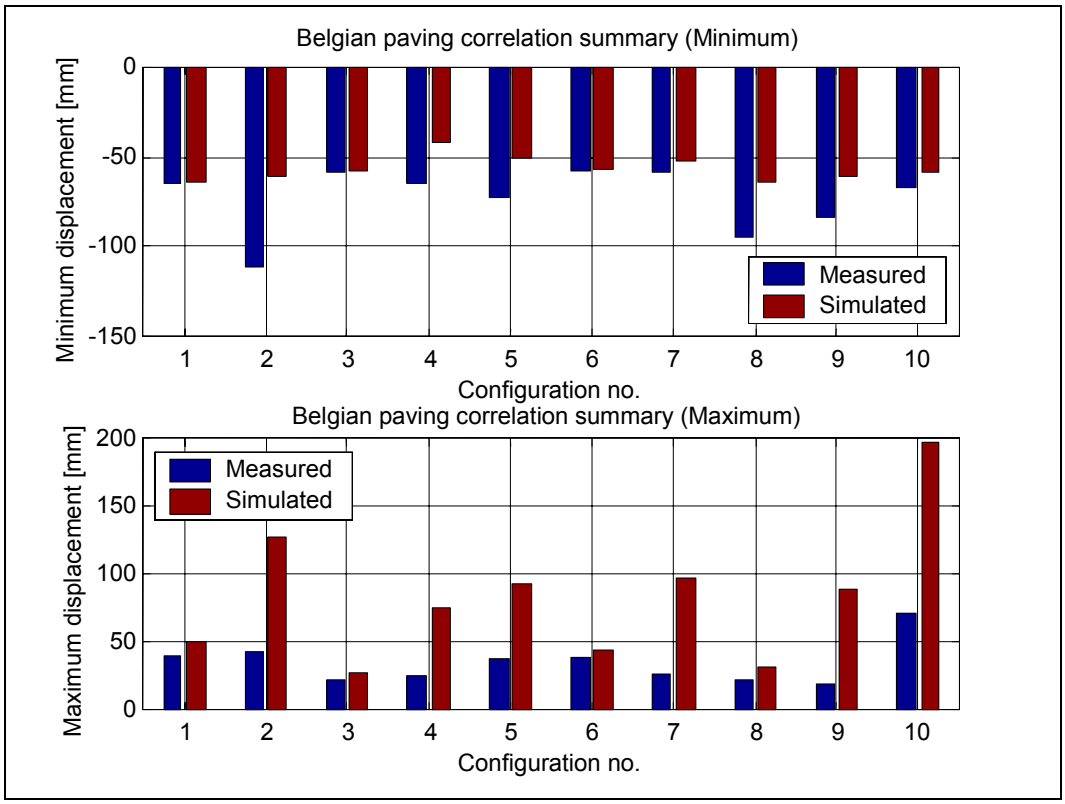


**Figure E-27: Belgian paving correlation summary (Minimum and maximum)**

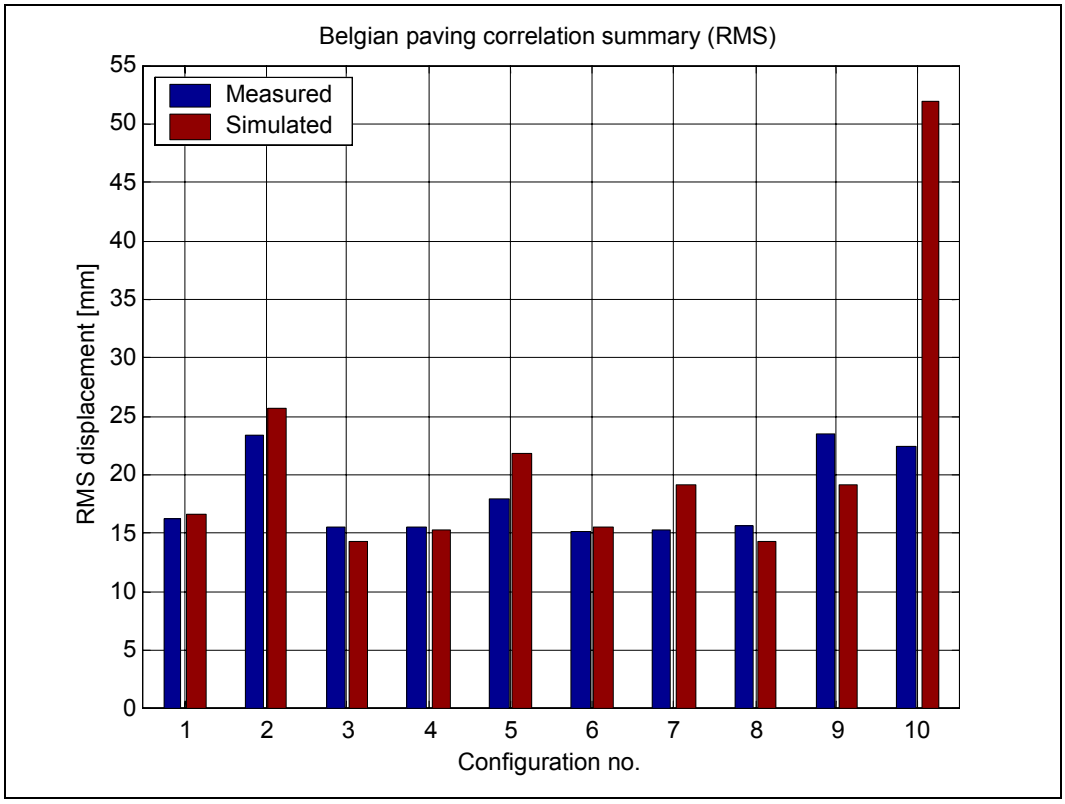


**Figure E-28: Belgian paving correlation summary (RMS)**

## E.4 Sine sweep correlation

For the sine sweep tests, a sine displacement input was supplied to the actuator. The sine wave had a constant amplitude of 15*mm*, while the frequency was linearly adjusted from 0.1*Hz* to 15*Hz* in 78*s*. Figure E-29 indicates the recorded actuator signal for the sine sweep tests. From this figure, it is clear that the frequency response of the actuator is not sufficient to follow the input signal at the higher frequencies. Table E-4 supplies a list of figures and the corresponding spring and damper settings for different correlation graphs.

**Table E-4: Spring/damper configuration for sine sweep tests**

| Figure number | Input | Spring state | Damper state |
|---|---|---|---|
| Figure E-30 | Sine sweep (15*mm* amplitude) | OFF | OFF |
| Figure E-31 | Sine sweep (15*mm* amplitude) | ON | OFF |
| Figure E-32 | Sine sweep (15*mm* amplitude) | OFF | ON |
| Figure E-33 | Sine sweep (15*mm* amplitude) | ON | ON |
| Figure E-34 | Sine sweep (15*mm* amplitude) | ON | Karnopp |
| Figure E-35 | Sine sweep (15*mm* amplitude) | OFF | Karnopp |
| Figure E-36 | Sine sweep (15*mm* amplitude) | ON | Holsher & Huang |
| Figure E-37 | Sine sweep (15*mm* amplitude) | OFF | Holsher & Huang |

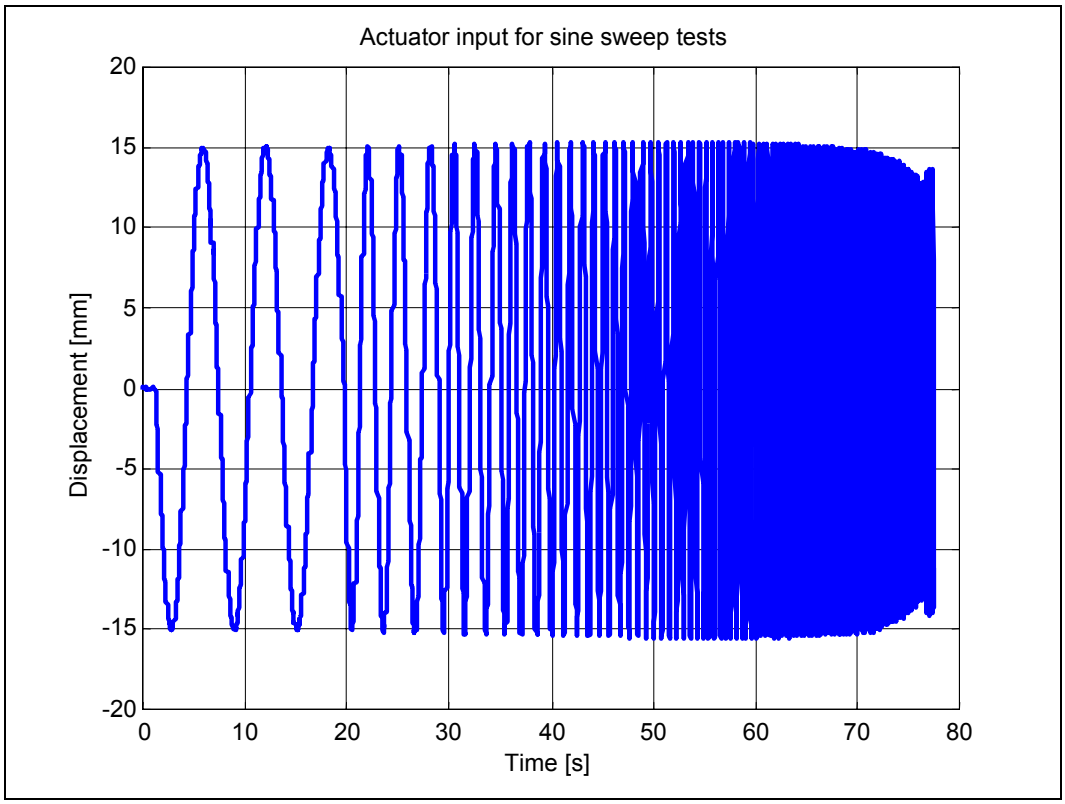


**Figure E-29: Sine sweep actuator input**

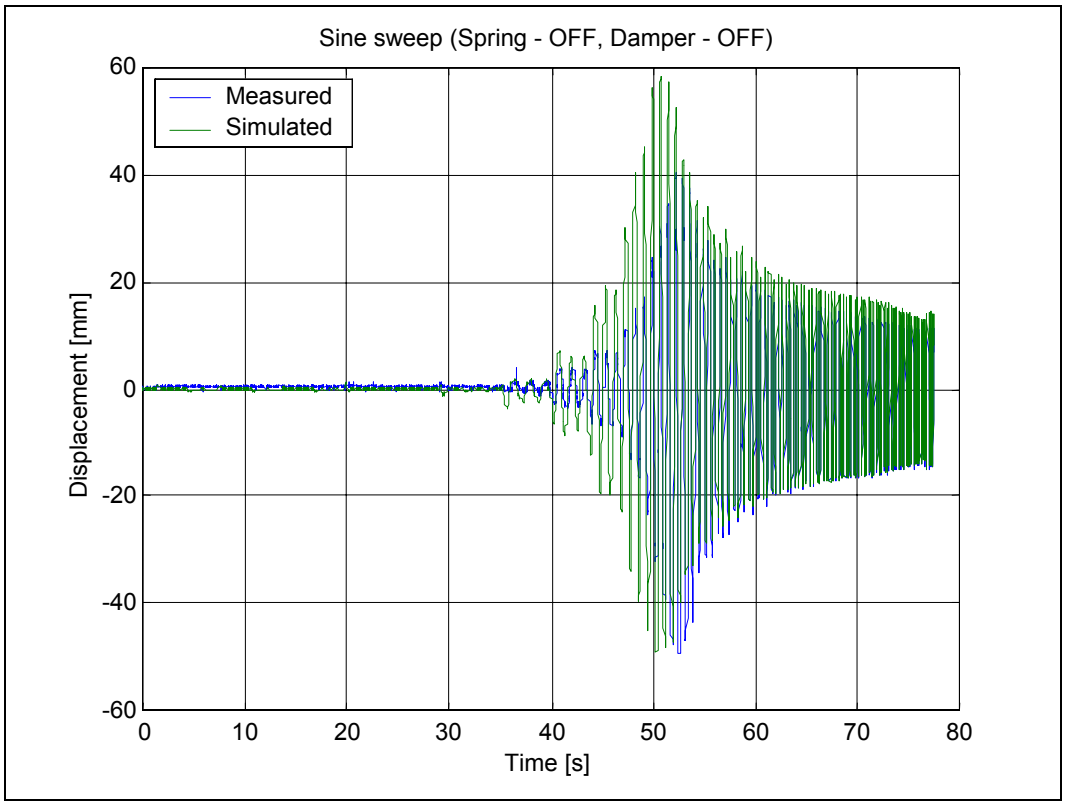


**Figure E-30: Sine sweep (Spring - OFF, Damper - OFF)**

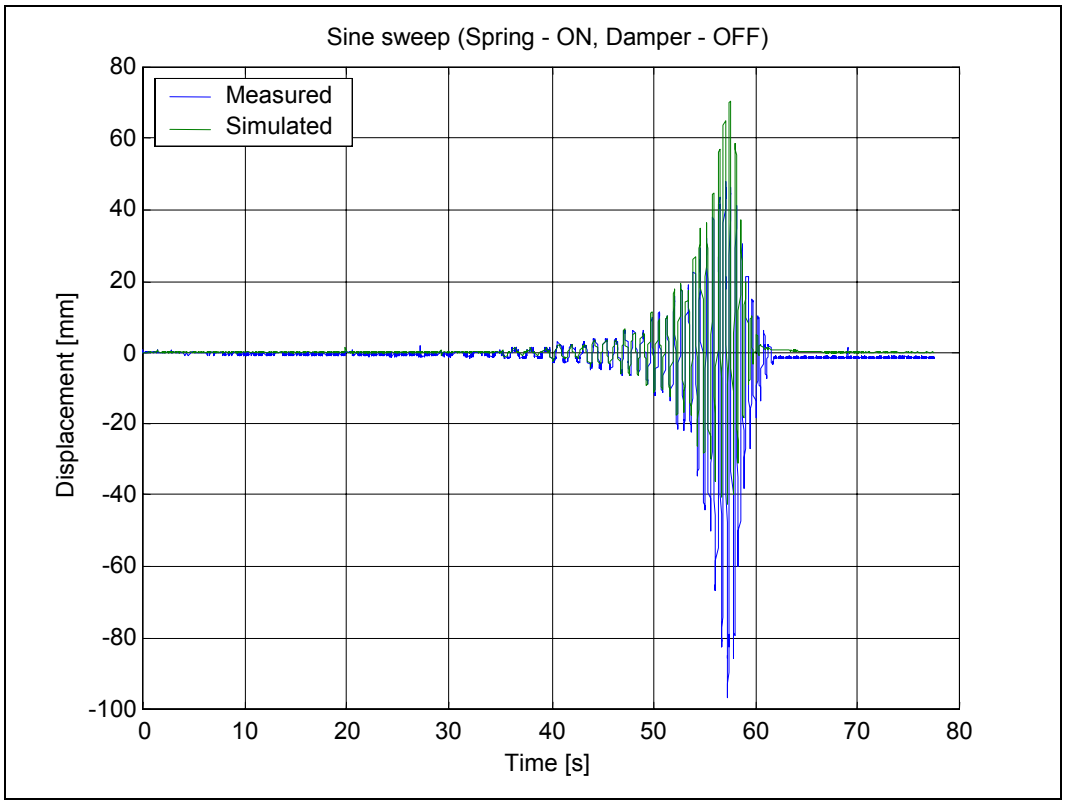


**Figure E-31: Sine sweep (Spring - ON, Damper - OFF)**

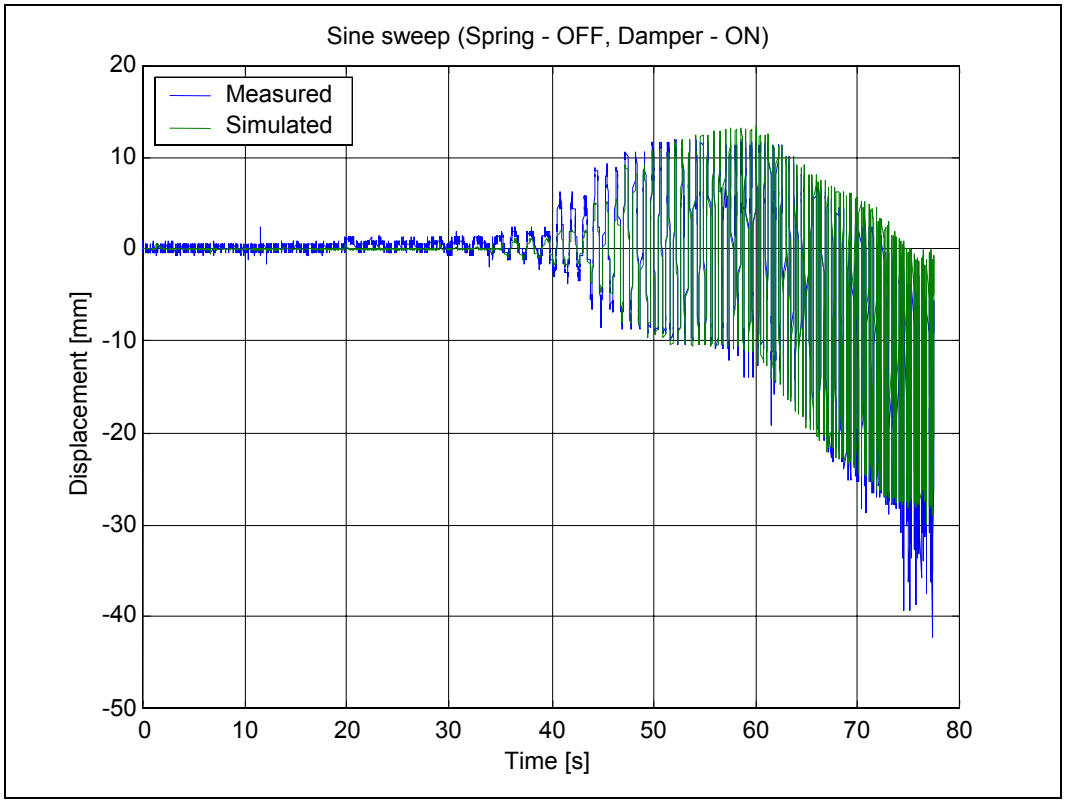


**Figure E-32: Sine sweep (Spring - OFF, Damper - ON)**

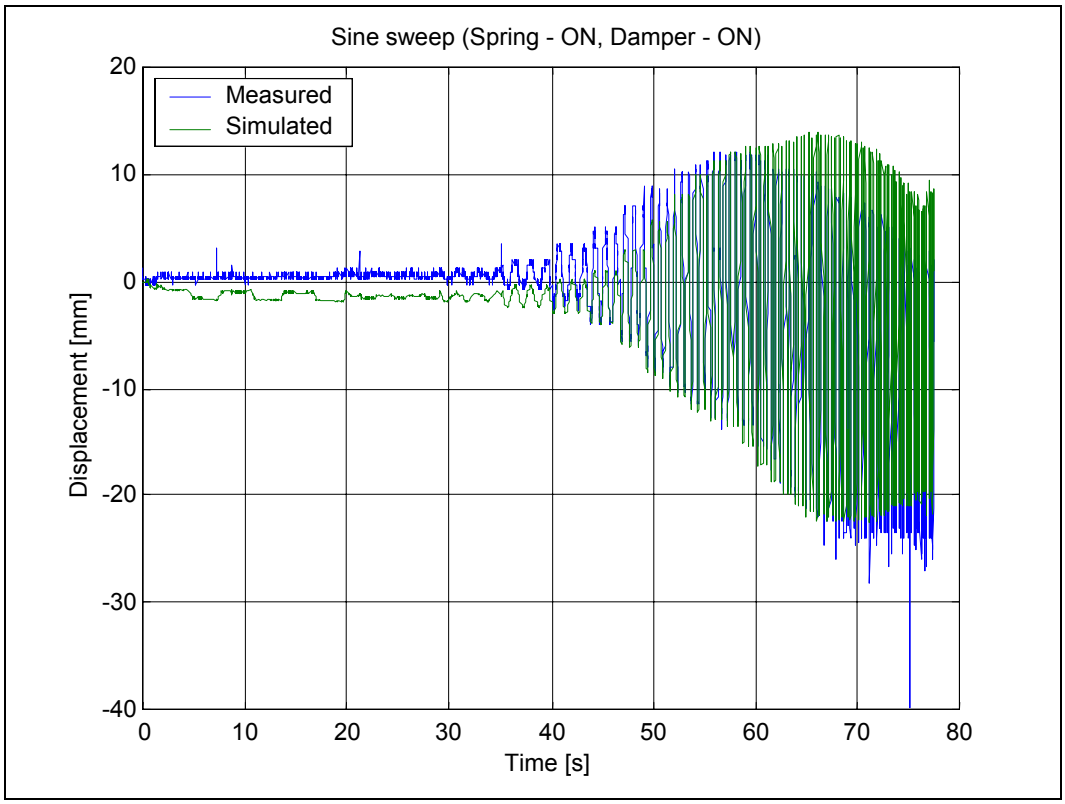


**Figure E-33: Sine sweep (Spring - ON, Damper - ON)**

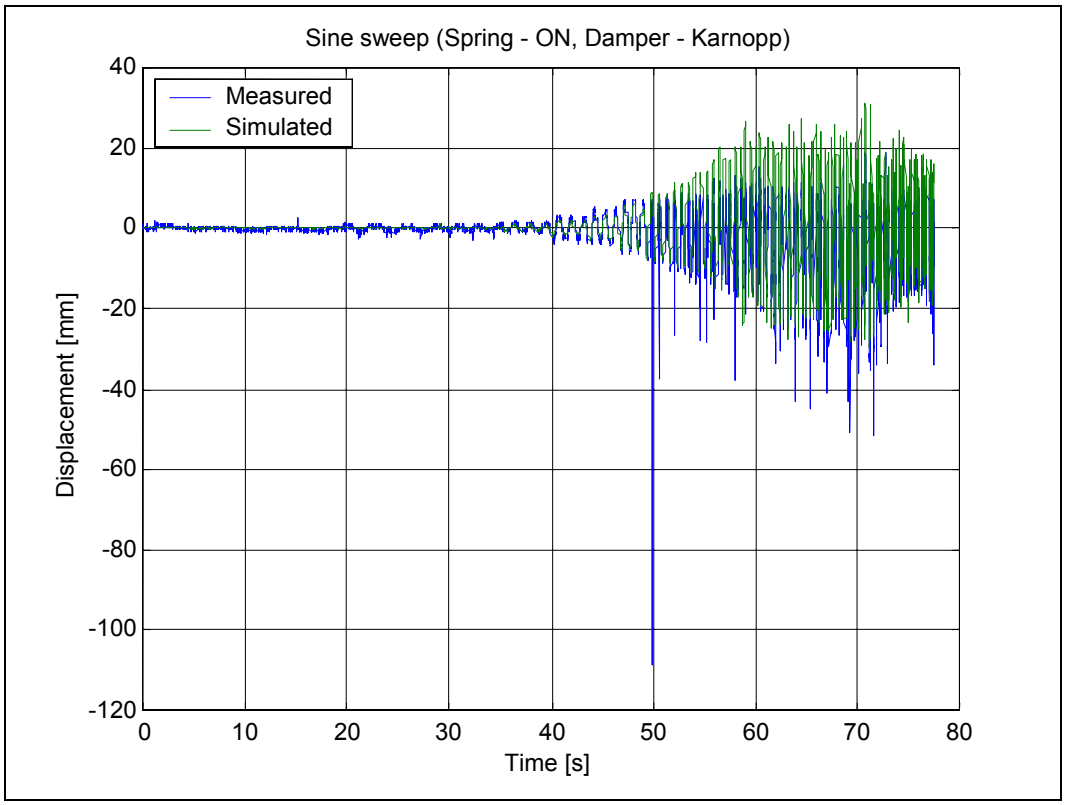


**Figure E-34: Sine sweep (Spring - ON, Damper - Karnopp)**

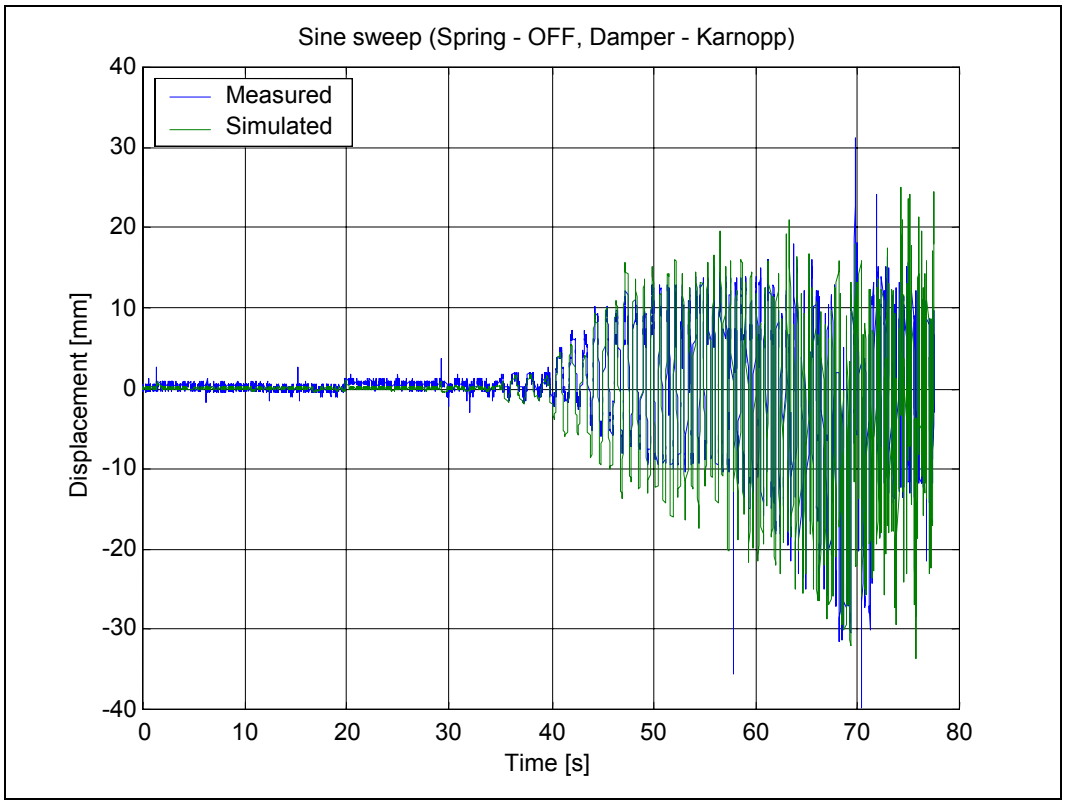


**Figure E-35: Sine sweep (Spring - OFF, Damper - Karnopp)**

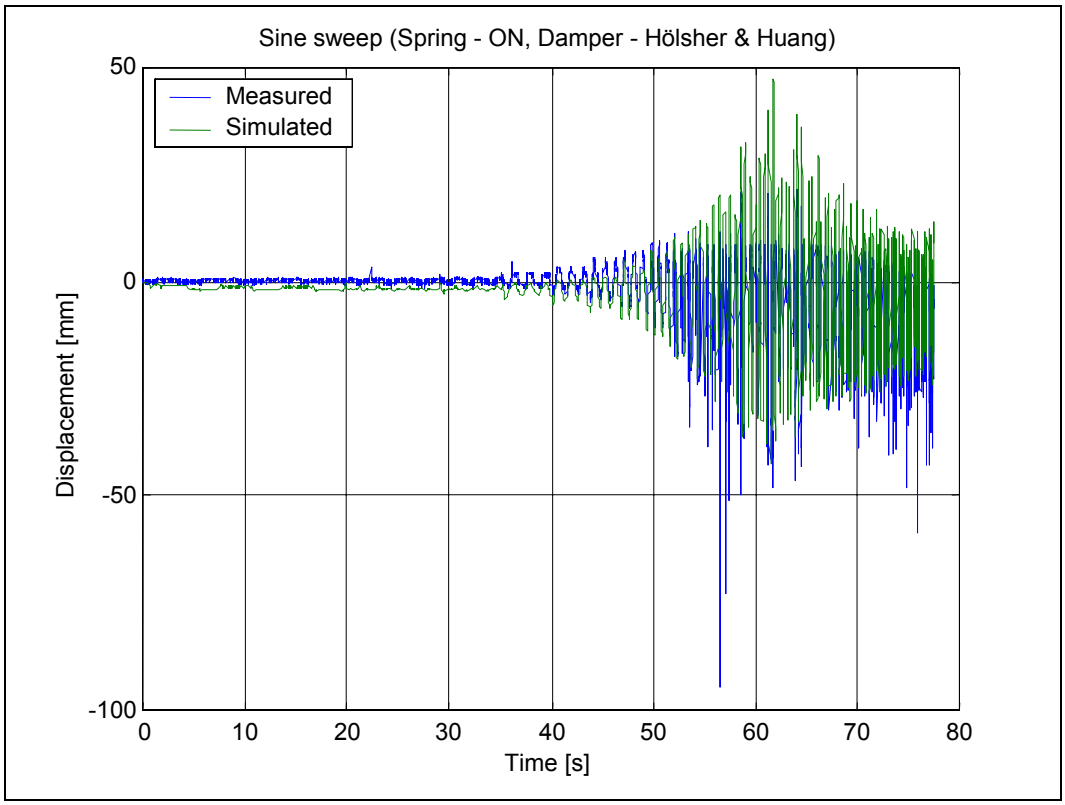


**Figure E-36: Sine sweep (Spring - ON, Damper - Hölscher & Huang)**

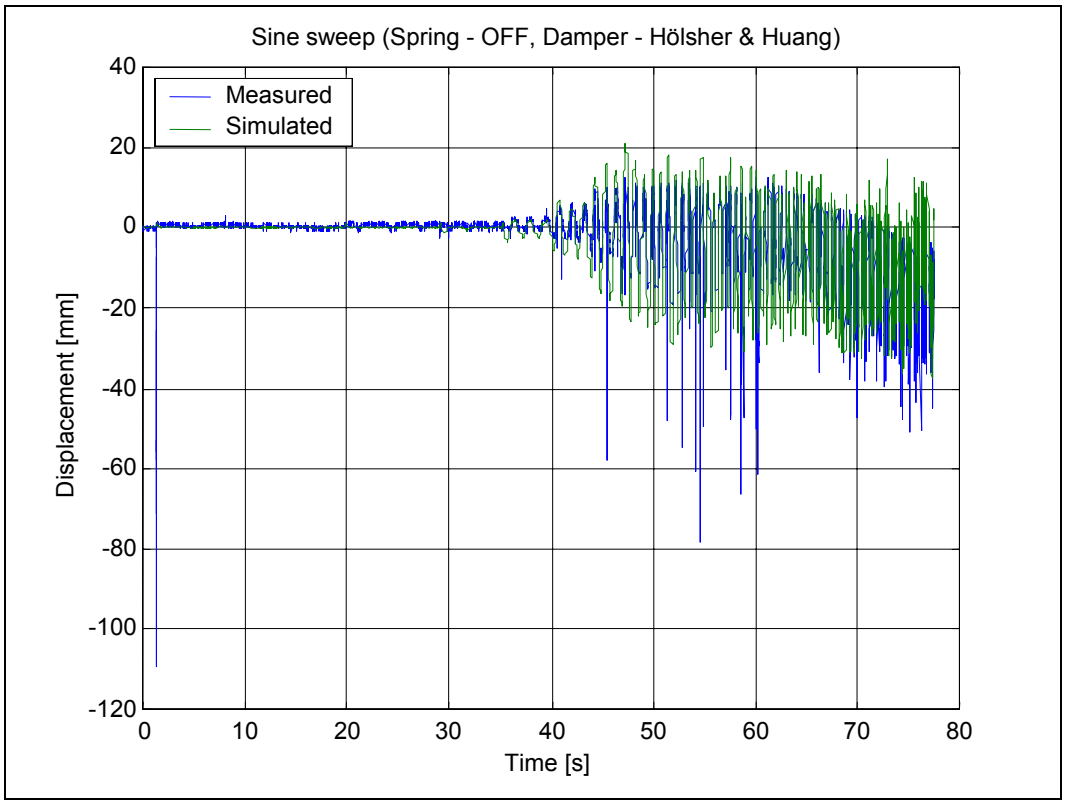


**Figure E-37: Sine sweep (Spring - OFF, Damper - Hölscher & Huang)**

The transmissibility between the input signal (Schenck displacement) and the sprung mass displacement was determined for the measured, as well as the simulated data. Table E-5 supplies a list of figures and the corresponding spring and damper settings for the transmissibility graphs.

**Table E-5: Spring/damper configuration for transmissibility graphs**

| Figure number | Input | Spring state | Damper state |
|---|---|---|---|
| Figure E-38 | Sine sweep (15mm amplitude) | OFF | OFF |
| Figure E-39 | Sine sweep (15mm amplitude) | ON | OFF |
| Figure E-40 | Sine sweep (15mm amplitude) | OFF | ON |
| Figure E-41 | Sine sweep (15mm amplitude) | ON | ON |
| Figure E-42 | Sine sweep (15mm amplitude) | ON | Karnopp |
| Figure E-43 | Sine sweep (15mm amplitude) | OFF | Karnopp |
| Figure E-44 | Sine sweep (15mm amplitude) | ON | Holsher & Huang |
| Figure E-45 | Sine sweep (15mm amplitude) | OFF | Holsher & Huang |

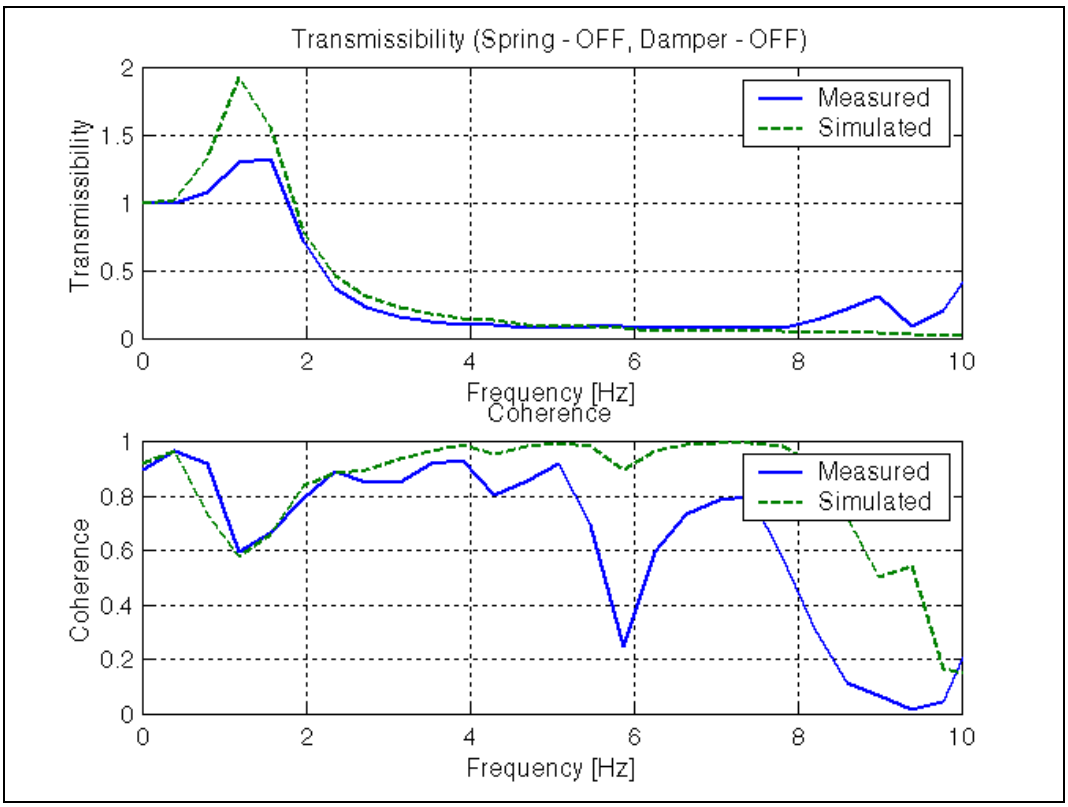


**Figure E-38: Transmissibility plot (Spring - OFF, Damper - OFF)**

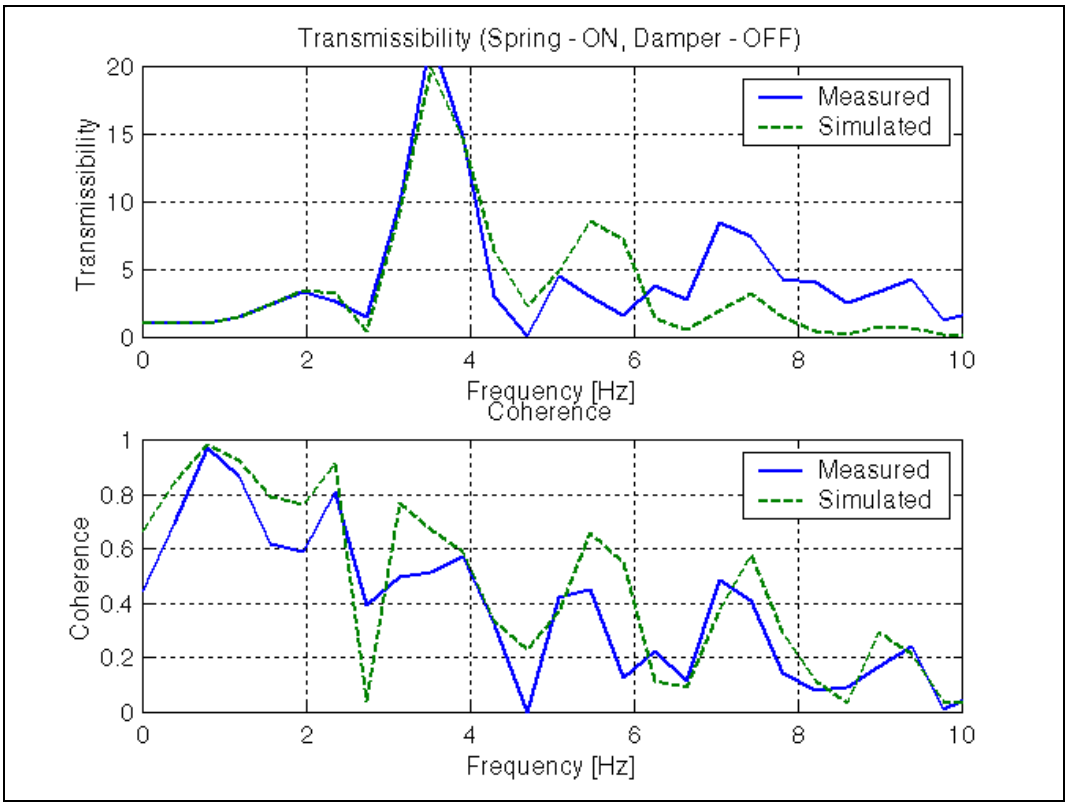


**Figure E-39: Transmissibility plot (Spring - ON, Damper - OFF)**

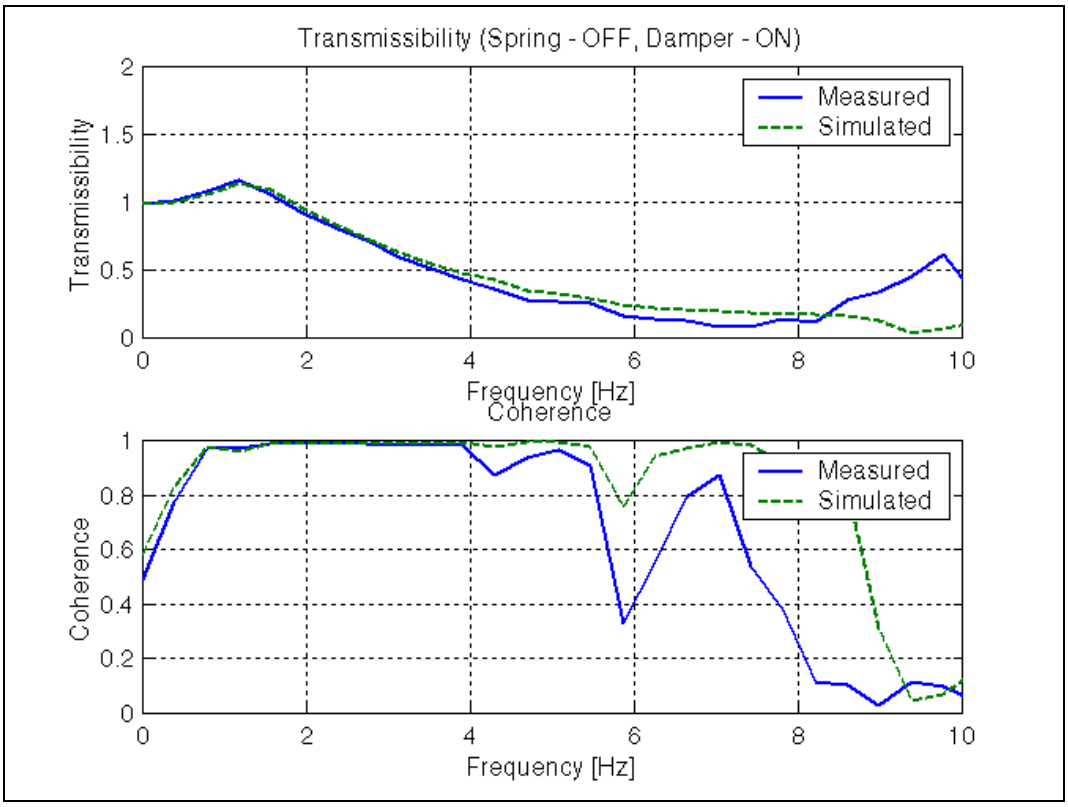


**Figure E-40: Transmissibility plot (Spring - OFF, Damper - ON)**

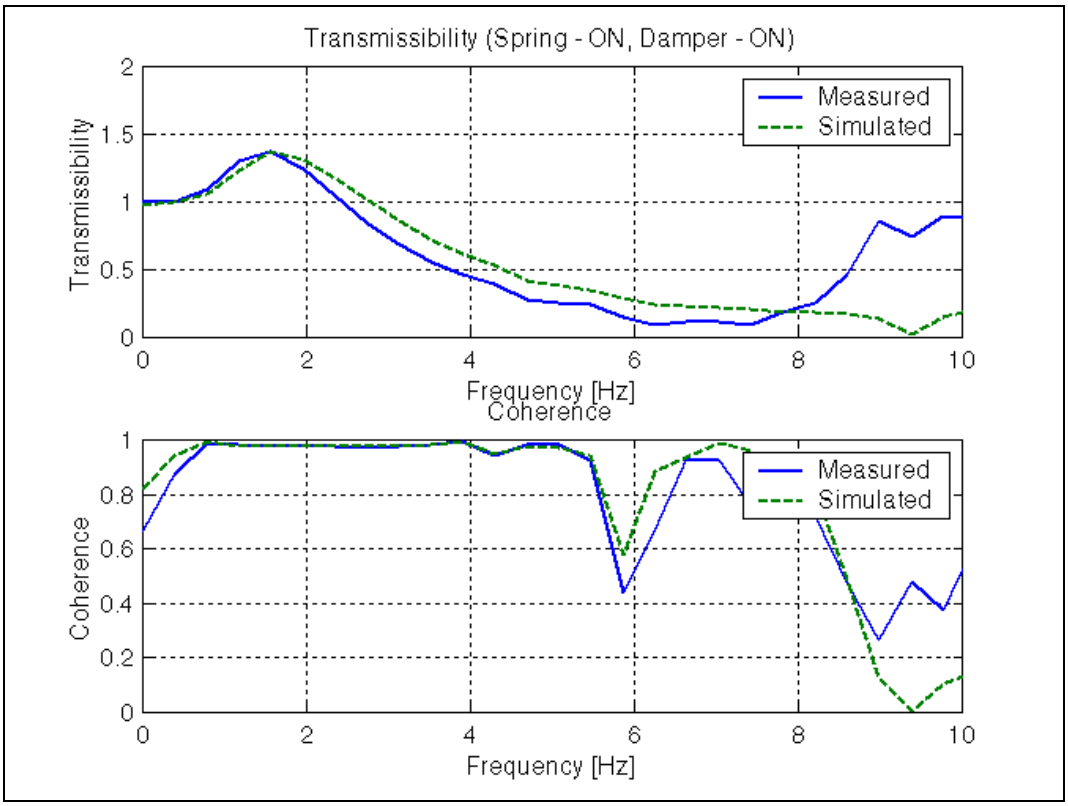


**Figure E-41: Transmissibility plot (Spring - ON, Damper - ON)**

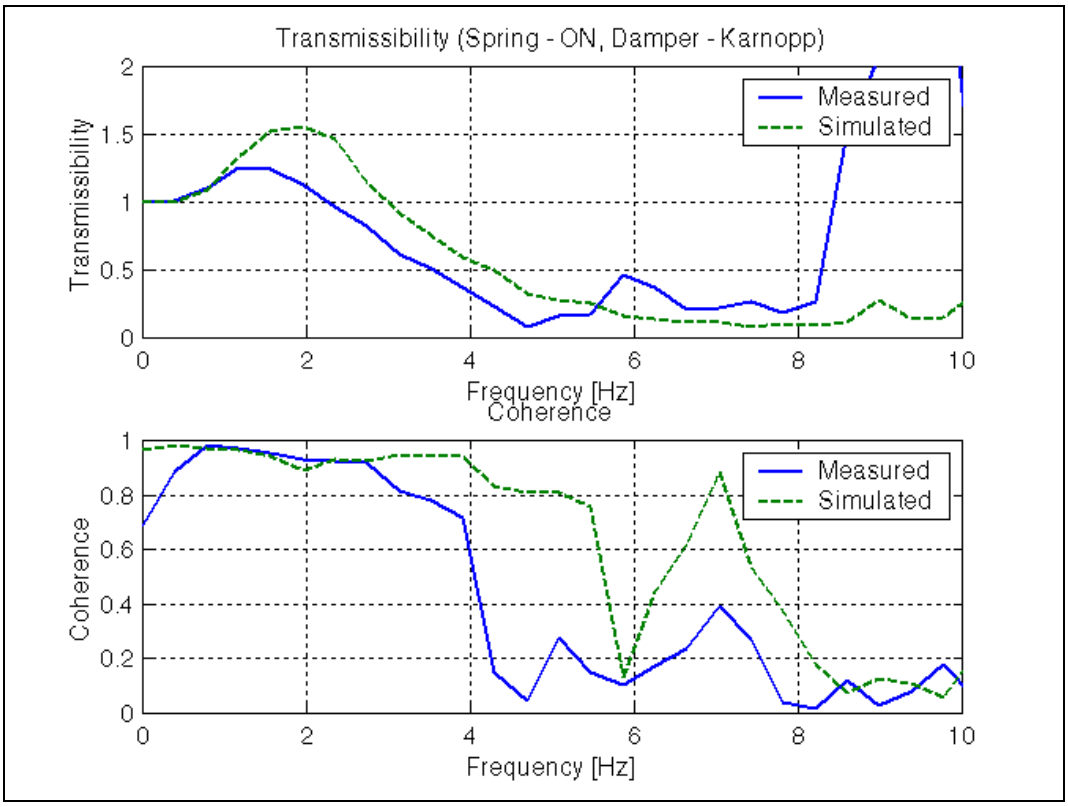


**Figure E-42: Transmissibility plot (Spring - ON, Damper - Karnopp)**

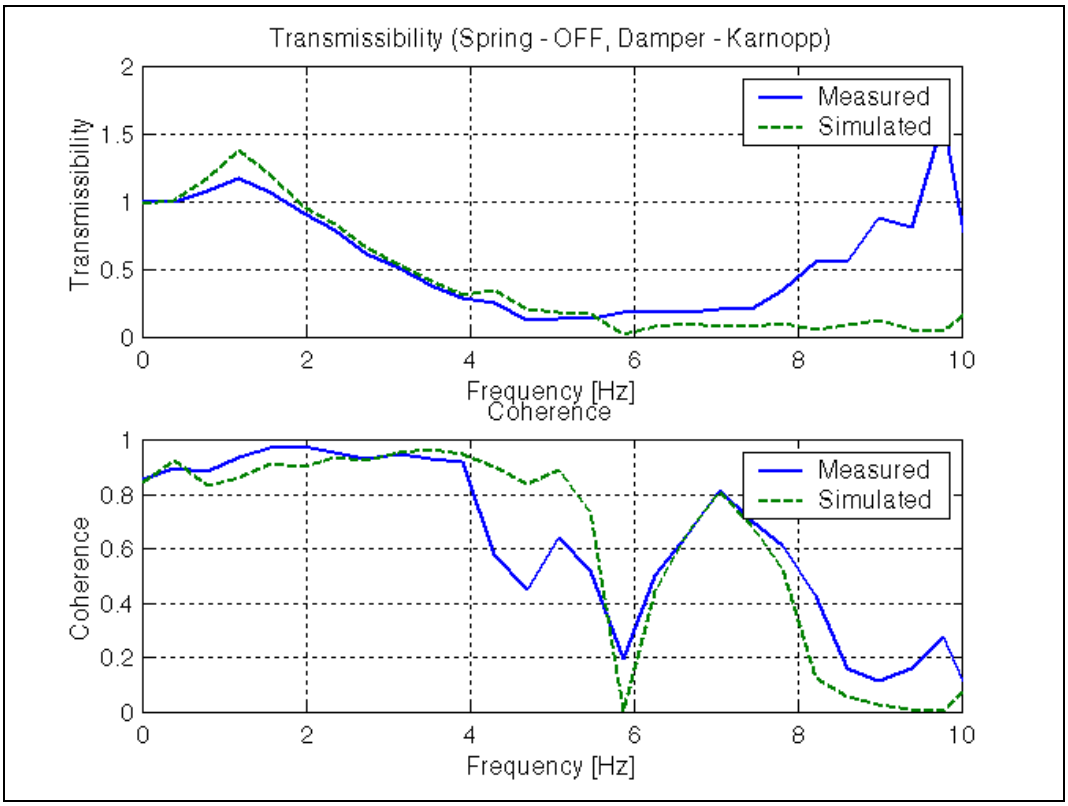


**Figure E-43: Transmissibility plot (Spring - OFF, Damper - Karnopp)**

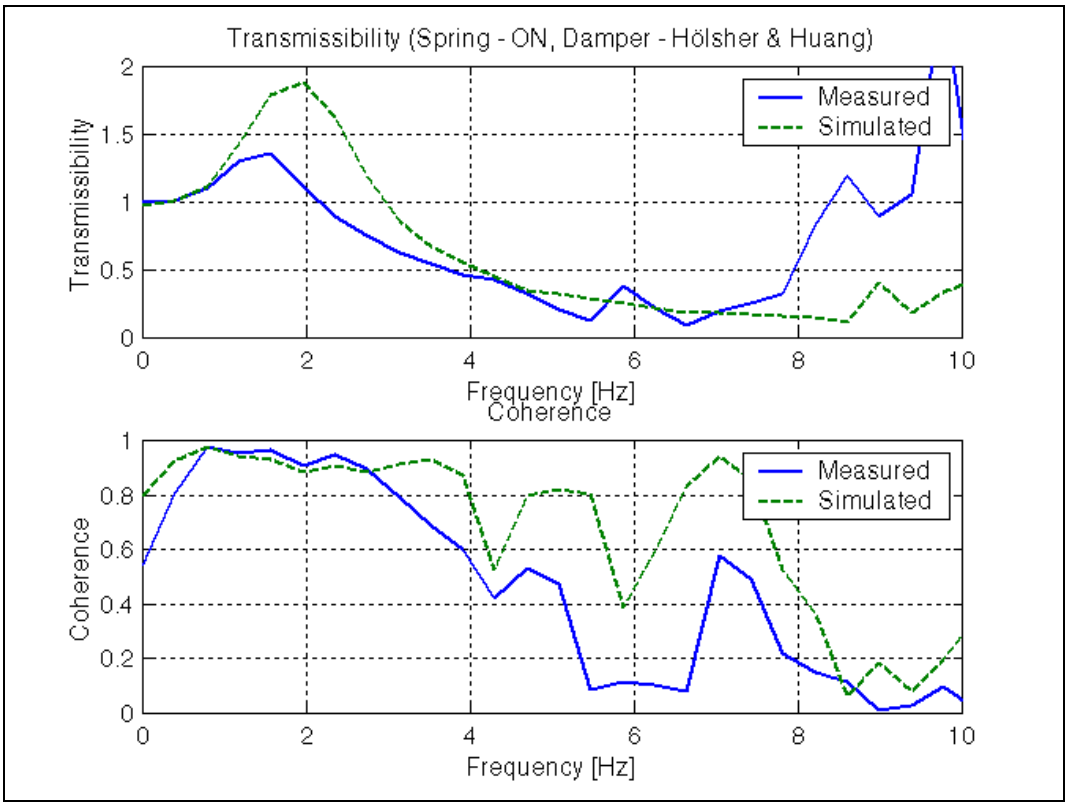


**Figure E-44: Transmissibility plot (Spring - ON, Damper - Hölscher & Huang)**

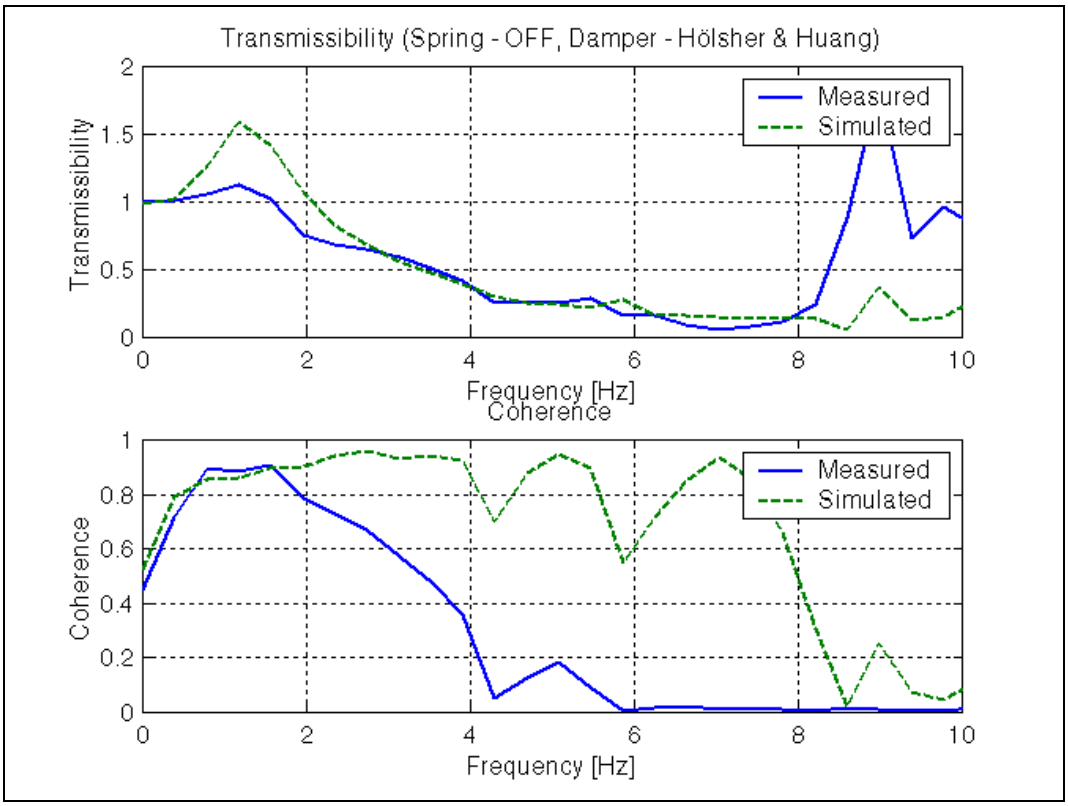


**Figure E-45: Transmissibility plot (Spring - OFF, Damper - Hölscher & Huang)**